WATER RESOURCE EVALUATION IN THE DANAKIL BASIN, ETHIOPIA: GROUNDWATER SUPPLY FOR POTASH SOLUTION MINING.

Luke Towers

Submitted in fulfilment of the requirements for the degree

Magister Scientiae in Geohydrology

in the

Faculty of Natural and Agricultural Sciences

(Institute for Groundwater Studies)

at the

University of the Free State

Supervisor: Fanie De Lange

Co-supervisor: Rowena Hay

July 2017

DECLARATION

I, LUKE TOWERS, hereby declare that the dissertation hereby submitted by me to the Institute for Groundwater Studies in the Faculty of Natural and Agricultural Sciences at the University of the Free State, in fulfilment of the degree of Magister Scientiae, is my own independent work. It has not previously been submitted by me to any other institution of higher education. In addition, I declare that all sources cited have been acknowledged by means of a list of references.

I furthermore cede copyright of the dissertation and its contents in favour of the University of the Free State.

Luke Towers

03 July 2017

ACKNOWLEDGEMENTS

I would hereby like to express my sincere gratitude to all who have motivated and helped me in the completion of this thesis:

- Umvoto Africa for the opportunity, motivation, lessons and support.
- The mining company, and other concessions in the region for making available the data and reports.
- The friendly Ethiopian people for their hospitality and the unforgettable experiences I had while in their country.
- The Danakil Mafia for the support both in and out of the field-special mention to Oom Dave, Captain and Dr Fanie Botha.
- Noel, Teresa and Amy for encouraging me. My friends, for helping me maintain a good balance and reminding me to make the most out of my experiences.

TABLE OF CONTENTS

LIST OF FIGURES

LIST OF TABLES

LIST OF ABBREVIATIONS

°	-	degrees
~	-	approximately
>	-	greater than
<	-	less than
%	-	percent
a	-	annum
ALOS		Advanced Land Observation Satellite
API	-	American Petroleum Institute
ASR	-	aquifer storage and recovery
AST		Aquifer Stress Test
ASTER	-	Advanced Spaceborne Thermal Emission and Reflection Radiometer
ASTM	-	American Society for Testing and Materials
BD	-	Bada-Danakil
BP	-	years before present
cm	-	centimetre
d	-	day
DA	-	Danakil block
DEM	-	digital elevation model
DM	-	Dallol Mound
DTW	-	Dallol Test Well
E	-	east
e.g.	-	for example
et al.	-	and others
EC	-	electrical conductivity (salinity)
EGM	-	earth gravitational model
EM	-	electromagnetic
ERM	-	Environmental Resources Management
ENE/ESE	-	east-northeast/east-southeast
FEFLOW	-	Finite Element subsurface FLOW system
Fm.	-	formation
GDEM	-	global digital elevation model
GIS	-	Geographical Information System
Gl		Gigalitres (billion litres)
GNSS	-	Global Navigation Satellite Systems
GPS	-	global positioning system
GSE	-	Geological Survey of Ethiopia
hm^3		cubic hectometre (SI unit for a million cubic metres)
HPZ	-	hydrostratigraphic parameter zone
i.e.	-	that is
IWRM	-	integrated water resource management
K	-	hydraulic conductivity
km	-	kilometre
km^2	-	square kilometre
km^3	-	cubic kilometre
kPa	-	kilopascal
kW	-	kilowatt
l	-	litre
m	-	metre
m^2	-	square metre
m^3	-	cubic metre
Ma	-	million years
mbgl	-	metres below ground level
mamsl	-	metres above mean sea level
mbmsl	-	metres below mean sea level
mg	-	milligram
MDRF	-	Main Danakil Rift-boundary Fault

Ml	-	Megalitre (million litres)
mm	-	millimetre
MOP	-	muriate of potash
MoW		Ministry of Water
mS	-	milliSiemens
µg	-	microgram
MWSFS	-	Mine Water Supply Feasibility Study
N	-	north
NASA	-	National Aeronautics and Space Administration
NE/NW	-	northeast/northwest
NNE/NNW	-	north-northeast/north-northwest
NU	-	Nubian block
p.	-	page
pp.	-	pages
Q	-	discharge
RES	-	Remote Exploration Services
RMC	-	Renda-Maglalla-Coma graben
s	-	second
S	-	Storativity
S_s	-	specific storage
S	-	south
SANS	-	South African National Standard
SANAS	-	South African National Accreditation System
SOP	-	sulphate of potash
SRTM	-	Shuttle Radar Topography Mission
SE/SW	-	southeast/southwest
SSE/SSW	-	south-southeast/south-southwest
T	-	transmissivity
TDEM	-	Time Domain Electromagnetic
TDS	-	Total Dissolved Salts
TEM	-	Transient Electromagnetic
USGS	-	United States Geological Survey
UTM	-	Universal Transverse Mercator
VES	-	Vertical Electrical Sounding
W	-	west
WGS	-	World Geodetic System
WHO	-	World Health Organisation
WNW/WSW	-	west-northwest/west-southwest
WWDSE	-	Water Works Design and Supervision Enterprise
y	-	year

CHAPTER 1
INTRODUCTION

1.1 RESEARCH FRAMEWORK

A potash mining company holds an exploration licence in the northern part of the Danakil Depression. Potash ore, an evaporite deposit, occurs on the floor of the Danakil Depression, approximately -120 metres below mean sea level (mbmsl). The occurrence of potash in the Danakil Depression is associated with rift magmatism, marine flooding, and deep brine cycling (Warren, 2015), making it a highly complex region from both a geological and hydrogeological perspective.

The Danakil Depression occurs in the northern part of the Afar Rift, which is part of the north-south-trending arm of the East African Rift System (Franzson *et al.*, 2015) (see **Figure 2-1**). The mining concession covers an area of 365 km^2 and lies southwest of the Ethiopian-Eritrean border. To the south lies the Danakil Desert and the renowned Mount Dallol (**Figure 1-2**). The Danakil Depression is considered by many to be the hottest inhabited place on earth (ERM, 2014) with average annual temperatures of 38°C and maximum temperatures reaching 50°C in summer months (Darrah *et al*., 2013).

Potash ore in the Danakil Depression is composed predominantly of sylvite (KCl), carnallite ($KMgCl_3 \cdot 6H_2O$), polyhalite [$Ca_2K_2Mg(SO_4)_4 \cdot 2H_2O$] and kainite ($MgSO_4 \cdot KCl \cdot 3H_2O$) (Orris *et al.*, 2010). These different deposits are divided into three members which have a dominant suite of potash minerals, namely the Sylvinite, Intermediate and Kainitite members (ERCOSPLAN, 2009). Extracted sylvite is used in the production of muriate of potash (MOP) fertilizers while kainite is used in the production of sulphate of potash (SOP) fertilizers. Bischofite ($MgCl_2 \cdot 6H_2O$) and halite (NaCl) are often also mined for the construction of evaporation pond basal layers at surface (Umvoto, 2014).

The mine is still in the exploration phase and plans to make use of solution mining techniques to mine the potash and other associated salts. This mining method requires large volumes of water. An estimated 30 million cubic metres (30 000 000 m^3) or 30 cubic hectometres (30 hm^3) of water is required per annum. This equates to approximately 80 million litres of water per day (80 Ml/d) for the projected 20-year life of mine, once fully

operational (Umvoto, 2015). Groundwater abstraction, surface water supply or ideally a combination of both will possibly be needed to meet this substantial water requirement. The scarcity of surface water in the region however, makes groundwater the more feasible option for meeting this water demand in terms of quantity, but not necessarily in quality.

Previous and on-going investigations carried out by several mining and exploration companies in the region, as well as the Ethiopian Ministry of Water and Energy (MoWE), indicated the presence of numerous springs at the toe of alluvial fans (Umvoto 2014a). The alluvial fans occur at the base of the Dogua Mountains (see **Figure 1-1**) along a rift related fault called the Main Danakil Rift-boundary Fault (MDRF) (Umvoto, 2015). These springs or seeps flow out onto the playa salt-mud flats and indicate a possible continuous flow of groundwater (see **Figure 1-1**). Three alluvial fans to the west of the mining concession are thus targeted for groundwater exploration and potential abstraction to meet the mine water demand.

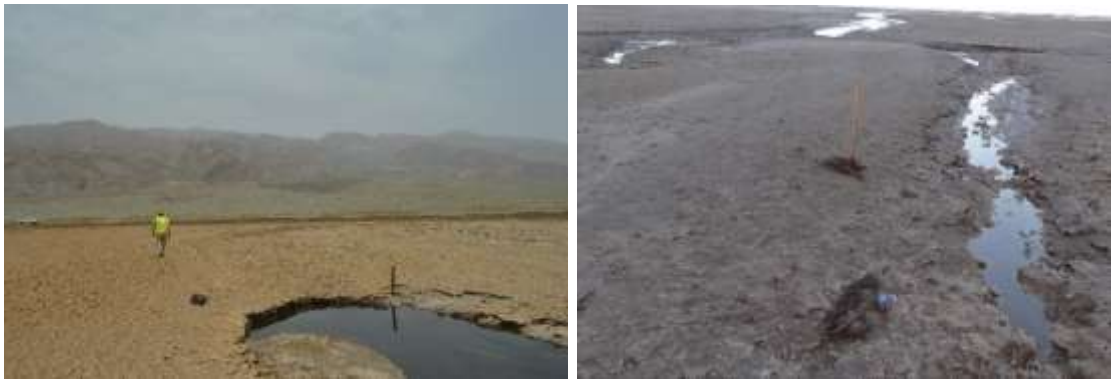

Figure 1-1 Groundwater seeps at the toe of the alluvial fans indicating a possible continuous flow of groundwater.

Previous works predominantly focused on alluvial fans found further south than the three fans under investigation in this study. The fans in this investigation were named from south to north as the Asabuya fan, Bussaba fan and the North Dogua fan, which together form the Dogua Alluvial Fan Complex (see **Figure 1-3**) (Umvoto, 2016a). A fourth, northern most fan, namely the Badah fan was not included in the investigation as groundwater abstraction or development from this fan was avoided due to the vulnerability of the community located at Badah Village which make use of shallow dug wells and a shallow borehole in the alluvial deposits (see **Figure 1-3**).

The remote and complex geographical, geological and meteorological setting of the study area has resulted in limited literature and data being available regarding groundwater potential within the region. Numerous studies pertaining to the active rifting, associated faulting and volcanism of the region have been carried out (Chorowicz, 2005; Darrah *et al.,* 2005; Frostick, 1997; Umvoto, 2016f). Research of such studies, along with additional field investigations and interpretations are used to assist in better defining regional and local components of the alluvial fan aquifers, their associated flow paths, hydrochemical signatures and recharge sources.

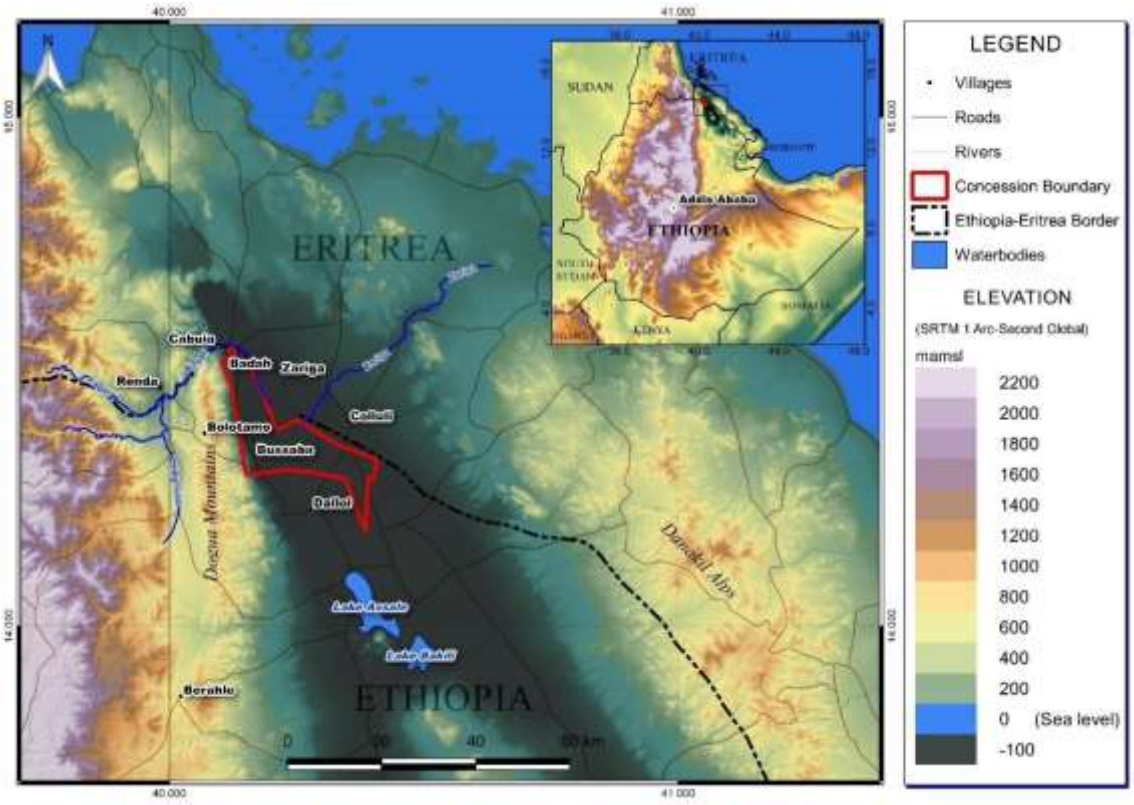

Figure 1-2 Regional location map depicting the study area and its associated elevation in meters above mean sea level (mamsl) (Umvoto, 2016a).

Figure 1-2 is a regional locality map based on Advanced Land Observing Satellite (ALOS) digital elevation data obtained from Umvoto (2016a). The mining concession boundary, as it is labelled, is illustrated as a red polygon shown in relation to major towns and villages (labelled black dots), river channels (blue lines), roads (brown lines) and the international border (dashed black line) within the northern part of the Danakil Depression. An insert at the upper right corner locates the figure within the broader context of Ethiopia, Eritrea and the southern Red Sea.

Figure 1-3 **Google Earth image of the four main alluvial fans adjacent to the mining concession. Three of these constitute the focus for groundwater exploration for supply to the potash mining operation.**

Figure 1-3 illustrates the location of alluvial fans that form from the Dogua Mountains. The Badah fan was excluded from field investigation and potential development. A green polygon represents the mining concession.

1.2 RESEARCH QUESTION

This study will address hydrogeological characterisation of three alluvial aquifers found in the Danakil Depression study area for potential sustainable water supply to the potash mining operation.

Research of literature and field investigations aims to obtain results for several different sub-disciplines within hydrogeology, but finally results are all used to answer the following research question:

Based on groundwater exploration and aquifer characterisation, do the three alluvial fan aquifers west of the mining concession hold groundwater resources of sufficient quantity

and of what quality, to meet the mine's water demand of 30 million cubic meters per annum over the 20-year life of mine?

1.3 AIM AND OBJECTIVES

1.3.1 Aim

To investigate groundwater resources for potash mining. The groundwater consulting company Umvoto Africa (Pty) Ltd. was appointed to undertake a groundwater exploration investigation and resource estimation of available water sources. This investigations aim was to evaluate the potential of alluvial fan aquifers for mine water supply. The author formed part of the project team for the investigation and was co-author of reports significant to this study.

The aim of this research thesis is to perform groundwater exploration and aquifer characterisation in support of a groundwater resource estimation for three alluvial fan aquifers within and adjacent to the mining concession.

1.3.2 Objectives

1. Carry out a literature review to better understand potash deposits, alluvial aquifers and the tectonic context of the hydrogeological system and its associated flows. Make use of relevant literature to characterise the geological, hydrogeological and climatic context of the groundwater flow system on a regional and local scale.
2. Summarise and review geophysical data to support the siting of monitoring and production boreholes. Interpretation of geophysical data to delineate physical boundaries and hydrostratigraphic detail of the aquifer system.
3. To better characterise lithology allowing for increased certainty in the geology, and better understand the geometry, hydraulic parameters and responses of the aquifer. This will be achieved through conducting field investigations such as drilling and test pumping boreholes in each of the three target fans.
4. Test pumping to collect and interpret data on aquifer time-drawdown response and recovery. This is to define aquifer characteristics such as volume, hydraulic properties, storage and sustainable yield potential, where possible.

5. Monitor water levels during field investigations to determine if there is any cross-fan interaction or basement rock and fan interaction in the upper fan areas to inform on numerical modelling boundary conditions.
6. Identify and evaluate hydrochemical signatures from collected samples to differentiate recharge sources and flow paths to the aquifer.
7. Evaluate and verify, as far as possible, the hypothesis of deep flow through basement rocks, via fault structures, and to what extent the aquifer is recharged by such flows as opposed to rainfall-infiltration components contributed by local fan catchments.
8. Review existing conceptual and numerical models and existing hydroclimatic, and recharge data, affording higher levels of confidence in the number of production boreholes needed to fulfil the mining operations requirements as well as the optimum pumping rates of each borehole from the different fans to sustainably abstract water without resulting in adverse effects on the physical integrity of the aquifer, regional groundwater levels and groundwater dependent communities.
9. Establish a reliable hydrogeological and climatic monitoring network that contributes to data collection and database development. This is to develop a higher confidence understanding of baseline conditions and seasonal variations.
10. Develop supply and demand scenarios for the mining operation with estimated groundwater volumes and yields to determine if it is hydrogeologically feasible to successfully and sustainably meet the water demand for the expected life of mine.

1.4 RESEARCH METHODOLOGY

The research methodology is based on literary research and exploratory field work to better understand the hydrotectonic, hydroclimatic and hydrogeological conditions of the study area. Interpretation of geophysical data and the establishment of weather stations within recharge and discharge areas was used to assist in this understanding.

Hydraulic testing was carried out via drilling three production- and five monitoring-boreholes for testing purposes. These production boreholes along with two pre-existing boreholes were test pumped for an extended period each and thereafter could recover as part of an Aquifer Stress Test (AST). Time-drawdown data obtained from test pumping was analysed and interpreted by making use of visual interpretations based on experience and first principles, supported by analyses with appropriate software

(AQTESOLV). Hydrochemical and isotope sampling, analyses and interpretation, to better define recharge sources and water quality considerations, was also conducted.

Results and interpretations from the afore mentioned works were incorporated into and used to update an existing conceptual and numerical groundwater flow model constructed in FEFLOW by Umvoto (2016e). The results of the Umvoto (2016e) numerical model were used to support well field design and predictive simulation to increase the level of confidence associated with resource estimation.

1.5 STRUCTURE OF THIS DISSERTATION

This dissertation is comprised of 10 chapters. **Chapter 1** serves as an introduction to the research project and incorporates the aims and objectives, methodology and location of the study area. The second chapter is a Literature Review of potash mining, alluvial fans and the tectonic context of the Danakil Depression. **Chapter 3** pertains to the physiography, geology and hydrogeology of the study area on both a regional and local scale. **Chapters 4 - 7** detail the methodology, results and discussion of the various works carried out to satisfy the initial objectives of the study as defined in **Section 1.3.2**. A regional conceptual and numerical groundwater model is discussed in **Chapter 8**. All the above is brought together in **Chapter 9** to provide a groundwater resource estimation based on demand, supply and development scenarios. **Chapter 10** details the conclusions of the study and incorporates recommendations for groundwater resource development for the mining operation in the future.

CHAPTER 2

LITERATURE REVIEW

2.1 TECTONIC CONTEXT OF THE DANAKIL DEPRESSION

The rift valley represents a series of adjacent, individual, highly faulted rift basins (Umvoto, 2015). Faulting within the rift creates distinct graben structures that are bordered by steep fault ridges (Chorowicz, 2005). These rift basins are cross cut and segmented by transform faults, transfer faults or accommodation zones which are areas of strain transfer across a rift (Umvoto, 2015), forming topographic ridges at the edges of the rift (Frostick, 1997). The half-graben is considered a crucial structural feature in a rift system. A half graben is an asymmetrical basin with one or two main border faults on one side of the basin (Frostick, 1997). Volcanic and sedimentary rocks are typical within a half graben, with the most deposition occurring along the main border fault of the rift (Chorowicz, 2005).

The East African Rift System (EARS) is the most recognised example of an active continental rift system where ocean floor spreading and microplate formation takes place within a continental, not oceanic, setting (Acton and Stein, 1991; Eagles *et al*., 2002 and Frostick, 1997). A microplate is a portion of continental crust that essentially acts rigidly during plate movement. Microplates may either extend to the asthenosphere or represent detached crustal blocks (Acton and Stein, 1991).

A prominent feature of the EARS is the Afar Triangle, representing a triple junction where rifting of the Somali, Nubian and Arabian tectonic plates occurs (Chorowicz, 2005; Eagles *et al*., 2002). This triple junction is formed where the Red Sea rift (Arabia plate – Nubia plate) meets the Gulf of Aden rift (Arabia plate – Somalia plate) east of Djibouti and where the Main Ethiopian Rift (Somalia plate – Nubia plate), the northern Afar rift and the Gulf of Aden rift meet in the Afar depression; the northern Afar rift occurs along the Danakil Depression and meets the Red Sea rift off the coast of Eritrea. (Eagles *et al*., 2002) (see **Figure 2-1**).

The northern segment of the Afar Triangle is represented by the Erta Ale volcanic belt, a typical oceanic ridge where the lithosphere's character experiences a transition between continental and oceanic (Chorowicz, 2005). The horst structure that occurs along the north-eastern border of the Afar Triangle, and represents a typical microplate

is called the Danakil Block. The Danakil depression occurs to the west and south west of the Danakil Block (Chorowicz, 2005).

Numerous authors have attempted to refine the geological history and evolution of the area, especially the kinematics of the Danakil block which represents an active microplate (Abbate *et al*., 2004; Chorowicz *et al*., 1999 and Eagles *et al*., 2002), but uncertainty and disagreement remain. A summary and expansion of such works is provided in Umvoto (2016f), but is not considered further for the purposes of this study.

The Danakil depression is filled with flood basalts that are overlain by clastic sediments and evaporite deposits. At the border of the rift, the evaporites are interbedded with wedges of alluvium from the surrounding plateau (Umvoto, 2015). The Ethiopian plateau to the west of the Danakil depression and the Danakil block to the east are both comprised of Precambrian metamorphic rocks. In the Ethiopian plateau the Precambrian basement rocks are overlain by sandstone, limestone and alkaline basalts while the Danakil block is bordered by recent volcanic material and recent Red Sea sediments along the coast (Abbate *et al*., 2004; Waltham, 2010).

Figure 2-1 Regional map of Ethiopia illustrating the western and eastern plateaus, the Afar region, Main Ethiopian rift and the Danakil Depression in relation to geology, major towns, water features and the Red Sea (Umvoto, 2015).

2.2 ALLUVIAL FANS

Alluvial fans are conical sedimentary features that form where a drainage element of a mountain catchment discharges into a basin (Blair and McPherson, 1994). Fan deposits typically occur where uplifted bedrock is eroded by drainage channels and the eroded

sediment is deposited in a lower lying area. Alluvial fans in arid regions offer ideal deposits for investigation (Blair and McPherson, 1994). Numerous factors influence the development of alluvial fans. Blair and McPherson (1994) detail conditions for alluvial fan development.; those considered of foremost importance are sufficient sediment supply, sediment accumulation, and adequate relief for vertical fan growth.

Groundwater potential of alluvial fans may be considered high as they transmit groundwater from high elevation regions into lower lying basins. This throughflow recharges aquifers in adjacent basins or is discharged as surface water within the basin (Blainey and Pelletier, 2008; Munevar and Marino, 1999).

Alluvial fan deposits are typically highly heterogenous with coarse grained and poorly sorted sediment, as is expected in debris flow and sheet flood deposits (Blair and McPherson, 1994). The elevation difference or slope and large grain size further increase the groundwater flow potential. Abstraction of groundwater from alluvial fans could lower the water table, which may result in destabilisation of slopes and subsidence along structural features such as faults and fracture zones. Faulting may intercept groundwater flow within an alluvial fan (Blair and McPherson, 1994).

Alluvial fan through flow is difficult to quantify for groundwater resource estimation. Identifying preferable infiltration locations and volumes is complicated by the heterogenous nature of the sediment and complex flood behaviour (Blainey and Pelletier, 2008).

Blainey and Pelletier (2008) report modelled results indicating that active depositional channels of alluvial fans have the highest permeability and are the locus of the highest infiltration rates. Furthermore, it was determined that fans with lower gradients showed increased infiltration with highest infiltration rates occurring near the apex of the fan. Through proving the primary influence of the surface permeability of fan sediments, Blainey and Pelletier (2008) highlight why the depositional history and climatic variation experienced by alluvial fans is important to understand from a groundwater perspective.

Figure 2-2 is a photograph of alluvial sediments of the Asabuya alluvial Fan. **Figure 2-3** is a photograph of active depositional channel flows in the Dogua alluvial fans and **Figure** 2-4 is a photograph of sheet flow during a rain event.

Figure 2-2 Alluvial sediments of the Asabuya Fan.

Figure 2-3 Photographs of active deposition and flow channels in the Dogua Alluvial Fans

Figure 2-4 Sheet flow down an alluvial fan after rainfall in the Dogua Mountains.

2.3 PREVIOUS WORKS

Several mining companies and the MoWE have undertaken groundwater exploration within the vicinity of the study area. These investigations however, are focussed on features such as alluvial fans, faults and geological formations that occur to the south of the current study area. The presence of the evaporite deposits, geological evolution of the area and the presence of the Dallol hydrothermal field indicate that groundwater within the region is likely to be highly saline to brine in nature.

The MoWE campaign focussed on water resources in the alluvial fans west of Dallol (WWDSE, 2013), which occur to the south of the fans under investigation in this study. These southern fans have a much larger aerial extent and have larger recharge catchment areas, possibly making them more attractive targets for groundwater supply, but they occur within and adjacent to other mining concessions and do not have the spatial convenience for development associated with the northern fans. These southern fans, named the Musley, Gehertu and Bacarti fans, also occur adjacent to the MDRF and are reported to have fresh water components (MWH, 2015d; WWDSE, 2013) where fresh groundwater is presumably transmitted via predominantly east-west trending faults

that are shared by fractured and potentially karstic aquifers to the west of the southern fans.

Thirteen test wells were drilled in the MoWE campaign with two wells still to be drilled. These were named Dallol Test Well (DTW1-10 and DTW13-15). The logs and pump test results of these investigations were used to augment and verify literature pertaining to the geology and hydrogeology of the region and are referred to throughout. Details of these boreholes are supplied in **Table 2-1** and their location in **Figure 2-5.**

Table 2-1 Summary of the MoWE drilling and pump testing results adapted from WWDSE (2013) and WWDSE (2015).

Borehole ID	Location	UTM E	UTM N	Elevation (mamsl)	Depth (mbgl)	SWL (mbgl)	Q (l/s)	T (m2/d)	Comment
DTW-1	Gehertu	627462	1576873	-5	189	99.59	44	3890	Groundwater is fresh and the yield was > 44 l/s with little draw down during pump testing.
DTW-2	Gehertu	626691	1576283	39.22	223	144	10	714	The water is brackish.
DTW-3	North Gehertu	627337	1578555	-70.76	91	43.3	60	8.67	The water is brackish.
DTW-4	Asabuya	622916	1584222	112.96	251	132.8	10	62.8	Fractured meta- sandstone aquifer
DTW-5	Musley	628438	1573114	5.168	152	45.19	6	5.48	The water is fresh , well is drilled close to escarpment
DTW-6	Bacarti	631676	1564435	27.107	160	40.7	-	-	Low discharge(2-3 l/s) from pre test by the available pump.
DTW-7	Saba	627010	1547959	137.417	250	44.6	-	-	Low discharge(2-3 l/s) from pre test by the available pump.
DTW-8	Saba	628837	1548947	99.93	170	25.76	-	-	Low discharge(2-3 l/s) from pre test by the available pump.
DTW-9	Saba	630771	1546472	57.04	250	26.2	-	-	Low discharge(2-3 l/s) from pre test by the available pump.
DTW-10	Saba	629306	1573479	-24	130	79.28	50	5190	Water quality is good
DTW-13	Elifan	609438	1575980	489	244	10.94	37.5	2565	Water quality is good
DTW-14	Simblele	612204	1564889	581	300	68.37	29	470	21.36m draw down during pump testing.
DTW-15	Simblele	612838	1566640	555	209	52.45	33.6	2510	Water quality is good

From data in **Table 2-1** it was noted that boreholes in the southern fans typically had high Transmissivity (T) values, were of varying quality and boreholes were potentially high yielding.

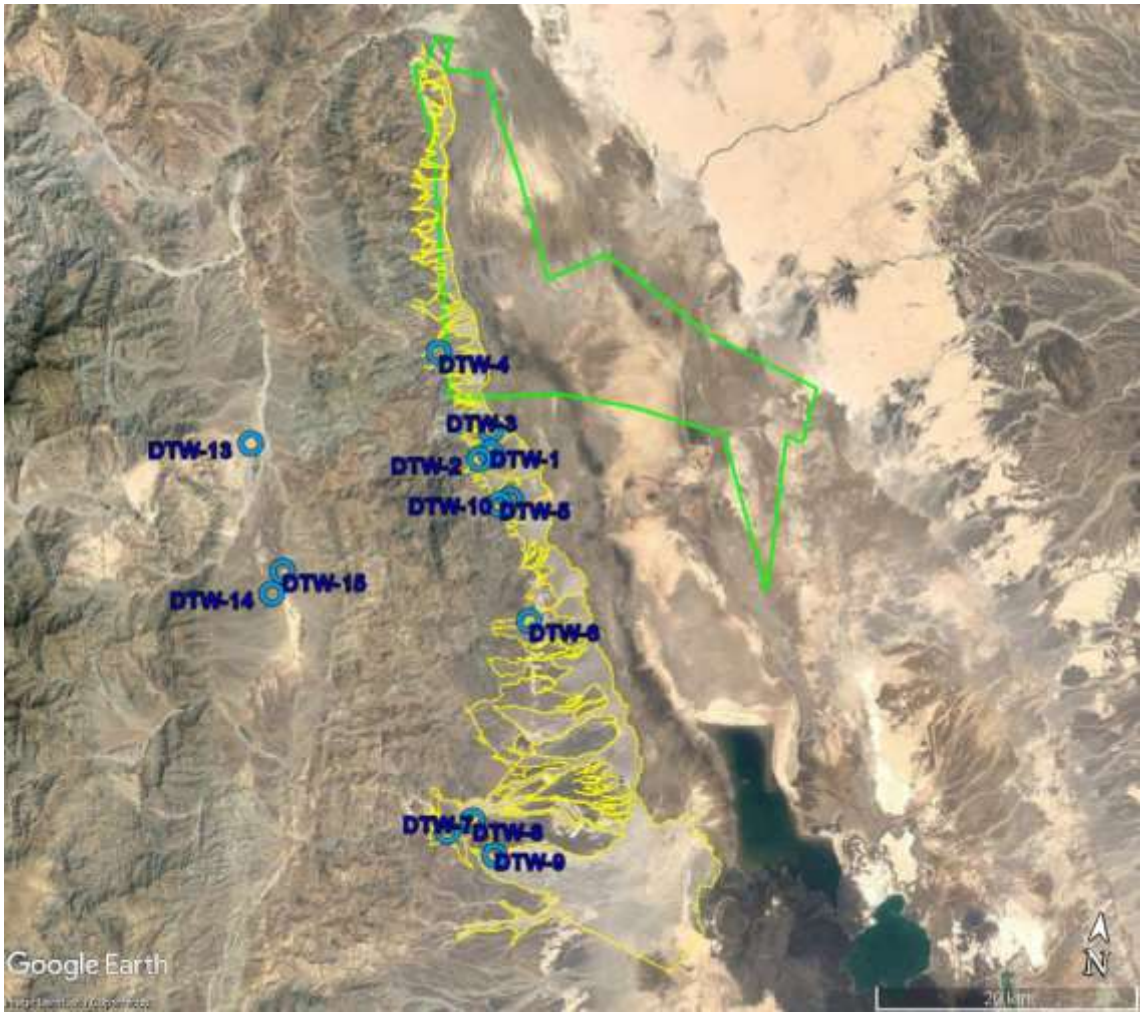

Figure 2-5 Google Earth image indicating the location of DTW wells drilled for MoWE

In **Figure 2-5** the MoWE boreholes are depicted by annotated blue circles south and south west of the alluvial fans under investigation shown as yellow polygons, adjacent to the mining concession represented by a green polygon.

Other mining companies in the region have also conducted groundwater exploration for potential potash mining. Data from these sources also predominantly pertains to the southern fans and were thus useful for discerning the regional flow paths, sources and sinks of the groundwater system within the depression. The complex geological setting of the region implies that there is a high variability in groundwater occurrence and quality throughout the region.

Two boreholes were drilled in the Asabuya and North Dogua fans respectively in 2015 for Umvoto (2015) to evaluate the potential of two of the northern alluvial fans. These boreholes were named RAJ-1 and RAJ-2, with RAJ-1 being present in the Asabuya fan

and RAJ-2 in the North Dogua fan. These boreholes were pump tested for 72 hours each. **Table 2-2**, **Table 2-3** and **Table 2-4** summarise the details of drilling and test pumping results of both these boreholes.

Table 2-2 Summary of drilling details for RAJ-1 and RAJ-2 drilled in 2015.

Borehole		RAJ-1	RAJ-2
Northing	N	1584915.94	1598422.61
Easting	E	624631.43	621478.57
Elevation	mamsl	-28	-94
End of Hole	mbgl	165	77
	masml	-193	-171
Rest Water Level	mbgl	79	31.5
	mamsl	-107	-125.5
Borehole Diameter and Depth	mm (mbgl)	600 (0-4.8)	600 (0-5)
		445 (4.8-165)	445 (5-77)
Casing Diameter and Depth	mm (mbgl)	473 (0-4) / solid API steel	473 (0-4) / solid API steel
		340 (0-113.5) / solid API steel	340 (0-46) / solid API steel
		330 (113.5-163.5) / 2 mm slotted API steel with 0.5 mm gauze screen	330 (46-76) / 2 mm slotted API steel with 0.5 mm gauze screen

Table 2-3 Summary of the Transmissivity calculated for RAJ-1 during step and constant discharge tests, and then recovery (Umvoto, 2015)

Pumping Test	Analytical Analysis	Solution	Transmissivity (m^2/d)
Step Test	AQTESOLV software	Theis (1935) unconfined aquifer	2179
Constant Discharge Test	AQTESOLV software	Theis (1935) unconfined aquifer	2297
Recovery	Time-recovery plot	Theis concept	2250

Table 2-4 Summary of the Transmissivity calculated for RAJ-2 during step and constant discharge tests, and then recovery (Umvoto, 2015)

Pumping Test	Analytical Analysis	Solution	Transmissivity (m^2/d)
Step Test	AQTESOLV software	Theis (1935) unconfined aquifer	1024
Constant Discharge Test	AQTESOLV software	Theis (1935) unconfined aquifer	1263
Recovery	Time-recovery plot	Theis concept	2034

From these data, the alluvial fans were classified as unconfined aquifers with high T values and relatively shallow water levels that had varying groundwater quality and boreholes of high yield potential (Umvoto, 2015).

CHAPTER 3

SITE DESCRIPTION

3.1 INTRODUCTION

The study area is situated in the north-eastern part of Ethiopia in the Danakil Depression of the Afar region and shares a border with Eritrea to the north (see **Figure 1-2**). The extent of the mining concession within the Danakil Depression is approximately 27 km north-south and up to 29 km east-west. A prominent feature to the south of the study area is the Dallol hydrothermal mound (see **Figure 3-1**).

Figure 3-1 Photograph of salt deposits, fumaroles and acid pools at Mount Dallol, south east of the study area.

In general, due to the remote location of the study area, limited literature is available regarding hydrogeology of the alluvial fans. Most available literature either directly refers to the regional Afar Rift and the East African Rift System (EARS) and associated tectonic process or Mount Dallol and its hydrothermal system.

3.2 PHYSIOGRAPHY

3.2.1 Regional Topography

Vast portions of Ethiopia are covered with volcanic rocks that rise to high elevations forming plateaus separated by rift basins with much lower elevations. The topography of Ethiopia is extensive and complex, but has been classified into five broad regions by Ayenew *et al.* (2008). These regions are the western highlands, western lowlands, eastern highlands, eastern lowlands and the rift valley.

The western and eastern highlands rise to between 1500 and 3000 meters above mean sea level (mamsl) with the highest mountains reaching 4620 mamsl (Alemayehu, 2006). These highlands consist of numerous mountain ranges and slope towards Sudan in the west and northwest forming the western lowlands. The eastern highlands slope east and south east towards Somalia (see **Figure 3-2**) to form the eastern lowlands (Ayenew *et al*., 2008).

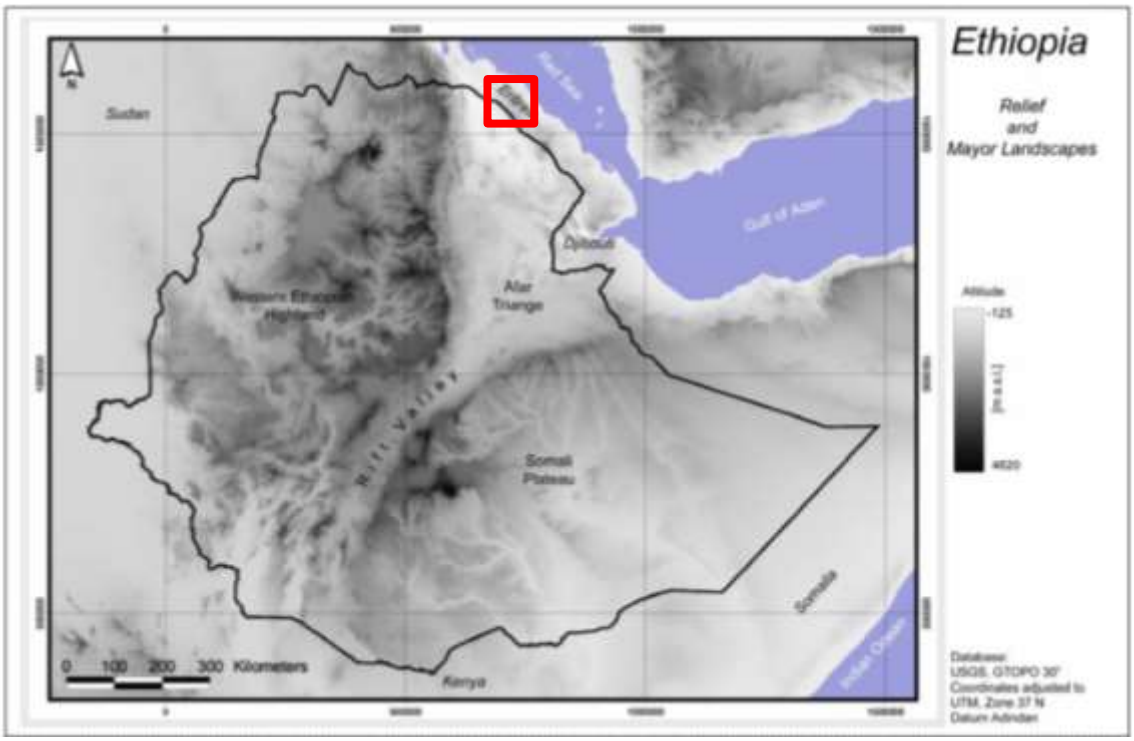

Figure 3-2 Regional Topographic map of Ethiopia (Thiemann, 2007).

Figure 3-2 from Thiemann (2007) clearly illustrates the Rift Valley, Afar Triangle, western and eastern Somali highlands.

A prominent topographic feature in Ethiopia is the Rift Valley (see **Figure 3-2**). It trends southwest-northeast and splits the highlands into north western and south-eastern segments. The Ethiopian Rift has two main sections: The Main Ethiopian Rift (MER) and the Afar Rift, which form the Afar Triangle which includes the Danakil Depression, the elevation of which drops as low as 120 mbmsl (Alemayehu, 2006).

The MER manifests at surface as a deep trench 40-60 km wide and up to 1000 m below the surrounding plateau (Ayenew *et al.*, 2008). The rift valley is surrounded by stepped grabens and slopes that rise to high elevations forming part of the larger Ethiopian Plateau (Alemayehu, 2006; Umvoto, 2014). The Danakil Depression stretches northwest into Eritrea towards the Red Sea; its northern most point being the Gulf of Zula (Mesfin and Yohannes, 2014). It was formed by rifting along the northern Afar Rift and is tectonically and volcanically still active (Umvoto, 2014a).

3.2.2 Local Topography

The study was carried out in the sloped basal fan area that has formed below the Ethiopian highlands, and reaches to the low-lying salt flats of the Danakil Depression (Holwerda and Hutchinson, 1968) (**Figure 3-3**). To the west of the study area, the Dogua Mountains rise to an elevation ranging between 700-2000 mamsl (see **Figure 3-3**). To the east is the Danakil block or Danakil Alps with elevations ranging between 800-3000 mamsl (Alemayehu, 2006; Mesfin and Yohannes, 2014).

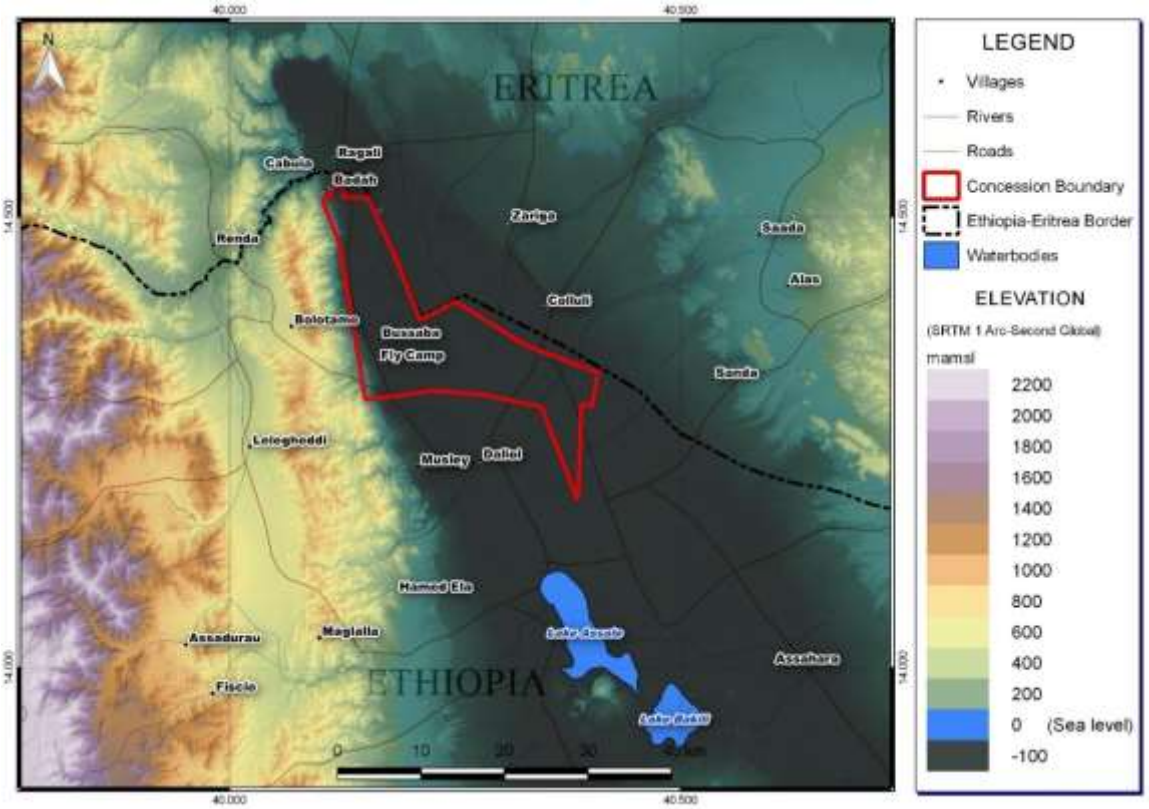

Figure 3-3 Local topographic map of the study area based on ALOS data (Umvoto, 2016a).

3.2.3 Geomorphology

The geomorphology of the region is dominated by high mountains with elevations over 2000 mamsl and large arid lowlands. About 80% of mountains higher than 2000 mamsl in Africa occur in the East African region *(*Abiye, 2010). The most characteristic features of Ethiopia are the prominent highland plateaus in the northwest to central and western parts of the country and deserts and semi-deserts towards the north, east and south (Umvoto, 2014a).

The geomorphology of the Danakil Depression includes (Hayward and Ebinger, 1996; Holwerda and Hutchinson, 1968; Umvoto, 2014a):

- Rifted graben structures forming the high cliffs of the Ethiopian plateau and the Danakil alps surrounding the depression;
- lower-lying slopes and foothills to the plateau formed by sedimentary sandstone and limestone outcrops;
- valleys and water eroded run-off features, known as wadis, in the higher lying areas that carry sediment down;

- recent alluvial fans formed at the base of the plateau in the west and the Danakil Alps in the east;
- a flat surface within the depression underlain by basaltic lavas and covered by evaporate, oceanic and lacustrine sediments;
- non-perennial salt pans and evaporation lakes; and
- interbasin grabens and ridges formed by recent volcanic activity such as the Erta Ale shield volcano, 80 km south of the study area.

A local slope map of the study area was made from the digital elevation model (DEM) by Umvoto (2016a). **Figure 3-4** illustrates that the flat morphology of the depression floor (salt flats) dominates the central part of the study area (slope <10°), while the western edge (Dogua Mountains) of the study area has steeper slopes (>15°). The transition between mountains and salt flats is very abrupt (Kebede, 2013), with gently sloped alluvial fans extending from the plateau to the depression floor (see **Figure 3-5**). These fans are associated with rift related faulting and represent recently active fault scarps (Umvoto, 2014a). The difference in slope is attributed to the sediments in the depression being more susceptible to erosion (flat slope) than the crystalline basement and volcanic rocks that comprise the plateau as it has steep slope and high elevation. Accommodation for the fans is made by extensional tectonics in the form of normal faulting.

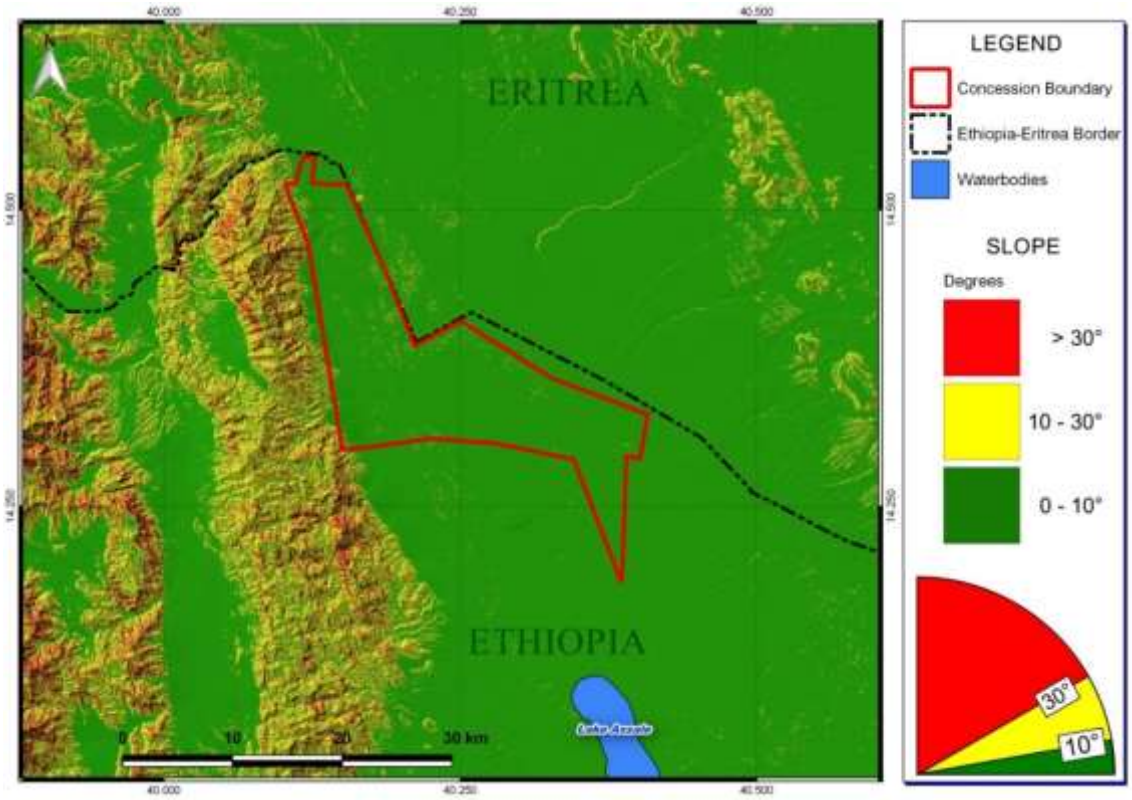

Figure 3-4 Local slope map of the study area (Umvoto, 2016a).

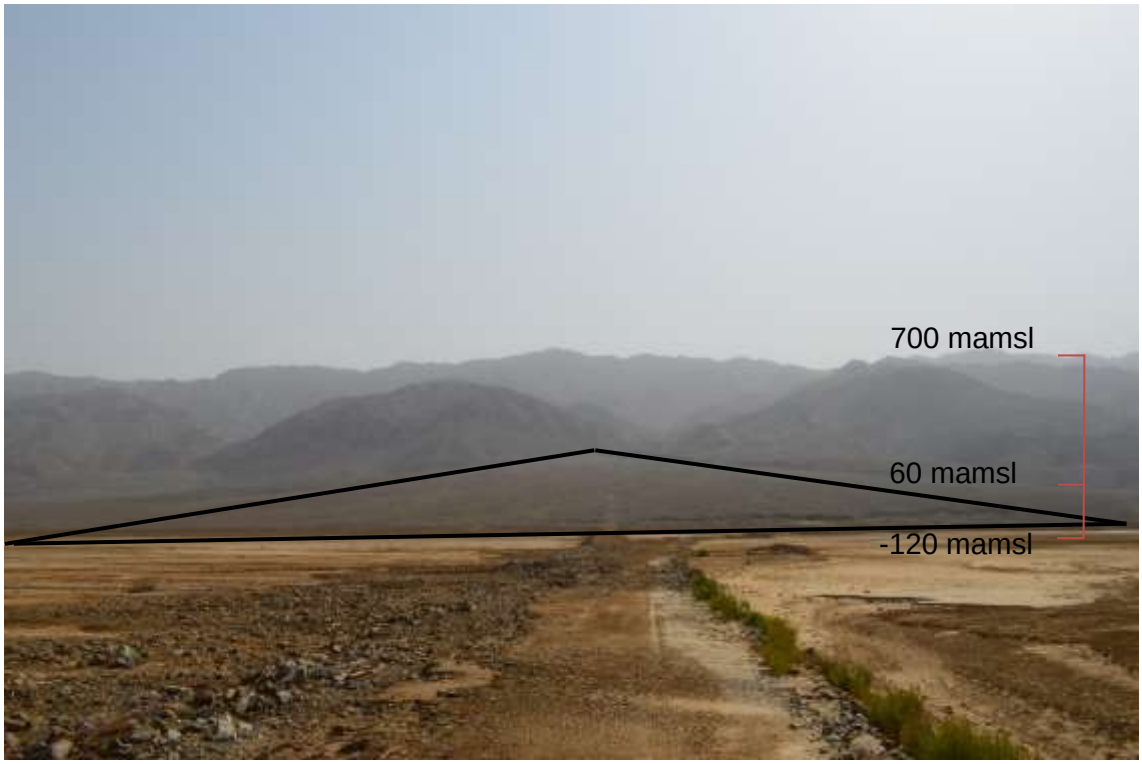

Figure 3-5 Photograph taken from floor of the Danakil Depression.

Figure 3-5 is a photograph orientated to the west depicting the western highlands, sloped basal fan area represented by a black triangle and salt flats. Average elevations have been superimposed to illustrate the drastic change in elevation.

3.2.4 Drainage

3.2.4.1 Regional Drainage

The Danakil basin's catchment area extends from the Ethiopian Plateau in the west to the Danakil Alps in the east (see **Figure 3-6** and **Figure 3-7**), with all runoff, rivers and streams flowing towards and ending in the endorheic Danakil Depression (Umvoto, 2014a). The rivers and streams are non-perennial or sub-surface flows that occur as steeply carved ravines within the plateau and as braided and meandering flows within the alluvial fan and lower lying areas of the depression (Holwerda and Hutchinson, 1968). The depression is bordered by the tributaries of the Ragali River in the west, one such tributary is the Lelegheddi River (**Figure 3-6**). The Lelegheddi River alluvium and the underlying limestone is a potential source of fresh water, but has not yet been explored.

A catchment area and watershed analysis done by Umvoto (2016a) from ALOS topographic data defined the major primary catchment of the northern Danakil endorheic drainage basin, and delineated the main secondary catchments within it (see **Figure 3-6**). Of interest are the smaller, tertiary-level basins on the eastern slopes of the Dogua Mountains, that drain through the wadis to the alluvial fans (see **Figure 3-7**).

The Ragali River flows in a northerly then easterly direction towards the village of Badah, where it flows out onto the salt flats (Holwerda and Hutchinson, 1968 and Kebede, 2013) (see **Figure 3-8**). The Ragali River flows at the subsurface as baseflow or as sheet wash within the depression (Umvoto, 2015). To the south, the Seba River flows east into Lake Assale. Two larger rivers occur to the northeast and southwest. These rivers, the Zaringa and Belinga Rivers flow from the Danakil Highlands in Eritrea southwest towards the depression and from the foothills of the plateau east towards Dallol (see **Figure 3-7**).

The Ragali River is the only perennial river close to the study area. The other largest nearby river, the river Awash, occurs far to the south and drains to the northeast through the rift floor, to Lake Abhe (Ayenew *et al.*, 2006). The Awash is part of the rift valley's internal drainage system and has been the subject of numerous studies (Alemayehu, 2006).

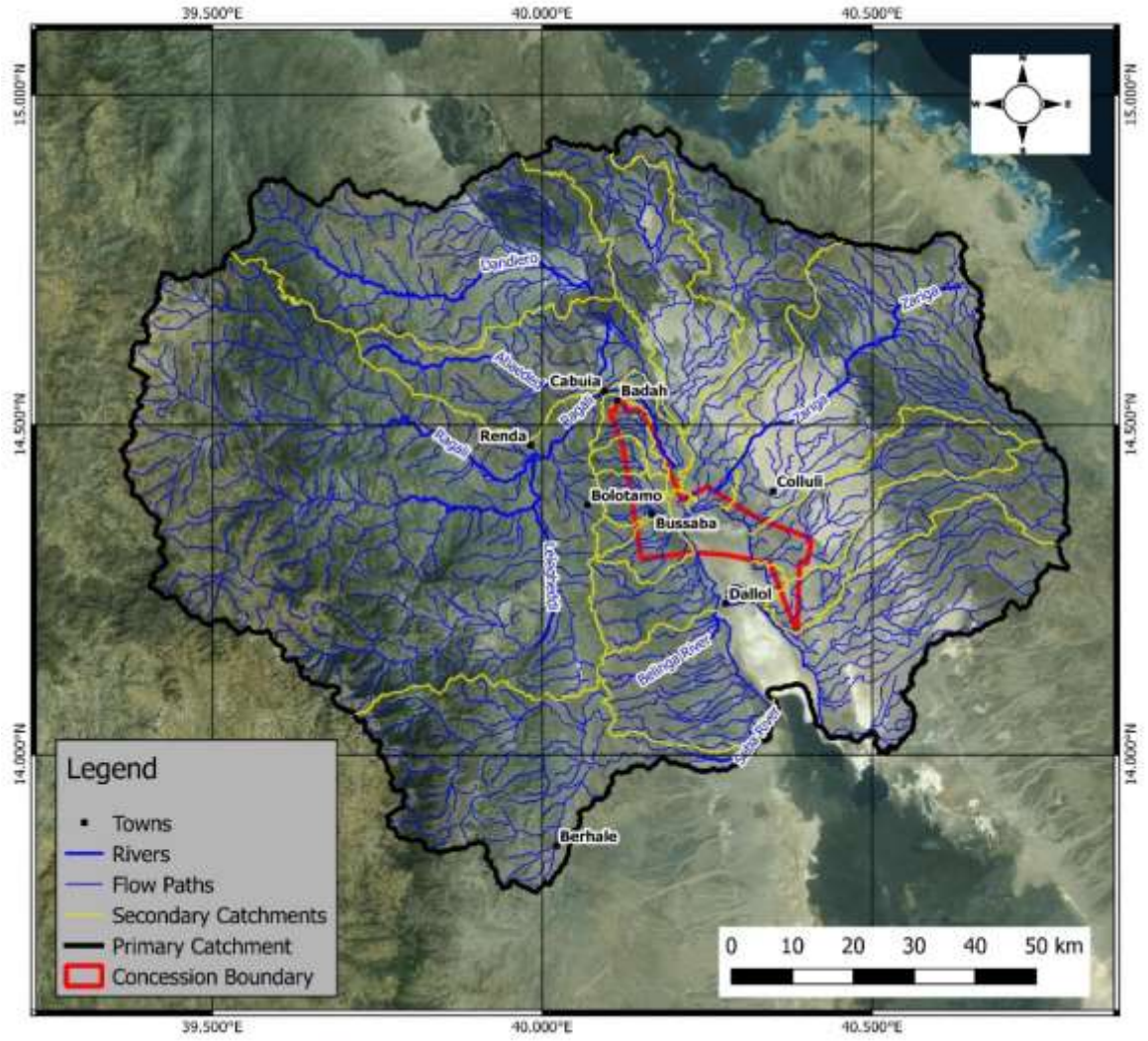

Figure 3-6 Regional drainage analysis map (Umvoto, 2016a).

Figure 3-6 shows the primary (black polygon) and secondary catchment area (yellow polygons) in which the mining concession (red polygon) is found.

3.2.4.2 Local Drainage Patterns

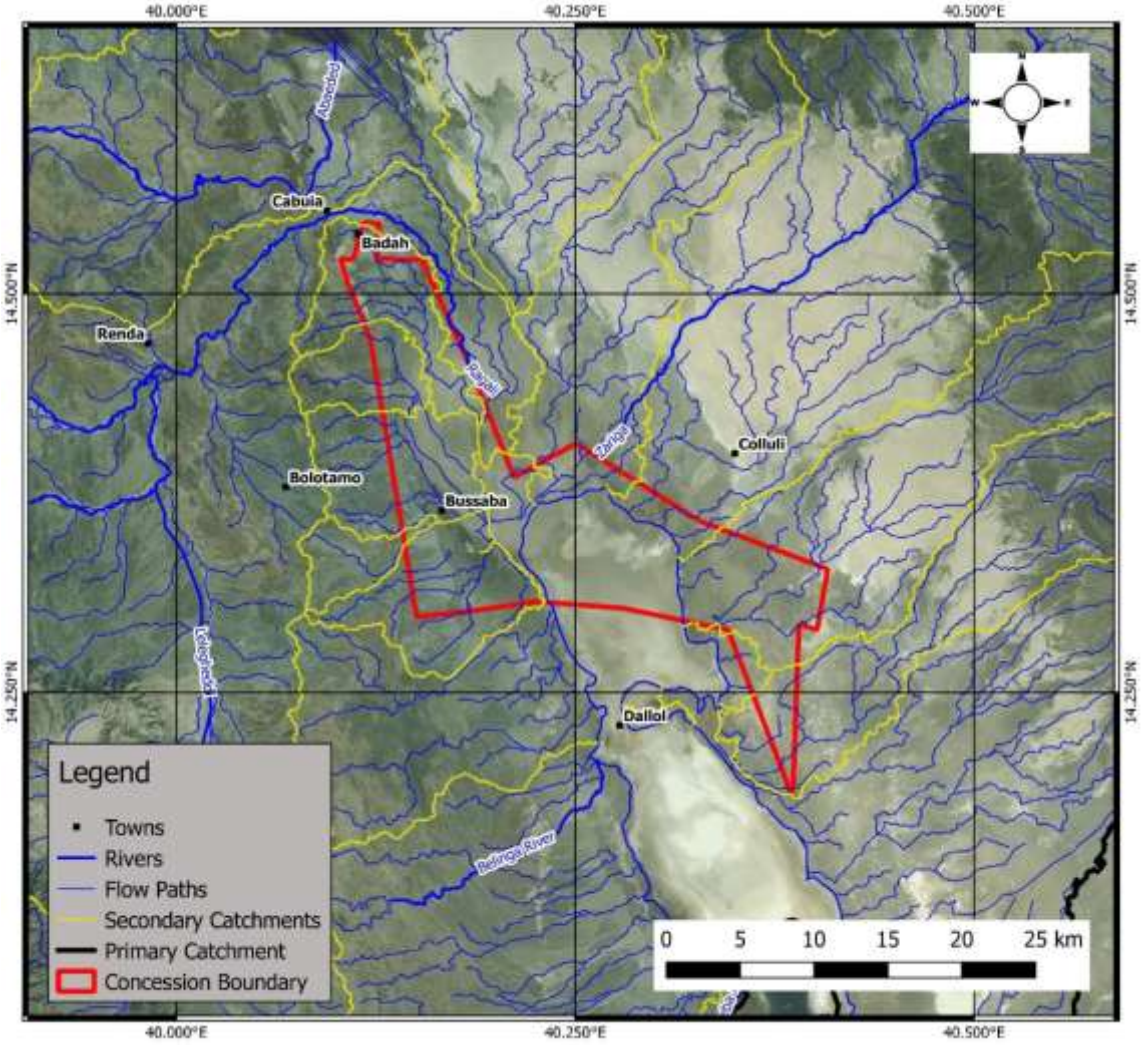

Figure 3-7 Local site drainage analysis (Umvoto, 2016a).

Figure 3-7 is a local drainage analysis of the study area (red polygon) showing the main rivers (thick blue lines), streams and runoff channels (light blue lines) and secondary catchment areas (yellow polygons).

Figure 3-8 Ragali River flowing out onto the salt flats.

Figure 3-8 is a photograph orientated north west showing the Ragali River flowing across the mud flats of the basin floor.

3.2.5 Climate

3.2.5.1 Regional Climate

The climate in the East African region is highly variable both spatially and temporally. The major climatic conditions in Ethiopia have been categorised by the United Nations Educational, Scientific and Cultural Organisation, UNESCO (2004) as: tropical in the south and south west; climatic in the highlands, and arid and semi-arid in the north eastern and south eastern lowlands.

Ethiopia has a monsoonal climate with distinct dry and wet seasons (ERM, 2014). Rainfall depends largely on the movement of moisture from the South Atlantic and South Indian Oceans. In arid and semi-arid lowlands, the rainfall is sparse and irregular (Abiye, 2010). Average annual rainfall across the region ranges from less than 100 mm per annum (mm/a) in the arid regions (Ayenew *et al.*, 2008) such as the Danakil Depression to over 2000 mm/a on the Ethiopian Plateau (Kebede, 2013).

The climate over Ethiopia is related to the topography of the country's climatic zones which are summarised in **Table 3-1** after Alemayehu (2006):

Table 3-1 Climatic classification of Ethiopia (Alemayehu, 2006).

Altitude (mamsl)	Mean Annual Temperature	Description	Local Name
3 300 and above	10 or less	cool	Kur
2 300 - 3 300	10 - 15	cool temperate	Dega
1 500 - 2 300	15 - 20	temperate	Woina Dega
500 - 1 500	20 - 25	warm temperate	Kola
below 500	25 and above	hot	Bereha

Within these climate zones, three locally named rainfall seasons are defined by Alemayehu (2006) and FAO (2005) as follows:

- "Kiremt" the summer, main rainy season during which long and heavy rainfall occurs, usually lasting from June to September, covering mostly the northern hemisphere of Ethiopia.
- "Bega" the dry winter season, lasting from October to February, during which everywhere except the central region is dry.
- "Belg" the light rainy season, usually from February to May. This season is the main source of rainfall in the south and south-eastern parts of Ethiopia.

The climate of the Danakil region is hot and dry with desert to semi-desert conditions. Average daily temperatures vary between 20-28 °C in winter and reach up to 50 °C in summer (Darrah *et al*., 2013). **Figure 3-9**, **Figure 3-10** and **Figure 3-11** represent the mapped Mean Annual Temperature (MAT), Potential Evapotranspiration (PET) and Mean Annual Precipitation (MAP) obtained from known weather stations in a 150-km radius of the mine concession (Umvoto, 2016d). From **Figure 3-9** it is seen that more temperate climates occur over the plateau ranging from 15-26 °C while the lowland and study area experience temperatures exceeding 35 °C. A similar pattern is observed in PET across the region with high levels in the lowlands and lower levels in the highlands (see **Figure 3-10**).

Figure 3-11 indicates a MAP below 100 mm/a for the study area, with over 800mm/a occurring in the west and central part of the mapped area. The main rainfall season in the Danakil region occurs during the spring-summer period (April to October). The Ethiopian national average rainfall lies in the order of 850-1000 mm/a (UNEP, 2010).

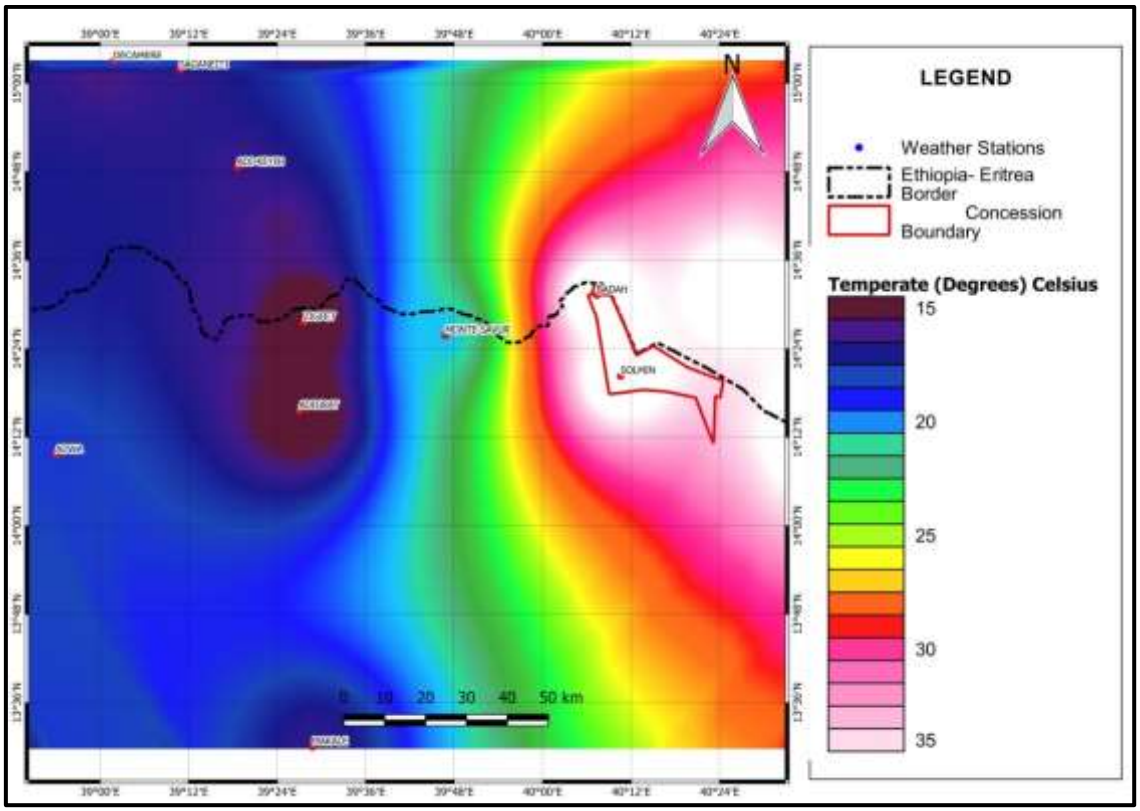

Figure 3-9 **Mean Annual Temperature from known weather stations within a 150 km radius of the mining concession (Umvoto, 2016d).**

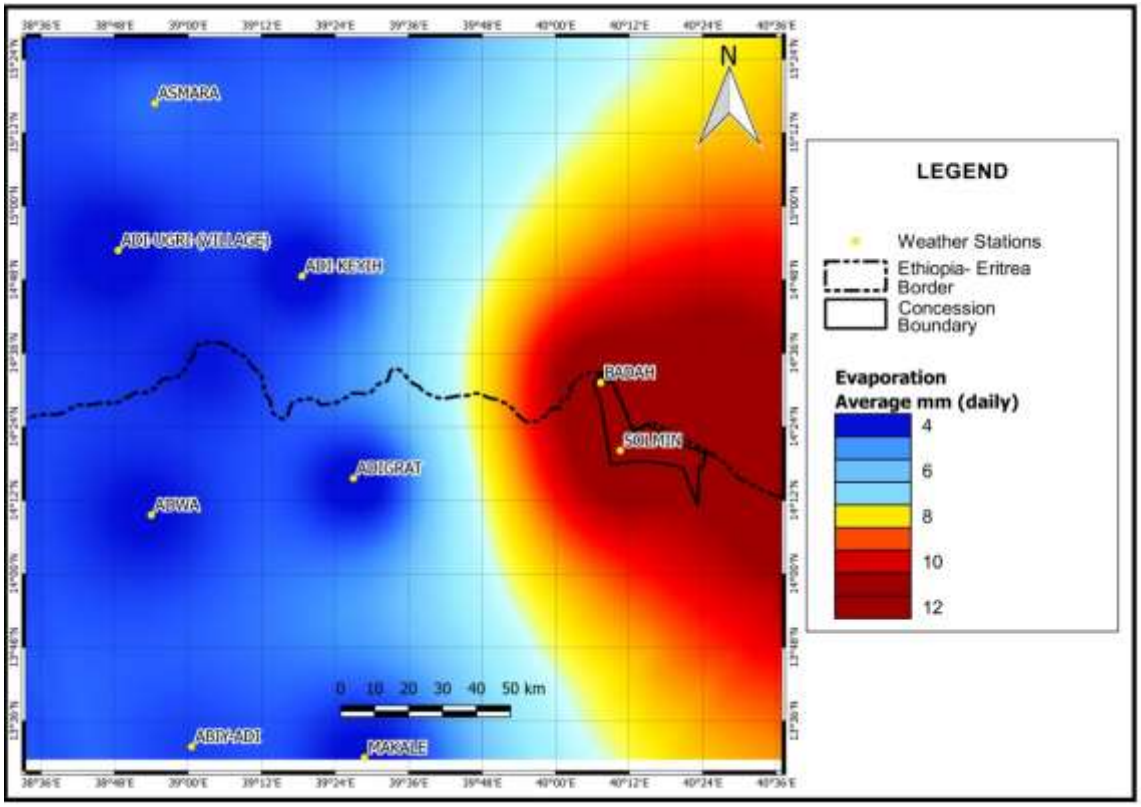

Figure 3-10 **Mean Annual Evaporation form known weather stations within a 150 km radius of the mining concession (Umvoto, 2016d).**

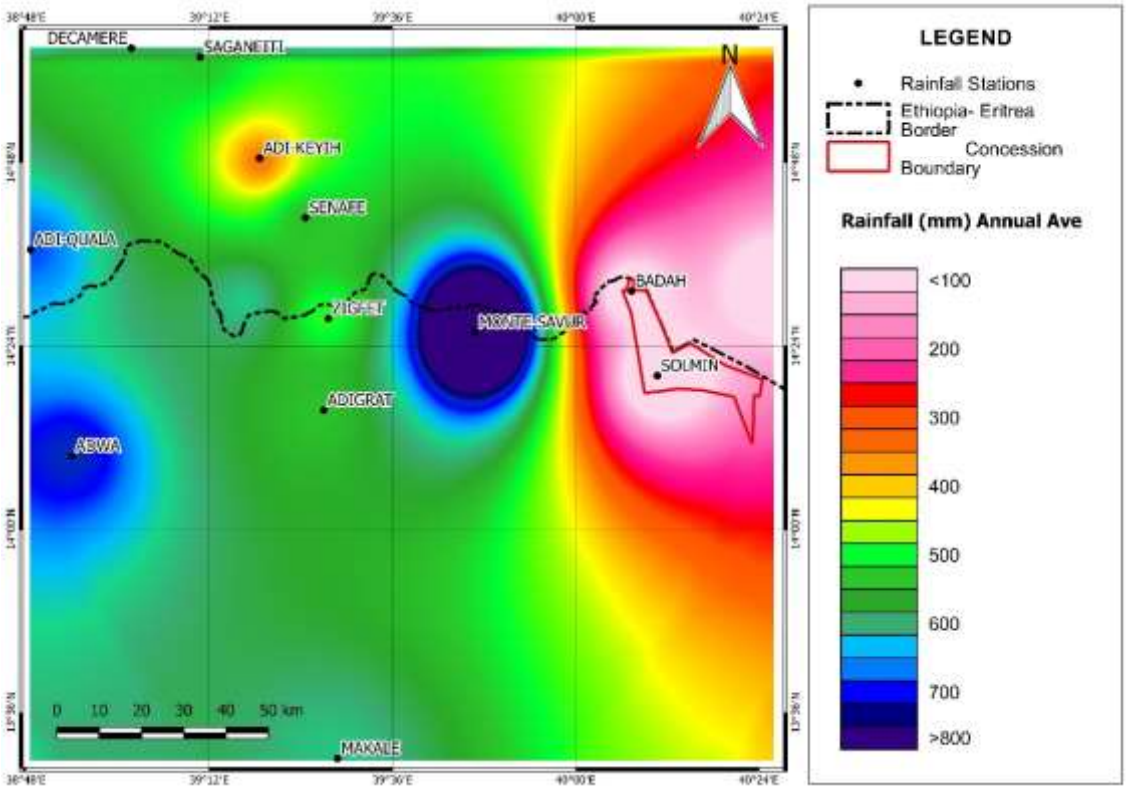

Figure 3-11 Mean Annual Precipitation from known weather stations within a 150 km radius of the mining concession (Umvoto, 2016d).

3.2.5.2 Local Climate

Few sources contain local climate data. Monthly average temperature values measured for Dallol (see **Figure 3-12**) between 1960 and 1966 is taken from Pedgley (1967) and shows average maximum temperatures exceeding 45 °C.

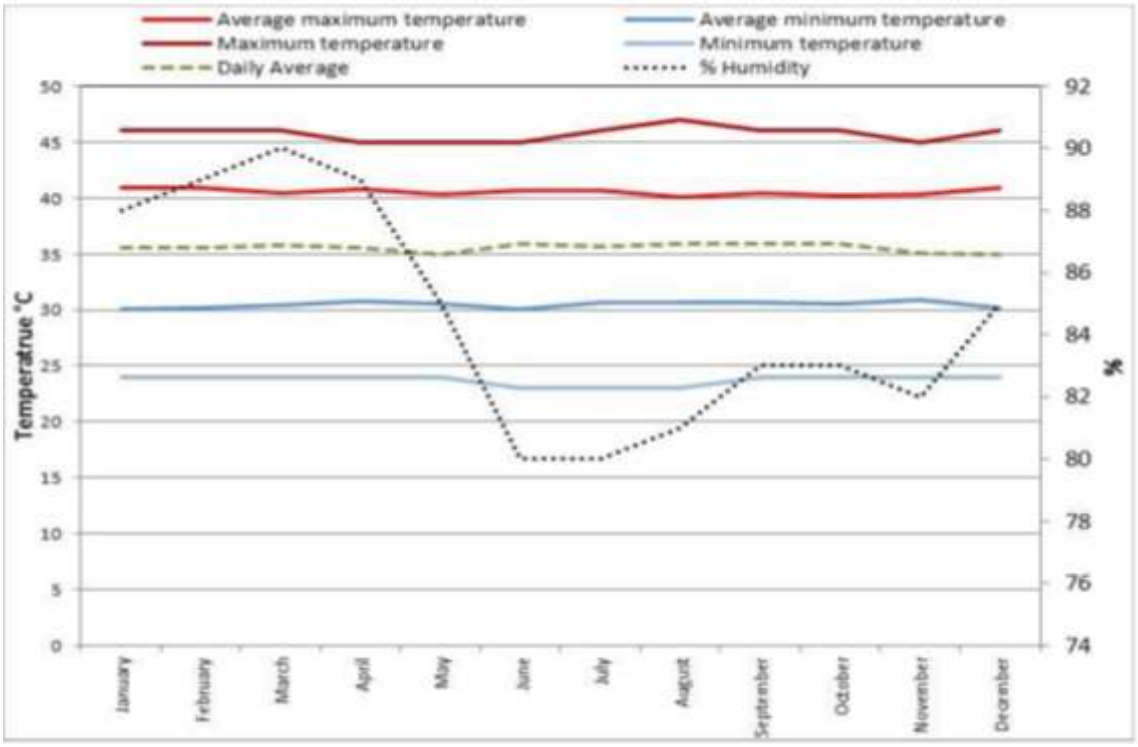

Figure 3-12 **Maximum, minimum, average maximum, average minimum and daily average temperatures recorded at Dallol between 1960 and 1966 (Pedgley, 1967).**

Various mining companies have automatic weather stations established in the region. Two weather stations located on the salt flats within the mining concession, Badah Camp Weather Station and Solmin Weather Station, recorded data between October 2014 and February 2016). To obtain data from the recharge zones of the alluvial fan aquifers, two additional weather stations were established in the Dogua Mountains to the west of the mining concession in April and May of 2016 (see **Figure 3-13**).

Figure 3-13 Photograph of Dogua Weather Station 2 (WS-2) within the Dogua Mountains.

The weather stations were named Dogua Weather Station-1 (WS1) and Dogua Weather Station-2 (WS-2) (see **Figure 3-14**). Parameters recorded include: temperature, pressure, relative humidity, wind speed and direction, solar radiation, precipitation and evapotranspiration. Evaporation data are only available for Badah, Dogua WS1 and Solmin. As the main contributing factors to groundwater recharge and monitoring, only temperature, pressure, rainfall and evapotranspiration are discussed in detail. The full meteorological data set for the four individual weather stations can be found in **Appendix A**.

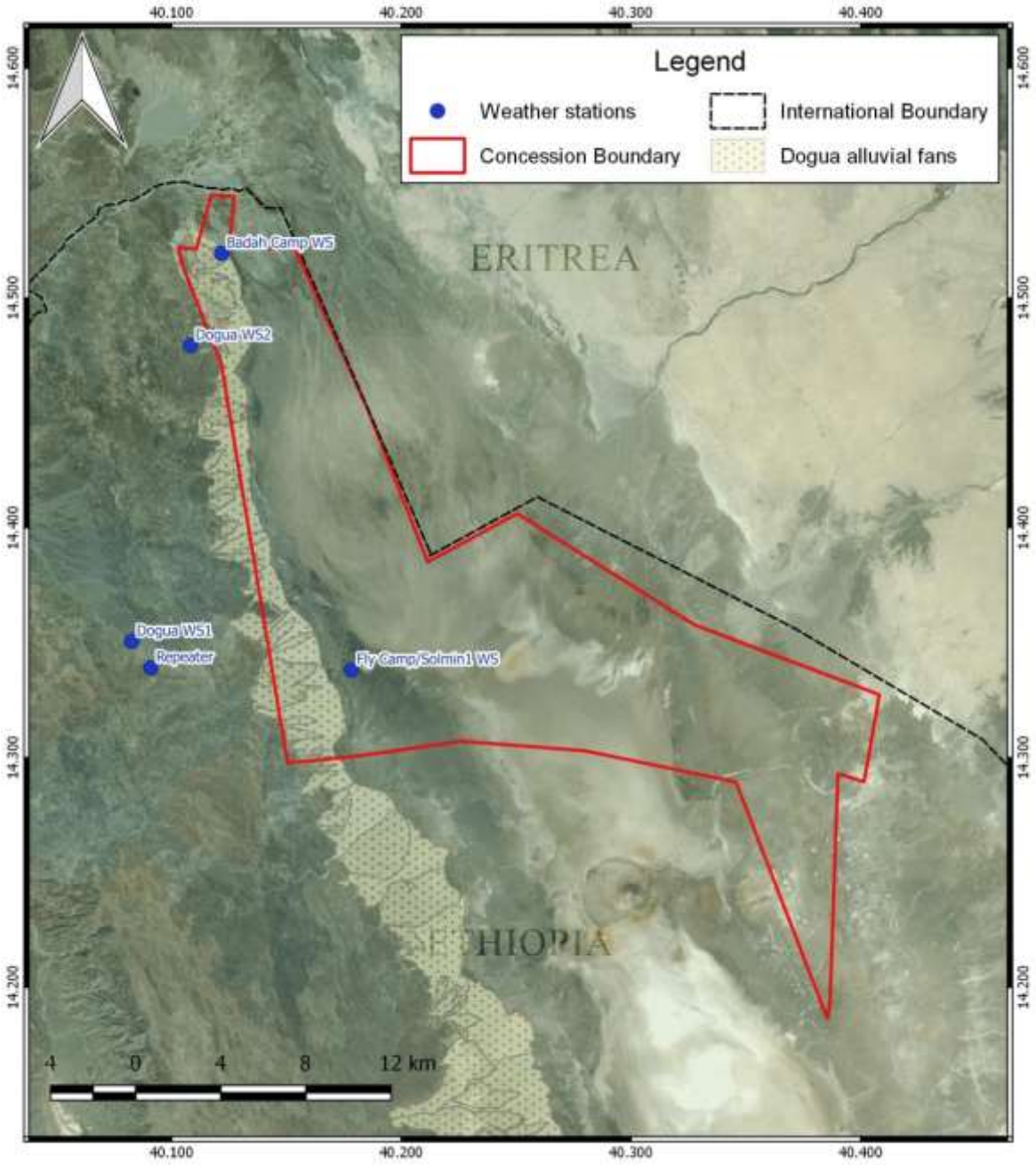

Figure 3-14 Locations of weather stations in the study area (Umvoto, 2016d).

Figure 3-14 illustrates locations of two newly established Dogua Weather Stations in the recharge zone of the Dogua Mountains, west of the concession (represented by a red polygon) and the two original weather stations located at Badah Camp and Solmin-1.

3.2.5.2.1 Temperature

Figure 3-15 shows that high temperatures persisted throughout the year with an average of 34.4°C and reaching 50°C in summer. Temperatures in July (summer) varied between 36-50°C and in January (winter) between 23-37 °C. Summer maximums coincided with the inflow of moist, warm air from Equatorial Africa and the Gulf of Guinea during the monsoon season (Umvoto, 2016d). The maximum and minimum temperatures of Badah Camp weather station were slightly lower than Solmin station (see **Figure 3-16**). This was interpreted to be because of Solmin station's lower elevation and location on the salt flats, and Badah station's position closer to the Dogua mountains (see **Figure 3-14**). Seasonal changes in temperature were clearly visible from the graphs.

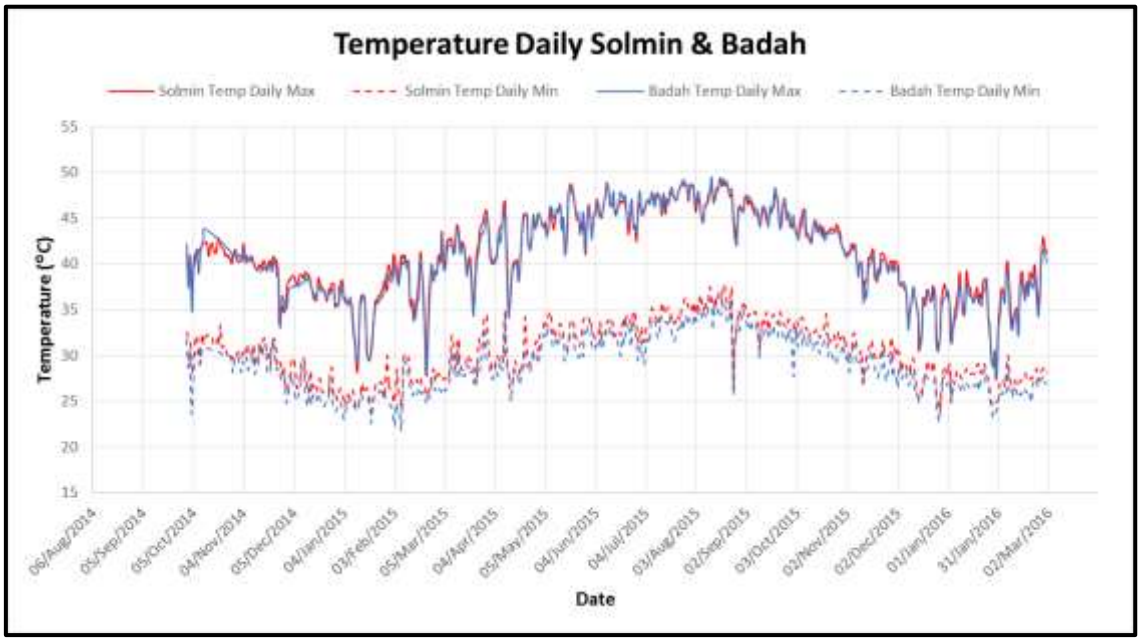

Figure 3-15 Maximum (solid lines) and minimum (dashed lines) temperatures at Badah Camp and Solmin-1 weather stations for the period October 2014 to March 2016.

These data were further supplemented by temperature readings obtained from May 2016 to November 2016 while field activities were underway (**Figure 3-16**).

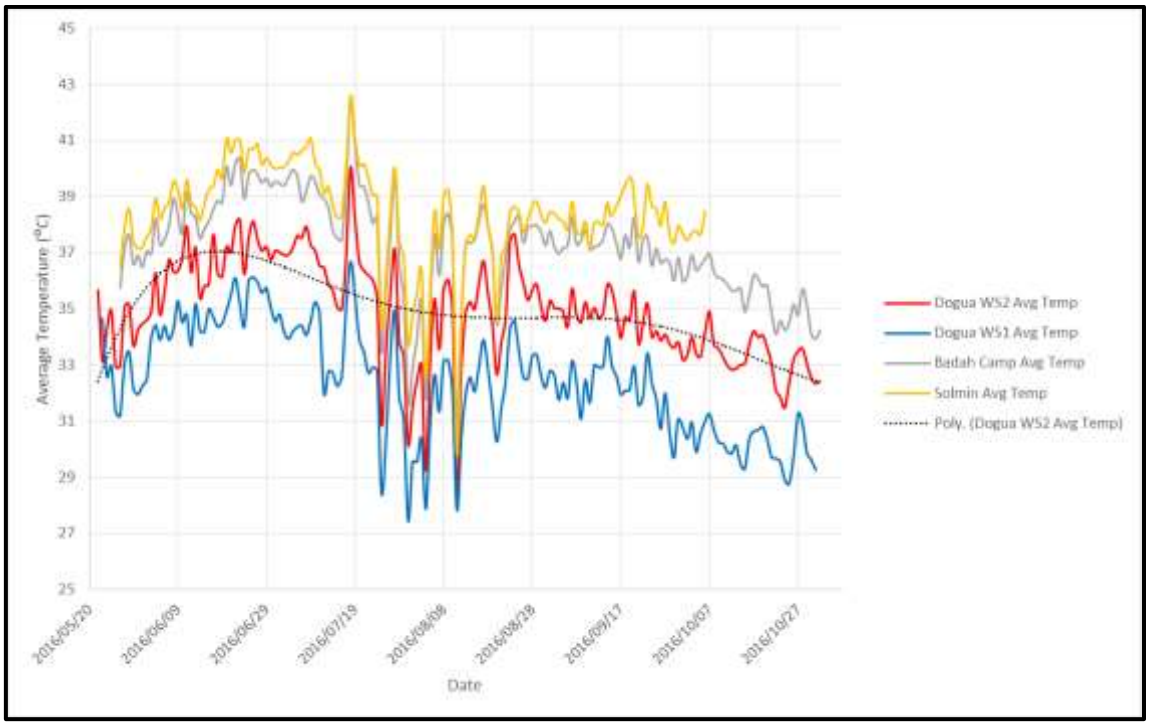

Figure 3-16 Average temperature recordings at Dogua WS2, Dogua WS1, Badah Camp and Solmin weather stations between 20 May 2016 and 31 October 2016

The average temperature recorded at all four weather stations followed a similar trend, but temperatures varied with elevation differences. The lower elevation, Solmin-1 and Badah Camp weather stations situated on the salt flats were between 2-3 °C higher than the high elevation Dogua WS1 and Dogua WS2 weather stations situated in the Dogua Mountains to the west. The trend line in **Figure 3-16** shows that peak temperatures were reached between mid-June to mid-July after which a decrease in temperatures in late-July to early-August was observed. This period of low temperatures corresponded with a high rainfall period recorded at all four weather stations (see **Figure 3-17**). The temperature stabilised, following the end of the Kiremt rainy season and the onset of autumn in September. Increased temperatures were commonly associated with northerly winds while southerly winds were associated with drops in temperature (see **Appendix A** for wind speed and direction results).

3.2.5.2.2 Rainfall

Rainfall in the study area was scarce but intense and normally occurred between June and September (Kiremt rainfall season), coinciding with a period of weaker winds (ERM, 2014). There was however, a shorter rain season in February and March (Belg

rainfall season), coinciding with a transitional period and the onset of the monsoon season (ERM, 2014). A difference in rainfall between the Solmin and Badah weather stations was noted for 2015, 51.28mm and 85.6 mm respectively, emphasizing the variability of rainfall across the study area.

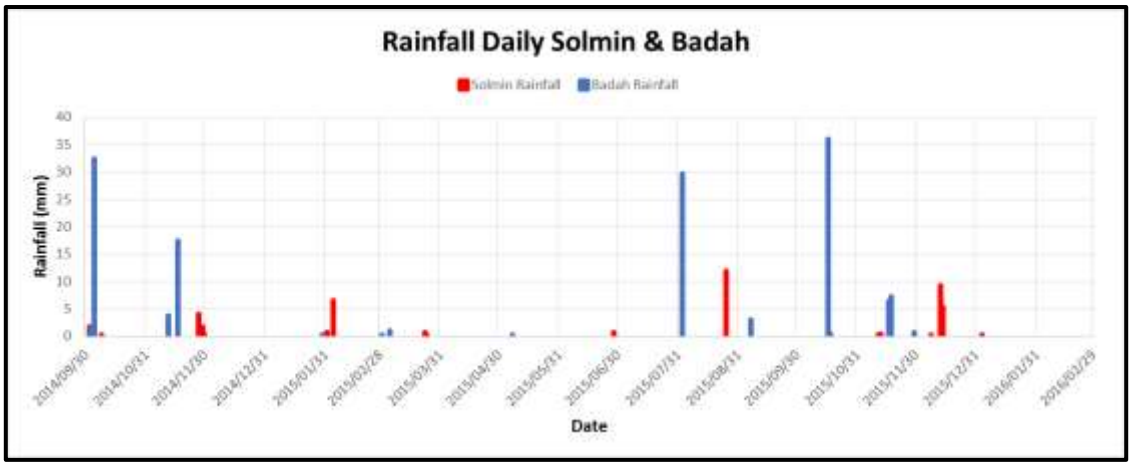

Figure 3-17 Rainfall recorded between October 2014 and March 2016 at Badah Camp and Solmin-1 weather stations (Umvoto, 2016d).

Daily rainfall plots for all four weather stations over the May 2016 to October 2016 period show that majority of the rainfall occurred in July and August corresponding to the Kiremt rainy season. **Figure 3-18** shows that there was a variation in rainfall across the four weather stations, indicating that rainfall is sporadic and localised. However, Badah Camp, Dogua WS1 and Dogua WS2 all received between 80 and 100 mm over the five-month period and Solmin was significantly drier, recording only 40 mm. Over the recording period, the higher elevation Dogua WS1 received the most rainfall. Flash flooding often occurred after a rainfall event as rainfall from the highlands drained toward the low-lying areas bringing vast amounts of sediment with it.

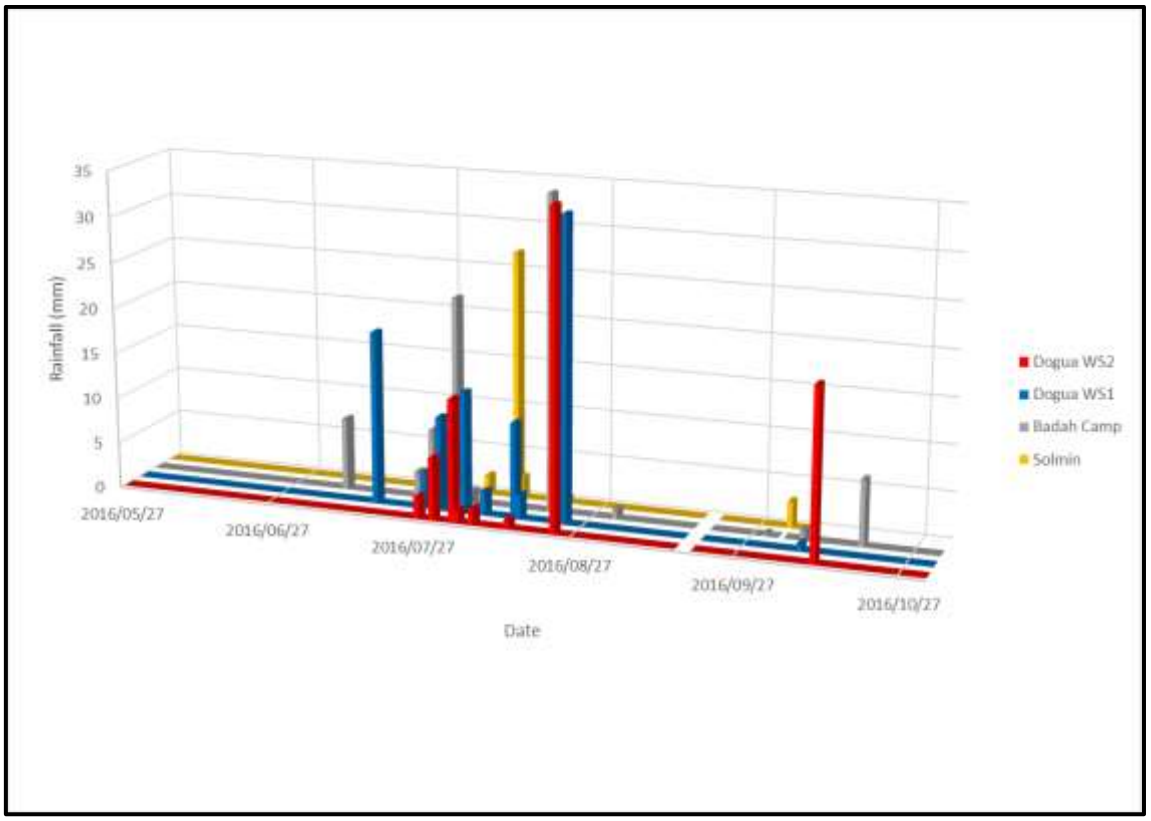

Figure 3-18 Daily total rainfall recordings at Dogua WS2, Dogua WS1, Badah Camp and Solmin-1 weather stations between 20 May 2016 and 31 October 2016 (Umvoto, 2016d).

3.2.5.2.3 Evaporation

Evaporation in the study area was approximately 11.6 mm per day, but with seasonal fluctuations between 18 mm/day in summer and 9 mm/day in winter (see **Figure 3-19**). This was interpreted to be due to a culmination of seasonal temperature, wind, relative humidity and solar radiation changes in the study area. See the similarities in trend lines of temperature and evaporation in **Figure 3-19**. Higher evaporation was recorded at the Solmin weather station because of its higher temperatures and solar radiation linked to its location on the exposed salt flats (see **Appendix A** for solar radiation, relative humidity and wind results).

Three of the weather stations, namely Dogua WS1, Badah Camp and Solmin-1 had evaporation pans that recorded actual evaporation, but for comparison purposes between all four stations, ETos was used (see **Figure 3-20**). ETos is a theoretical parameter, which is computed for shortgrass evaporation and accounts for factors such as latitude, longitude, altitude, temperature, wind speed and relative humidity (Allen *et al*., 1998 and Umvoto, 2016d).

Peak evaporation was linked to a peak in temperature on the same day. Evaporation was generally highest at Solmin-1, with Badah Camp having the lowest evaporation rate (see **Figure 3-20**). This was likely due to Solmin-1 having the highest temperature and wind speed and Badah having the lowest wind speed. Average daily ETos for Solmin-1, Dogua WS2, Dogua WS1 and Badah Camp over the six-month period was 8.74 mm, 7.33 mm, 6.97 mm and 6.71 mm respectively.

The actual recorded daily evaporation from the evaporation pans at Dogua WS1, Badah Camp and Solmin weather stations was higher than the theoretical ETos values, possibly due to effects of cloud cover and dust. Data gaps were noted in **Figure 3-21**, this was linked to the refilling of the evaporation pan at Solmin-1 and Badah and the pan drying out at Dogua WS1 due to access problems. Trend lines were added to **Figure 3-21** to illustrate the general trend over the recording period.

Evaporation followed a similar trend to temperature with an increase in late-June to early-July and a decrease in late-July to early-August. The decrease in evaporation was also associated with the increase in rainfall during that period. Average daily pan evaporation for Dogua WS1, Badah Camp and Solmin over the six-month period was 13.8 mm, 13.8 mm and 12 mm respectively. Solmin had the lowest rate because of data gaps linked to weekly refills, battery malfunctions and the pan drying out.

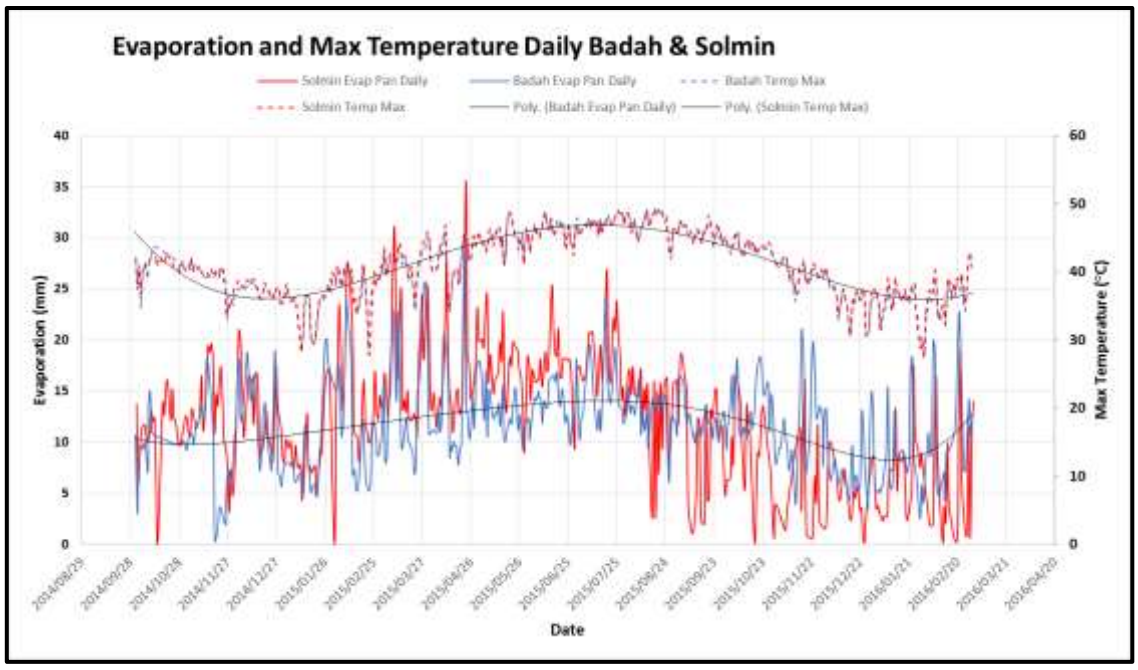

Figure 3-19 **Evaporation (solid lines) and temperature (dashed lines) recorded between October 2014 and March 2016 at the Badah Camp and Solmin-1 weather stations (Umvoto, 2016d).**

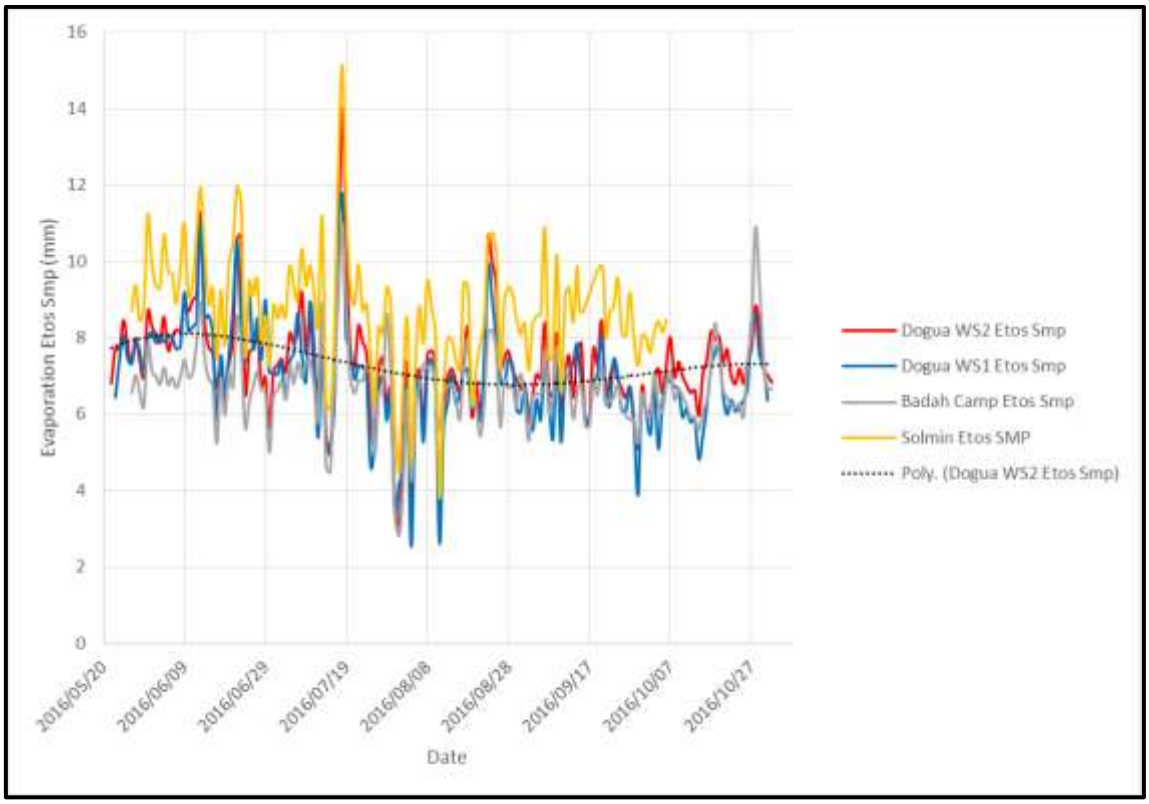

Figure 3-20 **Theoretical evaporation recorded as ETos at Dogua WS2, Dogua WS1, Badah Camp and Solmin weathers stations since 20 May 2016 (Umvoto, 2016d).**

Actual evaporation pan data recorded at Dogua WS1, Badah Camp and Solmin-1 weather stations is shown in **Figure 3-21**.

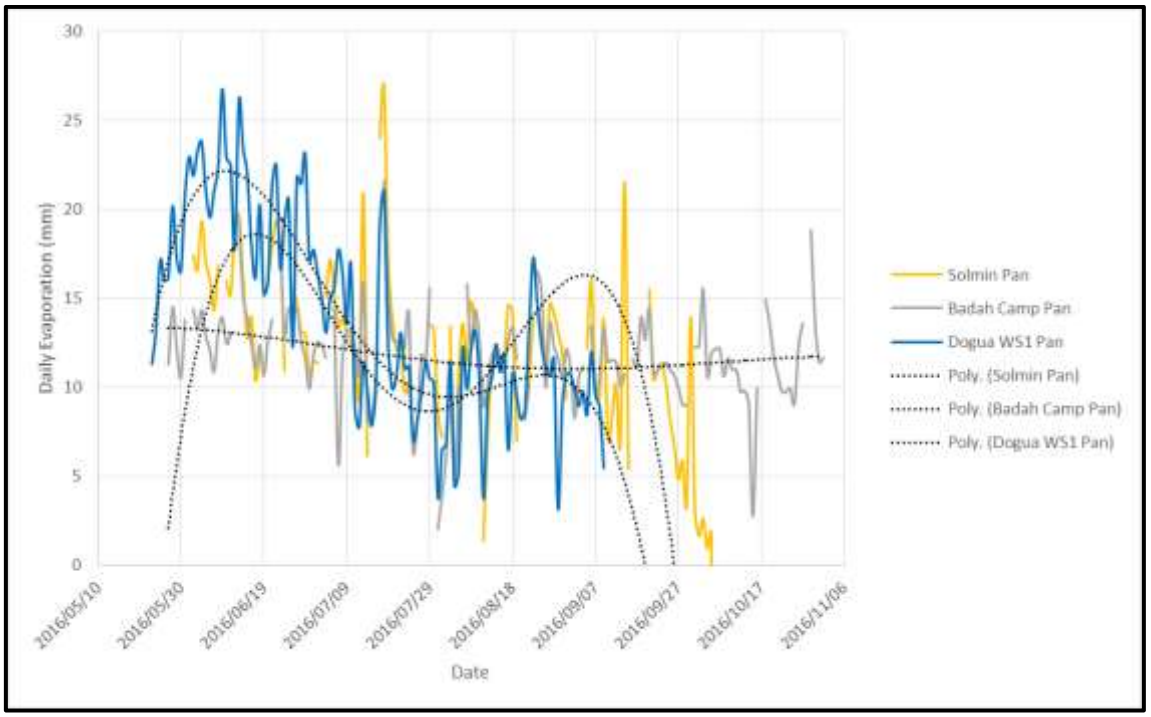

Figure 3-21 Actual evaporation recording from the evaporation pans at Dogua WS1, Badah Camp and Solmin weather stations (Umvoto, 2016d).

WS1 showed an exaggerated high evaporation for the first half of June, which was likely linked to start up errors, however this was seen to normalise over the remainder of the recording period. The sharp drop in evaporation at Dogua WS1 and Solmin was due to the pans drying out and Solmin's battery malfunctioning.

3.2.5.2.4 Pressure

Neither Solmin-1 nor Badah weather station was initially equipped or programmed to record pressure. Barometric measurements were thus limited to the May 2016 to November 2016 recording period.

Barometric measurements were uniform and constant for all weather stations for the duration of the recording period (see **Figure 3-22**). Regular pulsing with a weekly frequency was observed, likely linked to a weekly build-up of moisture. Barometric pressure measurements from all applicable weather stations were within expected limits and variations between stations were consistent with altitude differences (Umvoto, 2016d).

A slight decrease in pressure was observed in July, likely linked to the onset of the rainy season.

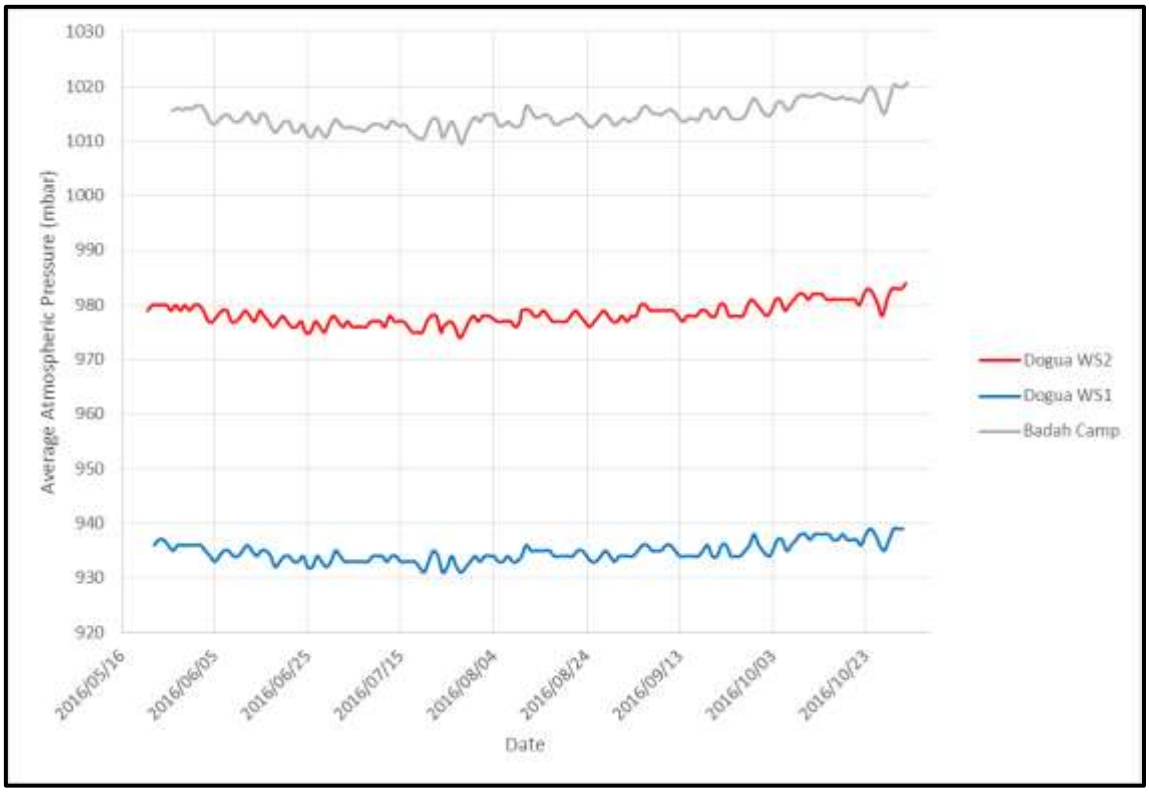

Figure 3-22 Average daily pressure recorded at Dogua WS2, Dogua WS1 and Badah Camp weather stations between May and October 2016 (Umvoto, 2016d).

3.2.5.3 Summary of Climate

From the Climograph created for WS-1 station (**Figure 3-23**) based on Peel *et al*. (2007), the Danakil Depression falls within the BWH category of the Köppen and Geiger classification.

The horizontal index lines at 22 °C, 18 °C, 10 °C and 0 °C represent the Köppen temperature parameters for B (Arid Climate), A (Tropical Climate), C (Temperate Climate) and D (Cold Climate) respectively. E for a Polar climate is not included in the graphs (Peel *et al.,* 2007).

- B - Arid - MAP<10x$P_{threshold}$
- W – Desert - MAP<10x$P_{threshold}$
- h – Hot - MAT≥18

*MAP = mean annual precipitation, MAT = mean annual temperature, $P_{threshold}$ = (if 70% of MAP occurs in summer then $P_{threshold}$ = 2 x MAT + 28) (Peel *et al*., 2007).

It was noted that the actual recorded evaporation was on average 1.7 times higher than the theoretical ETos value. This pattern was observed at all three weather stations that recorded both parameters and was therefore also applied to Dogua WS2 which only recorded ETos.

Temperature increased in June and July and then decreased as the rainy season as autumn approached.

Most of the rainfall fell in July and August known as the Kiremt rainy season. Rainfall occurred as a mixture of convection and orographic driven events, resulting in intense, episodic downpours which often resulted in flash flooding (Holwerda and Hutchinson, 1968).

Relative humidity increased with the onset of the rainy season in July. Field experience and hourly recordings showed that the mornings were extremely humid and then dropped as the temperature increased during the day.

The dominant wind direction in the Danakil Depression valley, recorded by Dogua WS2, Badah Camp and Solmin, was northerly due to it being funnelled by the roughly N-S orientated Dogua Mountains (Umvoto, 2016d). Dogua WS1 situated in the Dogua Mountains experienced a westerly wind direction which was the result of it being in a roughly E-W orientated valley extending through the Dogua Mountains (Umvoto, 2016d).

Total solar radiation recordings were similar for all four weather stations and showed a decrease during July and August associated with the rainy season, higher humidity and more cloud cover.

Barometric measurements were uniform and constant for all weather stations for the duration of the recording period with variations between stations consistent with altitude differences.

The newly installed automatic weather stations (Dogua WS1 and Dogua WS2), along with the existing weather stations (Badah Camp and Solmin-1) proved that a variation in climatic conditions across the study area, particularly in temperature and rainfall between the higher elevation recharge area of the Dogua Mountains and discharge area of the salt flats.

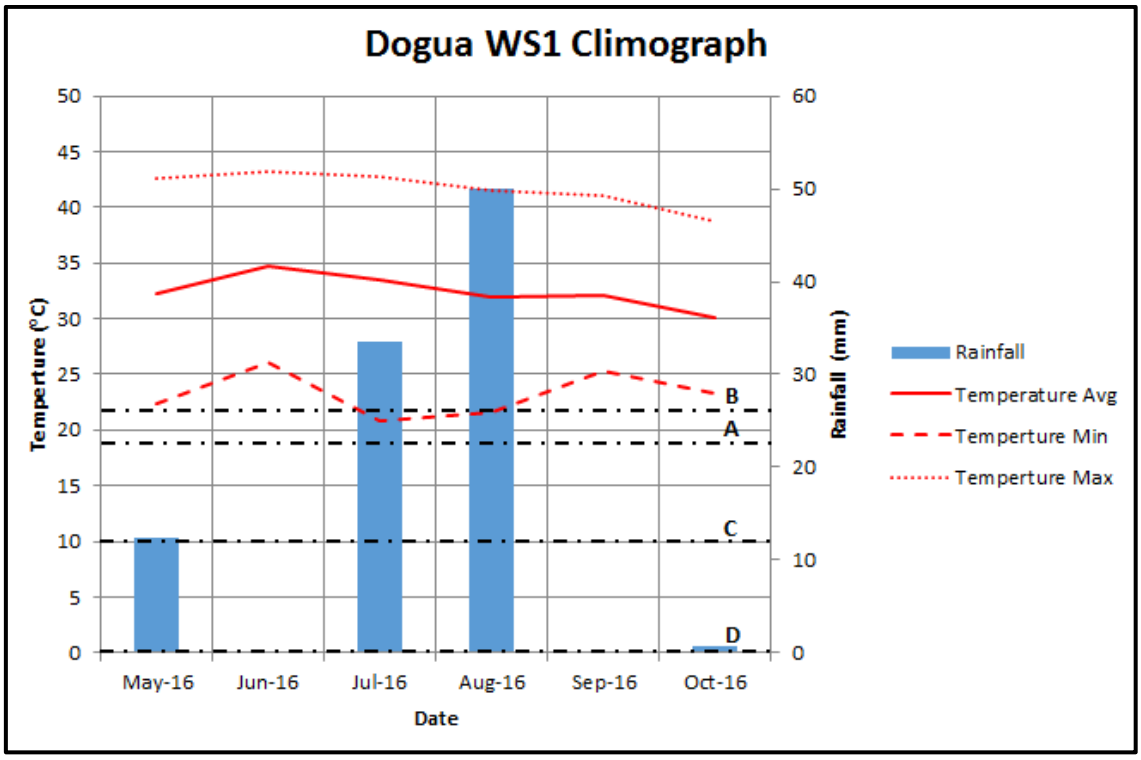

Figure 3-23 **Climograph of Dogua WS1 weather station showing average, maximum and minimum temperature and rainfall (Umvoto, 2016d).**

3.3 GEOLOGY

3.3.1 Introduction

Geological and hydrogeological fieldwork was undertaken to inform and better constrain the initial findings from literature. A large portion of the geological study relied on Geographic Information Systems (GIS) databases for regional geographic, geological and hydrological data and information which were acquired from numerous sources. Categories of databases used during lithological classifications and structural framework analyses included:

- from Kazmin (1972) the 1:2 000 000 geological map of Ethiopia; Geological Survey of Ethiopia (2009) the 1:2 000 000 geological map of Ethiopia; Brickmann and Kursten (1970) the 1:250 000 geological sketch map of the Danakil Depression.
- from Ethiopian Institute of Geological Surveys (1988) 1:2 000 000 hydrogeological map of Ethiopia; Kebede (2013) groundwater in Ethiopia maps.

3.3.2 Stratigraphy and Lithology

Data and information on regional and local geology and hydrogeology were sourced from various technical (RES, 2014a-b; Umvoto Africa, 2014a) and government reports (WWDSE, 2013), as well as other available reports and data sources (Knight Piesold, 2012; MWH, 2015a-d).

3.3.2.1 Regional Stratigraphy

The regional stratigraphy of the Danakil depression can be classified into three main divisions, from youngest to oldest in age (Holwerda and Hutchinson, 1968; Umvoto, 2015):

1. Quaternary (2.6-0 Million years old [Ma]) rocks, these are poorly cemented and weakly compacted playa-lake sediments, evaporites and alluvium continuously being deposited in the Danakil depression;
2. Paleogene and Neogene (66-2.6 Ma) clastic sedimentary rocks and volcanics, deposited in the Danakil depression in early stages of rift and basin development; and
3. Pre-Paleogene bedrock with clastic and carbonate sediments from the Jurassic era and early Palaeozoic (Permian) to Precambrian (Proterozoic) crystalline basement rocks.

Figure 3-24 is a geological map of the study area. The line trace labelled B-B' represents the line along which the cross section in **Figure 3-25** was constructed. These geological maps and **Table 3-2** that accompanies them are summarised below:

Table 3-2 Lithostratigraphy and Hydrostratigraphy after (Umvoto, 2016a).

Map Unit	Formation Name	Thickness (m)	Lithostratigraphy	Hydrostratigraphy	Age (Ma)
Qu	-	5-10	Alluvial and colluvial cover derived from weathering of the Danakil Alps and Dogua Mountains	Thin primary aquifers	Quaternary (un-differentiated) ~2.5-0 Ma
Qha	-	-	Palaeo-Lake Karum deposits	Evaporites, silts (aquiclude)	
Qh	-	500-2500?	Sand, silt, clay, diatomite, limestone and evaporates – Danakil potash ore zone (marine and lacustrine deposits)	Thin primary aquifers at surface, but predominantly evaporites (aquicludes)	
Qb	**Abaeded Formation**	-	Basalt flows, spatter cones and hyaloclastites (transitional between alkaline and tholeiitic)	Probable aquitard (Localised to Maraho cone near Badah)	Holocene <0.01 Ma
Q0	**Oss Formation**	-	Basalt	Probable aquitard (Localised to Eritrea)	Late Pleistocene ~0.03 Ma
Qa	**Alid Formation**	-	Acidic, silicic volcanics (rhyolite pumice)	Probable aquitard (Localised to Eritrea	Late Pleistocene ~0.035-0.01 Ma
Qdy / **Qdo**	**Dogua Formation**	100-300	Undifferentiated alluvial fan and debris-flows, intercalated with lacustrine and beach sediments	Primary aquifers in lenticular conglomerates and sands	Late Pleistocene – Recent ~0.2-0.02 Ma
Qp	**Zariga Formation**	5-50	Coralline reef, limestone, marl and gypsum (alluvial, lacustrine and marine sediments)	Local karstic aquifers	Late Pleistocene ~0.4-0.02 Ma
Qs	**Samoti Formation**	-	Basalt	Probable aquitard (Localised to Eritrea)	Pleistocene 1 Ma – 0.5 Ma
Qpd	**Dandiero Group**	~1000	Terrestrial deposits of fluvial, deltaic, lacustrine and alluvial-fan facies, containing fresh-water gastropods	Primary aquifers in lenticular conglomerates and sands	Pleistocene ~1Ma
QTa	**Afar Formation**	-	Hawaiite, mugearite, trachyte, andesine, ferro-basalts and stratoid basalts	(Localised to Badah in Circum concession, mainly within Eritrea)	Pleistocene 2.5 Ma-1.1Ma
Trs	**Danakil Group (“Red Sea Series”)**	150-350	Conglomerate, sandstone and Siltstone, with intercalated basalt flows and lacustrine sediments	Local primary and/or secondary (fractured-rock) aquifers in conglomerates and sandstones	Miocene-Pliocene ~20-2.5 Ma
Jt	**Antalo Group**	1080	Limestone with interbedded Agula Fm. shale, and overlying Amba Aradom Fm. conglomerate and sandstone	Possible karstic and fractured aquifers	Late Jurassic ~160-145 Ma
Ja	**Adigrat Formation**	300-820	Fe-rich sandstone, conglomerate (base) and grey shale (top)	Possible secondary (fractured-rock) aquifers	Late Triassic - Middle Jurassic ~230-160 Ma
gt4	-	>1520	Post-tectonic granite and syenite	Aquiclude	Late Proterozoic ~1000-540 Ma
gd	-		Granodiorite	Aquiclude	
dt	-		Diorite	Aquiclude	
PR2I	**Tsaliet Group**		Meta-andesite, meta-dacite, meta-rhyolite, chl-ser-graph phyllites, greenschist, limestone and quartzite	Aquiclude	

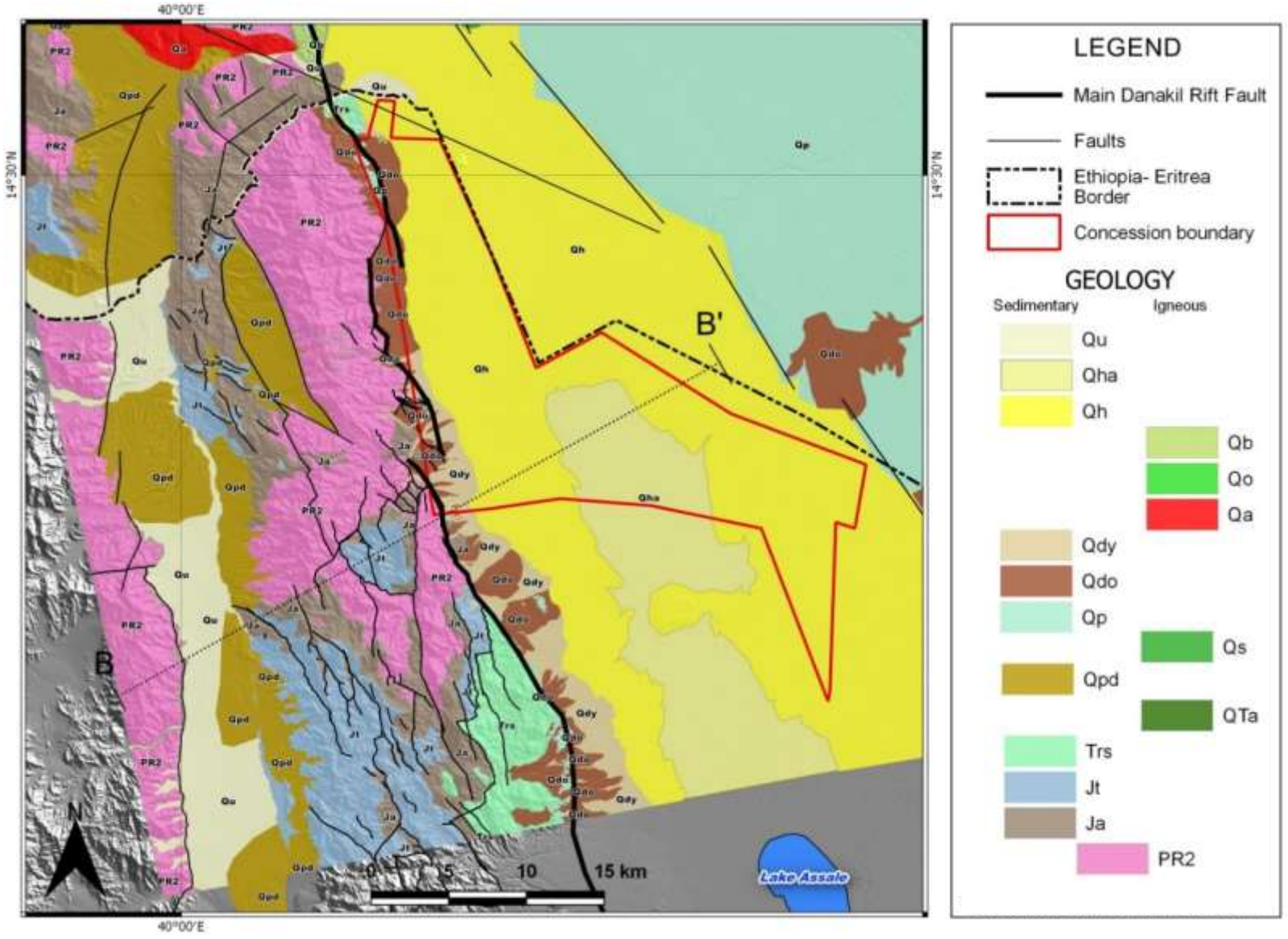

Figure 3-24 Local Geological Map (Umvoto, 2016a). See Table 3-2 for legend.

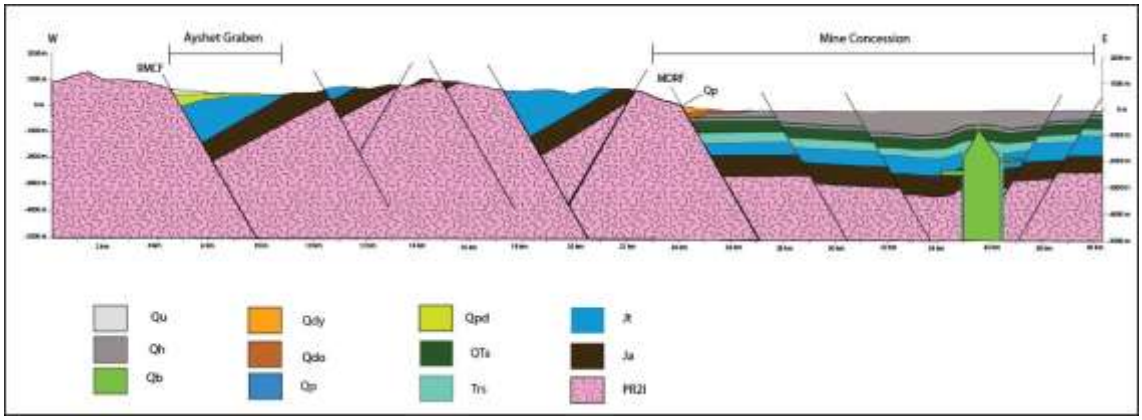

Figure 3-25 Schematic geological cross section through the line B-B' in Figure 2-26 (Umvoto, 2016a).

In a regional context, Cenozoic (Quaternary, Palaeogene and Neogene) rocks occur within the boundaries of the rift system as they were deposited after rifting had begun. Pre-Paleogene rocks are more extensive geographically and have been subject to older block faulting and folding that predate rifting (Umvoto, 2015). The pre-rift faulting is predominantly normal faulting which influenced rift formation and propagation in the early stages of continental extension (Mesfin and Yohannes, 2014). These fractures and faults are of hydrogeological significance as they juxtapose Jurassic and Proterozoic rocks (Mesfin and Yohannes, 2014) and create groundwater flow paths between the two units through the shared fractures and faults (Umvoto, 2015).

3.3.2.1.1 Precambrian Basement and Mesozoic Rocks

Neoproterozoic (1000-540 million years old [Ma]) crystalline basement rocks of the Arabian-Nubian Craton outcrop within the Ethiopian Plateau and the Danakil block, consisting of metamorphosed volcanic and sedimentary rocks of the Tsaliet Group (PR2 on **Figure 3-24**) (Gebresilassie *et al*., 2011; Mesfin and Yohannes, 2014). The highly deformed, fractured and faulted basement rocks were intruded by dykes and sills of diorite, granodiorite, granite and syenite, which then also underwent extensive metamorphism and deformation with the basement rocks (GSE, 2009; Holwerda and Hutchinson, 1968). The metavolcanics show a high degree of heterogeneity in original composition as well as metamorphic grade and consist of meta-andesites, meta-dacites, meta-rhyolites, chlorite-sericite-graphite phyllites, marbles, slate and quartzite (Umvoto, 2015). Per Holwerda and Hutchinson (1968), the phyllites of the Tsaliet Group likely exceed a thickness of 1500 m, and rest on top of an undefined thickness of Precambrian gneiss and migmatites.

The Tsaliet Group underlies Cretaceous to Late Jurassic (230-145 Ma) sedimentary rocks, which were deposited in a continental to shallow marine environment. The marine sequences were deposited during the Jurassic transgression of the Indian Ocean, from intra-continental rifting during the Gondwanan break-up (Gebresilassie *et al*., 2011; Umvoto, 2015). Within the study area these sedimentary sequences are represented by the Adigrat Formation (Ja in **Figure 3-24**) sandstones and the Antalo Group limestones (Jt in **Figure 3-24**).

The Adigrat Formation reaches thicknesses of between 300-1600 m and is described as an un-fossiliferous, coarse-grained, red arkosic sandstone (Holwerda and Hutchinson,1968; Mesfin and Yohannes, 2014; MWH, 2015a) (see **Figure 3-26**). The formation fines upward from conglomerate at the base to grey shale at the top. Ferruginous sandstone beds common to the Adigrat Formation give it a distinct red colour (Holwerda and Hutchinson, 1968).

Figure 3-26 **Adigrat Formation (background right), overlying (contact represented by the black dashed line) the grey shales of the basement Tsaliet Group (foreground left), within the Asabuya Fan wadi.**

The conformable Antalo Group, which is 1080 m thick and composed of intercalated fossiliferous limestone and marl, is overlain by the Agula Formation shale and Amba Aradom Formation sandstone (Gebresilassie *et al*., 2011; Holwerda and Hutchinson, 1968). The lower Antalo Group (see **Figure 3-27**) is described as “a dense, grey, locally fossiliferous marine limestone…” (Holwerda and Hutchinson, 1968) locally intruded by mafic dykes and sills. These intrusions are more extensive and frequent in the underlying Adigrat Formation. The upper Antalo Group is described as an “impure, thin-bedded, grey-blue, fossiliferous limestone with lenticular gypsum beds of up to 5 m thick occurring near the top of the group…” (Holwerda and Hutchinson, 1968).

Figure 3-27 **Light-grey to brown coloured, folded and faulted limestones of the lower Antalo Group, within the Musley Fan wadi. A fresh water spring occurs in the river bed.**

After deposition of these Cretaceous to Late Jurassic sediments, the region was affected by tectonic uplift and erosion, which resulted in the formation of a peneplain (Gebresilassie *et al.*, 2011).

The Adigrat Formation and Antalo Group are potential fractured rock and karstic aquifers respectively. The outcrop geometry and thickness of the units is however, difficult to determine due to the extensive faulting of both units and their juxtaposition against each other and the basement rocks of the Tsaliet Group. (Umvoto, 2015).

3.3.2.1.2 Neogene-Pliocene Sediments and Volcanics

Profuse eruption of volcanic rock, up to 3 km thick, occurred from approximately 30 Ma, resulting in the rifting that formed the Danakil Depression. These volcanic sequences, which overlie the Danakil block, form the base of the Danakil depression. There is a transition in composition from basaltic at the base of the pile to andesitic and rhyolitic at the top (Gebresilassie *et al.*, 2011).

Pleistocene to Recent (2.5-0 Ma) volcanic rocks of the Afar, Samoti, Alid, Oss and Abaeded Formations have erupted in and around the Danakil Depression and are comprised of hawaiite, mugearite, trachyte, andesine basalt, ferrobasalt, rhyolite, spatter cones and hyaloclastites ranging in composition from alkaline to tholeiitic (Umvoto, 2016a). The Afar volcanics are usually intercalated with the Danakil Group sediments described below (Kazmin, 1972). The Abaeded Formation volcanics surface around Badah village. The Samoti, Alid and Oss Formation volcanics are mainly localised to Eritrea (Umvoto, 2016a).

The Danakil Group (Trs) or Red Series (Abbate *et al.*, 2004; Mesfin and Yohannes, 2014) was deposited during the Miocene to Pliocene (23-2.6 Ma) and consists of Lower, Middle and Upper sub groups. "…Limestone and mudstone units were likely deposited during Miocene-Pliocene marine incursion into the Danakil Depression, whereas conglomerates are likely debris-flow or alluvial fan erosional deposits…" sourced from the plateau (Umvoto, 2015). Boreholes drilled for the MoWE's DTW campaign (WWDSE, 2013) intersected parts of the Danakil Group in some of the DTW wells (see **Table 3-3**). The Danakil Group outcrops are also observable north west of Badah village and south from the Musley fan which may mean that the Danakil Group has been displaced by faulting along the main rift fault. If the Danakil Group has been down faulted, then it ought to be present beneath the alluvial fans at the western edge of the depression (Umvoto, 2015).

The Lower Danakil Subgroup consists of "…blueish grey marl overlain by marly limestone…" (Brinckmann and Kursten, 1970). A survey of the outcrops and DTW rock chips (MWH, 2015a) confirmed that the Lower Danakil Subgroup is not exposed in the Musley Fan wadi immediately to the west of borehole DTW5 and that the subgroup was not intersected in DTW boreholes to the north of DTW5 (see **Figure 2-5**). Probable Lower Danakil Subgroup limestone was encountered at the base of DTW5 (2 m thick) and southwards at DTW7 (30 m thick), but in both cases, the drill holes were terminated in this limestone so the thickness was not proven beyond 30 m (MWH, 2015a).

Outcrop of this subgroup has been verified in the field to the south and south west of the mining concession, by survey and drilling works carried out (MWH, 2015a; WWDSE, 2013). The thickness of the intersected limestones however, were not determined in the DTW holes. **Table 3-3** below is sourced from MWH (2015a) and summarises the formations and their respective thickness intersected in the DTW campaign.

Table 3-3 Formation thickness intersected in the DTW campaign (MWH, 2015a)

Sub-Group or Formation	Symbol	Thickness of Formation in Each Well									
		DTW-1	DTW-2	DTW-3	DTW-4	DTW-5	DTW-6	DTW-7	DTW-8	DTW-9	DTW-10
Alluvial Fan Sands &Gravels	Qt	192	158	90	40	6	6	0	6	28	130
Upper Danakil	tss		Absent		Absent	Absent	Absent	40	94	76	
	tc		Absent		Absent	30	32	78	Not Identified	Absent	
	tcs		Absent		Absent	Not Identified	Not Identified	Not Identified	Not Identified	Absent	
Afar Basalts	B2		Absent		Absent	Absent	Absent	Absent	28	Absent	
Middle Danakil	tssv		Absent		Absent	34	52	40	44	Absent	
	t's (Upper)		Absent		Absent	40	36	42		Absent	
	t's (Lower)		Absent		Absent	40	34	20		Absent	
Lower Danakil	t'c		Absent		Absent	2		30		Absent	
	t'cy		Absent		Absent					Absent	
Antalo Limestone	j2		64		Absent					Absent	
Adigrat Sandstone	j1				Absent					Absent	
Palaeozoic \ Precambrian	ps				211					146	
Total Borehole Depth:		192	222	90	251	152	160	250	172	250	130

The Middle Danakil Subgroup consists of "…chocolate brown sandstones and chocolate brown to violet conglomerates…" (Umvoto, 2015) (see **Figure 3-28**). The sandstones and conglomerates are overlain by partially cemented gravels, sands and silts (Brinckmann and Kursten, 1970). In borehole cuttings of DTW wells, the latter conglomerate units are easily identified due to the red to dark red colours and consistent thickness of the conglomerates which act as a distinctive marker bed (MHW, 2015a). These units are well exposed in the Musley Fan wadi (see **Figure 3-28**), south of the study area, where 80-130 m of red sands, red conglomerates and red sandstones are observed (MHW, 2015a).

The Upper Danakil Subgroup consists of "…red to yellow-grey, clayey, gravelly, sandy silts, which are underlain by intercalated creamy to grey marls and limestones with localised grey coral reef limestone..." (Brinckmann and Kursten, 1970).

Figure 3-28 Reddish to purplish-brown coloured conglomerates of the Middle Danakil Subgroup, within the Musley Fan wadi.

While the borehole logs of the MoWE's DTW wells do not record the full Upper Danakil Subgroup thicknesses, the full thickness of the marl and limestone unit was determined to be 30-78 m from two of the boreholes, with the minimum thickness of the sandy silt unit ranging from 40-94 m (MWH, 2015a).

3.3.2.1.3 Quaternary Sediments

The Zariga Formation (Qp) (Brinckmann and Kursten, 1970), also called the Enkafala Formation (Abbate *et al.*, 2004) unconformably overlies the Danakil Group along the western side of the rift basin. At certain locations, the oldest Pleistocene alluvial fans are also overlain by the Zariga Formation. The Zariga formation represents a marine ingression into the northern Danakil depression (Umvoto, 2015). It is predominantly comprised of "…laminated gypsum and marls with oolitic and reef limestone…" (Holwerda and Hutchinson, 1968). Field observations and measurements undertaken in the Badah area verify the Zariga's thickness to range between 30 and 50 meters (Umvoto, 2015). Marine fossils present within the Zariga Formation (see **Figure 3-29**) have been dated as Middle to Late Pleistocene [200 000 to 24 000 years before present (BP)] (Abbate *et al.*, 2004).

Figure 3-29 Marine fossils-coral (left) of the Zariga Formation (right) with karstic structures visible in the Zariga formation.

Late Pleistocene (200 000 BP) to Holocene alluvial fans (Qdy and Qdo in **Table 3-2** and **Figure 3-24**), occur where wadis or ravines drain the Dogua Mountains. These alluvial deposits were named as the Dogua Formation by Umvoto (2015) (see **Figure 3-30**). The fans consist of coarse alluvial sands and gravels, with interbedded, lenticular sandy silts and clays in parts (MWH, 2015a).

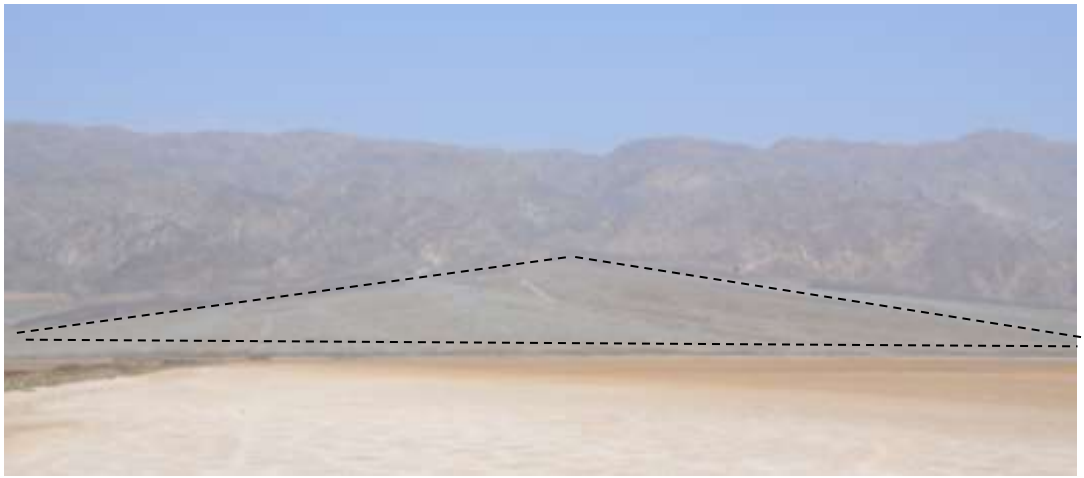

Figure 3-30 Quaternary Alluvial Fans formed where the Dogua mountains drain out onto the salt flats of the depression.

Figure 3-31 is a Sentinel 2A False Colour Composite (FCC) of the study area and is useful in delineating outcrops of different lithological units, their contacts and large drainage features.

Figure 3-31 False Colour Composite of the Danakil Depression and western Dogua Mountains from Sentinel 2A European satellite.

The metabasites and other magmatic rocks of the Neoproterozoic Tsaliet Group basement in the northern portion of the Dogua Mountains have a dark orange-red colour (labelled **1** in **Figure 3-31**). The phyllites of the Tsaliet Group basement have a blueish colour (labelled **2** in **Figure 3-31**). The overlying Cenozoic-Jurassic Antalo Group limestones and Adigrat Formation sandstones (labelled **3** in **Figure 3-31**) are pinkish-red in colour, with the Adigrat Formation sandstones having a slightly more orange tinge.

The Dogua Formation gravels (labelled **4** in **Figure 3-31**) and Lelegheddi River valley sediment have the same colour as the lithology they drain. Fans draining the Tsaliet phyllite are thus blue and the fans draining the Antalo Group and Adigrat Formation are pink, while some are mixed colours as they drain more than one type of geology. The Danakil Depression salt flats (labelled **5** on **Figure 3-31**) are bright red, while Dallol can be seen in the bottom right corner is yellow (labelled **6** in **Figure 3-31**).

3.3.3 Structural Geology

The Dogua Mountains represent a tilted horst block structure that forms the footwall block of the MDRF (Umvoto, 2015). The MRDF trends roughly north-south along the western edge of the Dogua Mountains (see **Figure 3-32**). Fault orientation and patterns that cross cut the Dogua Mountains play an important role in controlling the direction of groundwater flow toward the Danakil basin. The most recent phase of deformation is characterised by north-south-trending structures parallel to the MDRF (Umvoto, 2015). An older series of north east-south west (NE-SW) and north west- south east (NW-SE) structures are also inferred from the lithology in the Dogua Mountains. Older structures are not observed in the younger alluvial deposits, and are therefore interpreted as structures that may have been formed during Jurassic rifting and opening of the Indian Ocean, or even Cenozoic rifting and separation of the Somalian Plate from the Nubian Plate (Umvoto, 2015). More recent deformation has reactivated these structures, creating transfer faults along the older NE-SW striking faults that cross-cut the MDRF. Structural mapping carried out by Umvoto (2015) and Umvoto (2016a) based on satellite imagery indicated that these structures extend into the Dogua Mountains which increases the likelihood of them being significant conduits of groundwater flow from the plateau to the alluvial fans. This is particularly the case in the southern region near the Musley Fan, where rocks of the Antalo Group are down faulted against the alluvial fans.

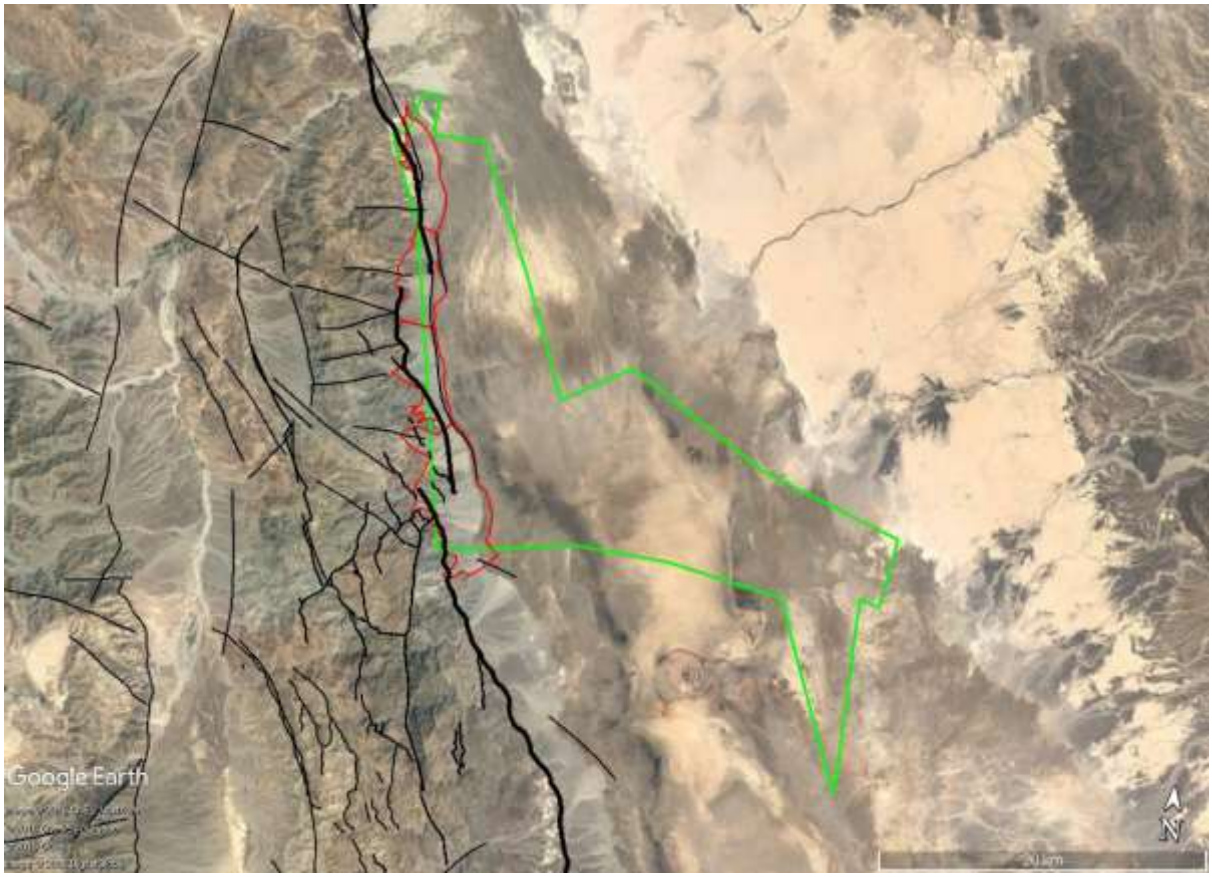

Figure 3-32 Fault and fracture mapping carried out using Google Earth with smaller structures near the concession verified in the field. The thick, black roughly north-south trending line represents the MDRF.

One of these structures, separates the Dogua horst into northern and southern sections (Umvoto, 2016f). This separation is a crucial factor in evaluating the potential for fracture throughflow from the plateau to the alluvial fans (Umvoto, 2016f). The southern section of the Dogua Horst has Precambrian basement rock as well as portions of the Jurassic-Cretaceous sedimentary rocks (Antalo Group and Adigrat Formation) while the northern section lacks any outcrop of these sediments and is comprised predominantly of Precambrian basement rock. This difference in lithologies has implications for the likelihood and quality of water that is transferred through the faults to the alluvial fan aquifers. Limestones and sandstones of the Jurassic-Cretaceous sediments store and consequently transmit fresher quality water into the southern fans (MWH, 2015d; WWDSE, 2013), while Precambrian basement predominantly acts as an aquitard and seemingly allows limited amounts of potentially poorer quality water to recharge the northern fans.

Faulting within the rift is complex and extensive with numerous fault splays off the MDRF creating a step-like pattern. Some such faults associated with the MDRF were mapped to be present below and in some cases, transect the alluvial fans. This was confirmed in the geophysical survey carried out as is discussed in **Chapter 4**. The presence of such faults within the alluvial fans implies a possible source of vertical recharge where water of numerous possible origins flows vertically into the fans via faults and may be considered a possible source of vertical recharge to the aquifer. This may have implications for pump test data analysis as numerous assumptions coupled with analytical analysis techniques are rendered invalid if such a recharge source is present (Driscoll, 1986).

3.4 HYDROGEOLOGY

3.4.1 Introduction

Groundwater is used in several towns in and around the Danakil Depression and by mining companies conducting exploration within the depression. While large volumes of water are not currently used for mining exploration programmes, water demand will increase once solution mining of the potash deposits commences. Local communities depend on surface, well and borehole water-sources many of which were surveyed during a hydrocensus carried out in the region by ERM (2012). In the northern part of the Badah-Danakil area, two boreholes have been equipped with pumps. The Bada-Admerug well supplies the mine's exploration camp and is equipped with a currently non-functional reverse-osmosis (RO) plant. It is also used by the local community for its domestic and stock-watering needs (Umvoto, 2014b). The Bada-Ermile well is of higher quality and potable, but has a similar yield to the Bada-Admerug well. The village of Hamdale or Hamad Ela has two wells with manual pumps on which they are dependant (Umvoto, 2014b).

3.4.2 Groundwater Occurrence

3.4.2.1 Regional Groundwater Occurrence

Generally, groundwater occurrence varies to a large degree depending on the local geology. The most productive aquifers are usually found in shear zones and tectonic discontinuities (Umvoto, 2014b). Abiye (2010) reviewed the transboundary aquifers in east Africa, and elaborated on the Precambrian Ethiopian-Eritrea aquifer.

The Precambrian metamorphic basement with intrusive rocks and tertiary lava flows dominates the geology of the aquifer on the escarpment to the west of the Danakil Depression. This aquifer occurs west of the site on the plateau and north of the site in Eritrea. The basement rocks have undergone greenschist metamorphism and contain joints, fracture zones and weathered layers which produce secondary aquifers within this broader aquifer. Quartz veins, 10-50 m weathering zones and intrusive dolerite and other mafic dykes represent groundwater targets in the basement. In general boreholes in the basement are drilled to an average depth of 50 m or shallower and average yields are reported to be approximately 2.7 litres per second (l/s). Most the basement lithologies are, however, aquicludes and hydraulic conductivities in metavolcanic rocks are recorded as being low, in the order of 0.1 m/day. Springs are rare, but occur along regional fractures. Groundwater exploitation within basement rocks occurs on a small-scale in the form of dug wells and occasional boreholes.

Jurassic limestone and cretaceous sandstone deposited on this highly-fractured crust imply high groundwater potential aquifers in the Danakil Depression. The northern part of the depression contains Triassic quartz-rich sandstones that extend into Eritrea which also represent high groundwater potential aquifers. Productivity of these aquifers will be dependent on thickness and lateral extent of the formations.

Ayenew *et al*. (2008) confirms that the fractured volcanics covered with thick quaternary sediments of alluvial fans at the shoulder of the rift are the most productive aquifers because of faulting and the occurrence of relatively permeable unconsolidated sediments. Lateral continuity of aquifers and groundwater flow might be locally disrupted by major faults. In this case groundwater is forced to flow parallel and sub-parallel to the axis of the rift, but to a large degree the groundwater contours are a subdued imitation of the topographic contours (Umvoto, 2014b).

3.4.2.2 Local Groundwater Occurrence

Locally groundwater is channelled along the dominant faults within the plateau north towards the Ragali River (Umvoto, 2014b). Adjacent to the Danakil block similar large-scale faults occur which possibly channel deep-seated groundwater towards the south. Groundwater flow directions are based on fault orientation, topography and slope (Umvoto, 2014b). The weathered regolith and fractured rock aquifer of the basement material is therefore a poor aquifer to target with respect to groundwater, east of these faults. The various compartments of the basement material have also been divided into numerous faulted blocks resulting in smaller recharge areas for each block. The great distance and elevation of these fractured rock aquifers from the study site also makes

these aquifers economically unviable. With regards to recharge these aquifers would, however, most likely be more sustainable in the long-term (Umvoto, 2014b).

Groundwater movement along the larger north-south oriented faults is expected to be large as numerous smaller faults show interconnectivity with the large regional faults (see **Figure 3-32**). The large faults represent secondary aquifers of possibly high groundwater potential and likely good water quality. These faults occur between 12-23 km north-west and west of the site area, but are elevated at 150-950 m above the site area. Ridges, ravines and rough terrain makes these targets difficult to access with regards to exploration and drilling.

The Adigrat and Antalo aquifers are of unknown thickness in the lowlands and at the edge of the plateau. These units could represent extensive aquifers at depth, but the lack of lateral extension due to erosion and faulting limits groundwater potential (Umvoto, 2014b). Faults along the edge of these blocks may represent better groundwater targets west and south west of the site area.

The Danakil Group or Red Sea series represents a large primary aquifer of unknown thickness to the south west, west and underlying alluvial fan deposits of the site area. This aquifer though extensive, may however be of brackish to saline water quality (Umvoto, 2014b).

The alluvial fan aquifer including alluvium and excluding the clays and saline material at the base of the Danakil depression is of moderate to possibly high groundwater potential. The water quality in these alluvial fans will be fresh to brackish water quality as is seen through the testing of some of the DTW boreholes (WWDSE, 2013). Numerous faults underlie and occur along the eastern edge of these alluvial fan deposits and discharge may occur from these faults into the overlying fans. The impact of which may cause uncertainty in pump test result analysis.

3.4.3 Hydrostratigraphy

The lithostratigraphy of the Danakil Depression is given in **Table 3-2** and was grouped into four broad hydrostratigraphic units (Umvoto, 2015):

1. The Precambrian metavolcanic and metasedimentary basement rocks of the Tsaliet Group constitute a relatively impermeable, low yielding, poor quality aquitard.

2. Adigrat Formation and Antalo Group fractured sandstones and limestones, respectively representing more permeable fractured rock or karstic aquifer units with good quality water.
3. Danakil Group and Zariga Formation fine-grained sediments, which are unlikely to constitute a significant regional source of fresh groundwater, although local primary or fractured-rock aquifers are potentially present in conglomerates and sandstones of the Middle Danakil Subgroup, while local karstic aquifers may be present in the limestones of both the Danakil Group and Zariga Formation.

4. Dogua Formation alluvial fans on the west side of the rift basin, which form a major, regional primary aquifer.

While limestones are known to be high yielding karstic aquifers, certain geological and hydrological characteristics of the Antalo Group diminish its potential to form a regional, large-scale aquifer system and have resulted in limited or no karstification of the limestones in certain areas of northern Ethiopia (Umvoto, 2015). This is confirmed in the field while driving from Mekelle to Badah, where no karstic structures are visible within the well exposed limestones. Some of these characteristics include the absence of large scale regional faulting, reduction of limestone thickness due to interbedding of shales and marls and the formation of isolated blocks due to dissection by regional and local faults and rivers. (Kebede, 2013). It has however, been proposed that if faults and fracture zones that dissect the Antalo Group are targeted for groundwater use, sustainable fresh water yields can be attained (Kebede, 2013).

The rocks of the Danakil Group and Zariga Formation represent the Quaternary rift and shallow-marine sediments and are unlikely to constitute a significant regional source of fresh groundwater. Local primary or secondary fractured-rock aquifers are potentially present in the conglomerates and sandstones of the Middle Danakil Subgroup (Umvoto, 2015).

The Dogua Formation alluvial fans on the western side of the rift basin form a major, regional primary aquifer. These alluvial fans formed by accretion of debris-flow and flash-flood deposits above an active fault in the developing half graben (Umvoto, 2015). Dating of the oldest Zariga Formation fossils indicate that these alluvial fans have formed over the last 200 000 years (Abbate *et al*., 2004). These sheet-flood events are highly energetic near the source and in the wadis, but flow velocity dissipates as it is spread over a wider area. Coarse boulder- to cobble sized material is therefore deposited higher up on the slope of the alluvial fans, and there is generally an overall gradation down to

sands and silt toward the fan toe. The sorting affects the porosity and permeability of the fan and therefore there are likely to be gradual but significant changes in hydraulic conductivity between the fan head and the toe. These physical changes affect the flow of groundwater over and through the fans, and will also impact on the subsurface storage capacity (Umvoto, 2016a).

The Dogua Formation deposits have been considered as the "…primary water supply target for the proposed mining of potash due to their high transmissivity and the store of good quality water in some of the fans…" (MWH, 2015a). The well records from the MoWE drilling campaign prove that the Dogua Formation thickness in the two largest alluvial fans (Musley and Gehertu Fans) is close to 200 m, but the Asabuya, Bussaba, North Dogua and Badah Fans have a smaller catchments and horizontal extents likely resulting in maximum thicknesses being smaller than the larger fans. Drilling of two boreholes in the Asabuya Fan (RAJ-1 and DTW-4) to 186 mbgl and 165 mbgl respectively, and a borehole in the North Dogua Fan (RAJ-2), drilled to 77 mbgl, only intersected alluvial fan material. This indicates that the thicknesses suggested by the Moving Loop Electromagnetic (MLEM) survey are a realistic indicator of fan thickness (Umvoto, 2015).

There are two distinct ages of alluvial fans within the Dogua Formation (see **Figure 3-33**), visibly indicated by dark greyish brown desert varnishing on the older fans (Qdo in **Figure 3-24**), which have in turn been cross-cut by lighter coloured, younger fan channels and deposits (Qdy in **Figure 3-24**). There are less distinct regions on the fans where young fans are in a transition from young to old and these can be considered an intermediate age.

Figure 3-33 Google Earth image indicating the old (dark brown) and new (light grey) alluvial fans of the Dogua Formation. The margins of the new and old fan portions have been outlined.

Zariga Formation sediments was seen, remotely and in the field, to overlie the upper portions of the older fans in certain sections of the Badah and Bussaba Fans, indicating that the oldest sediment of the fans is older than the depositional period of the Zariga Formation which as per Umvoto (2015) was during the Eemian, between 130 000-115 000 BP.

It is important to note that to the west of the target fans, the Precambrian basement outcrops in the Dogua Mountains, while further south, adjacent to the Musley fan and part of the Asabuya fan, the Cenozoic-Jurassic rocks are exposed and juxtaposed against the quaternary fans. This implies that fresh water is likely to be transmitted via interconnected fault and fracture zones from the west into the southern fans, but no such through flow is expected into the northern fans due to the Precambrian rock acting as an aquitard. This is likely to cause a considerable difference in recharge sources and hydrochemical signatures between the southern and northern fans.

3.4.4 Groundwater Recharge

The main source for groundwater recharge in the entire East African Region is rainfall in excess of 1000 mm/a, mostly summer rain originating from the Atlantic Ocean, in the Ethiopian Highlands. Accordingly, the recharge varies between 400 mm/a in the highlands and less than 50 mm/a in dry low lying regions such as Afar (Abiye, 2010).

While not providing much detail for the study area, the recharge map (**Figure 3-34**) shows that the site area receives less than 50 mm/a recharge to groundwater from precipitation and the lowlands and plateau between 50-150 mm/a. Recharge rates vary between 150-250 mm/a to the south east on the escarpment, far outside the study area.

Despite the relatively high recharge in the highlands, some lowland aquifers remain unproductive because they are isolated by impermeable tectonic lineaments and do not receive any of the highland groundwater recharge. Hence, the groundwater potential of aquifers is strongly related to the geomorphology, geology, climate and environmental setting (Abiye, 2010).

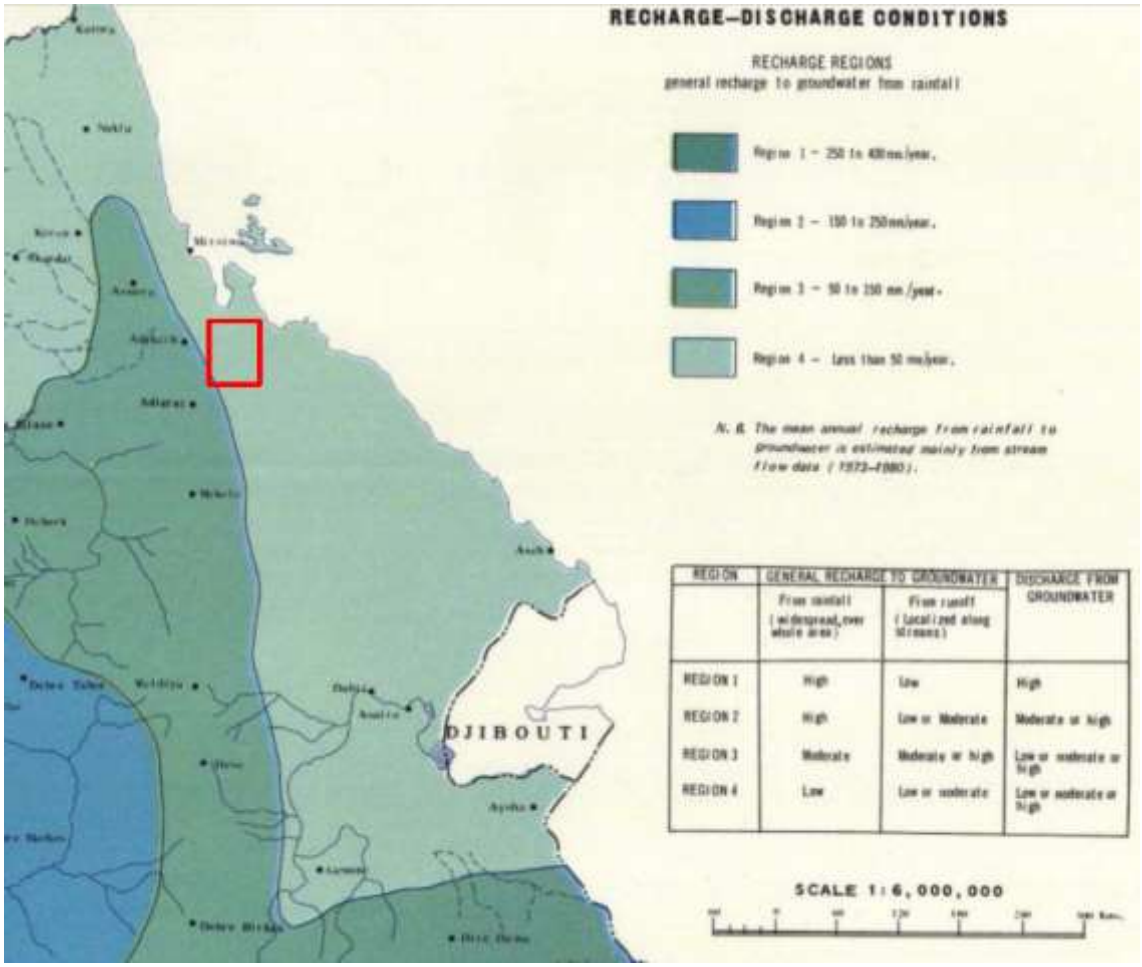

Figure 3-34 Regional Groundwater Recharge surrounding the study area (red square) (EIGS, 1988).

More detailed local scale recharge estimations were carried out and are detailed in **Chapter 8** as input to the numerical model developed by Umvoto (2016e).

3.4.5 Groundwater Flow and Discharge

Understanding of groundwater flow implies that the unevenly carved topography of the western plateau intercepts the recharge generated in the highlands and valleys. This recharge is expected to be channelled towards dominant faults and move towards the north, where it is channelled and discharged into the Ragali River. To the east of these faults groundwater is interpreted to move in an easterly direction or along localised faults. Groundwater in aquifers in the lowland hills flows east into the Danakil depression with possible discharge at springs. The floor of the Danakil depression therefore acts as a discharge area or sink where water is evaporated or flows south towards Lake Assale.

Deep groundwater in the fractured basalts emerges as hot springs surrounding the Dallol hydrothermal complex.

In a diagram taken from Umvoto (2014b) the schematic conceptual understanding of flow paths to the Danakil Depression is illustrated (**Figure 3-35**). Groundwater from the fractured basement in the highlands and intergranular and karstic rocks in the gentler slopes discharges in an easterly direction. Some of the discharge ends up as stream flow, whereas the main discharge path is evapotranspiration.

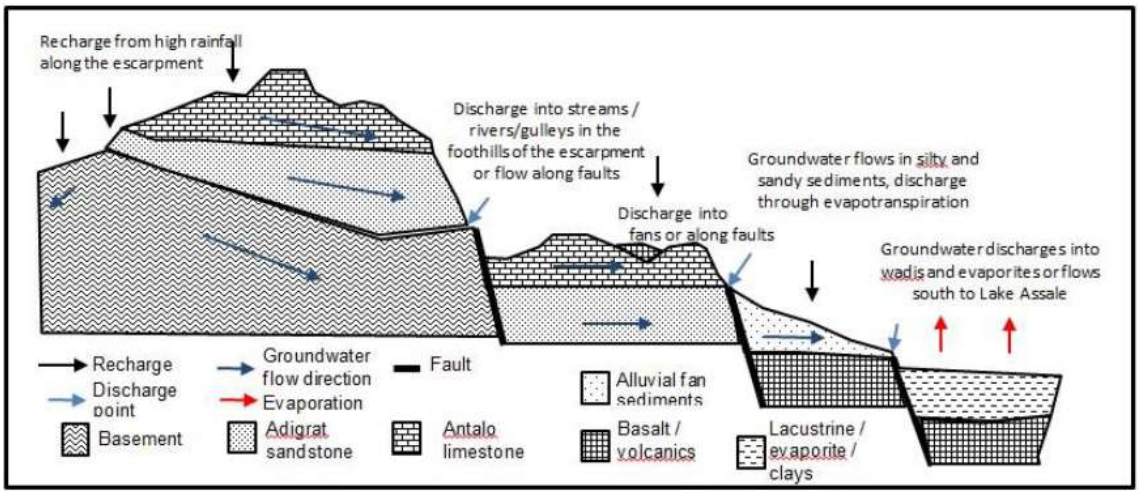

Figure 3-35 Conceptual hydrogeological sketch of the Danakil Depression (Umvoto, 2014b).

3.4.6 Hydrocensus

A hydrocensus was carried out in the region by ERM (2014). Details of boreholes and wells surveyed and six of the boreholes drilled for the MoWE are listed in **Table 3-4** and **Table 3-5**.

Six of the DTW boreholes drilled into alluvial fans along the escarpment west of the study area were surveyed as part of the hydrocensus. During drilling, boreholes intersected boulders, clay, sand, alluvium and gravel beds in DTW1 to DTW3 and other granitoid, clay, sand, gravel, quartzite and metasediments in DTW4 to DTW6. Boreholes DTW1 to DTW3 were pump tested at 44 l/s, 10 l/s and 60 l/s respectively and have a borehole width of between 6-17 inches with most the boreholes drilled at 10-inch diameter. The drawdown in the near to 24-hour constant yield test in these three boreholes was between 1.1 m, 6 m and 6.8 m respectively. The salinity of the boreholes was, however, highly variable, and ranged from 114 - 6170, milli-Siemen per meter (mS/m), from fresh to brackish. Should this data prove accurate, the alluvial fan should be able to supply

sufficient groundwater to the mine site. The highest target areas with regards to the alluvial fans would be on the faults, but these may deteriorate water quality. The head of the fans where streams and gulley's open to form the alluvial fans may be of fresher water quality.

Table 3-4 Summary of the details of boreholes and wells obtained during a hydrocensus of the study area after (ERM, 2014).

Site ID	Latitude	Longitude	Elevation (mamsl)	Type	Depth (mbgl)	Casing height (magl)	Static water level (mbgl)	Yield (l/s)	Equipment Installed	Use	Sampled by ERM	Comment
Groundwater												
APBH01	13.99545	40.18592	100	Borehole		0.89	16.59		Submersible pump	Construction and domestic	Yes	
APBH02	14.56579	40.02567	665	Borehole		1.2			Submersible pump	Domestic and livestock	Yes	
APBH03	14.21889	40.21171	-78	Borehole					None	Domestic and livestock	Yes	
APHS01	14.21175	40.31802	-126	Hot Spring					None	Domestic and livestock	Yes	
APHS02	14.23598	40.29644	-88	Hot Spring					None	Domestic and livestock	Yes	
APDW01	13.87278	40.05514	702	Dug well					None	Domestic and livestock	Yes	
APDW02	14.08319	40.27223	-91	Dug well		105			Manual Pump	Domestic and livestock	Yes	
APDW03	14.08064	40.27381	-96	Dug well		2			Submersible pump	Domestic and livestock	No	
APDW04	14.07911	40.27486	-95	Dug well		0			Manual Pump	Domestic and livestock	Yes	
APTR01	14.23292	40.22223	-112	Trench					None	Stormwater management	Yes	
APEXP01	14.18675	40.2646	-115	Borehole		1	2.9		None	Exploration hole	No	
APEXP02	14.19338	40.28012	-116	Borehole		0.49	0		None	Domestic and livestock	Yes	
APBH04/ Bada Admerug well	14.52548	40.1175	-96	Borehole	46	1	13	3	Pump and generator	Domestic and livestock	Yes	Slightly saline, RO plant for treatment Supplies G&B camp with water
Bada-Ermile Well	14.54378	40.12131	-90	Borehole	46		12.5	3	Pump and generator	Domestic and livestock	No	Potable, maximum yield 3 l/s, sustainable yield 2 l/s at 20 hours/day. Specific capacity 19.6 m^2/d, Transmissivity 33.7 m^2/d and storativity 0.00085

Table 3-5 Summary of the hydrocensus data obtained from six of the DTW boreholes (ERM, 2014).

Borehole Name	Latitude	Longitude	Elevation (mamsl)	Type	Total Depth (mbgl)	Depth of Casing (mbgl)	Static Water Level (mbgl)	Yield (l/s)	Pump Installation (mbgl)	EC (mS/m)	TDS (mg/l)	pH	Temperature (°C)
DTW-1	14.26061	40.181574	-9	Borehole	192	162	99.5	(44)	119.15	5964	357.6	7.1	45.6
DTW-2	14.25532	40.1744	41	Borehole	223	214	144	(10)	145.08	109	6.6	6.4	53.8
DTW-3	14.27583	40.180495	-70	Borehole	91	88	43.3	(60)	52.75	181	11.1	6.4	44.8
DTW-4	14.32725	40.139773	115	Borehole	251	250.25	127.3		170	11	675.0		37.1
DTW-5	14.22659	40.190442	4	Borehole	152	150.1	50			8	502.8		38.1
DTW-6	14.14798	40.220029	25	Borehole	160	145	40.7						

CHAPTER 4

GEOPHYSICS AND BOREHOLE SITING

4.1 INTRODUCTION

To support the identification and delineation of the alluvial aquifers over the Dogua Formation alluvial fans and to assist in siting boreholes, Moving Loop Electromagnetic (MLEM) ground geophysical surveys were carried out over the Dogua Formation alluvial fans (RES, 2014a; RES, 2016; Umvoto, 2016a). Survey lines were walked in east-west and north-south directions along the eastern edge of the Dogua Mountains.

4.2 MOVING LOOP ELECTRO MAGNETIC SURVEY

4.2.1 Methodology

The results of the LMEM survey were used to site boreholes in the Dogua Formation with the purpose of meeting the research study objectives. The 2016 survey was conducted as a follow-up to a similar investigation carried out in 2014 by RES (2014a), which provided additional up-fan traverses on the alluvial fans previously surveyed on basin parallel profiles.

All the MLEM soundings were inverted using UBC EM1DTM software to create an electrical conductivity model (UBC-University of British Colombia, EM-Electromagnetics, 1D-one dimensional models, T-time domain observations, M-magnetic sources and receivers) (Umvoto, 2016a). EM1DTM is a one-dimensional inversion programme which creates a layered conductivity model using the values of the measured magnetic field for arrangements of source and receivers (RES, 2016). Transmitter waveform, loop geometry and receiver position were effectively modelled (Umvoto, 2016a). Results were output as a series of one-dimensional models for each MLEM sounding which was juxtaposed to create a two-dimensional image of the subsurface for data collected along a line, or a 3D image if the data was collected over a grid (RES, 2016). **Figure 4-1** illustrates the locations of the different traverses included in the MLEM survey.

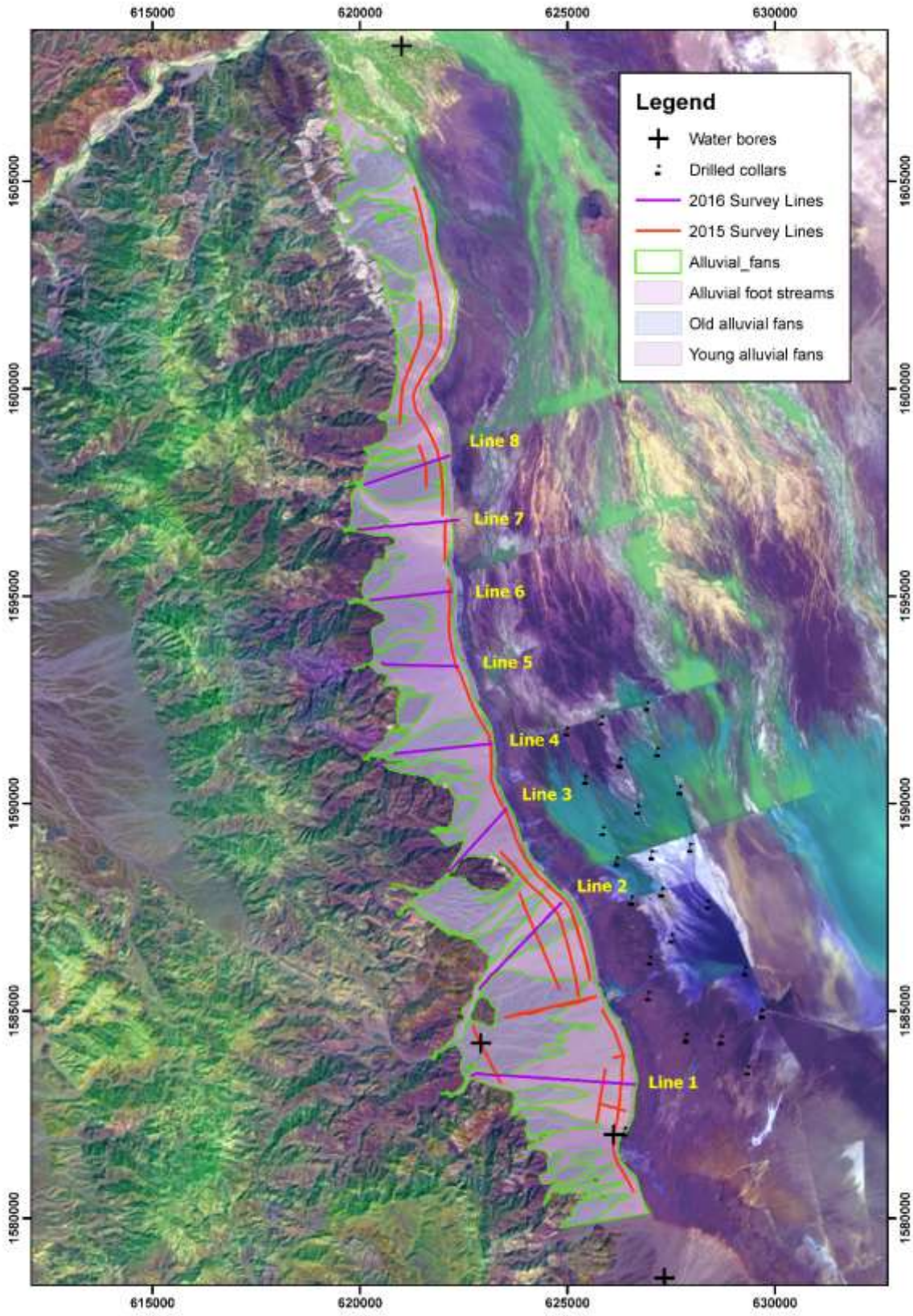

Figure 4-1 **Locality map illustrating the MLEM traverses over the Dogua Formation (RES, 2016)**

4.2.2 Results

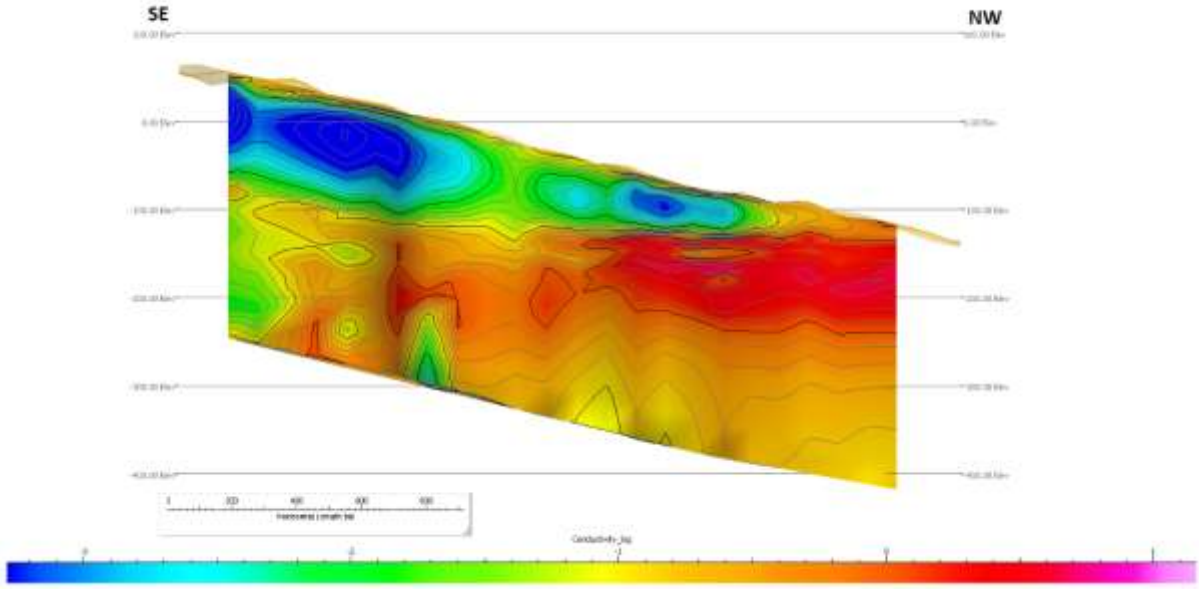

Figure 4-2 Example of the 1D inversion obtained from traverse line 2 (Umvoto, 2016a).

Figure 4-2 illustrates the shallow low conductivity blue layer overlying a more conductive green-to-red layer. The contact between these two layers was seen to be sharp and laterally extensive, and is therefore interpreted to represent the top of the water table, the boundary between saturated and unsaturated zones. This allowed the alluvial fan thickness to be estimated as can be seen in **Figure 4-3.** A maximum thickness was determined to occur toward the centre of the fan and did not exceed 160 meters. From this, useful assumptions regarding the overall geometry and shape of the alluvial fan were deduced. Each individual fan appeared to deepen from the contact with basement rock in the west, to a point near the centre of the fan after which it once again became shallower further east.

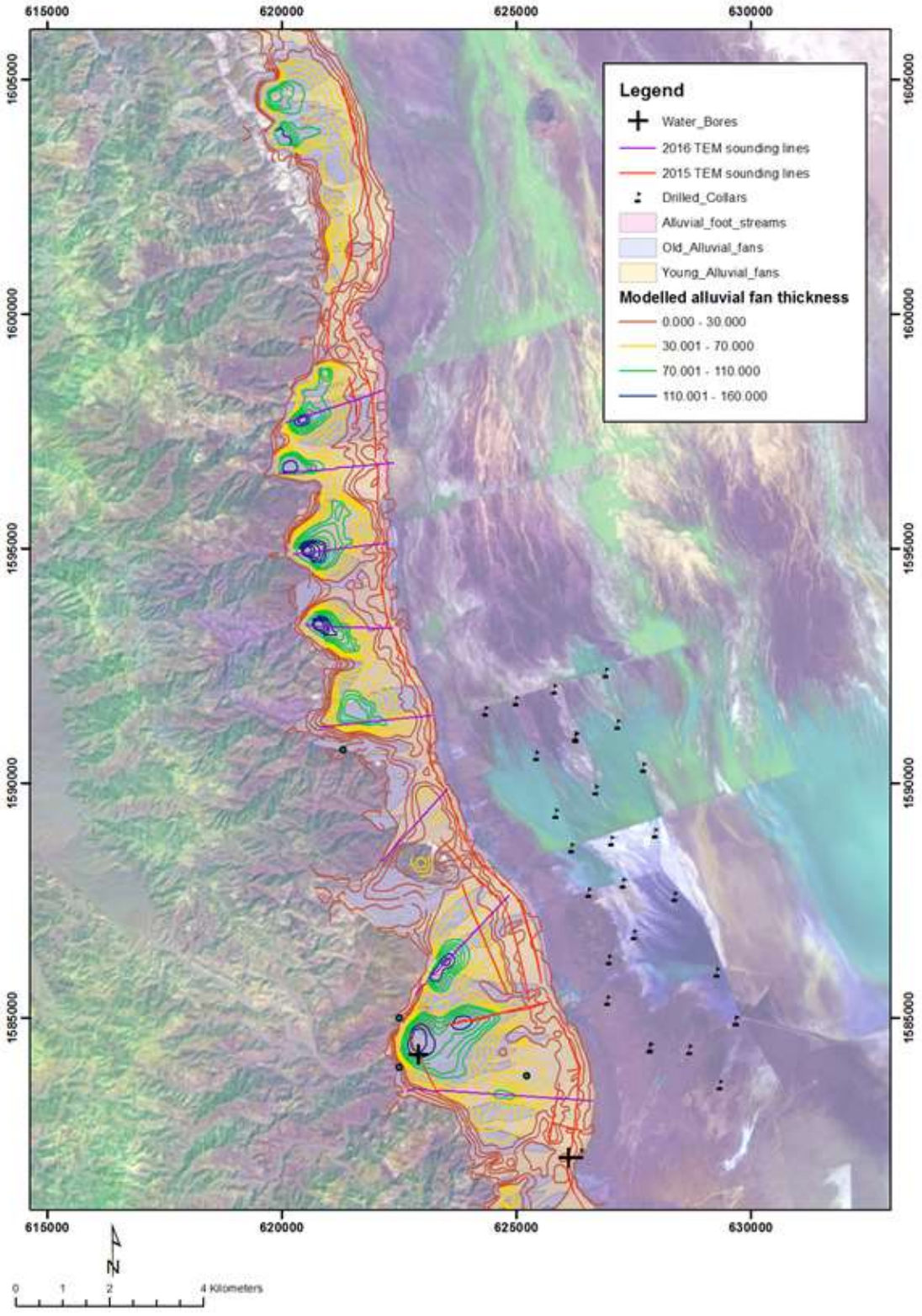

Figure 4-3 **Modelled alluvial fan thickness generated from field and remote sensing mapping (lateral) and inverted Time Electromagnetic (TEM) soundings (RES, 2016).**

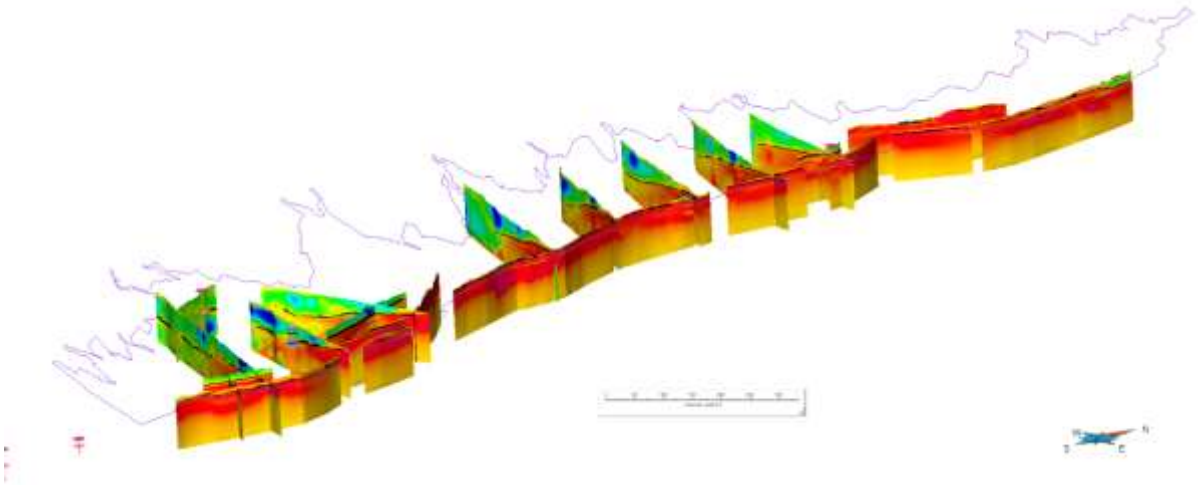

Figure 4-4 **Inverted 2D conductivity-depth sections from 2014 and 2016 MLEM data (Umvoto, 2016a).**

Figure 4-4 outlines the mapped alluvial fan contacts. Base of the resistive cover or top of conductor has been highlighted with a black line and represents the water table. The image is orientated north west and has a 5x vertical exaggeration (Umvoto, 2016a). Low conductivity, blue areas, can be seen to run through each fan from south to north and represent rift related faulting on which production boreholes were sited where drilling depth were achievable.

Optimal results were obtained using an unconstrained starting model with 25 layers, 300m depth of investigation, relatively conductive half-space, and Generalised Cross Validation (GCV) inversion method (RES, 2016). Results from the earlier 2014 MLEM survey were reprocessed and inverted using the same methodology to allow for overlap between the two surveys. The 2014 results were less informative due to their north south orientation elucidating very little of the fans structure as opposed to east-west orientated lines. Selected soundings were removed from the 2014 data where transmitter problems occurred and these lines were re-surveyed (Umvoto, 2016a).

4.2.3 Discussion

EM survey stations were collected amounting to 20 km of MLEM traverse data on the Dogua alluvial fans.

The salt units present in the basin floor were displayed as highly conductive units, sub cropping on the eastern edge of the alluvial fans (see **Figure 4-4**). These units were traced under moderately resistive alluvial fan sediments and provided a useful marker for estimating the alluvial fan thickness (Umvoto, 2016a). More resistive bedrock was apparent on the western edge of the fans. In the basin floor, depth of penetration was limited by conductive salt units although some structures and multiple conductive units were mapped in the upper 50 m (RES, 2016). This conductive unit corresponded well with groundwater levels obtained in previous drilling campaigns (Umvoto, 2015; WWDSE, 2013) carried out in the area.

A shallow resistive unit, followed by a continuous, thin conductive unit, which was in-turn underlain by more resistive units was apparent beneath all the traverses. The continuous conductor was interpreted to be related to a basal clay unit, or more likely, the water table situated above more resistive bedrock (Umvoto, 2016a).

4.3 BOREHOLE SITING

4.3.1 Dogua Formation Fans Borehole Siting

The geology and geophysical results were used to review and finalise positions and inform preliminary designs for three production boreholes in the Dogua Formation. As previously mentioned, these boreholes were named AY-P01 in the Asabuya Fan, BS-P01 in the Bussaba Fan and DN-P01 in the North Dogua Fan. In addition, five exploration or potential monitoring boreholes were sited in the Asabuya, Bussaba and North Dogua fans. These were named AY-M01 and AY-M02, BS-M01 and DN-M01 and DN-M02 respectively.

Borehole sites within the Dogua Formation targeted fault structures, depicted by the blue, less conductive zones, from the MLEM survey results (RES, 2016) (see **Figure 4-5**). These structures as well as the middle and younger, active portion of the fans were selected for their greater hydraulic potential, where better flow paths were expected (see **Table 4-1**). Most sites within the Dogua Formation were located on the north-south trending MDRF. Monitoring boreholes were sited above and below the production boreholes on the fans, or where specific geophysical anomalies were seen.

The alluvial fans appeared as low-conductive layers or wedges overlying more conductive units (see **Figure 4-4**). In the Dogua Formation this highly conductive material

correlated with and likely represented either basinal salt deposit wedges, or the water level of the highly saline groundwater encountered during drilling and test pumping of RAJ-1, RAJ-2 and DTW boreholes in the region.

Table 4-1 details the location, estimated water table depth and intended borehole depth of the boreholes sited in the Dogua Formation along with a brief description of the target site. In **Figure 4-5** faults are displayed by the black lines and coincide with the lower conductive, blue zones in the image. Boreholes were sited on these faults, but in this example the production borehole (BS-P01) targets a minor fault due to deeper drilling and pumping depths required on the higher MDRF.

Table 4-1 Proposed production and exploration or monitoring borehole sites in the Dogua Formation. Estimated water table depth based on geophysical survey results (Umvoto, 2016a).

Target Sites		Location (WGS 84 / UTM 37 P)		Elevation	Water Table Depth	Borehole Depth	Target Site Description
Fan	BH ID	m E	m N	mamsl	mbgl	mbgl	
Asabuya	AY-P01	624214	1586873	-60	120	170	Main Danakil Rift-Boundary Fault and two overlapping younger, active fans
	AY-M01	623733	1586443	-15	88	120	Younger, active fan and upgradient of AY-P01
	AY-M02	624677	1584600	-20	90	110	Main Danakil Rift-Boundary Fault and younger, active fan, upgradient of RAJ-1
Bussaba	BS-P01	622229	1591336	-30	85	160	Minor fault and younger, active fan
	BS-M01	622378	1591361	-45	152	160	Main Danakil Rift-Boundary Fault and younger, active fan, upgradient of BS-P01
Dogua North	DN-P01	621613	1596765	-85	32	124	Middle of two overlapping younger, active fans
	DN-M01	621126	1596728	-50	64	90	Minor fault and upgradient of DN-P01
	DN-M02	621675	1598363	-95	19	50	Main Danakil Rift-Boundary Fault and younger, active fan, upgradient of RAJ-2

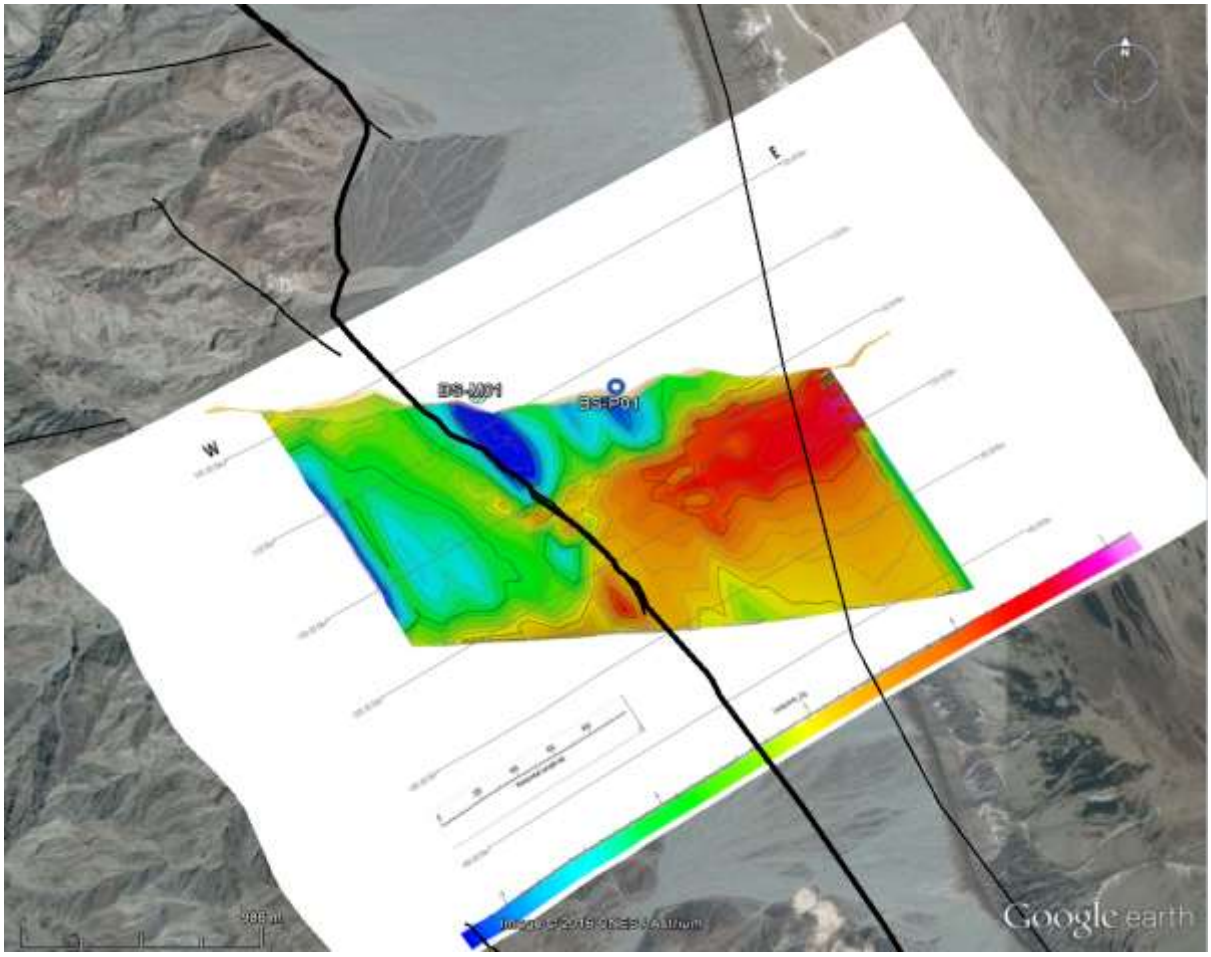

Figure 4-5 **Line 4 of the 2016 MLEM Survey conducted showing where borehole BS-P01 was sited over a low conductive zone representing a fault associated with the MDRF (Umvoto, 2016a).**

CHAPTER 5
BOREHOLE DRILLING

5.1 INTRODUCTION

This chapter summarises the results of the drilling and design of three production sized and five monitoring sized boreholes into the Dogua Alluvial Fan Complex. Drilling and design details of the two production sized boreholes, RAJ-1 and RAJ-2, drilled in 2015 in the Asabuya and North Dogua fans respectively (see **Section 3.2**), are also summarised.

The borehole sites selected to be drilled were AY-P01, AY-M01 and AY-M02 within the Asabuya Fan, BS-P01 and BS-M01 within the Bussaba Fan, DN-P01, DN-M01 and DN-M02 within the North Dogua Fan complex (see **Figure 5-7**),

Special consideration had to be given to design and construction of the boreholes due to the high temperature and salinity of the groundwater which is corrosive to casing and equipment and prone to scaling. The downhole geophysical logs, drilling penetration rates and rough borehole logs are included in **Appendix B**.

5.2 METHODOLOGY

Direct rotary drilling techniques (see **Figure 5-1**) were used to drill all the boreholes within the Dogua Formation. This was deemed the most suitable method based on the alluvial nature of the aquifer. Drilling fluid used was bentonite (sodic montmorillonite) which carried drill chips to the surface, helped maintain hydrostatic pressure in the borehole, prevented likelihood of borehole collapse, while simultaneously sealing the borehole walls to prevent fluid loss and cooling the drill bit. Fluid viscosity was measured on site with a typical marsh funnel.

Figure 5-1 **Mud rotary drilling technique. Shown is the smaller KLR rig drilling at DN-M02.**

Two drilling rigs were used to complete the drilling of the eight different boreholes. A large Ingersoll Rand (IR) rig and a smaller KLR rig. It was planned that the IR rig would be used to drill production sized boreholes and the KLR rig used to drill the smaller diameter monitoring boreholes.

Drilling of production boreholes commenced with a 22-inch (559 mm) tungsten carbide tricone bit and 18.5-inch (470 mm) starter casing installed to a depth of 3 mbgl. Drilling of pilot holes then continued with the 12.5-inch (317 mm) bit until target depths were attained. Thereafter the boreholes were reamed to final depth with the 17.5-inch (445 mm) reamer bit to achieve the desired diameter and cased or screened with 12.5-inch 316L stainless steel lengths (see **Figure 5-2**) of screen or casing.

Figure 5-2 Wire wrap 316L stainless steel screen.

Continuous slot screen (wire wrap) made form 316 L stainless steel was selected for its tensile and compressive strength, aperture size and design, which prevents sands from being sucked into the well during pumping (Driscoll, 1968).

Drilling of monitoring boreholes commenced with a 14-inch (356 mm) tricone bit and 13-inch (330 mm) starter casing installed to a depth of 3 mbgl. Thereafter drilling proceeded with the 10-inch (254 mm) drill bit to target depth with 6.5-inch (165mm) casing and screen installation. Reaming was not necessary due to the smaller diameter of the monitoring boreholes.

Rock chips recovered (see **Figure 5-3**) were logged per the SANS 633:2007 South African National Standard for Profiling, percussion borehole and core logging in Southern Africa standard (Standards South Africa, 2007) and the Munsell colour chart was used to describe the colour of the rock chips. Rock chips were collected for every meter drilled and in combination with the measured rest water level were used to determine the configuration of screen and casing installation. Screens were only installed below the water table and where there was a limited likelihood of fines entering the borehole. For intervals where fines were present, such as clay layers, solid or blind casing was used to prevent inflow of fines.

Figure 5-3 Manual logging of drill rock chips in 1 metre intervals.

Water needed for drilling was sourced from a combination of the Ragali River, when accessible and from the Badah village well.

Prior to casing installation, once target depth had been achieved, downhole electrical logging was carried out. Resistivity (long and short normal) and Spontaneous Potential (SP) parameters were surveyed for. These investigations, were variable in their accuracy and success, but the preliminary results were compared to that of the MLEM results and informed on borehole design based on downhole lithology and water table depth (see **Figure 5-4**). The electrical logging is typically useful for discerning different strata present in the borehole. In this case however, it did not indicate the presence of any defined clay layers or changes from sedimentary rock to igneous or metamorphic rock. When coupled with the drill chips, it was seen that the strata in the boreholes were too similar or relatively undifferentiated throughout and electrical logging was thus most useful in discerning the position of the water table rather than highlighting any major lithological changes, as these were not present (Driscoll, 1986).

Figure 5-4 Receiver unit used for downhole electrical logging.

A gravel pack or sleeve consisting of 4-9 mm river gravel was inserted into the annulus between the casing and borehole wall (see **Figure 5-5**). This acted to stabilise the borehole and the casing within it, while simultaneously increasing the conductivity immediately around the casing allowing water to flow easily into the borehole. The gravel pack was also useful for filtering water, by trapping a portion of the fines before they entered the well. Ideally well rounded and sorted gravel is used, but due to the remote location, the gravel sourced was not very well sorted or rounded (see **Figure 5-5**). Passing the gravel through a sieve prior to inserting it into the annulus assisted in constraining the degree of sorting, but not necessarily roundness.

Figure 5-5 **4-9 mm gravel pack inserted into the annulus between the casing and borehole wall.**

Borehole development (see **Figure 5-6**), by compressed air and surging, was carried out prior to well-head construction. Different boreholes were developed for varying amounts of time. Development typically continued for 12 hours per borehole or until the water expelled from the borehole was deemed to be at least 90 % clear of fines.

Hydrochemical samples (see **Figure 5-6**) were collected at the end of development and sent to an accredited laboratory for detailed analysis, the results of which are incorporated and discussed in **Chapter 7**.

Figure 5-6 **Hydrochemical sampling carried out during borehole development.**

Due to the uncertainty of the thickness or depth to the base of the alluvial aquifers and the drilling rigs capability, it was expected that most or all the boreholes drilled would only partially penetrate the aquifer, having possible head loss implications for time-drawdown analysis during pumping (Driscoll, 1986).

5.3 RESULTS

The final locations of the boreholes present in the Dogua Alluvial fans can be seen in **Figure 5-7** below. Included in the image are the two RAJ boreholes both drilled in 2015.

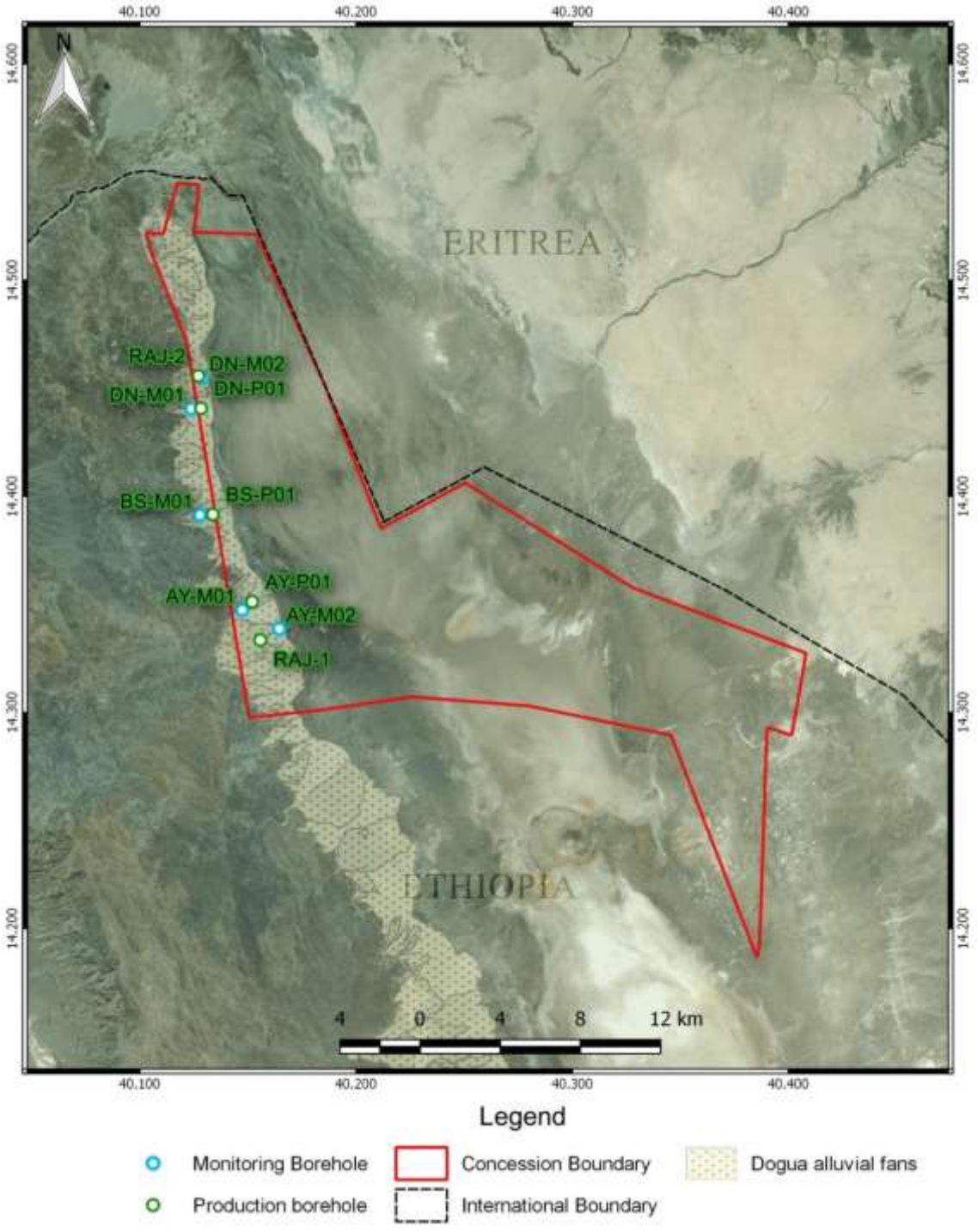

Figure 5-7 **Final location of boreholes present in the Dogua Alluvial Fan complex in relation to the mining concession (red polygon).**

5.3.1 Monitoring Boreholes

5.3.1.1 DN-M01

The lithological log and borehole construction details of monitoring borehole DN-M01 are provided in **Figure 5-8** along with the blow yield achieved during development and the rest water level as measured after the borehole could rest for a day.

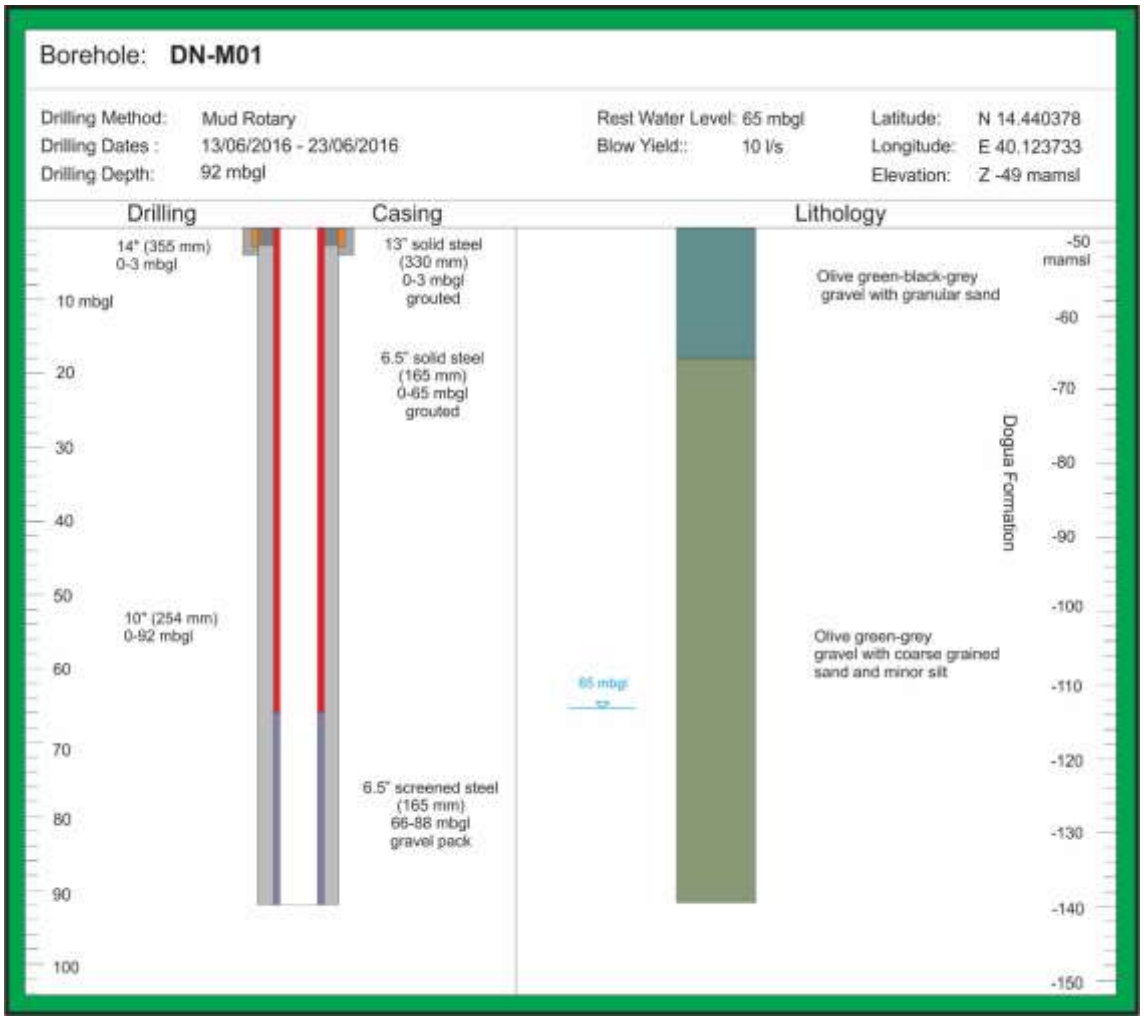

Figure 5-8 Lithological log, borehole design and drilling details for DN-M01.

5.3.1.2 DN-M02

The lithological log and borehole construction details of monitoring borehole DN-M02 are provided in **Figure 5-9** along with the blow yield achieved during development and the rest water level as measured after the borehole could rest for a day.

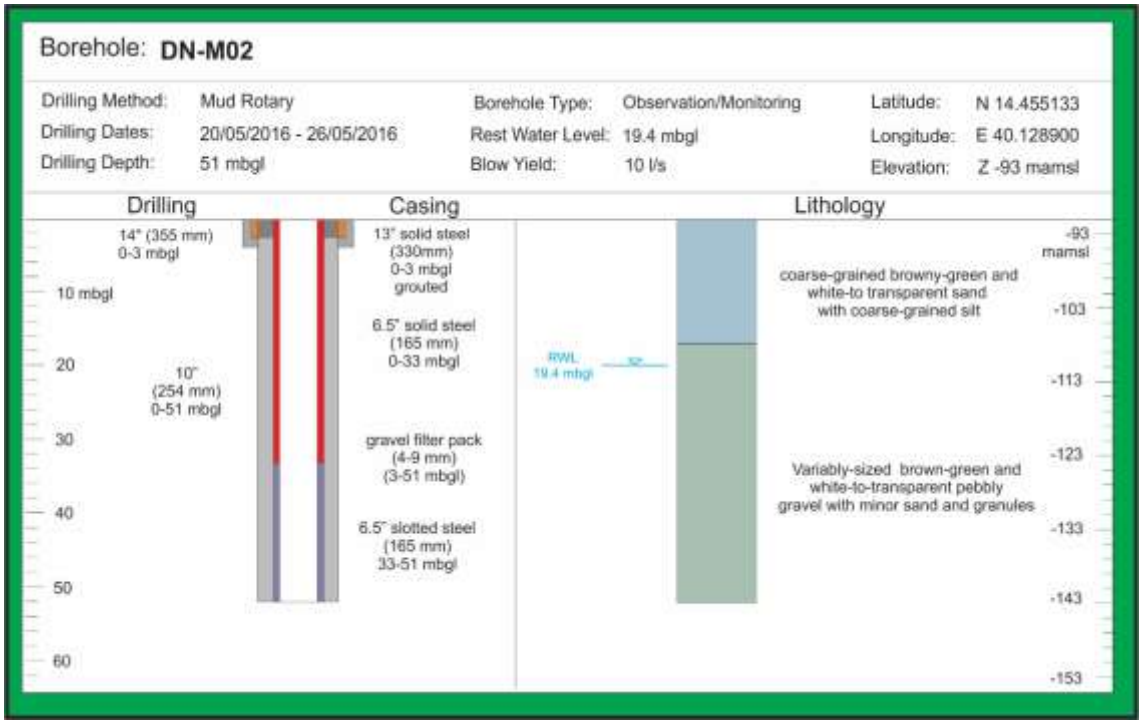

Figure 5-9 Lithological log, borehole design and drilling details for DN-M02.

5.3.1.3 BS-M01

The lithological log and borehole construction details of monitoring borehole BS-M01 are provided in **Figure 5-10** along with the blow yield achieved during development and the rest water level as measured after the borehole could rest for a day.

Figure 5-11 is an example of the final well head construction carried out on the monitoring and production boreholes. All the boreholes had a 1 m x 1 m x 1 m concrete block constructed around it at surface and were capped to prevent any contamination. Production boreholes were finalised in a similar manner, but provision was made for boreholes to be equipped.

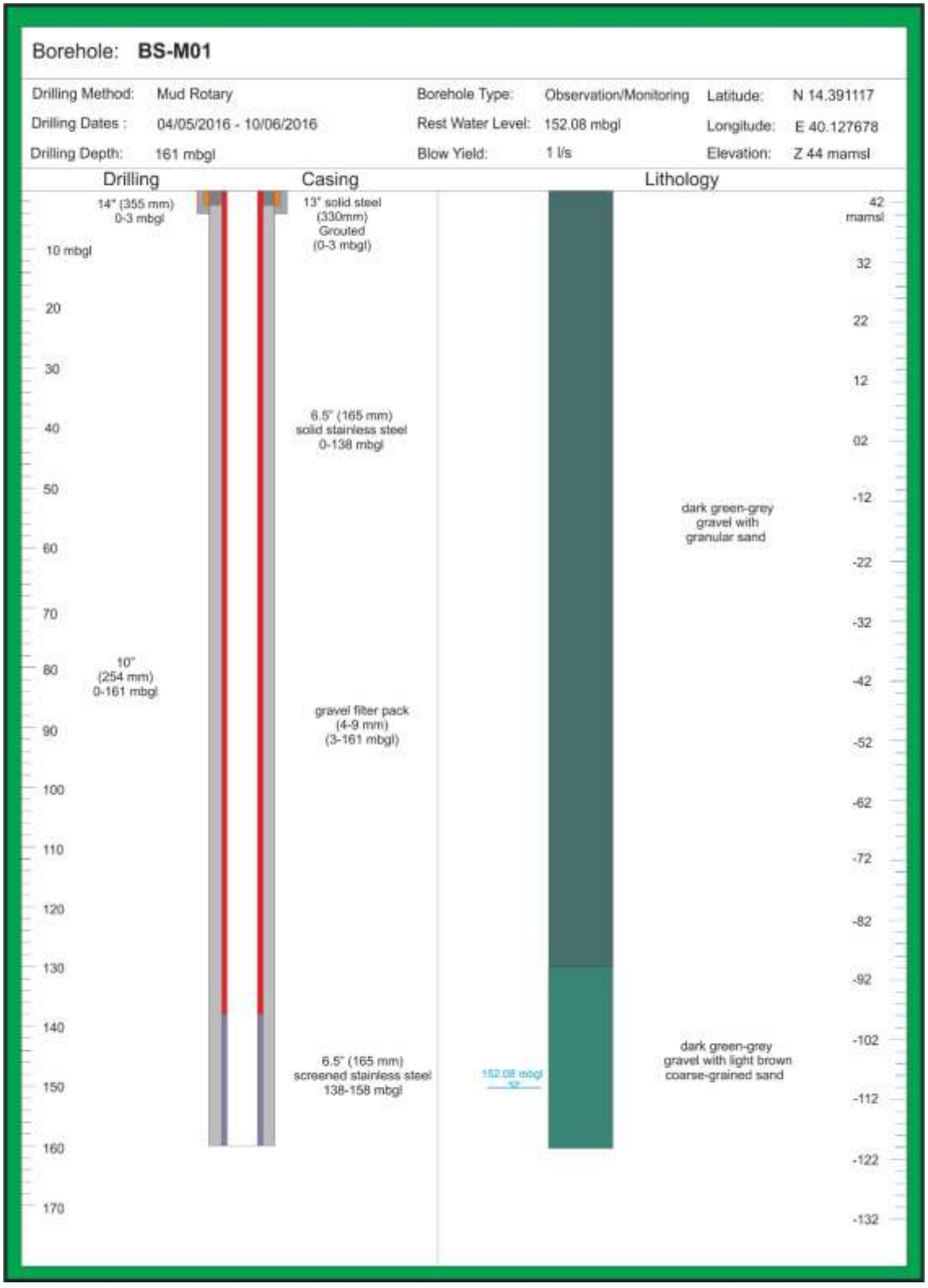

Figure 5-10 Lithological log, borehole design and drilling details for BS-M01.

Figure 5-11 Final well head construction at BS-M01 and BS-P01.

5.3.1.4 AY-M01

The lithological log and borehole construction details of monitoring borehole AY-M01 are provided in **Figure 5-12** along with the blow yield achieved during development and the rest water level as measured after the borehole was left to rest for a day.

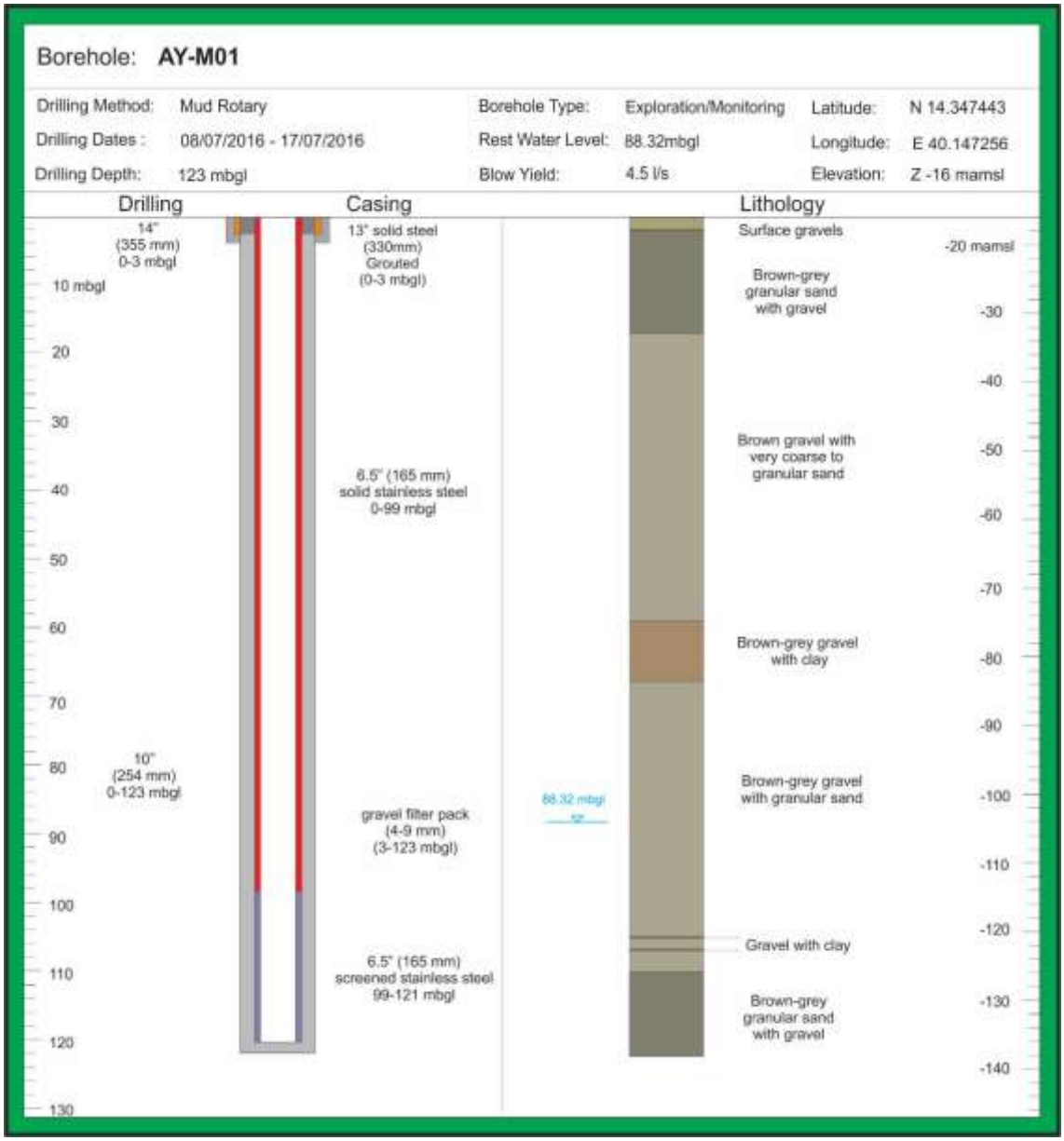

Figure 5-12 Lithological log, borehole design and drilling details for AY-M01.

5.3.1.5 AY-M02

The lithological log and borehole construction details of monitoring borehole AY-M02 are provided in **Figure 5-13** along with the blow yield achieved during development and the rest water level as measured after the borehole could rest for a day.

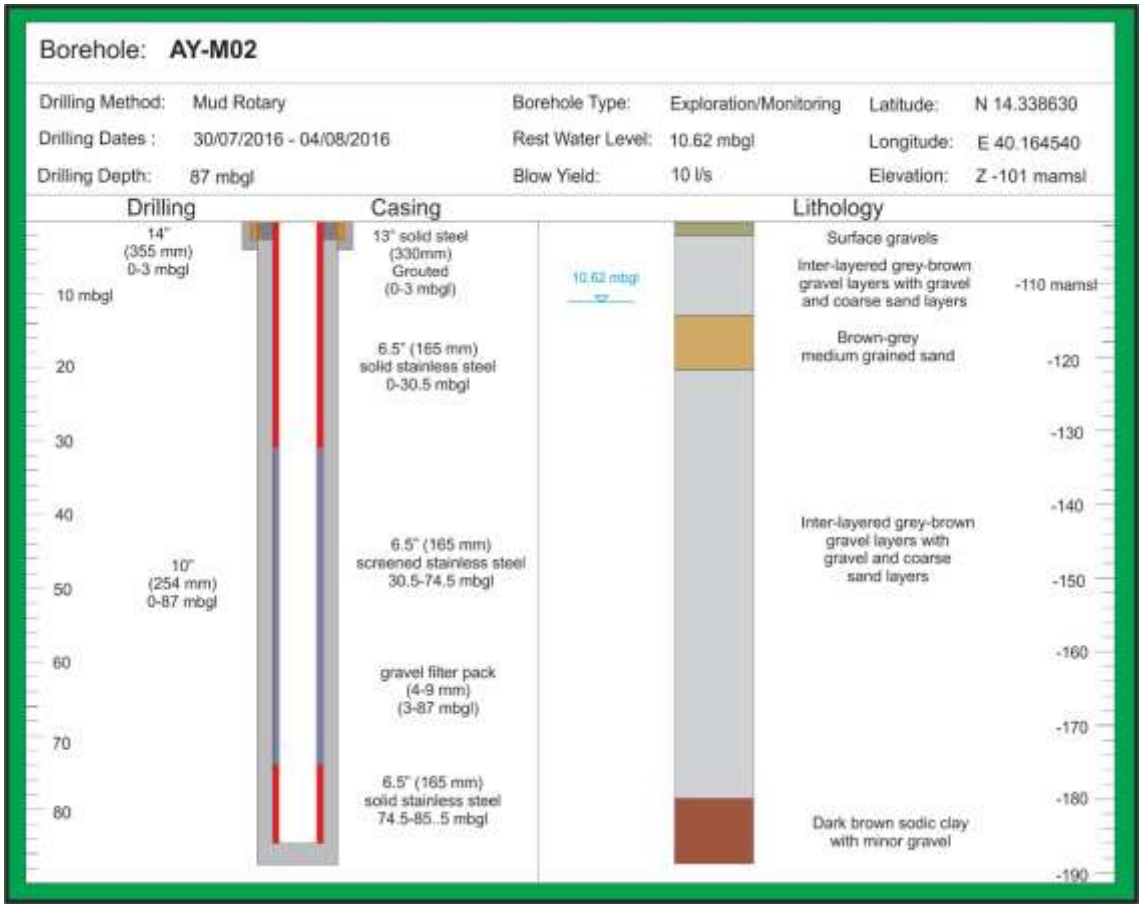

Figure 5-13 Lithological log, borehole design and drilling details for AY-M02.

5.3.2 Production Boreholes

5.3.2.1 DN-P01

The lithological log and borehole construction details of production borehole DN-P01 are provided in **Figure 5-14** along with the blow yield achieved during development and the rest water level as measured after the borehole could rest for a day.

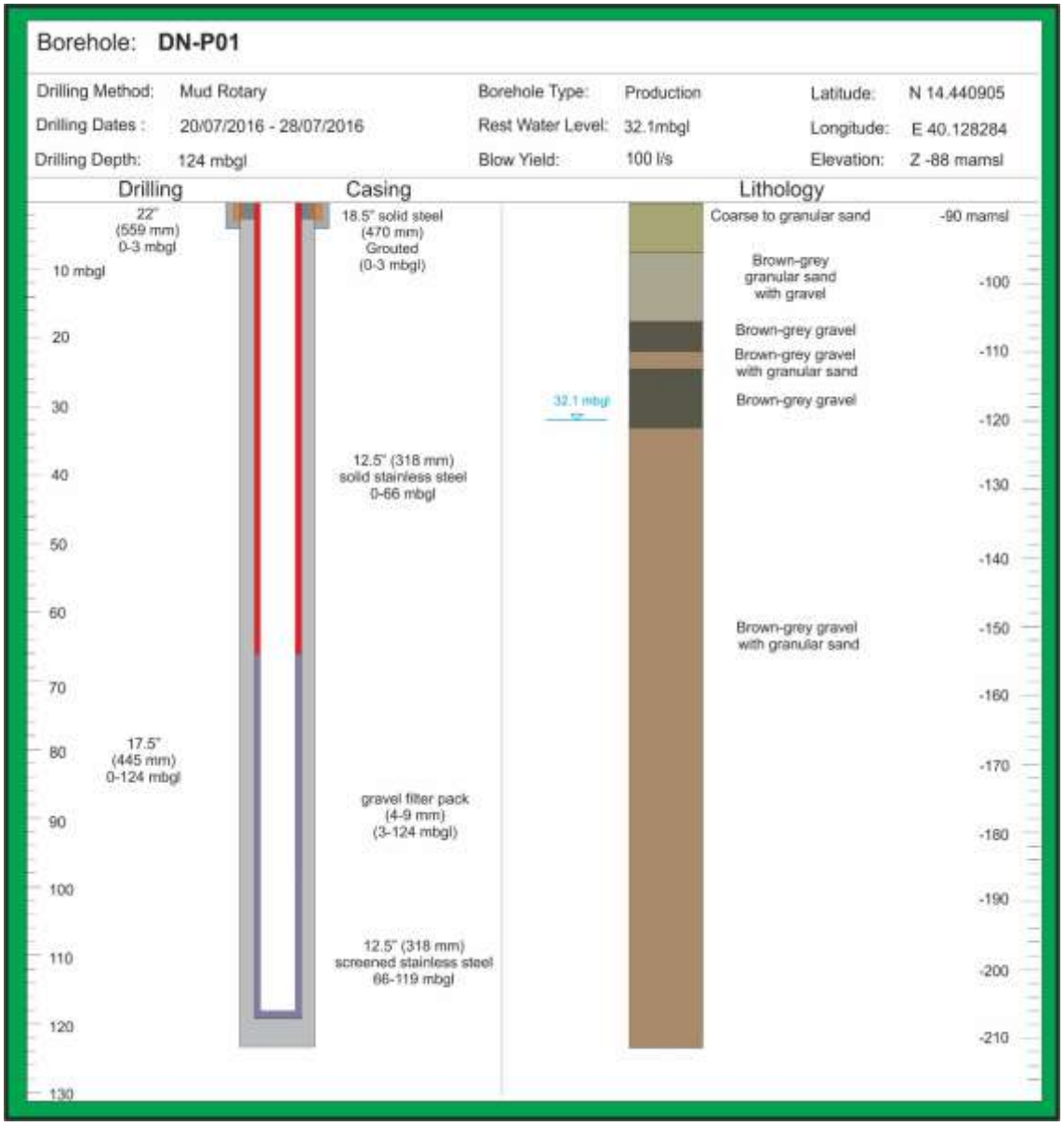

Figure 5-14 Lithological log, borehole design and drilling details for DN-P01.

5.3.2.2 BS-P01

The lithological log and borehole construction details of production borehole BS-P01 are provided in **Figure 5-15** along with the blow yield achieved during development and the rest water level as measured after the borehole could rest for a day.

5.3.2.3 AY-P01

The lithological log and borehole construction details of production borehole AY-P01 are provided in **Figure 5-16** along with the blow yield achieved during development and the rest water level as measured after the borehole could rest for a day.

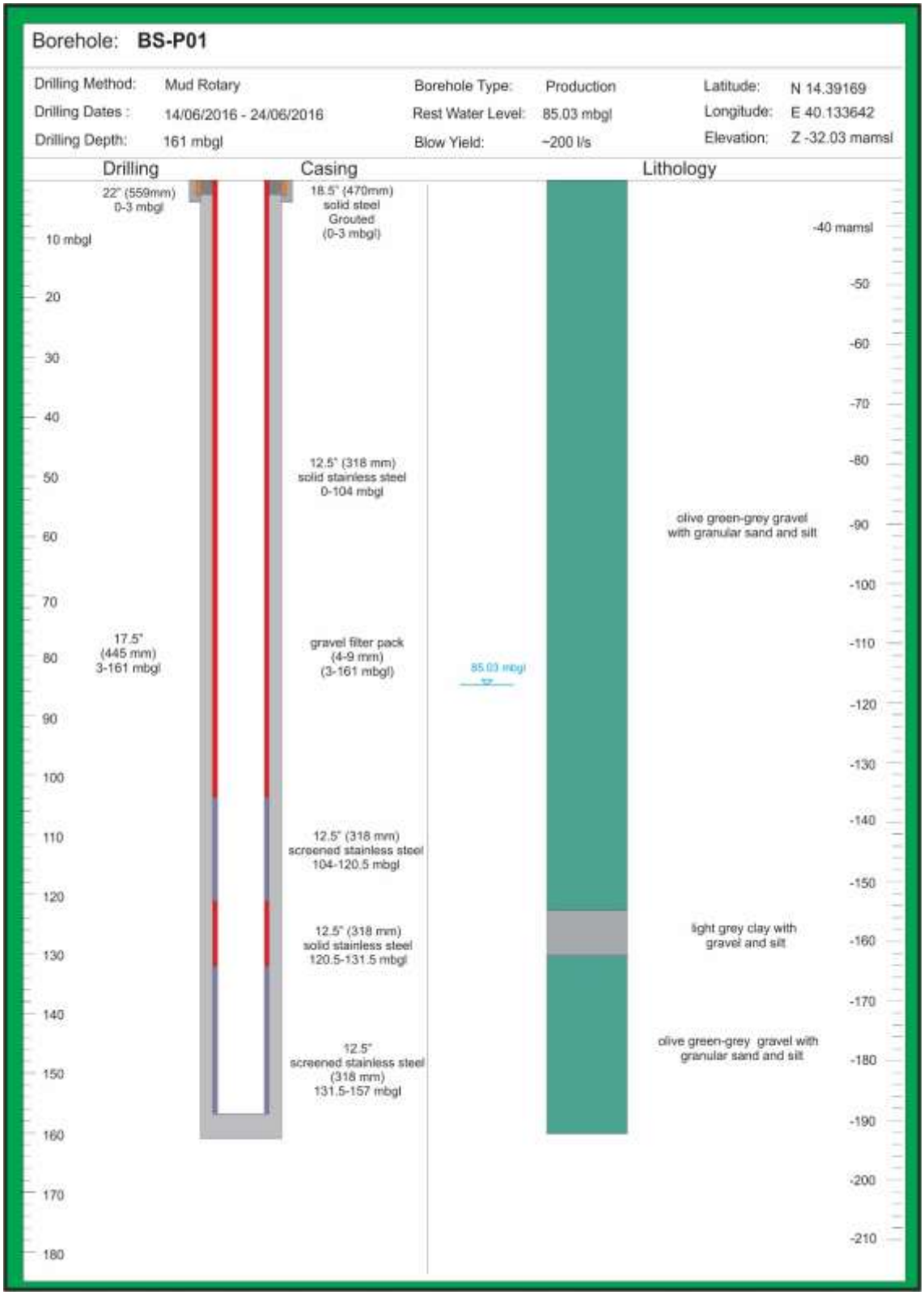

Figure 5-15 Lithological log, borehole design and drilling details for BS-P01.

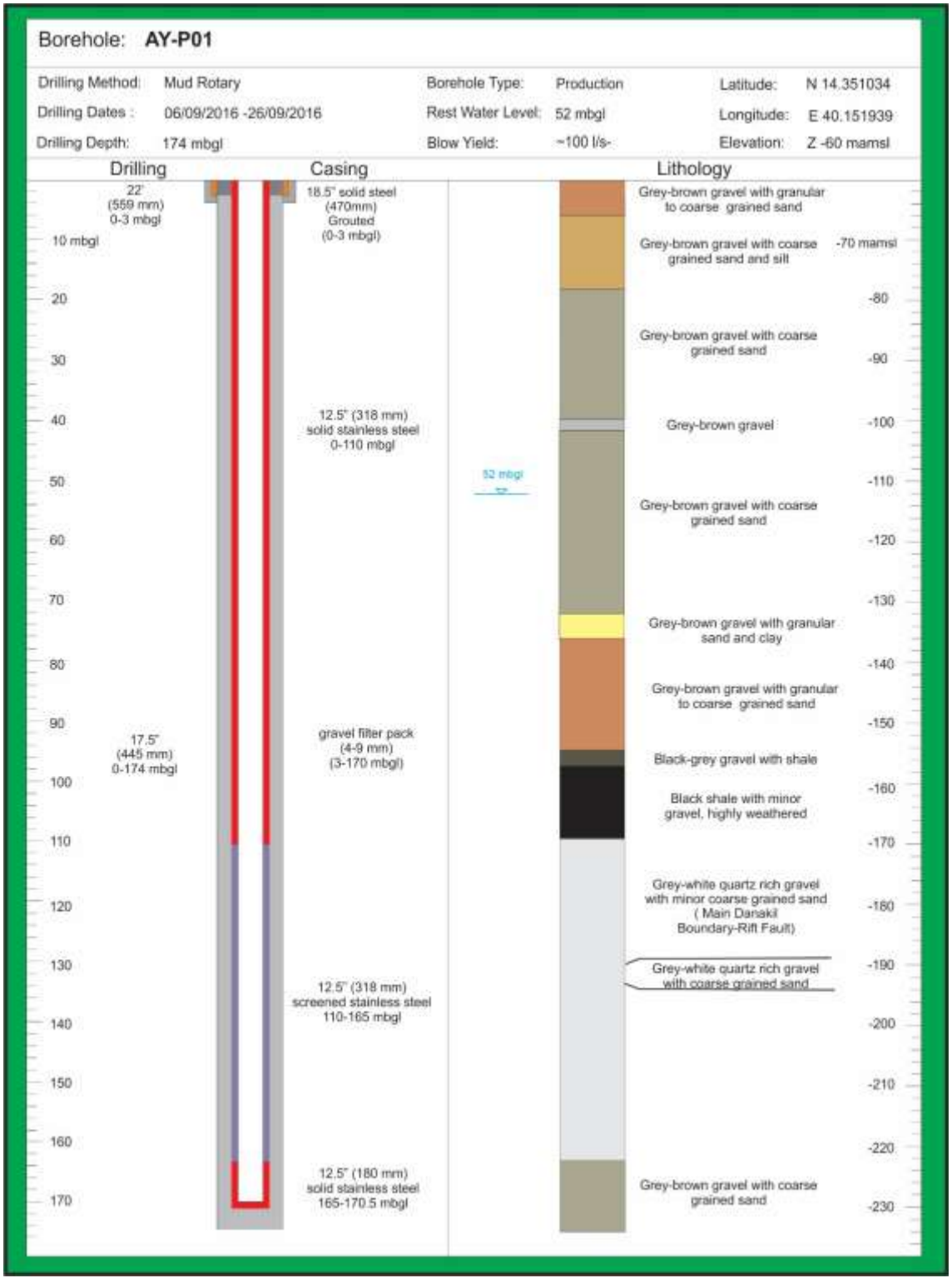

Figure 5-16 Lithological log, borehole design and drilling details for AY-P01.

Figure 5-17 Hand held EC and pH meters used to measure water quality in the field after development.

5.4 DISCUSSION

5.4.1 Monitoring Boreholes

5.4.1.1 DN-M01

Drilling of DN-M01 was hampered by mud loss at a depth of 18 mbgl; the borehole was grouted to stabilise the hole. The target depth of 90 mbgl was achieved after 10 days of drilling with minor rig repairs and maintenance having taken place.

Rock chips recovered from 0-18 mbgl were composed of variably sized dark green black gravel. Rock chips from depth 18-90 mbgl were composed of green-grey gravel with coarse grained sand and minor silt. There was very little variation in the rock chips

composition throughout and no evidence of any confining clay layers (MWH, 2015a) was present in the rock chips.

Downhole electrical logging took place prior to casing installation and while sufficient drilling mud was still present in the borehole. The results of the geophysical logging were inconclusive and deemed to be erroneous. The borehole was re-logged the following day (see **Appendix B** for geophysical logs). A positive anomaly at 60 mbgl correlated well with the inferred water table depth from the MLEM surveys.

The borehole design is illustrated in **Figure 5-8**. Casing comprised 66 m of 6.5" blank stainless-steel casing that was inserted between 0 and 66 mbgl and 22 m screened stainless steel casing between 66-88 mbgl. 4-9 mm gravel packing was inserted from 3-90 mbgl and the upper 3 m were grouted to prevent any contamination.

Well development by compressed air continued for approximately 15 hours. A stable blow yield of 10 l/s was measured. On site groundwater quality assessments (see **Figure** 5-17) indicated that the water was near neutral (pH = 7.1), but highly saline (E.C. > 4000 $\mu S.cm^{-1}$) with a temperature of ~40°C. A sample was collected for further hydrochemical analyses.

5.4.1.2 DN-M02

Drilling began at DN-M02 with the smaller KLR rig, but proved to be slow and progress was delayed by mud loss at a depth of 17 mbgl. Drilling was thus resumed with the bigger IR rig, and the viscosity of the drilling mud was increased. Steady progress was made thereafter and the target depth of 50 mbgl was reached within 8 days. Reaming and geophysical logging took place prior to casing installation

Rock chips recovered from the upper 17 metres of the borehole, which was drilled by the smaller KLR rig, revealed dark brown to dark green gravel with coarse-grained sand and silt. The lower 34 metres were composed of variably sized dark green and dark brown gravel with granular and coarse-grained silt. No distinct confining clay layers where intersected.

Downhole electrical logging was carried while sufficient drilling mud was still present in the borehole. The resistivity log (blue and red graphs in **Appendix B**) show a sharp drop in resistivity at approximately 20 mbgl. This is interpreted as the depth of the water table, which was later measured to be 19.4 mbgl. No noticeable anomalies were present in the spontaneous potential log (green graph in **Appendix B**).

The borehole design is illustrated in **Figure 5-9**. Casing installed comprised of 18 meters of 6.5” screened stainless steel casing, made up of two 5.5 m lengths and two 3.5 m lengths which were installed between 33 and 51 mbgl. The remainder was cased with six lengths of 5.5 m long 6.5” stainless steel blank casing each with a length of 5.5 m.

4-9 mm gravel pack was inserted between 3 and 51 mbgl. The borehole was developed for 12 hours with a stable blow yield of approximately 5 l/s. On site groundwater quality assessments indicated that the water is neutral (pH = 7.0), but highly saline (> 4000 µS.cm^{-1}) with a temperature of 46°C. Samples were collected for further chemical analyses.

Final well head construction was delayed by 3 days as the aggregate needed for mixing cement was not on site. To complete the well, suitably sized gravel was collected from the alluvial fan material and final grouting and well head construction was completed.

5.4.1.3 BS-M01

Drilling began and surface casing was installed to a depth of 3m. The grout holding the surface casing in place failed after 18 m of drilling and was re-grouted. Good progress was made and the target depth of 160 mbgl was reached after 5 days of drilling.

Drilling AY-M01 lithology from drilling chips is as follows (see **Figure 5-10**):

- 0 and 131 mbgl - dark-green gravels with minor coarse-grained sand.
- 132-161 dark green gravel with a component of light brown coarse-grained sand.

Drillers also reported that very little bentonite was needed to sustain mud viscosities below 120 mbgl indicating that there may be a higher clay content below this depth however, no evidence for the presence of significantly thick confining clay layers was present in the rocks chips.

Downhole electrical logging showed a positive anomaly at a depth of 130 mbgl (**Appendix B**). This correlated well with depth to the water table inferred from MLEM surveys. The static water level was however, later measured to be significantly lower at 152 mbgl.

The borehole design is illustrated in **Figure 5-10**. Casing was installed and comprised of 22 m of 6.5” screened stainless steel casing that was inserted between 138 and 160 mbgl and 138 m of 6.5” blank stainless-steel casing between 0 and 138 mbgl.

4-9 mm gravel pack was inserted from 3-160 mbgl and the upper three metres were grouted.

The well was developed for 16 hours achieving a blow yield of <1 l/s. This low yield has been attributed to the fact there was not enough water pressure to push the water out of the well during development; the small column of water present (10 m) was blown into the aquifer through the screened portion and did not effectively reach surface level. Water was poured down the borehole to assist in removing drilling fluid and fines from the well. On-site groundwater quality assessment indicated that the water is only slightly alkaline (pH = 8.0), yet highly saline (E.C.>4000 µS.cm^{-1}) and a temperature of 36°C. Water samples were collected for more detailed chemical analyses.

5.4.1.4 AY-M01

Drilling was initiated and took 8 days to complete. A starter casing was installed and grouted to a depth of 3 mbgl. Good drilling progress was made to a depth of 68 mbgl, when mud loss was experienced. Saw dust and bentonite balls were dropped down the borehole to plug the cavity, which proved to be successful, with drilling continuing to the target depth 123 mbgl. Drilling AY-M01 lithology from drilling chips is as follows (see **Figure 5-12**):

- 0-3 mbgl – surface gravels and granular sands,
- 3-18 mbgl – brown-grey granular sand with gravel,
- 18-60 mbgl – brown gravel with granular sand,
- 60-69 mbgl – brown gravel with grey clay,
- 69-109 mbgl – grey gravel with granular sand, with minor clay present with gravel at 105 mbgl and 107 mbgl,
- 109-123 mbgl – very coarse grained to granular sand with gravel.

Downhole electrical logging showed an anomaly at a depth of 90 mbgl across all three types (SP, long and short resistivity) (**Appendix B**). This correlated well with depth to the water table inferred from the MLEM surveys. The static water level was later measured to be at 88.3 mbgl.

The borehole construction is illustrated in **Figure 5-12**. Casing was installed and comprised of 99 m of 6.5” blank stainless-steel casing between 0-99 mbgl, and 22 m of 6.5” screened stainless steel casing between 99-121 mbgl.

4-9 mm gravel pack was inserted into the annulus between the casing and borehole wall from 3-160 mbgl, whereas the top 3 m of annulus was grouted.

The well was developed for 14 hours achieving a blow yield of 4-5 l/s. On-site groundwater quality assessment indicated that the water is slightly alkaline (pH = 7.3), highly saline (E.C.>4000 µS.cm^{-1}), and a temperature of 45.7°C. Water samples were collected for more detailed chemical analyses.

5.4.1.5 AY-M02

AY-M02 proved to be the most challenging borehole to drill within the Dogua Formation alluvial fans. Drilling first began with considerable mud loss occurring at depths of 8 mbgl and 10 mbgl. Thus, it was decided that drilling would be restarted at a new position on the drill pad. Substantial mud loss was encountered again at 23 mbgl, which continued despite the viscosity of the mud being increased. These near surface mud losses were believed to be caused by the intersection of an adjacent, highly permeable north-north-east and south-south-west (NNE-SSW) orientated fault zone. Although such losses were not expected, as the RAJ-1 production borehole had been drilled adjacent to the current location and into the same fault without extensive delays or mud loss issues (Umvoto, 2015). It was decided that the hole would be grouted to seal the fluid pathway (and prevent mud loss), and as the grout would take some days to set, the decision was made to pause drilling and revisit the site at a later stage. Three metres of starter casing was installed and the borehole was grouted down to 23 mbgl, and the rig was moved to drill other monitoring boreholes.

When drilling at AY-M02 was resumed following grouting an additional mud loss occurred at 27 mbgl. Drilling started again with the 27 mbgl mud loss ceasing and drilling continued to 43 mbgl. At 41 mbgl however considerable and irrecoverable mud loss and borehole collapse were experienced. It was decided to once again pause drilling and seek a solution to the mud loss. Saw dust and bentonite balls were dropped down the hole to plug the cavity and minimise the mud loss experienced at 41 mbgl. This proved to be effective, but once again an irrecoverable mud loss was encountered at 50 mbgl. The borehole was grouted with gypsum in a final effort to overcome the mud loss, but was declared abandoned when further penetration could not be achieved. It was decided to re-locate AY-M02 to a new site approximately 1.3 km down-fan of the initial AY-M02 site, which would be a shallow borehole (<70 mbgl).

Mobilisation of the KLR rig to the AY-M02 Fly Camp site took place, with drilling progress being good to the estimated depth of 70 mbgl, thereafter it was decided to continue drilling until the basement be intersected, this happened at 78 mbgl. Drilling continued to the completion depth of 87 mbgl. AY-M02 lithology from drilling chips were as follows (see **Figure 5-13**):

- 0-3 mbgl –surface gravels
- 4-14 mbgl – brown-grey gravel alternating with gravel and coarse-grained sand
- 15-21 mbgl – brown-grey medium grained sand
- 22-78 mbgl - brown-grey gravel alternating with gravel and coarse-grained sand
- 79-87 mbgl – dark brown sodic mud with minor gravels

Downhole electrical logging was carried out but, no anomaly linked to water level could be found in any of the parameters (SP, long and short resistivity) because the survey started at a depth of 13 mbgl, below the static water level of 10 mbgl (**Appendix B**).

The borehole construction is illustrated in **Figure 5-13**. Casing was installed and comprised of 41.5 m of 6.5" blank stainless-steel casing between 0-30.5 mbgl and 74.5-85.5 mbgl, and 44 m of 6.5" screened stainless steel casing between 30.5-74.5 mbgl.

4-9 mm gravel pack was inserted into the annulus between the casing and borehole wall from 3-85.5 mbgl, whereas the top 3 m of annulus was grouted.

The well was developed for 12 hours achieving a blow yield of 10 l/s. On site groundwater quality assessment indicated that the water is acidic (pH = 5.4), highly saline (E.C.>4000 $\mu S.cm^{-1}$) and a temperature of 43 °C. Water samples were collected for more detailed chemical analyses.

5.4.2 Production Boreholes

5.4.2.1 DN-P01

Drilling began at a diameter of 22", with 18.5" diameter starter casing installed and grouted to a depth of 3 mbgl. Drilling continued at a diameter of 12.5" until the target depth of 124 mbgl was attained after approximately 7 days. Once the target depth was reached, the borehole was reamed twice at 17.5" diameter to a depth of 124 mbgl to ensure casing and screen installation would not be hindered.

Downhole electrical logging took place and an anomaly was observed at 32 mbgl across all three types (SP, long and short resistivity), which correlated well with the expected depth to the water table inferred from the MLEM survey carried out. The rest water level was later measured at 32.1 mbgl. DN-P01 lithology from drilling chips was as follows (see **Figure 5-14**):

- 0-4 mbgl – grey, medium to coarse grained sand
- 5-8 mbgl – coarse to granular sand

- 9-18 mbgl – brown-grey granular sand with grave
- 19-124 mbgl – grey-brown gravel with granular sand, with certain intervals showing a greater occurrence of granular sand than others

Casing installation at DN-P01 comprised of 66 m of 12.5” blank stainless-steel casing between 0-66 mbgl and 53 m of 12.5” screened stainless steel casing between 66-119 mbgl. Casing however, was blocked at 86 mbgl due to boulders collapsing from the surface and jamming the casing at 20 mbgl. The casing was pulled and the borehole reamed for a third and fourth time. During reinstallation of the casing another boulder jammed the casing, requiring it be pulled again and a fifth reaming conducted. Thereafter the casing was successfully installed to a depth of 119 mbgl.

4-9 mm gravel pack was inserted into the annulus between the casing and borehole wall from 3-119 mbgl, whereas the top 3 m of annulus was grouted.

The well was developed for 12 hours. The water expelled from the borehole during development was deemed to be 95% clean, but development was ceased due to the amount of expelled water de-stabilising the rigs’ jacks and creating a safety risk. On-site groundwater quality assessment indicated that the water is acidic (pH = 5.4), highly saline (E.C.>4000 µS.cm^{-1}), and a temperature of 49.1°C. Water samples were collected for more detailed chemical analyses.

5.4.2.2 BS-P01

Drilling began at a diameter of 22”, with starter casing of 18.5” diameter installed and grouted to a depth of 3 mbgl. Drilling continued at a diameter of 12.5” until the target depth of 160 mbgl was reached after 6 days. Reaming of the borehole at 17.5” diameter had commenced when hydraulic failure resulted in the rig being idle for a day. Repairs were carried out and reaming continued to target depth of 160 mbgl. The borehole was reamed a second time at the same diameter to ensure the hole was open and that casing would not get stuck during installation. Mud loss was experienced during the second ream, but the borehole walls remained stable. BS-P01 lithology from drilling chips was as follows (see **Figure 5-15**):

- 0 and 122 mbgl light - dark green gravel with minor coarse-grained sand and silt.
- 122 - 130 mbgl light-grey clay with gravels and minor silt
- 130 - 160 mbgl dark green gravels with brown coarse-grained sand.

Downhole geophysical logging revealed no noticeable anomalies, however a gradual decrease in the short normal resistivity was observed between 80-90 mbgl. This

correlated well with depth of the water table inferred from the MLEM survey carried out (see **Appendix B**).

The borehole design is illustrated in **Figure 5-15**. Casing was installed and comprised of 25.5 m of 12.5" screened stainless steel casing that was inserted between 131.5-157.5 mbgl. The potentially confining clay layer was cased off with 11 m of 12.5" solid stainless-steel casing between 120.5-131.5 mbgl to prevent any fines from entering the borehole. 16.5 m of stainless steel screen was again installed between 104-120.5 mbgl. From 0-104 mbgl 12.5" solid stainless-steel casing was installed.

4-9 mm gravel pack was inserted from 3-160 mbgl and the well was developed for 22 hours. A blow yield was challenging to record as the flow of water was not constant, but pulsed as the compressor lacked volume to maintain the flow of water. It was estimated that the yield was 200 l/s per pulse.

On site groundwater quality assessment revealed that the groundwater is slightly acidic (pH = 6.2) and is highly saline (EC > 4000 µS.cm^{-1}) with a temperature of 44°C.

5.4.2.3 AY-P01

Drilling began with the IR rig, but was hindered by mud loss throughout and finally abandoned. Drilling was relocated to a new site, 30 meters away. Drilling resumed at a diameter of 22", with starter casing of 18.5" diameter installed and grouted to a depth of 3 mbgl. Drilling continued at a diameter of 12.5", until mud loss was encountered at a depth of 81 mbgl. To overcome the mud loss saw dust and bentonite balls were dropped down the borehole. Reaming at 17.5" diameter was undertaken to 81 mbgl, whilst the bentonite and sawdust sealed the cavity, this proved successful and drilling at 12.5" diameter continued. Target depth of 174 mbgl was achieved, with reaming at 17.5" diameter taking place thereafter. AY-P01 lithology from drilling chips was as follows (see **Figure** 5-16):

- 0-6 mbgl – grey-brown gravel with coarse to granular sand;
- 7-18 mbgl – grey-brown gravel with coarse grained sand and silt;
- 19-40 mbgl – grey-brown gravel with coarse grained sand;
- 41-43 mbgl - grey-brown gravel;
- 44-71 mbgl – grey-brown gravel with coarse grained sand;
- 72-76 mbgl - grey-brown gravel with coarse grained sand and clay;
- 77-95 mbgl - grey-brown gravel with coarse to granular sand;
- 96-99 mbgl – black-grey gravel with shale;

- 100-109 mbgl – black shale with minor gravel, highly weathered;
- 110-129 mbgl – grey-white quartz rich gravel with minor coarse-grained sand;
- 130-133 mbgl - grey-white quartz rich gravel with coarse grained sand;
- 134-162 mbgl - grey-white quartz rich gravel with minor coarse-grained sand;
- 163-174 mbgl - grey-brown gravel with coarse grained sand.

The quartz rich gravel between 110-162 mbgl was interpreted to be associated with the Main Danakil Rift-Boundary Fault.

Downhole electrical logging was done but, no anomaly linked to water level could be found in any of the parameters (SP, long and short resistivity) (**Appendix B**). A large anomaly at 81 mbgl was noted across all three parameters. This was likely associated with the sawdust that was used to plug the cavity at 81 mbgl.

The borehole construction is illustrated in **Figure 5-16.** Casing was installed, but became stuck at 148 mbgl, this was finally overcome and casing installed to the bottom of the borehole at 170.5 mbgl. The casing comprised of 115.5 m of 12.5" blank stainless-steel casing between 0-110 mbgl and 165-170.5 mbgl, and 55 m of 12.5" screened stainless steel casing between 110-165 mbgl.

4-9 mm gravel pack was inserted into the annulus between the casing and borehole wall from 3-170.5 mbgl, whereas the top 3 m of annulus was grouted.

The well was developed for 12 hours, achieving an estimated blow yield of 100 l/s. On site groundwater quality assessment indicated that the water is slightly acidic (pH = 6), highly saline (E.C.>4000 $\mu S.cm^{-1}$), with a temperature of 56.2°C. Water samples were collected for more detailed chemical analyses.

5.5 SUMMARY AND CONCLUSION

The location and details of all boreholes in the Dogua Alluvial Fan Complex are shown in **Figure 5-7**, **Table 5-1** and **Table 5-2**.

Table 5-1 Summary of the monitoring borehole drilling and design.

2016 Monitoring Boreholes						
Dogua Mountains Alluvial Fans						
Borehole		**DN-M01**	**DN-M02**	**BS-M01**	**AY-M01**	**AY-M02**
Northing	m N	1596747.88	1598342.72	1591303.68	1586459.28	1585493.72
Easting	m E	621131.57	621678.17	621579.34	623711.97	625580.89
Latitude	N	14.440566	14.454959	14.391331	14.347443	14.338630
Longitude	E	40.123795	40.128938	40.127701	40.147256	40.164540
Elevation	mamsl	-59.29	-98.59	34.35	-15.83	-101.00
End of Hole	mbgl	90	51	161	123	87
	masml	-149	-150	-127	-139	-188
Rest Water Level	mbgl	63.92	19.1	152.08	88.32	10.62
	mamsl	-123.21	-117.69	-117.73	-104.15	-111.62
Borehole Diameter and Depth	mm (mbgl)	375 (0-3)	375 (0-3)	375 (0-3)	375 (0-3)	375 (0-3)
		254 (3-90)	254 (3-51)	254 (3-161)	254 (3-123)	254 (3-87)
Casing Diameter and Depth	mm (mbgl)	330 (0-3) / solid steel	330 (0-3) / solid steel	330 (0-3) / solid steel	330 (0-3) / solid steel	330 (0-3) / solid steel
		165 (0-66) / solid stainless API steel	165 (0-33) / solid stainless API steel	165 (0-138) / solid stainless API steel	165 (0-99) / solid stainless API steel	165 (0-30.5) / solid stainless API steel
		165 (66-88) / screened stainless API steel	165 (33-51) / screened stainless API steel	165 (138-158) / screened stainless API steel	165 (99-121) / screened stainless API steel	165 (30.5-74.5) / screened stainless API steel
						165 (74.5-85.5) / solid stainless API steel

Table 5-2 Summary of the production borehole drilling and design.

Dogua Mountains Alluvial Fans Production Boreholes						
Year		**2015**		**2016**		
Borehole		**RAJ-1**	**RAJ-2**	**DN-P01**	**BS-P01**	**AY-P01**
Northing	m N	1584915.51	1598418.41	1596787.75	1591346.86	1586859.68
Easting	m E	624632.08	621480.64	621615.31	622219.72	624215.02
Latitude	N	14.333446	14.455652	14.440905	14.391693	14.351034
Longitude	E	40.155716	40.127109	40.128284	40.133642	40.151939
Elevation	mamsl	-27.83	-84.40	-88.46	-32.03	-60
End of Hole	mbgl	165	77	124	160	170
	masml	-193	-161	-212	-192	-230
Rest Water Level	mbgl	78.95	30.9	32.1	85.03	52
	mamsl	-106.78	-115.30	-120.56	-117.06	-112.00
Borehole Diameter and Depth	mm (mbgl)	600 (0-4.8)	600 (0-5)	559 (0-3)	559 (0-3)	559 (0-3)
		445 (4.8-165)	445 (5-77)	430 (3-124)	430 (3-160)	430 (3-170)
Casing Diameter and Depth	mm (mbgl)	473 (0-4.8) / solid API steel	473 (0-5) / solid API steel	483 (0-3) / solid steel	483 (0-3) / solid steel	483 (0-3) / solid steel
		340 (0-113.5) / solid API steel	340 (0-46) / solid API steel	320 (0-66) / solid stainless API steel	320 (0-104) / solid stainless API steel	320 (0-110) / solid stainless API steel
		340 (113.5-163.5) / screened API steel	340 (46-76) / screened API steel	320 (66-119) / screened stainless API steel	320 (104-120.5) / screened stainless API steel	320 (110-165) / screened stainless API steel
		-	-	-	320 (120.5-131.5) / solid stainless API steel	320 (165-170.5) / solid stainless API steel
		-	-	-	320 (131.5-157) / screened stainless API steel	-

All the boreholes drilled, as well as the RAJ-1 and RAJ-2 boreholes were partially penetrating the unconfined alluvial aquifer. This may have implications in pump test data analyses.

Water-table measurements from all drilling undertaken, the elevations of springs, seeps and lower-reach stream profiles, assuming the water table was 1 m below river surfaces, informed a regional piezometric map (see **Figure 5-18** and **Figure 5-19** below). **Figure** 5-18 is a water level map in mamsl covering the North Danakil basin, computed by bicubic spline interpolation from the water level of newly drilled Dogua Formation boreholes which are annotated, other wells in the region shown as blue dots and surface hydrology constraints provided by seeps and fan-wadi and salt flat drainage channels shown as black lines. Ethiopia Eritrea border which is shown as a black dashed line and the mining concession boundary as a red polygon. The data control on the western side of the map is considered limited to poor.

Figure 5-19 is a water level map in mbgl obtained by subtracting the modelled piezometric surface in **Figure 5-18** from the ALOS AW3D30 digital elevation model.

When the width of the accessible water table was set to <100 m, it was seen to be greatest around the head of the Asabuya fan in the south-eastern part of the mining concession and narrowest around the faulted western boundary of the alluvial fans between the Bussaba and North Dogua areas.

When considering these water level maps in conjunction with probable flow paths using the structural geology and hydrostratigraphy, these data and information informed the differences and in some cases the similarities in the hydrogeological and hydrological setting of the Dogua Alluvial fans in the north compared to the Musley, Gehertu and Saba fans in the south. Hydrochemical analyses and interpretation further increased confidence in such interpretations.

The drilling results of boreholes drilled in the Asabuya fan were particularly useful as AY-M02, which was drilled near the toe of the fan indicated a fan thickness of at least 79 m, while the location of RAJ-1 in the middle of the fan showed a minimum thickness of 170 m. These values were combined with the results of the geophysics and increased confidence in determining the geometry of the fan. The drilling depths attained as well as the measurable water levels between the top, middle and bottom of the fan could thus also contribute to estimating potential volume of storage within the fan.

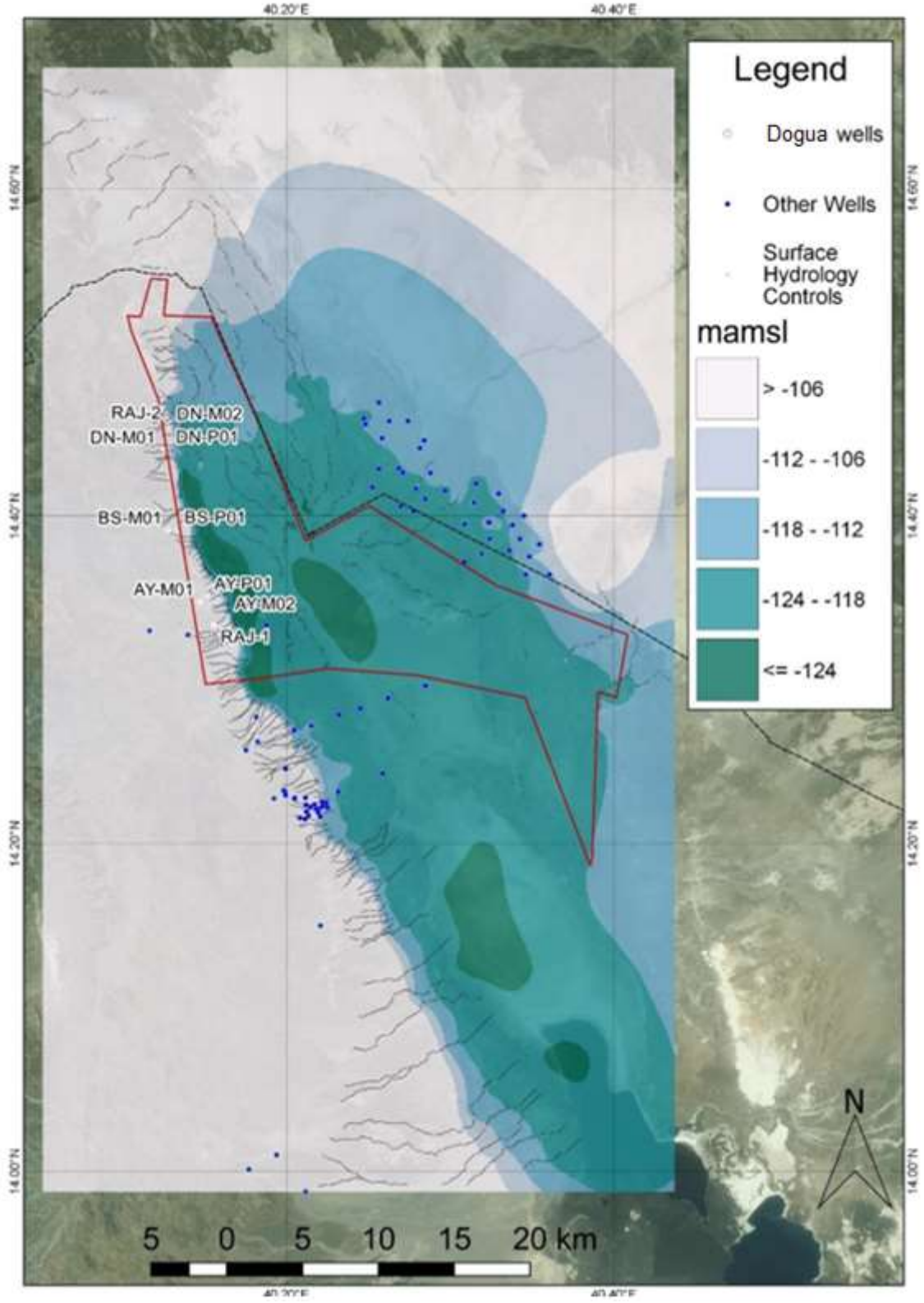

Figure 5-18 Water level map in mamsl of the Norther Danakil basin around the study site area (red polygon) (Umvoto, 2016g).

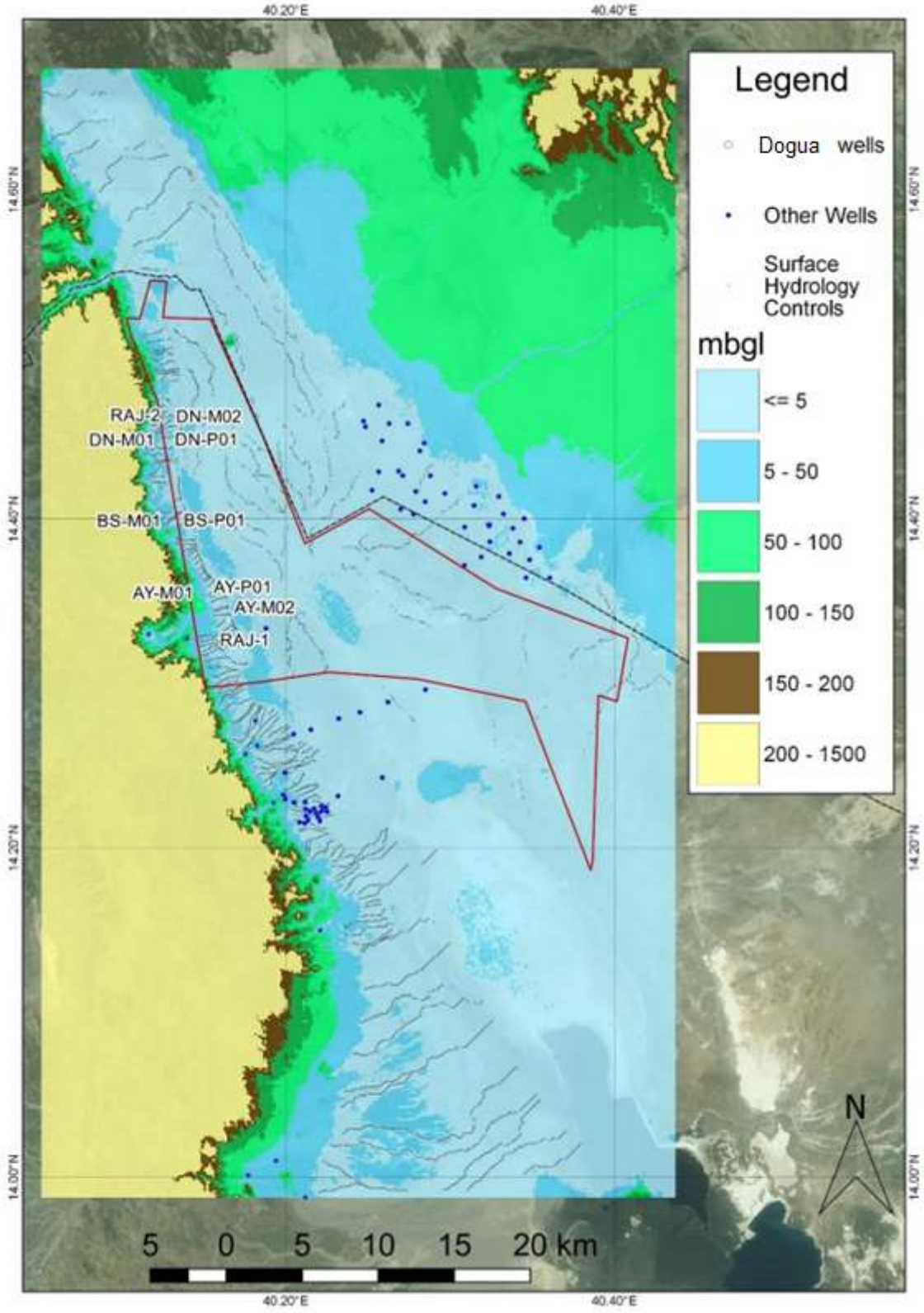

Figure 5-19 Water level map in mbgl based on Figure 4-19 above (Umvoto, 2016g).

CHAPTER 6

TEST PUMPING AND AQUIFER STRESS TEST

6.1 INTRODUCTION

Eighty-hour pump testing was carried out at DN-P01, BS-P01 and AY-P01. It was originally planned for the tests to each consist of a step-drawdown test and recovery, to determine the optimal discharge rate for the Constant Rate Test (CRT). After this the CRT would continue for 72 hours followed by recovery measurements to within 95% of the rest water level prior to pumping. The AST would then be conducted at the predetermined discharge rate with each borehole pump being switched on 24 hours apart until all five boreholes were being pumped simultaneously.

The purpose of the pumping test and the Aquifer Stress Test (AST) was twofold: to estimate the sustainable yield of the boreholes and to determine aquifer parameters based on time-drawdown data and any possible cross-fan interactions. The sustainable yield can be defined as "…the pumping rate of a borehole or wellfield that can be sustained by the aquifer system over a long period without harming the environment and decreasing the available amount of water for future generations..." (Umvoto, 2016c). Further to this, Vivier (2013) states: "…The concept of sustainability does not only cater for the environment, but also for people (social) and the economy (business)."

Pump test data and interpretations from the two boreholes drilled in 2015 within the North Dogua fan (RAJ-2) and the Asabuya fan (RAJ-1) were considered in the design of the pump tests. These earlier CRT's indicated that boreholes in the alluvial fans could sustain pumping rates of 50 l/s and that the groundwater was highly saline and had high temperatures between 40 – 60 °C. Pump test analyses of these previously tested boreholes showed that with the Theis (1935) solution for unconfined aquifers that the aquifer had high T values ranging between 1000 – 2500 m^2/d (Umvoto, 2015).

The conceptual model adopted an unconfined nature and related water released from storage to the Specific Yield as will be further described in Chapter 10. The AST data was interrupted by mechanical maintenance requirements which resulted in the long-term AST at each hole being comprised of a series of shorter tests with recovery periods in-between. Removing recovery and reinitiated periods to display the entire AST as a single test incorporates too much uncertainty and lowers confidence in data to be used in analytical analyses. It does however still effectively illustrate the length at which the

aquifer was pumped and any change in the water levels of boreholes and the aquifer. Such small variations in drawdown (0.2-0.4 m) over such large periods of time (and likely influence by earth tide fluctuations at such low altitudes), can be considered near negligible from a theoretical point of view and some tests thus achieve steady state. Observation borehole data would in this instance be useful to determine if the hydraulic gradient remains constant and if steady state conditions did develop with time (Kruseman and de Ridder, 1976).

Analytical analyses of the 80-hour test pump data were carried out and is discussed further. The AST data was also analysed but is used predominantly to illustrate the lack of cross fan interaction over long pumping periods and the large volume of water which was removed from the aquifer without adversely affecting the water table within the aquifer.

The pump test data analyses for the AST are not discussed in full and any graphics relating thereto are incorporated in **Appendix C**. This chapter however, focusses on the results and discussion of the individual 80-hour tests as carried out at boreholes DN-P01, BS-P01 and AY-P01.

6.2 METHODOLOGY

6.2.1 Individual Test Pumping

The pump used for each of the individual 80-hour tests was a 5-stage, 93 Horse Power (HP) submersible pump that was immediately started at its full capacity using a Perkins 400 kVA generator and run on a Variable Frequency Drive (VFD) control panel. At the pump's full pumping capacity, the water level within the all boreholes stabilised within 5 minutes. Due to the small amount of drawdown recorded a step test was not conducted and the constant discharge test was carried out for 80 hours, as opposed to the intended 8 hours of steps and 72 hours of constant discharge. This was done for all three production boreholes tested. After 80 hours of pumping, the pump was switched off and recovery measured.

Water levels were measured manually with a dip meter at specified times as per the Ethiopian Ministry of Water format (see **Table 6-1**). All water levels recorded were compensated for collar height and height of the observation pipe. To mitigate infiltration or potential recharge, the discharged water was directed into a plastic lined trench that allowed water to continuously flow off the fan and down onto the salt flats (see **Figure 6-1**). Level loggers or pressure transducers were installed in the production and monitoring wells to support the manually collected data as well as to test their functionality prior to the AST. Groundwater samples were collected for hydrochemical analyses prior to the end of the pump test. On site hydrochemical assessments of pH, temperature and EC were measured manually twice daily to monitor for any obvious changes in water quality and indication of varying groundwater source paths. The discharge rate during the individual 80-hour pump tests was measured by means of a 90 ° V-notch (**Figure 6-1**).

Table 6-1 **Time intervals between measurements as per the Ethiopian Ministry of Water and Energy Standard**

Time since pumping started (or stopped)	Time intervals between measurements in minutes
0-5	0.5
5-10	1
10-20	2
20-60	5
60-120	10
120-180	20
180-360	30
360-1440	60
1440-4800	120

Figure 6-1 **Photographs illustrating the V-notch used to measure discharge and the plastic lined trench that transmitted water down the fan to prevent recirculation during pumping.**

Time drawdown data was then plotted on different graphs and erroneous data removed as part of the Quality Control (QC) process. Both the manually collected data, as well as the data recorded by the level logger was analysed. There was a good correlation between the manually collected data and the level logger data, with the level logger data providing temperature measurements as well. Level logger data was compensated for pressure variations during testing. Pressure readings were obtained from the weather stations surrounding the various sites (within 300 m) at similar elevations (Badah Camp

weather station and Solmin-1 weather station). The data was interpreted visually based on the shape and slope of the curves obtained and analysed analytically by means of AQTESOLV version 4.50-Professional software. The analytical methods selected in AQTESOLV were Theis (1935) adapted by Hantush (1961) for a partially penetrating aquifer, and Cooper Jacob (1946). C. E. Jacob developed a procedure (Jacob, 1944) that corrects drawdown data for the reduction in an unconfined aquifer's saturated thickness resulting from groundwater abstraction by a pumping well and thereby enables pumping tests in unconfined aquifers to be interpreted by methods for nonleaky confined aquifers such as the Cooper Jacob (1946) solution. In addition to these analytical solutions, other solutions pertinent to unconfined aquifers such as Neuman (1974) were also applied to the data for comparative reasons. Various solutions were tested to determine which curve the test pump data best suited. Different fans responded differently to testing, which attests to the high degree of heterogeneity within the alluvial fan aquifer complex.

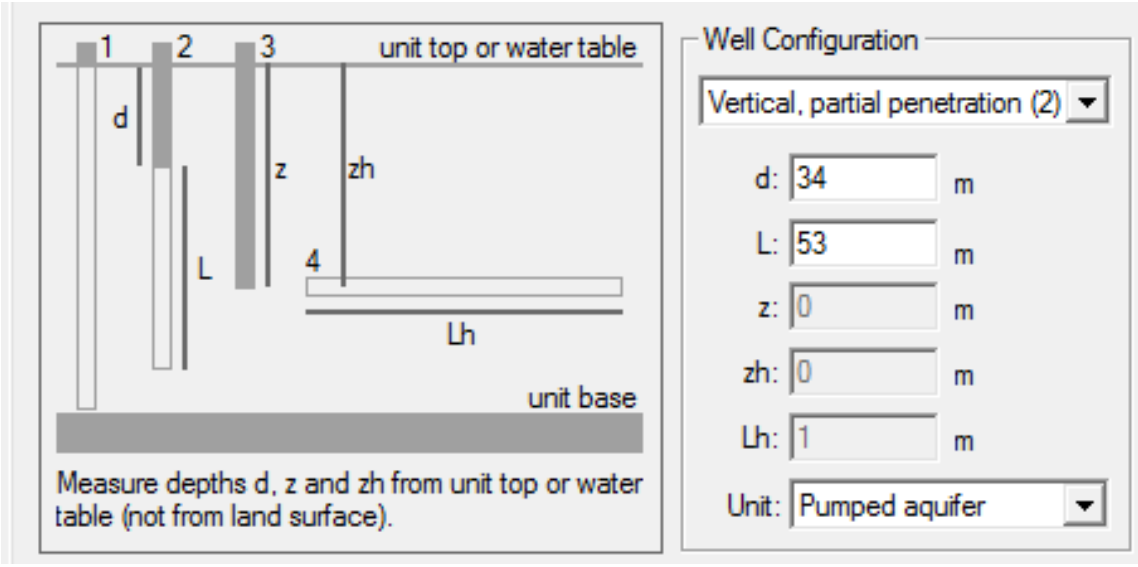

Figure 6-2 Input and settings required for each borehole in AQTESOLV software.

The value represented by the letter d in **Figure 6-2** is taken from the top of the water table to the top of the screen, while the value for L is derived from the top of the screened portion to the base of the screened portion for each borehole.

The data was also plotted in FC software, developed by the Institute of Groundwater Studies (IGS) at the University of the Free State (UFS) for interpretational and comparative purposes. FC was however, developed for fractured rocks (secondary

aquifers) and not for primary aquifers. FC makes use of the Cooper Jacob Method to determine aquifer parameters but is especially useful for determining the sustainable yield of the boreholes. This was done for comparative purposes as the results from each fan responded in separate ways when pumped. Conducting test pump analysis on the pumped well elevates the uncertainty of the parameters determined due to turbulence and frictional forces acting within the pumped well (Kruseman and de Ridder, 1976). A lack of observation data however requires the pumped wells be analysed to offer some insight to aquifer parameters for input to the numerical model. This further highlights the importance of observation data in obtaining reliable storage related parameters as distance is a vital component of all storage related calculations. Assuming the aquifer system responds in an unconfined manner, the Specific Yield (S_y) would indicate how much water can be drained from the interconnected pore space within the aquifer under the force of gravity (Kruseman and de Ridder, 1976). This implies the Specific Storage (S_s) would be small enough to disregard (Driscoll, 1986) and the S_y would offer an indication as to how effectively water would drain from the aquifer under force of gravity while pumping.

6.2.2 Aquifer Stress Test (AST)

The methodology for the AST followed closely that of the individual pump tests. For the AST, the three production boreholes, namely AY-P01, BS-P01 and DN-P01 were each equipped with a 6-stage 67 kW Vansan SS08-160 submersible pump, a 75 kW Schneider soft starter panel and a 67 kW Vansan motor with a 75 kW winding (see **Figure 5-2**). All the Vansan pumps were stainless steel to prevent corrosion of the impellers and pump housing. The 75 kW winding was engineered to account for the elevated temperature and salinity of the groundwater. Unforeseen static head in three of the boreholes (AY-P01, RAJ-2 and BS-P01) required that between one and four impellers be removed (**Figure 6-3**) to lower the current (Ampere) to within the operational limit of the motor and pump (140 Ampere). Additional complications arose through the poor construction of the cable joints as no crimping tool or insulation resistance tester was available on site. The cable joints experienced dead shorts (**Figure 6-4**) which in turn caused the thyristors in the soft starter panels to blow. The panels had to be replaced with 75 kW transformer (impedance) panels (**Figure 5-4**) which elevated the risk of motor burn out as the replacement panels would not act as a fail-safe to protect the motor as the soft starter panels had. This required that the current on the three phases be monitored closely at least twice a day.

The two pre-existing production boreholes, namely RAJ-1 and RAJ-2 were each equipped with a Grundfos SP160-5 submersible pump with a 67 kW Franklin Electric motor and were run on star-delta panels (see **Figure 6-5**). The Grundfos pumps however, were not suitable for the prevailing groundwater conditions and were subject to corrosion which later posed numerous challenges in successfully commissioning RAJ-1 and RAJ-2. During the AST, the tie rod of the pump at RAJ-1 broke and the pump fell down the hole as it came loose from its housing. The pump was replaced with a 13-stage 57 kW pump that required 4 impellers to be removed and a special coupling to be fabricated for the pump to fit the main riser pipe (see **Figure 6-4** and **Figure 6-6**). The pump at RAJ-2 also ceased operating after a few days. The pump was pulled and it was determined that the drive shaft seal on the motor had become stiff resulting in water ingress to the motor. RAJ-2 was then also equipped with a Vansan motor and pump, identical to the other three wells. These pumps were all powered by diesel generators which varied between 300- 450 kVA.

Figure 6-3 **Photograph of the Vansan pumps installed at AY-P01, BS-P01, DN-P01 and RAJ-2 respectively, a 6-stage pump and a stainless-steel impeller that was removed.**

Figure 6-4 **Photograph of the Grundfos pumps installed in RAJ-1 and RAJ-2. Corrosion to the tie rod and pump housing is evident.**

Figure 6-5 **Photographs depicting a shorted cable join due to incorrectly sized ferrules and crude crimping. The image on the far right depicts the replacement transformer (impedance) panel used after the soft starter panels were damaged.**

Figure 6-6 **Photographs of the RAJ-1 pump housing that broke and resulted in the pump falling down the well, the 13-satge pump and the modified coupling fabricated for the rental pump.**

Discharge or flow rates were measured at each borehole by flow meters that were installed when the boreholes were being equipped. Gate valves were installed to allow the discharge to be controlled, however closing the gate valve too much (reducing the flow rate) resulted in the static head increasing which in turn caused the ampere to increase. For this reason and to stress the aquifer as much as possible, the pumps were set to pump at full capacity and were not strictly operated per their pumping curves.

These challenges faced in commissioning the boreholes caused a deviation from the initial plan to bring each borehole online within 24 hours of one another. In addition to this, the generators used to power the pumps required servicing every 250 hours and some were coupled to a changeover switch to alternate every 12 hours. This resulted in down time of pumping in which recovery of the water level could occur.

Water levels were measured manually at specified times as per the Ethiopian Ministry of Water format, with time intervals being added for long term testing (see **Table 6-2**). To mitigate infiltration or potential recharge, the discharged water was directed into a plastic lined trench that allowed water to continuously flow off the fan and down onto the salt flats where it could evaporate. Automatic level loggers were installed in the production and monitoring wells to support the manually collected data, they recorded the temperature and dynamic water level in 5 minute intervals. Only the manual data is

presented, but where interesting temperature variations are noted, the level logger data is shown.

Data obtained was cleaned as part of the QC process and run through AQTESOLV, in the same manner as the individual test pump data was. Semi-log and log-log graphs were also created to better evaluate potential changes in water level that may sometimes be overlooked in the raw data plots. Recovery measurements were not included in the AQTESOLV data sets as recovery occurred too rapidly for it to have any overarching influence on the Transmissivity values obtained. Due to the lack of any measurable changes in water level occurring in the monitoring boreholes during and after the AST, no reliable storage estimations were obtainable. This indicates the importance of reliable observation data in test pump analysis. Distance measurements to quantify the radius of influence are critical unknowns required to solve for reliable Storage values. The results of the AST analysis are included in Appendix C. The 80 hour test pump data is used to determine initial aquifer parameters as input to the numerical model. AST data was also analysed, but due to the frequent disruptions, is not incorporated in full. AST water levels were also used to calibrate the numerical model (see **Chapter 8**).

Table 6-2 Time intervals between measurements during the AST as per the Ethiopian Ministry of Water Standard with additional intervals for long term testing.

Time since pumping started (or stopped)	Time intervals between measurements in minutes
0-5	0.5
5-10	1
10-20	2
20-60	5
60-120	10
120-180	20
180-360	30
360-1440	60 (1 hourly)
1440-4320	120 (2 hourly)
4320-7200	180 (3 hourly)
7200-10080	240 (4 hourly)
10080-20160	720 (12 hourly)
20160-37440+	1440 (24 hourly)

6.2.2.1 Challenges Encountered

Various challenges, including the harsh environment and isolated location, hindered the progress of the AST and are summarised below:

- High salinity water resulted in dip meters getting coated in salt and needing to be cleaned before functioning correctly;
- Generators needed to be serviced every 250 hours, resulting in water level recovery;
- Pumps needed to be modified by removing impellers to compensate for unforeseen static pressure;
- Cable joints shorted (dead short) causing the control panel to burn out, this was the result of bad joints because of no crimping tool being used;
- VFD could only be borrowed for ten days until it was demobilised from site, there after BS-P01 was shut down;
- Rust on the old RAJ-1 pump which resulted in the tie rod breaking and the pump and motor unit falling down the borehole;
- Pump at RAJ-1 only able to yield 25 l/s at 100 m head.

Despite these practical challenges to overcome, 603 370.7 m^3 of groundwater was pumped in total and individual boreholes were pumped for between 280 and 925 hours which delivered between 38 000 and 208 000 m^3 each.

6.3 RESULTS

6.3.1 DN-P01

The intended 80 hour constant discharge test at DN-P01 was interrupted by mechanical failure of the generator and thus resulted in a 53 hour test. **Figure 6-7** shows the drawdown time response of pumping at DN-P01 at a constant discharge rate of 54 l/s.

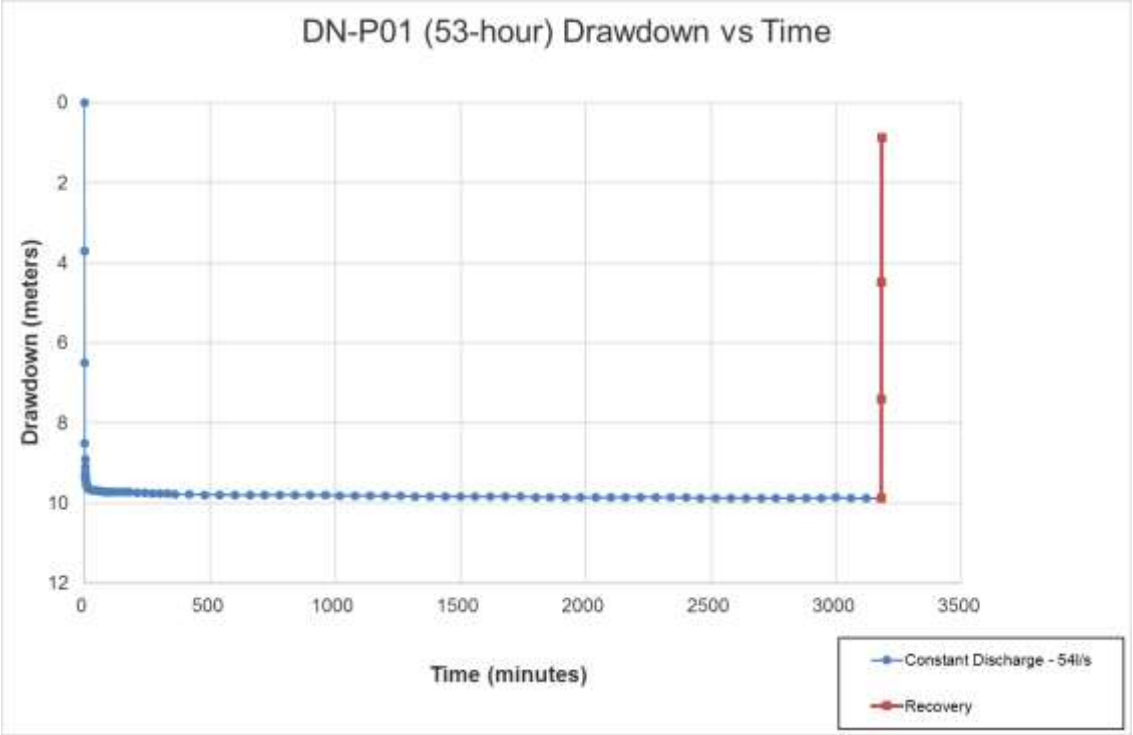

Figure 6-7 Manually recorded drawdown versus time graph at DN-P01.

Figure 6-8 is a semi-log plot of the drawdown time data measured at DN-P01 for 53 hours. **Figure 6-9** is the log-log plot of drawdown versus time data from DN-P01 while **Figure 6-10** represents the AQTESOLV processing and **Figure 6-11** the logger data representation of the drawdown and temperature versus time data.

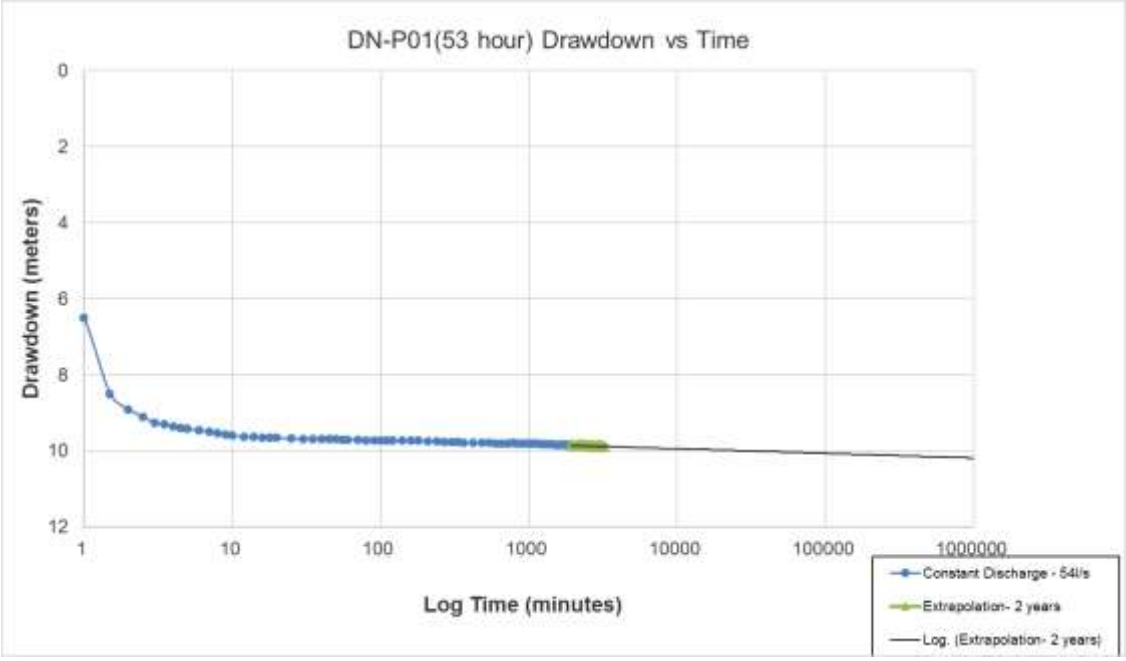

Figure 6-8 **Semi-log graph of manually recorded drawdown versus time data for 53 hours of pumping at DN-P01 with extrapolation to ~2 year of pumping.**

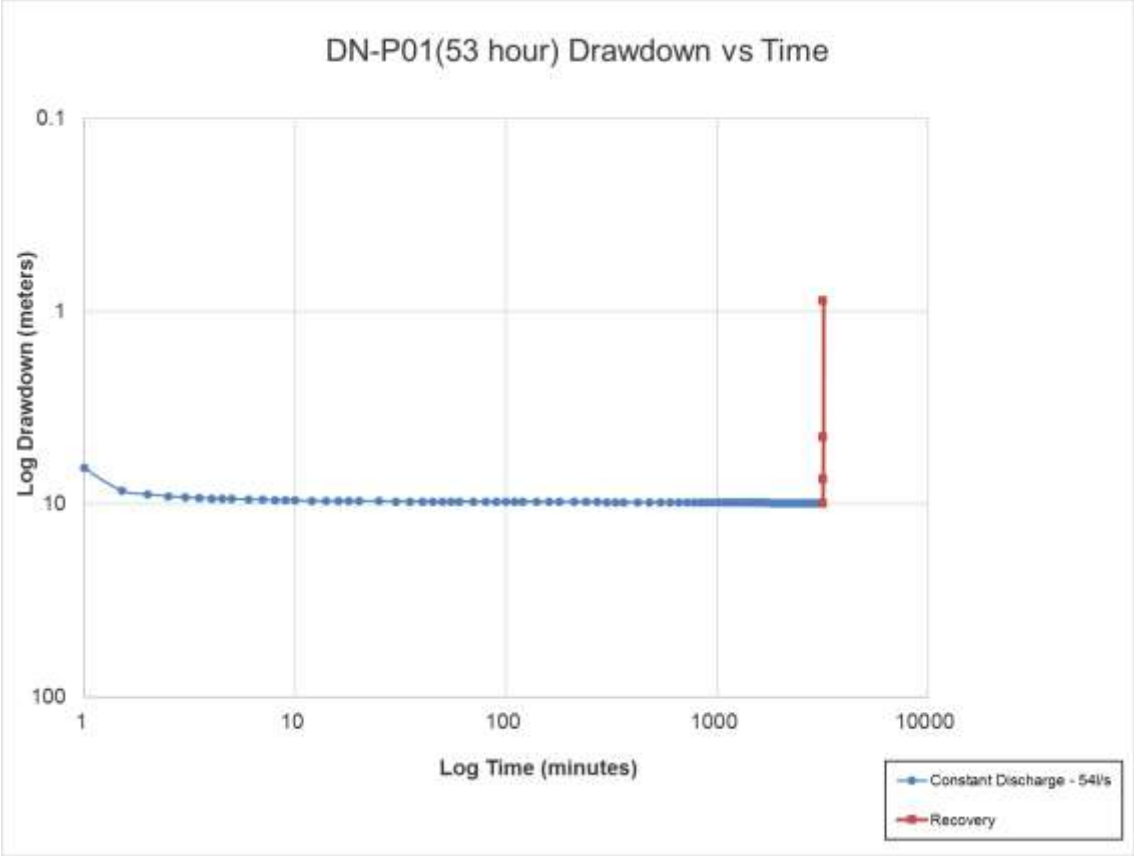

Figure 6-9 **Log-log graph of manually recorded drawdown versus time data at DN-P01**

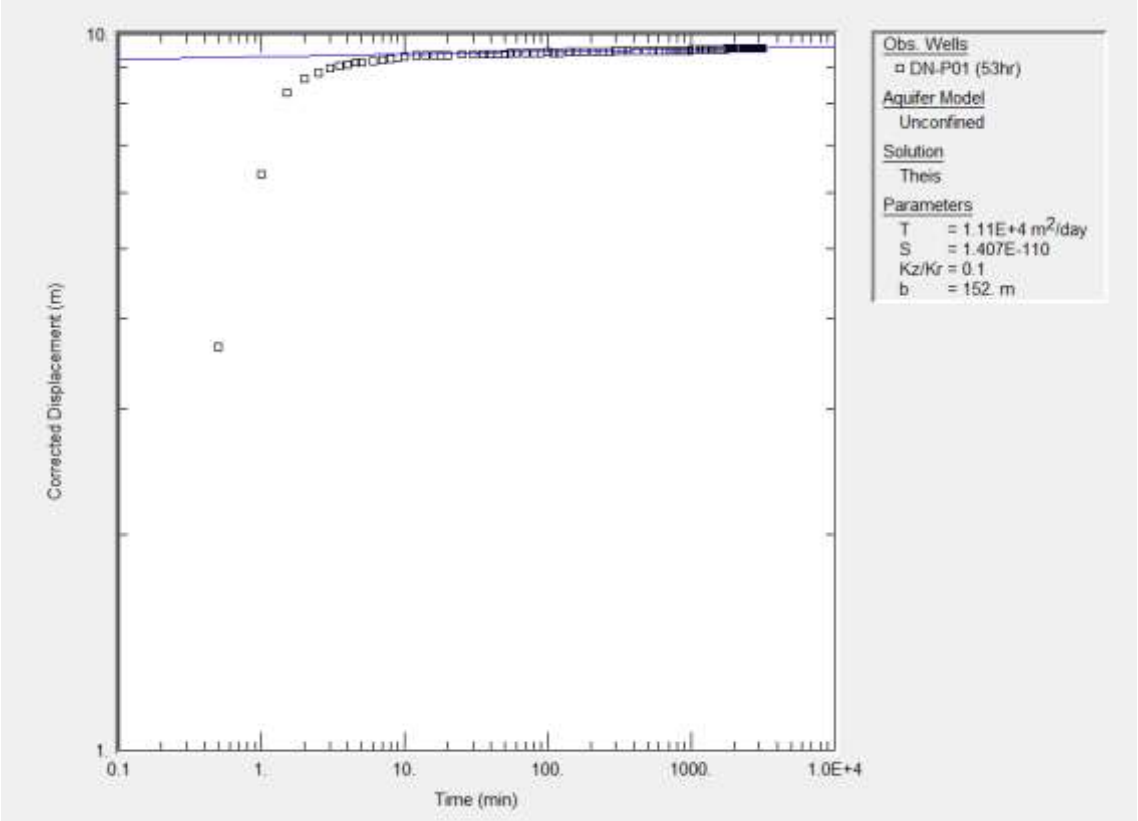

Figure 6-10 **Log-log graph in AQTESOLV software of drawdown versus time data of DN-P01 with adjusted Theis (1935) for partially penetrating, unconfined aquifer curve fitted.**

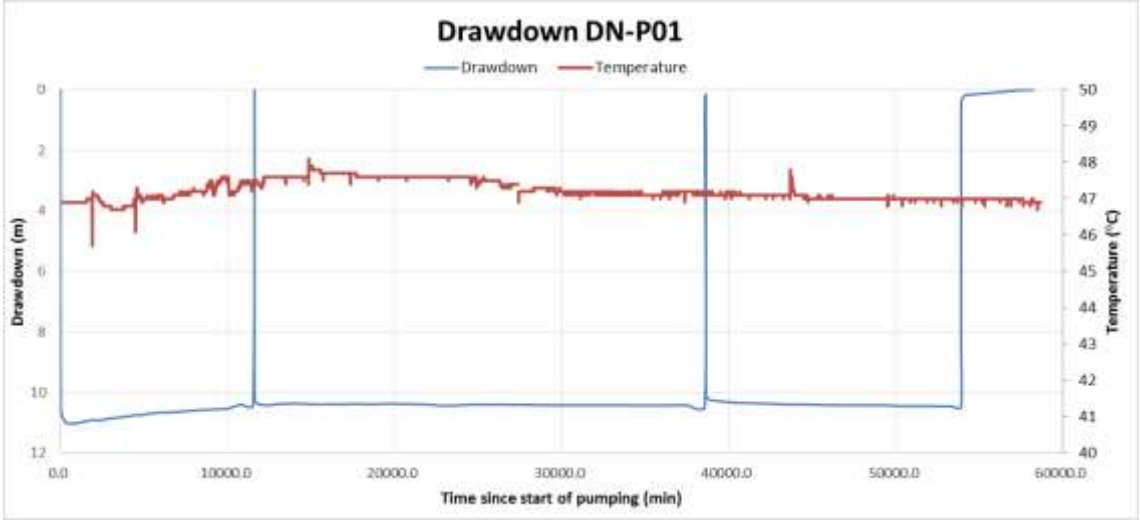

Figure 6-11 **Drawdown and temperature versus time graph of long term pumping at DN-P01 as recorded by the level logger during the AST.**

6.3.2 BS-P01

Figure 6-12 shows the drawdown time response of test pumping at BS-P01, with a constant discharge rate of 47.5 l/s.

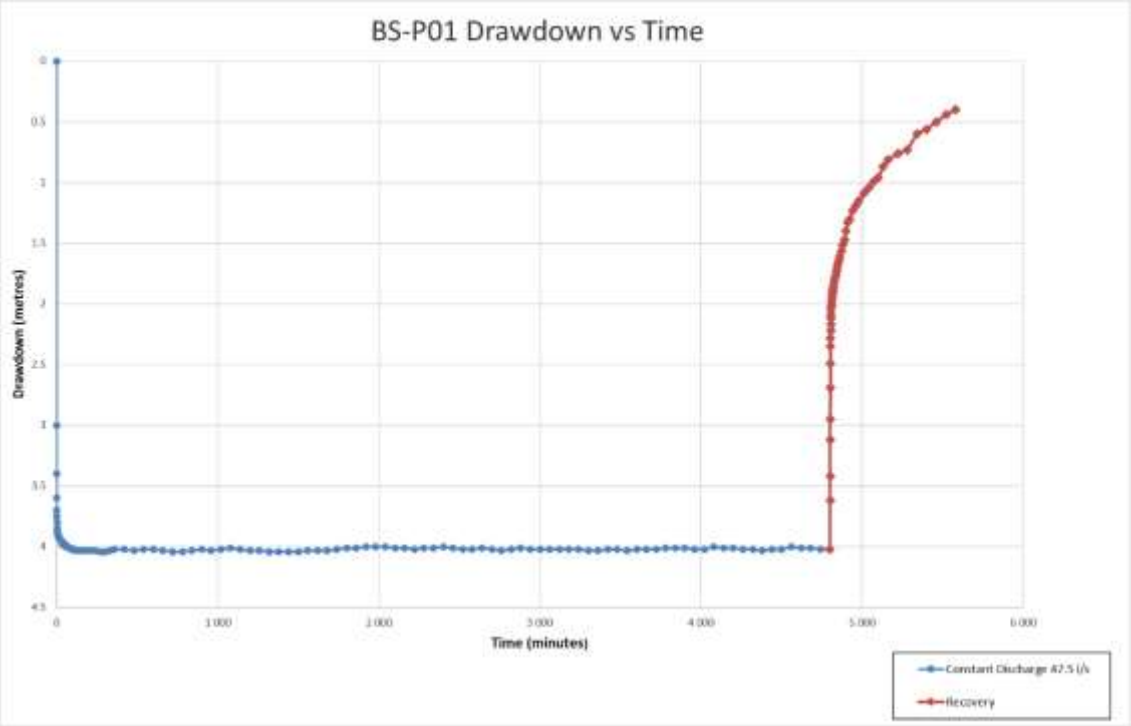

Figure 6-12 Manually recorded drawdown versus time graph of pumping at BS-P01.

Figure 6-13 is a semi-log plot of the drawdown time data measured at BS-P01 for the duration of the test. **Figure 6-14** is the log plot of drawdown versus time data from BS-P01 while **Figure 6-15** represent the AQTESOLV processing and **Figure 6-16** logger data representation of the drawdown time data and temperature during the AST.

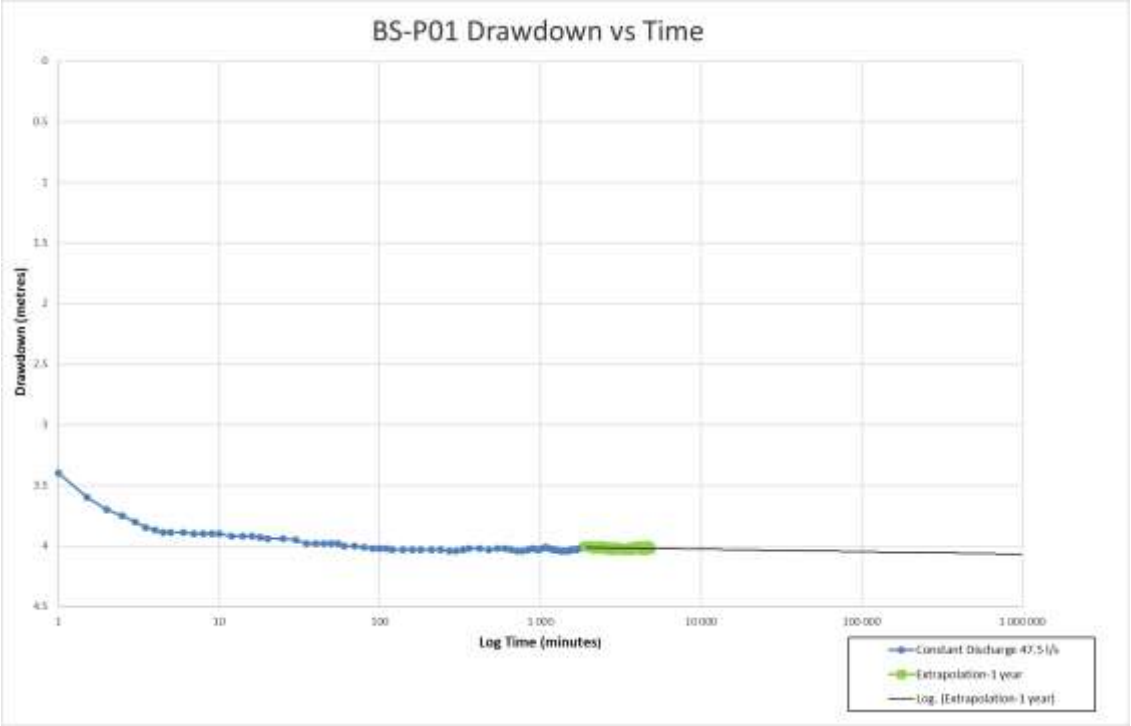

Figure 6-13 **Semi-log graph of manually recorded drawdown versus time data for 80 hours of pumping at BS-P01 with extrapolation to ~2 year of pumping.**

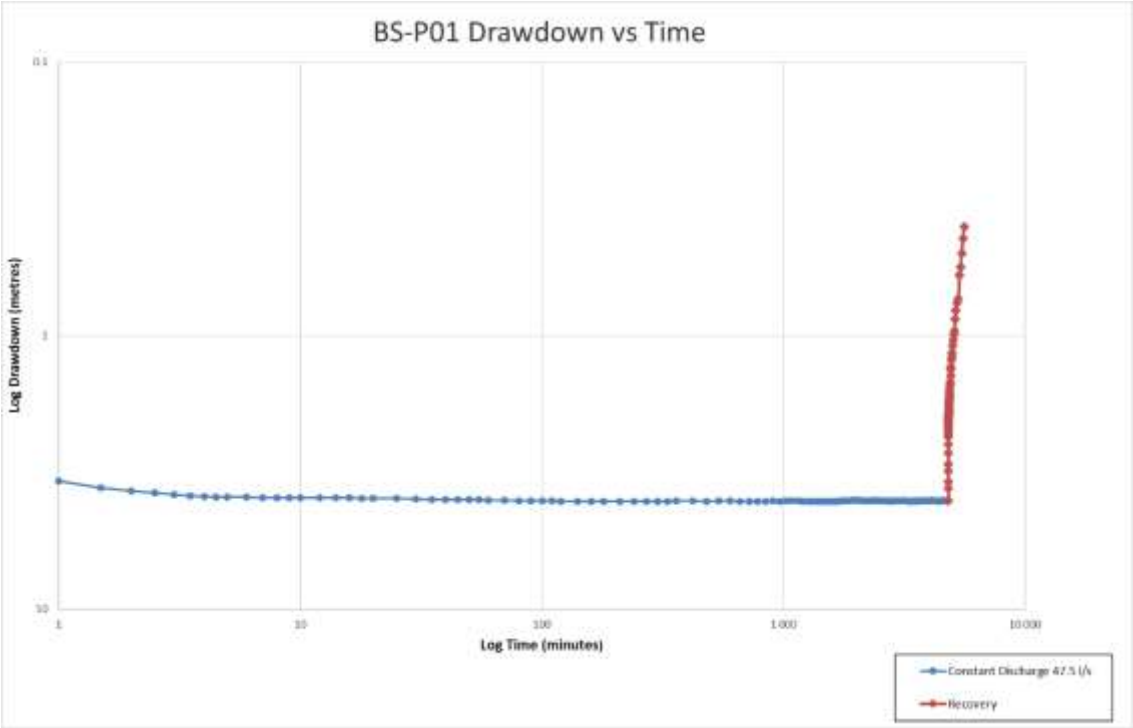

Figure 6-14 **Log-log graph of manually recorded drawdown versus time data at BS-P01 during test pumping**

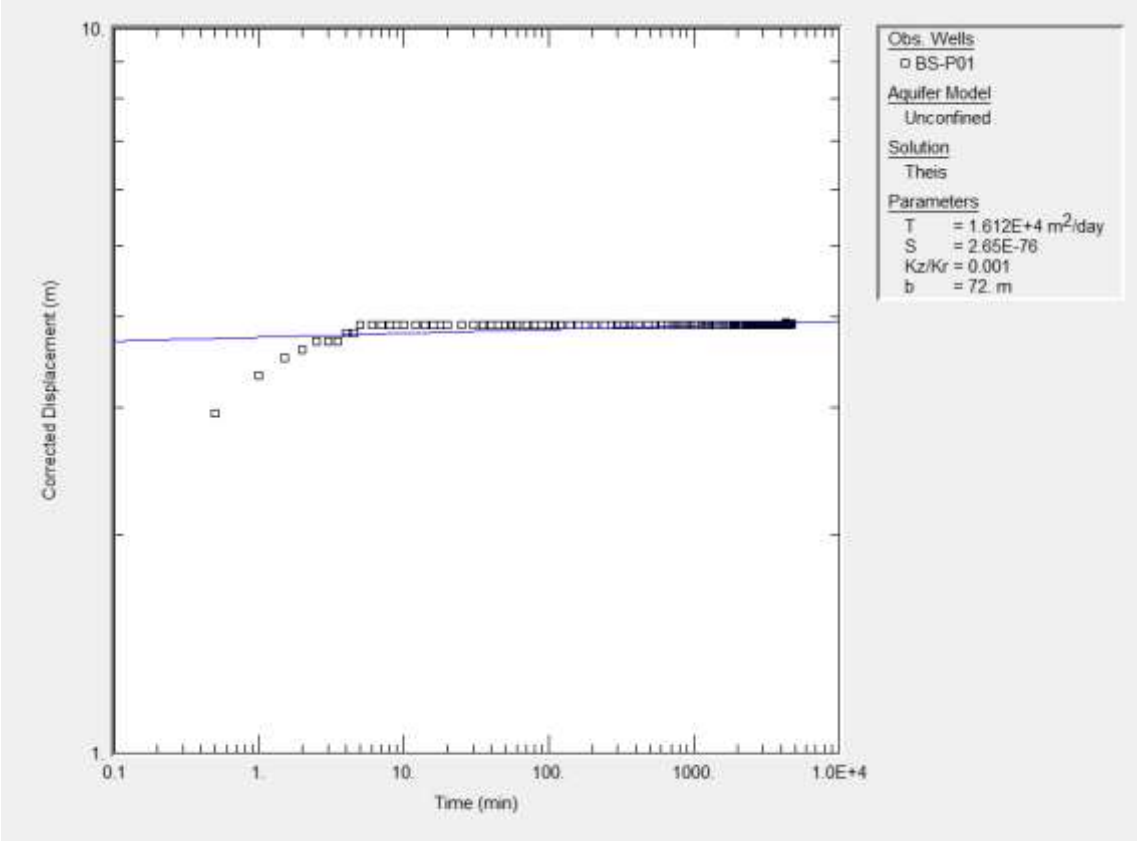

Figure 6-15 **Log-log graph in AQTESOLV software of drawdown versus time data of BS-P01 with adjusted Theis (1935) for partially penetrating, unconfined aquifer curve fitted.**

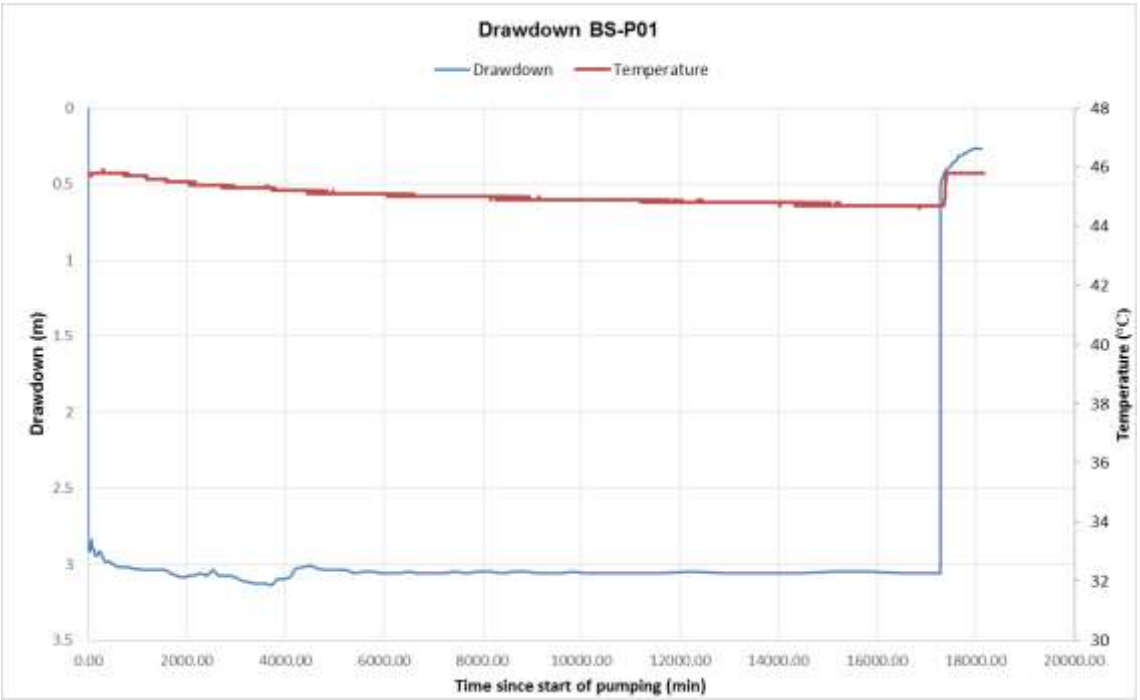

Figure 6-16 **Drawdown and temperature versus time graph of long term pumping at BS-P01 as recorded by the level logger during the AST.**

6.3.3 AY-P01

Figure 6-17 shows the drawdown time response of pumping at AY-P01 with a constant discharge rate of 56 l/s.

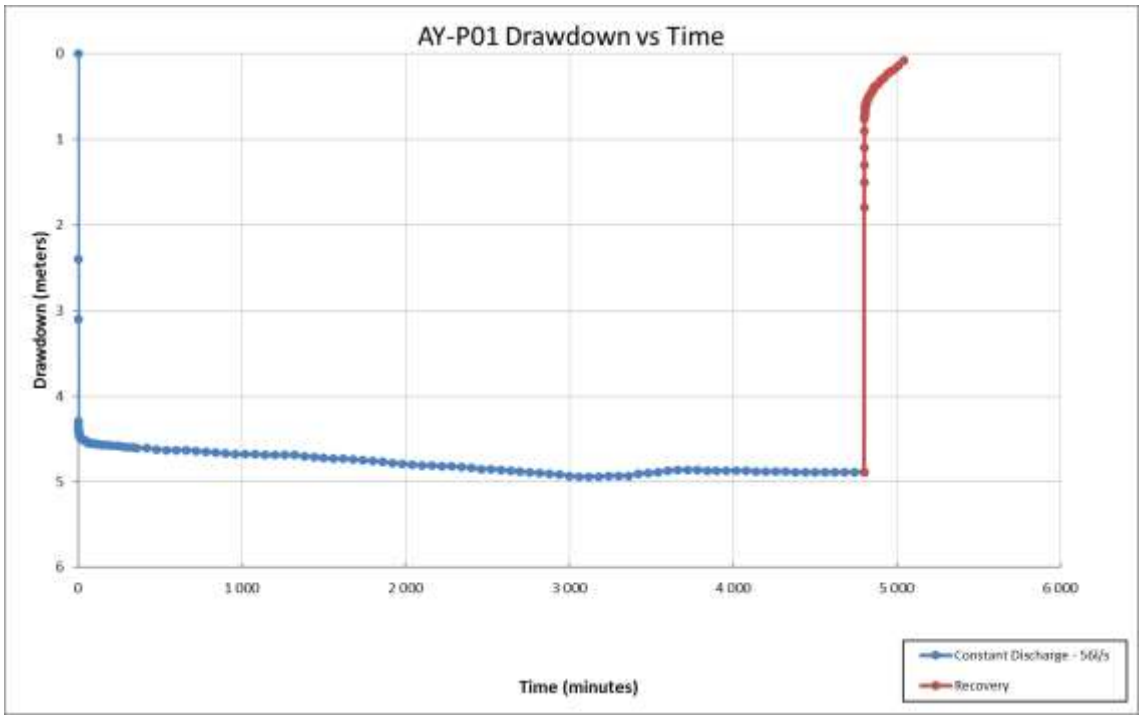

Figure 6-17 Manually recorded drawdown versus time graph of test pumping at AY-P01.

Figure 6-18 is a semi-log plot of the drawdown time data measured at AY-P01 for the duration of test pumping. **Figure 6-19** is the log-log plot of drawdown versus time data from AY-P01 while **Figure 6-20** represent the AQTESOLV processing and **Figure 6-21** logger drawdown and temperature data during the AST.

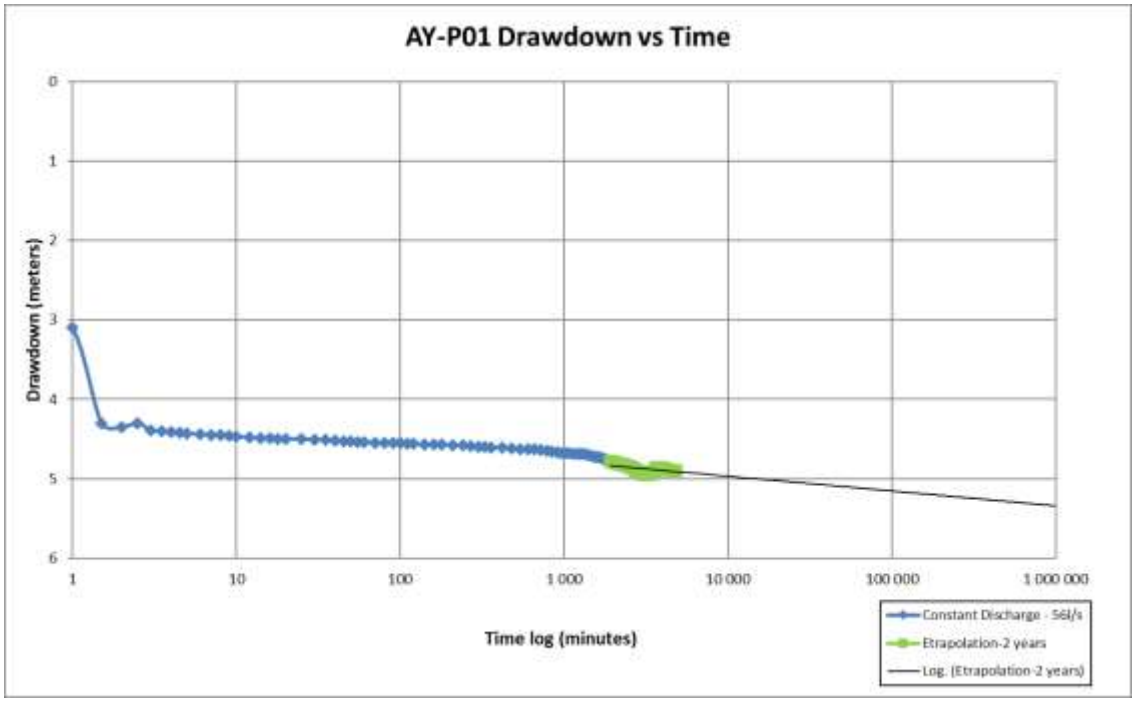

Figure 6-18 **Semi-log graph of manually recorded drawdown versus time data for test pumping at AY-P01 Semi-log graph of manually recorded drawdown versus time data for 80 hours of pumping at AY-P01 with extrapolation to ~2 year of pumping.**

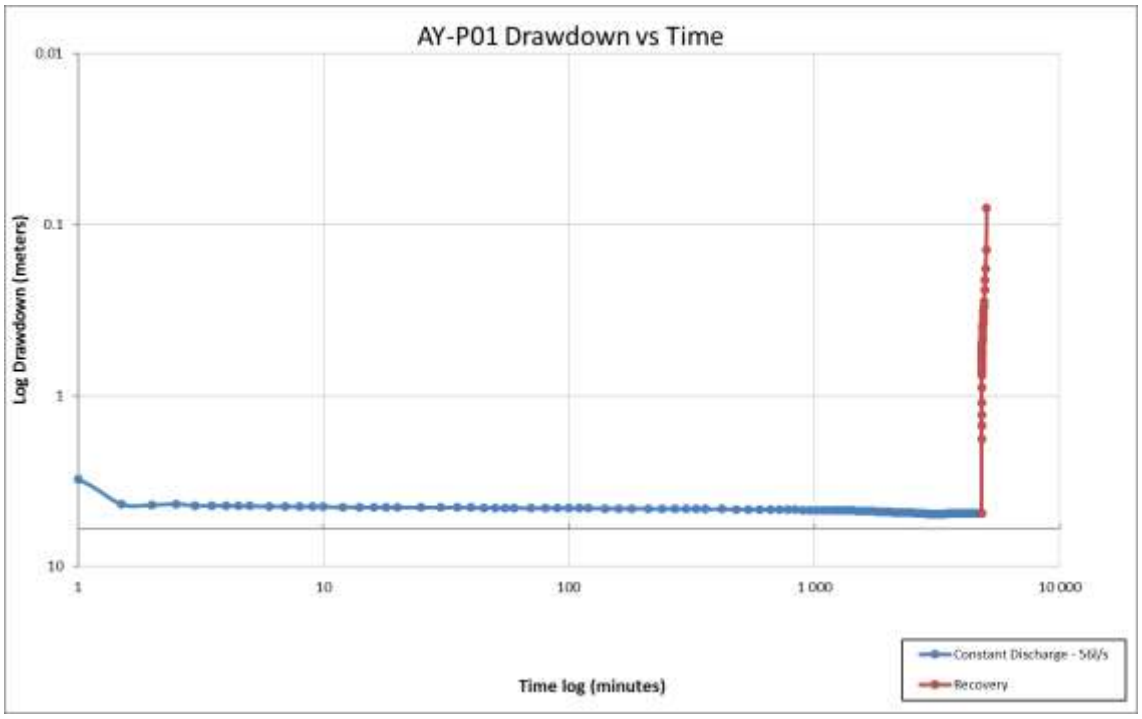

Figure 6-19 **Log-log graph of manually recorded drawdown versus time data at AY-P01.**

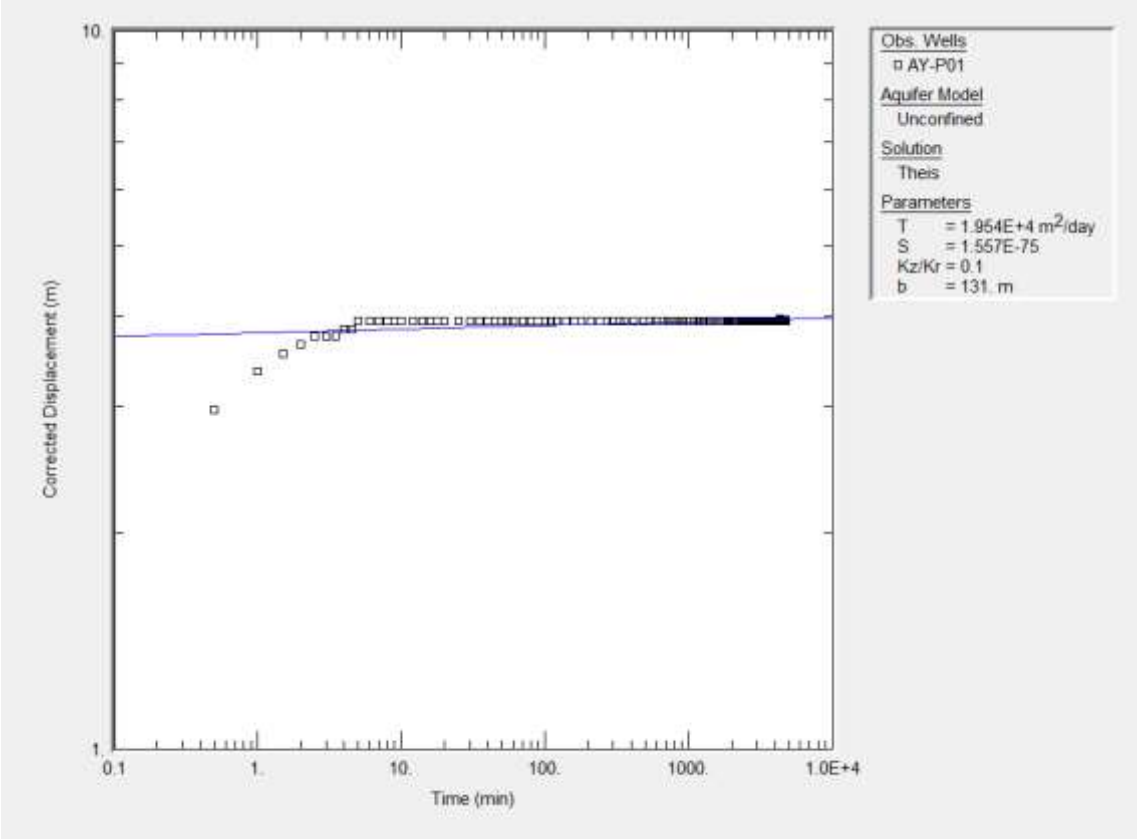

Figure 6-20 **Log-log graph in AQTESOLV software of drawdown versus time data of AY-P01 test pumping.**

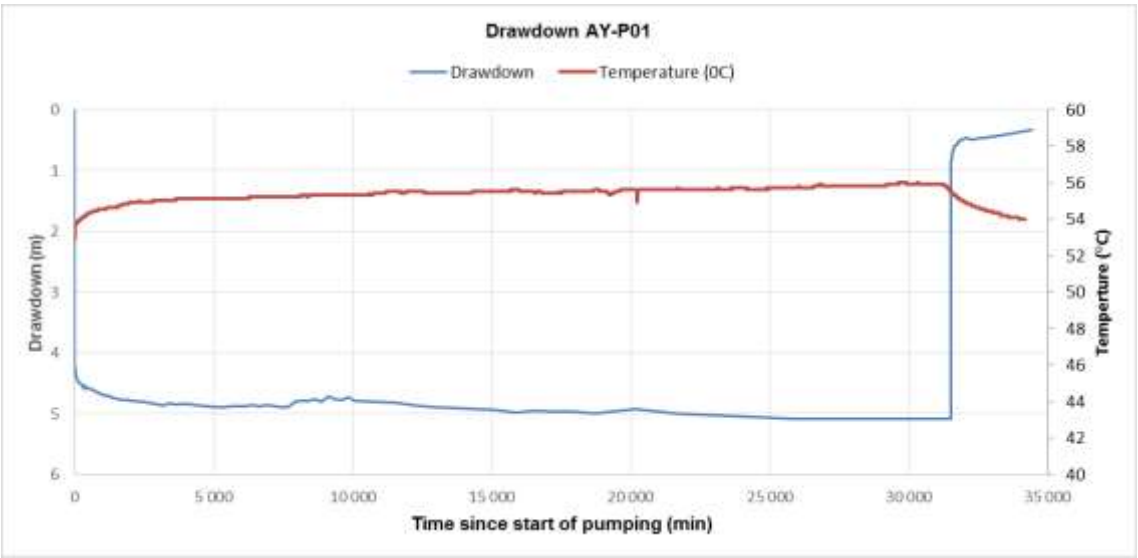

Figure 6-21 **Drawdown and temperature versus time graph of long term pumping at AY-P01 as recorded by the level logger during the AST with stop times removed.**

6.3.4 RAJ-1 and RAJ-2

Figure 6-22 and **Figure 6-23** represent the drawdown and temperature versus time response as recorded by the level loggers at RAJ-1 and RAJ-2 during the AST respectively. These boreholes did not have individual constant discharge tests conducted.

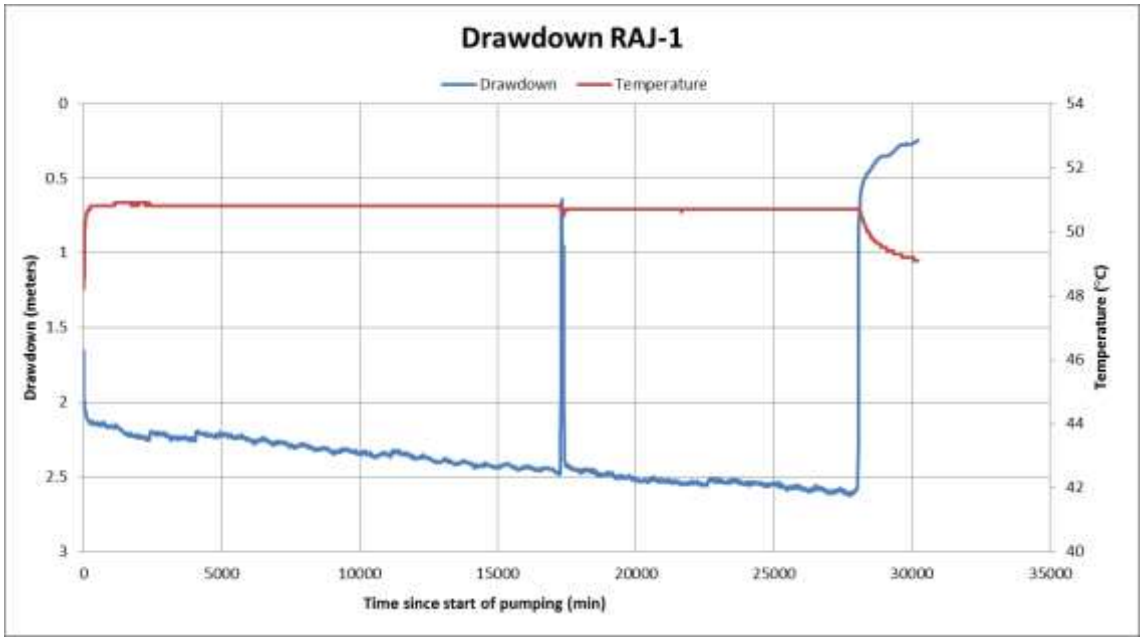

Figure 6-22 Drawdown and temperature versus time graph of long term pumping at RAJ-1 as recorded by the level logger.

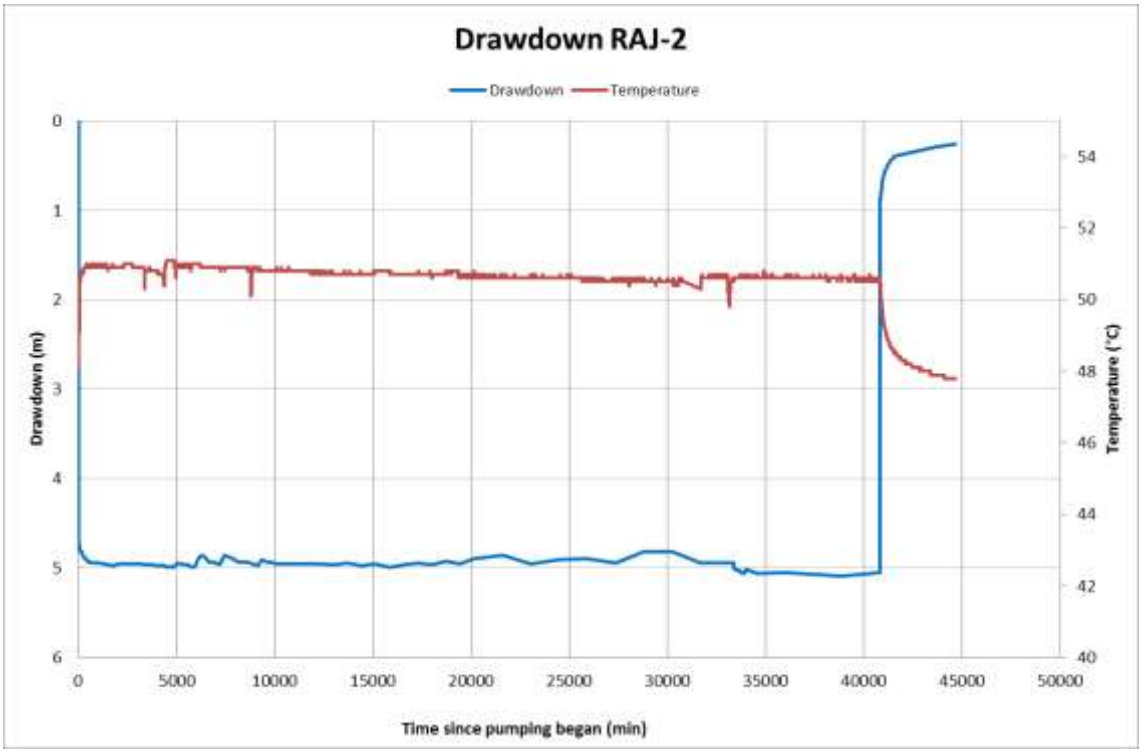

Figure 6-23 Drawdown and temperature versus time graph of long term pumping at RAJ-2 as recorded by the level logger.

6.4 DISCUSSION

6.4.1 DN-P01

Test pumping of DN-P01 commenced at 11:00 on the 22nd of August. The submersible pump was installed at a depth of 100 mbgl, ~68 m below the rest/static water level of 32.10 mbgl. The pump was started at full capacity and due to its depth obtained a yield of 54 l/s. The discharge rate was determined by a 90° V-notch. The constant discharge test ran for ~53 hours before the pump failed and the test was forced to come to an end and recovery measured.

On site groundwater quality assessments were conducted at various stages throughout the test and indicated that the water is acidic (pH=5.4), likely highly saline with an EC of >400 mS/m, and a temperature of ~49.1°C. No change in groundwater quality was observed during the 53-hour constant discharge test. Water samples were collected for more detailed chemical analyses after 24 and 48 hours respectively.

Figure 6-7 represents the curve of the manually recorded drawdown versus time since start of pumping for 53 hours of testing. The recovery was recorded when the pump stopped and it can be seen that recovery was near instantaneous. The water level drops

9 m from 32.10 mbgl to 41 mbgl within the first 2 minutes after which the water level stabilizes at ~41.97 mbgl. This represents a drawdown of 9.88 m at a constant discharge of 54.1 l/s. For the remainder of the test the water level fluctuates between 41.94 and 41.98 mbgl. This implies a well efficiency of 100% and that the aquifer is not being sufficiently stressed. In order to give insight into any major boundary conditions and increase confidence in hydraulic parameters and aquifer response, the well may need to be pumped for a longer period of time. This is further supported by the fact that the water levels measured twice a day in the monitoring wells DN-M01 and DN-M02 did not change and remained at 63.9 mbgl and 19.09 mbgl respectively for the duration of pumping.

Figure 6-8 and **Figure 6-9** represent semi-log and log-log plots of the time drawdown data for interpretational analyses. Extrapolation of the drawdown data on **Figure 6-8** from 32-53 hours for 1 million minutes (~2 years) shows that if no boundaries are intercepted, the drawdown will remain above the Available Drawdown limit. The change in drawdown is small over a large period of time, implying steady state conditions were achieved and that the discharge rate of 54 l/s is sustainable. **Figure 6-9** highlights how rapid recovery was after pumping ceased.

Figure 6-10 illustrates that the adapted Theis (1935) solution has a good fit apart from the initial drawdown- this could be due to the well bore storage effect experienced in the initial 5 minutes of the constant discharge test. No evidence of a delayed response or aquifer leakage is present. Curve matching was done manually under the “Visual” tab. The resulting Transmissivity of 11 100 m^2/day is high, but in the same order as the results obtained for the RAJ-1 and RAJ-2 tests conducted by Umvoto (2015). Due to the unconfined nature of the aquifer, the saturated thickness presumably changes as pumping progresses and drawdown increases. Dividing the T value obtained by the aquifer saturated thickness under natural conditions, a Hydraulic Conductivity (K) value of 73 m/day is obtained.

To conduct the AST, a submersible pump was installed at a depth of 70 mbgl, 40.68 m below the static water level of 29.32 mbgl. The pump started at 68 l/s but was then reduced to 62.5 l/s for the remainder of the test by partially closing the gate valve that had been installed. Two generator services took place during the 38-day constant discharge test with the water level recovering each time (see **Table 6-3**). The discharge rate was determined by a flow meter. **Table 6-4** represents the results of the aquifer parameters determined via analytical analyses of the test pump data.

Table 6-3 Summary of the AST at DN-P01

AST	Duration (minutes)	Start	End	Flow Rate (l/s)	RWL (mbgl)	Drawdown (meters)	Recovery (meters)	Recovery (minutes)	Comment
1st	11520	2016/10/08 11:40	2016/10/15 16:35	68	29.37	11.04	0.11	100	Service
2nd	28710	2016/10/15 18:25	2016/11/04 16:55	62.5	29.37	10.45	0.15	75	Service
3rd	15265	2016/11/04 18:15	2016/11/15 08:40	62.5	29.37	10.46	0	3360	End of AST

No change in groundwater quality was observed over the 38-day constant discharge test. Water samples were collected for more detailed chemical analyses after 7, 16 and 37 days respectively. Stable and radiogenic isotope samples were also collected after 27 and 34 days respectively. The results and discussion of these hydrochemical samples can be found in **Chapter 6**.

The small changes in drawdown over an extended period of time support results from the individual tests and further elude to the likelihood that steady state flow was achieved (see **Figure 6-11**). This is in theory only and would require consistent hydraulic gradients observed in observation wells that had measurable effects from pumping (Kruseman and De Ridder, 1976). To give insight into any major boundary conditions and increase confidence in hydraulic parameters, specifically storage values and aquifer response, the well needs to be pumped for a longer period and possibly a higher rate to further extend the cone of depression to an observation point. The high yield potential and lack of observation data over long periods suggests that observation boreholes be installed within 5, 10 and 20 m of the pumped well and then be retested. This is further supported by the fact that the water levels measured in the monitoring wells, DN-M01 (500 m away) and DN-M02 (1.5 km away), remained constant at 64.23 mbgl and 19.67 mbgl respectively throughout the test.

After 38 days, the pump was switched off and recovery measured. Recovery was initially very rapid and the water level continued to recover to the static water level of 29.37 mbgl after 3360 minutes.

Assumptions linked to analytical analyses of the data may be invalid due to the possibility and likelihood of there being a vertical recharge source in the form of the underlying rift related faults. It is proposed that this would not respond as a recharge boundary, but as a deep source of water recharging the alluvial aquifer vertically with geothermally driven waters flowing along the rift related faults.

Figure 6-11 shows temperature remained relatively constant throughout the 38-day test with a slight increase between 10 000 and 30 000 minutes.

Table 6-4 Summary of aquifer parameters obtained from test pumping DN-P01

BH ID	Transmissivity (m^2/day)	Thickness (m)	Hydraulic Conductivity (m/day)
DN-P01	11 100	152	73.03

Recovery data would be useful to determine T coefficient by means of a Horner Plot using the Theis concept. The recovery however, is too rapid to give any measurable change in residual drawdown over a single log cycle, as it is near instantaneous.

6.4.2 BS-P01

Test pumping of BS-P01 commenced at 10:30 on the 13th of August. The submersible pump was installed at a depth of 120 mbgl, 35 m below the rest/static water level of 85 mbgl. The pump was started at full capacity and due to its depth was only able to obtain a yield of 47.5 l/s. The discharge rate was determined by a 90° V-notch.

On site groundwater quality assessments were conducted at various stages throughout the test and indicated that the water is acidic (pH=6), likely highly saline with an EC of >400 mS/m, and a temperature of ~46.6°C. No change in groundwater quality was observed during the 80 hour constant discharge test. Water samples were collected for more detailed chemical analyses after 24 and 80 hours respectively.

Figure 6-12 represents the curve of the manually recorded drawdown versus time since start of pumping for 80 hours of testing. The water level drops 3 m from 85 to 88 mbgl within the first 30 seconds and steadily continues to drop for one and a half hours after which the water level stabilizes at ~89.03 mbgl. This represents a drawdown of 4.03 m at a constant discharge of 47.5 l/s. For the remainder of the test the water level fluctuates between 89.01 and 89.04 mbgl. This implies a well efficiency of 100% and that the aquifer is not being sufficiently stressed. In order to give insight into any major boundary conditions and increase confidence in hydraulic parameters and aquifer response, the well needs to be pumped for a longer period of time. This is further supported by the fact that the water levels measured twice a day in the monitoring well BS-M01 did not change and remained at 152.32 mbgl for the duration of pumping.

The pump was turned off at 18:30 on the 16th of August, after 80 hours of pumping, and the recovery rate measured. **Figure 6-12** shows that the water level had recovered to 85.4 mbgl after 13 hours (within 95% of the original water level).

Figure 6-13 and **Figure 6-14** represent semi-log and log-log plots of the time drawdown data for interpretational analyses. Extrapolation of the drawdown data on **Figure 6-13** from 34-80 hours for 1 million minutes (~2 years) shows that if no boundaries are intercepted, the drawdown will remain above the Available Drawdown limit. The change in drawdown is small over a large period of time, implying steady state conditions were achieved. It can thus be concluded that the discharge rate of 47.5 l/s is sustainable. Similar considerations as detailed for DN-P01 apply to the results obtained from BS-P01 in terms of the requirement for observation data to inform on storage parameters and increase confidence in analytical data requirements and assumptions.

Figure 6-15 illustrates that the adapted Theis (1935) solution has a good fit at late time- although the drawdown does seem to decrease during early time, making it challenging to fit a curve. This is possibly due to the effect of recharge from underlying rift related faults and potential pressure differentials within the aquifer or fault system. No evidence of a delayed response or aquifer leakage is present. Curve matching was done manually under the "Visual" tab. The resulting Transmissivity of 16 120 m^2/day is high, but in the same order as the results obtained for the RAJ-1 and RAJ-2 tests conducted by Umvoto (2015) and as obtained for borehole DN-P01. Due to the unconfined nature of the aquifer, the saturated thickness presumably changes as pumping progresses and drawdown increases. Dividing the T value obtained by the aquifer saturated thickness under natural conditions, a conservative Hydraulic Conductivity (K) value of 223 m/day is obtained (see **Table 6-6**).

The first attempt to commence pumping at BS-P01 as part of the AST failed due to a dead short in the cable joint (see **Table 6-5**). A Variable Frequency Drive (VFD) was used for the remainder of the test. The submersible pump was installed at a depth of 110 mbgl, 24.79 m below the rest water level of 85.21 mbgl. The pump was initially started at 68 l/s but was then reduced to 45 l/s for the remainder of the test due to the limitations of the VFD being used. The discharge rate was determined by a flow meter.

Table 6-5 Summary of the AST at BS-P01

AST	Duration (minutes)	Start	End	Flow Rate (l/s)	RWL (mbgl)	Drawdown (meters)	Recovery (meters)	Recovery (minutes)	Comment
1st	180	09/10/2016 11:00	09/10/2016 14:00	68	85.21	-	-	-	Dead short cable joint
2nd	17353	12/10/2016 16:35	24/10/2016 17:48	45	85.21	3.05	0.27	839.5	Spare control panel removed

No change based on site measurements of groundwater quality was observed over the 12-day constant discharge test. Water samples were collected for more detailed chemical analyses after 7 days. No further sampling for isotope analysis could be done due to the pumping test ending when the VFD was removed prior to the end of the other borehole tests.

The small changes in drawdown over an extended period of time (**Figure 6-16**) support results from the individual tests and further elude to the likelihood that steady state flow was achieved. This is in theory only and would require consistent hydraulic gradients observed in observation wells that had measurable effects from pumping (Kruseman and De Ridder, 1976). To give insight into any major boundary conditions and increase confidence in hydraulic parameters, specifically storage values and aquifer response, the well needs to be pumped for a longer period and possibly a higher rate to further extend the cone of depression to an observation point. The high yield potential and lack of observation data over long periods suggests that observation boreholes be installed within 5, 10 and 20 m of the pumped well and then be retested. This is further supported by the fact that the water levels measured in the monitoring well, BS-M01 (600 m away), remained constant at 152.32 throughout the AST.

After 12 days, the pump was switched off and recovery measured. Recovery was initially very rapid and the water level continued to recover to 0.27 m below the static water level of 85.21 mbgl after 839.5 minutes. There was a gradual decrease in temperature over the duration of the pumping test, with the temperature then increasing once the pump was turned off and recovery began.

Figure 6-16 shows a steady decrease in temperature as pumping progresses. As soon as the pump was switched off, the temperature can be seen to near instantaneously increase. This response was found to be unusual and in contradiction with the temperature trends experienced during pumping at the other boreholes. BS-P01 was drilled furthest off the fault identified in the MLEM geophysical surveys. This could imply that during pumping, cooler water present in storage within the alluvial aquifer is being

drawn into the well and the sudden change in pressure when the pump is switched off causes an influx of hotter deep, fault related or hydrothermal water to flow into the borehole.

Table 6-6 Summary of parameters obtained from test pumping BS-P01

BH ID	Transmissivity (m^2/d)	Thickness (m)	Hydraulic Conductivity (m/d)
BS-P01	16120	72	223,9

6.4.3 AY-P01

Test pumping of AY-P01 commenced at 10:30 on the 29th of September 2016. The submersible pump was installed at a depth of 74 mbgl, 22.69 m below the rest/static water level of 51.31 mbgl. The pump was started at full capacity with a yield of 56 l/s. The discharge rate was determined by a 90° V-notch.

On site groundwater quality assessments were conducted at various stages throughout the test and indicated that the water is acidic (pH=5.6), likely highly saline with an EC of >400 mS/m, and a temperature of ~58.3°C. Water samples were collected for more detailed chemical analyses after 30 and 80 hours respectively.

Figure 6-17 represents the curve of the manually recorded drawdown versus time since start of pumping. The water level drops 2.4 m from 51.31 to 53.71 mbgl within the first 30 seconds and steadily continues to drop for an hour after which the water level stabilizes at ~55.85 mbgl. This represents a drawdown of 4.55 m at a constant discharge of 56 l/s. For the remainder of the test the water level fluctuates between 55.86 and 56.2 mbgl. At ~3480 minutes the drawdown is seen to decrease slightly and continue at a pseudo steady state for the remainder of the test. This implies a well efficiency of 100% and that the aquifer is not being sufficiently stressed and is possibly still developing during testing. To give insight into any major boundary conditions and increase confidence in hydraulic parameters and aquifer response, the well needs to be pumped for a longer period. This is further supported by the fact that the water levels measured twice a day in the monitoring well AY-M01 did not change and remained at 88.32 mbgl for the duration of pumping. The pump was turned off at 18:30 on the 3rd of October 2016, after 80 hours of pumping, and the recovery rate measured. **Figure 6-17** shows

that the water level had recovered to 51.39 mbgl after 4 hours (within 95% of the original water level).

Figure 6-18 and **Figure 6-19** represent semi-log and log-log plots of the time drawdown data for interpretational analyses. Extrapolation of the drawdown data on **Figure 6-18** from 36-80 hours for 1 million minutes (~2 years) shows that if no boundaries are intercepted, the drawdown will remain above the Available Drawdown limit. The change in drawdown is small over a large period of time, implying steady state conditions were achieved and that the discharge rate of 56 l/s is sustainable. **Figure 6-19** highlights how rapid recovery was after pumping ceased.

Figure 6-20 illustrates that the adapted Theis (1935) solution is best fitted to the late time data, several other analytical curves were used to obtain a good match, but the Theis (1935) curve was best suited. The decrease in drawdown as seen from ~3480 minutes may be a result of a delayed response or aquifer leakage or could represent the development of the borehole progressing as pumping continues and drilling fluid is removed from the immediate vicinity around the borehole or in the borehole screens, allowing for more efficient flow of groundwater into the well. Curve matching was done manually under the “Visual” tab. The resulting Transmissivity of 19 540 m^2/day is high, but in the same order as the results obtained for the RAJ-1 and RAJ-2 tests conducted by Umvoto (2015) as well as the tests done at DN-P01 and BS-P01. Due to the unconfined nature of the aquifer, the saturated thickness presumably changes as pumping progresses and drawdown increases. Dividing the T value obtained by the aquifer saturated thickness under natural conditions, a Hydraulic Conductivity (K) value of 149.2 m/day is obtained. **Figure 6-21** shows a steady increase in temperature as pumping progressed. As soon as the pump was switched off, the temperature can be seen to gradually decrease. This response is interpreted to be due to AY-P01 intersecting a major fault at depth. It is possible that water or hydrothermal fluid was being extracted directly from the fault during pumping and that when the pump was switched off, the temperature decreased as water held in storage in the alluvial aquifer then flowed into the borehole. This implies that there is a possible vertical source of recharge below the aquifer. No impact from pumping any of the other boreholes was visible in any of the monitoring or pumped boreholes during the AST. Based on the high T values obtained, it is no likely that such an effect will be visible until larger volumes are abstracted at a greater rate.

Table 6-8 represents the results of the aquifer parameters determined via analytical analyses of the test pump data.

To conduct the AST, a submersible pump was installed at a depth of 110 mbgl, 59.99 m below the rest water level of 50.01 mbgl. The pump was initially started at 68 l/s but was then reduced to 62.5 l/s for the remainder of the test, along with the removal of two impellers. The discharge rate was determined by a flow meter.

On site groundwater quality assessments were conducted at various stages throughout the test and indicated that the water is acidic (pH=5.85), likely highly saline with an EC of >400 mS/m, and a temperature of ~58.2°C. No change in groundwater quality was observed over the 22-day constant discharge test. Water samples were collected for more detailed chemical analyses after 7 and 20 days respectively. Stable and radiogenic isotope samples were also collected after 10 and 20 days respectively. The results and discussion of these hydrochemical samples can be found in **Chapter 6.** **Table 6-7** illustrates the differences between pump start up due to generator services and electrical problems.

Table 6-7 Summary of the AST at AY-P01

AST	Duration (minutes)	Start	End	Flow Rate (l/s)	RWL (mbgl)	Drawdown (meters)	Recovery (meters)	Recovery (minutes)	Comment
1st	720	10/10/2016 09:45	10/10/2016 21:45	68	-	-	-	-	Dead short in cable joint
2nd	8680	15/10/2016 18:00	21/10/2016 18:40	61.5	50.13	4.89	-	-	Dead short in cable joint
3rd	31575	25/10/2016 11:00	16/11/2016 09:15	62.5	50.13	5.09	0.34	2920	End of AST

The small changes in drawdown over an extended period of time support results from the individual tests and further elude to the likelihood that steady state flow was achieved (see **Figure 6-21**). This is in theory only and would require consistent hydraulic gradients observed in observation wells that had measurable effects from pumping (Kruseman and De Ridder, 1976). To give insight into any major boundary conditions and increase confidence in hydraulic parameters, specifically storage values and aquifer response, the well needs to be pumped for a longer period and possibly a higher rate to further extend the cone of depression to an observation point. The high yield potential and lack of observation data over extended periods suggests that observation boreholes be installed within 5, 10 and 20 m of the pumped well and then be retested. This is further supported by the fact that the water levels measured in the monitoring well, AY-M01 (800 m away), remained constant at 88.66 mbgl throughout the test.

After 22 days, the pump was switched off and recovery measured. Recovery was initially very rapid, and the water level continued to recover to 0.34 m below the static water level

of 50.13 mbgl after 2920 minutes. There was a general increase in the water temperature as pumping progressed and then a decrease once the pumps were shut off and recovery began.

Assumptions linked to analytical analyses of the data may be invalid due to the possibility and likelihood of there being a vertical recharge source in the form of the underlying rift related faults. It is proposed that this would not respond as a recharge boundary, but as a deep source of water recharging the alluvial aquifer vertically with geothermally driven waters flowing along the rift related faults.

Figure 6-21 shows a steady increase in temperature as pumping progressed. As soon as the pump was switched off, the temperature can be seen to gradually decrease. This response is interpreted to be due to AY-P01 intersecting a major fault at depth. It is possible that water or hydrothermal fluid was being extracted directly from the fault during pumping and that when the pump was switched off, the temperature decreased as water held in storage in the alluvial aquifer then flowed into the borehole. This implies that there is a possible vertical source of recharge below the aquifer. No impact from pumping any of the other boreholes was visible in any of the monitoring or pumped boreholes during the AST. Based on the high T values obtained, it is no likely that such an effect will be visible until larger volumes are abstracted at a greater rate.

Table 6-8 Summary of aquifer parameters obtained from test pumping AY-P01

BH ID	Transmissivity (m^2/d)	Thickness (m)	Hydraulic Conductivity (m/d)
AY-P01	19540	131	149,2

Recovery data would be useful to determine T coefficient by means of a Horner Plot using the Theis concept. The recovery however, is too rapid to give any measurable change in residual drawdown over a single log cycle, as it is near instantaneous.

6.4.4 RAJ-1

The submersible pump was installed at a depth of 100 mbgl, 21.03 m below the rest water level of 78.97 mbgl. The original Grundfos pump fell down the borehole due to the binding-tie rod rusting and breaking (see **Table 6-9**). A 13 stage 55 kW submersible

pump was then obtained; it too had four impellers removed to compensate for the unforeseen static pressure. The pump ran at 25 l/s for the duration of the test and discharge was initially measured using a v-notch and later a flow meter.

Table 6-9 Summary of the AST at RAJ-1

AST	Duration (minutes)	Start	End	Flow Rate (l/s)	RWL (mbgl)	Drawdown (meters)	Recovery (meters)	Recovery (minutes)	Comment
1st	Failed to start	-	-	-	-	-	-	-	Pump fell down hole
2nd	17280	24/10/2016 16:00	5/10/2016 16:00	25	78.97	2.5	0.64	45	Service
3rd	10720	5/10/2016 17:20	13/11/2016 04:00	25	78.97	2.3	0.24	2175	Control board blew

On site groundwater quality assessments were conducted at various stages throughout the test and indicated that the water is acidic (pH=6.45), likely highly saline with an EC of >400 mS/m, and a temperature of 50.4°C. No change in groundwater quality was observed over the 20-day constant discharge test. Water samples were collected for more detailed chemical analyses after 7, 16 and 22 days respectively. Stable and radiogenic isotope samples were also collected after 11 days. Additional samples could not be collected due to the pumping test ending when the thyristors of the control box blew.

Figure 6-22 shows a relatively constant temperature as pumping progressed. As soon as the pump was switched off, the temperature can be seen to gradually decrease. This response is interpreted to be due to RAJ-1 being drilled directly over a major fault traceable at surface. It is possible that deep water or hydrothermal fluid was being extracted directly from the fault during pumping and that when the pump was switched off, the temperature decreased as water held in storage in the alluvial aquifer then flowed into the borehole. This implies that there is a possible vertical source of recharge below the aquifer. No interaction between any of the boreholes was observed during the AST. It can be seen from **Figure 6-22** that the drawdown was steadily increasing during the AST, this is assumed to be sue to the low discharge rate and it is believed when comparing the results to the initial constant discharge test results as obtained from Umvoto (2015), that insufficient discharge rate resulted in the abstraction always being from well bore storage and that the pump rate was too low to induce sufficient flow within the aquifer for the measurements to be wholly representative of aquifer behaviour, but more likely a result of borehole construction and the previously determined high T value of the fan allowing sufficient water to flow toward the borehole.

6.4.5 RAJ-2

The AST of RAJ-2 commenced after two previous attempts failed due to generator problems and motor being destroyed by water ingress (see **Table 6-10**). The submersible pump was installed at a depth of 40 mbgl, 9.16 below the static water level of 30.74 mbgl. The pump was initially started at 58.8 l/s, but after removing one impeller to compensate for the unforeseen static pressure it was discharged at 62.5 l/s for the remainder of the test. The discharge rate was determined by a flow meter.

Table 6-10 Summary of AST at RAJ-2

AST	Duration (minutes)	Start	End	Flow Rate (l/s)	RWL (mbgl)	Drawdown (meters)	Recovery (meters)	Recovery (minutes)	Comment
1st	1440	07/10/2016 10:15	08/10/2016 10:15	58.8	30.74	-	-	-	Generator failed
2nd	720	11/10/2016 15:30	12/10/2016 03:30	58.8	30.74	-	-	-	Motor blew
3rd	40800	18/10/2016 08:00	15/11/2016 16:00	66.7	30.74	4.93	0.26	3860	End of AST

On site groundwater quality assessments were conducted at various stages throughout the test and indicated that the water is acidic (pH=6.2), highly saline with an EC of > 400 mS/m and a temperature of 50 °C. No change in groundwater quality was observed over the 28-day constant discharge test. Water samples were collected for more detailed chemical analyses after 7, 16 and 27 days respectively. Stable isotope and radiogenic isotope samples were also collected after 17 and 27 days respectively.

Figure 6-23 shows a relatively constant temperature as pumping progressed. As soon as the pump was switched off, the temperature can be seen to gradually decrease. This response is interpreted to be due to RAJ-2 being situated near a rift related fault. It is possible that water or hydrothermal fluid was being extracted directly from the fault during pumping and that when the pump was switched off, the temperature decreased as cooler water held in storage in the alluvial aquifer then flowed into the borehole. This implies that there is a possible vertical source of recharge below the aquifer. The water level measurements are erratic in nature when compared to other borehole data in the region and are believed to be due to excessive turbulence in the borehole which may be a result of borehole construction and the materials used. This is supported by the fact that rust particles could be seen in the discharged water because of the borehole casing corroding.

6.5 AQUIFER AND BOREHOLE PARAMETERS

6.5.1 Specific Capacity

This unit for Specific Capacity (S_c) is cubic meters pumped per day per meter of drawdown (m^3/day/m). The discharge or flow per day is thus divided by the distance the water level in the well has drawn down.

$$\frac{Yield}{Drawdown} = \frac{\mathrm{m}^3/day}{s} \qquad (1)$$

As pumping time increases, so the Specific Capacity decreases. In theory, zero drawdown correlates with a maximum specific capacity as the saturated thickness is remaining constant (Driscoll, 1986). This was however not the case during the constant discharge test as the saturated thickness did not change after early time as pumping continued (see **Table 6-11**).

Table 6-11 Specific Capacity per borehole.

BH ID	Yield (m^3/d)	Drawdown (m)	Sc (m^3/d/m)
DN-P01	4665	9,9	472,2
BS-P01	4104	4,0	1018,4
AY-P01	4838	4,6	1063,3
RAJ-1 (AST)	2160	2,3	939,1
RAJ-2 (AST)	5763	4,93	1169,0

6.5.2 Transmissivity and Hydraulic Conductivity

Time drawdown data was analysed by means of the Theis (1935) solution adapted by Hantush (1961) for a partially penetrating aquifer, and Cooper Jacob (1946). C. E. Jacob developed a procedure (Jacob, 1944) that corrects drawdown data for the reduction in an unconfined aquifer's saturated thickness resulting from groundwater abstraction by a pumping well and thereby enables pumping tests in unconfined aquifers to be interpreted by methods for nonleaky confined aquifers. The results obtained using the two different solutions were very similar and thus the Theis related solution was deemed most suitable due to the accommodation for partial penetration.

The recovery data was rapid and was therefore not useful for gaining T values as changes in drawdown occurred near instantaneously, not allowing data to cover an entire log cycle as would be required by methods such as a Horner Plot (Horner, 1951).

The Transmissivities calculated using the AQTESOLV software were all high but consistent with the Transmissivity of unconsolidated alluvial fans and other boreholes in the Dogua Mountain fans and while some fans had the highest T values, their K values were affected by the known aquifer thickness used (see **Table** 6-12).

Table 6-12 Summary of the analytical analysis for the production boreholes during October-November 2016

BH ID	T (m^2/d)	K (m)
DN-P01	11100	73,6
BS-P01	16120	223,9
AY-P01	19540	149,2

While the T values of the alluvial fans were undoubtedly very high as could be seen by the toe seeps, recovery data, small drawdown levels and a lack of drawdown in observation wells, there remained a moderate degree of uncertainty in the T values obtained. This was due to the potential influence of rift related faults recharging the aquifer vertically from depth. This would have caused many of the assumptions coupled with the Theis solution to be invalid. In addition to this is the uncertainty introduced by conducting test pump analyses on the pumped well and not having any observation data.

6.5.3 Storage

The aquifer was classified as an unconfined aquifer with a water table open to atmospheric pressure. In unconfined aquifers, the Storativity is typically represented by the Specific Yield (S_y) as the Specific Storage is so small that it is often neglected (Driscoll, 1986 and Kruseman and De Ridder, 1976). Due to the lack of observation data to add a distance element to the analytical solutions, storage values could not be determined.

Due to the uncertainty surrounding storage related parameters, values determined through numerical groundwater model calibration are deemed representative for storage yield calculations. While these values are also useful for input to the numerical model, S_y is one of the key parameters for which sensitivity analysis would provide some insight

to during various scenarios of the numerical model run. Typical S_y values quoted in literature for gravel material as encountered in the fans ranges from 0.15-0.23 (Umvoto, 2015).

6.5.4 Water Levels

Water levels were monitored throughout the drilling and test pumping as illustrated in **Figure 6-24** and **Figure 6-25**. A noteworthy observation was a water table gradient between the southern (Asabuya Fan) and northern boreholes (Bussaba and North Dogua Fans), the water level dropped 12 meters over 14 kilometres, at a gradient of 1:0.00086 meters (0.86 mm every meter). **Figure 6-24** shows that water levels of the production boreholes recovered almost immediately to their original level once the AST was stopped. AY-P01 recovered to its original water level at the start of the AST, but prior to that its water level was lower, this was likely due to it still recovering from drilling and the 80-hour constant discharge test and the pores still been blocked with mud from drilling.

Figure 6-25 shows water levels within all the monitoring boreholes remained relatively constant throughout the monitoring period and showed no effects from the AST. The lack of monitoring data prior to the initiation of the AST also allowed for uncertainty as to baseline and seasonal trends in water level. DN-M01 was removed from the data set as it was damaged and buried by alluvial material during a storm, resulting in sediment blocking the borehole.

Figure 6-26 illustrates the change in water level from before the AST to during pumping and then once recovery was complete after the AST. The water level contours were constrained by water level data from within the boreholes and the fan toe seeps. This showed that there are two water mounds or high points, the Asabuya Fan to the south and the North Dogua Fan to the north, with the Bussaba Fan in the middle forming a low point. The water therefore possibly flows northward and southward to the Bussaba Fan.

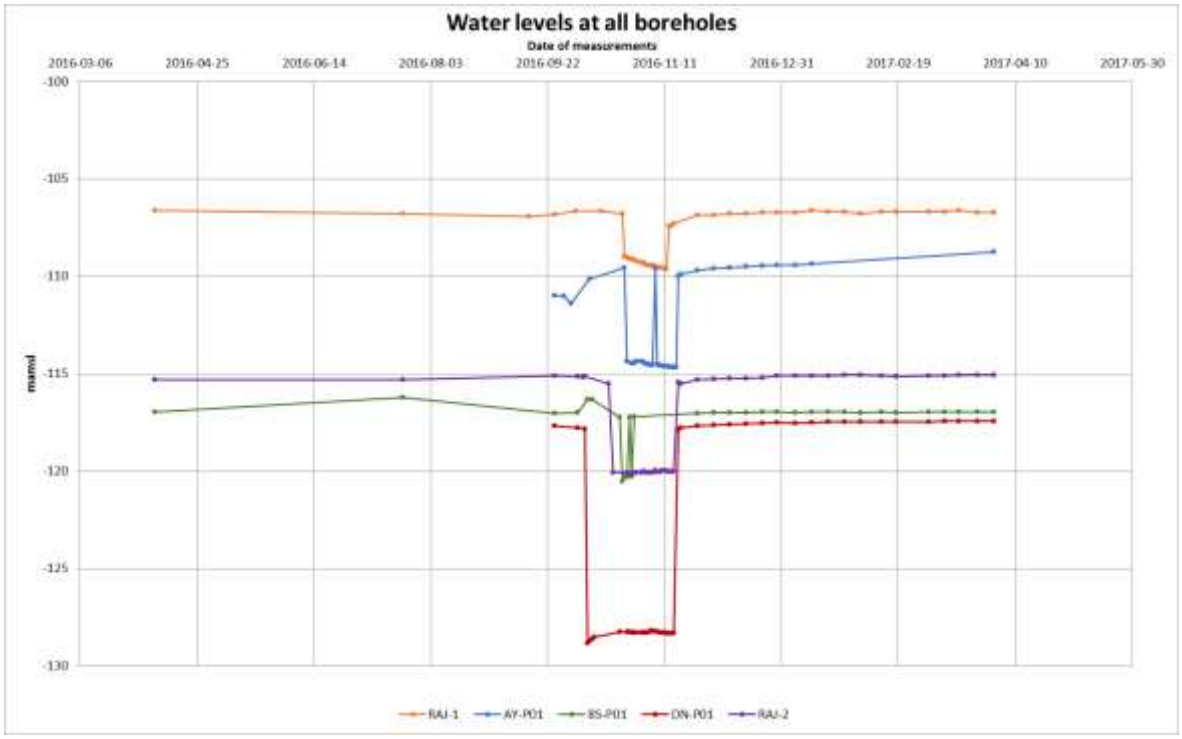

Figure 6-24 Summary of production borehole water levels pre, during and post AST, measured manually. Gradient from south to north is noticeable.

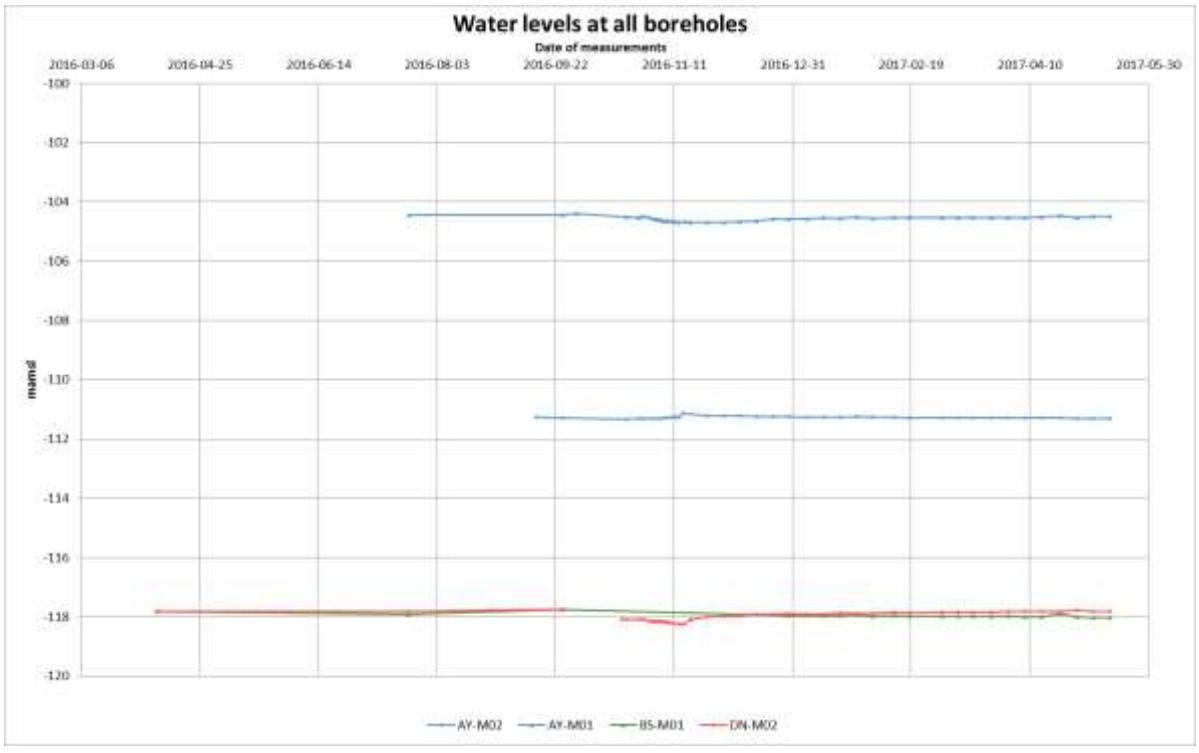

Figure 6-25 Summary of monitoring borehole water levels pre, during and post AST, measured manually. Gradient from south to north is noticeable.

The Asabuya Fan showed an increase in water level up the fan at a gradient of 0.0085. The other fans showed a decrease in water level up the fan with a gradient of 0.007 and 0.12 for the Bussaba and North Dogua Fans respectively. The increase in water level at Asabuya could show that there is some western recharge from the Dogua Mountains and the decrease at the northern fans shows that there is no western recharge, but possibly northern/southern recharge. The high T values implied that a shallow cone of depression developed during pumping that should typically have a large radius. The radius is important for storage calculations, but the lack of observation borehole data limited the possibility of reliable storage calculations being carried out.

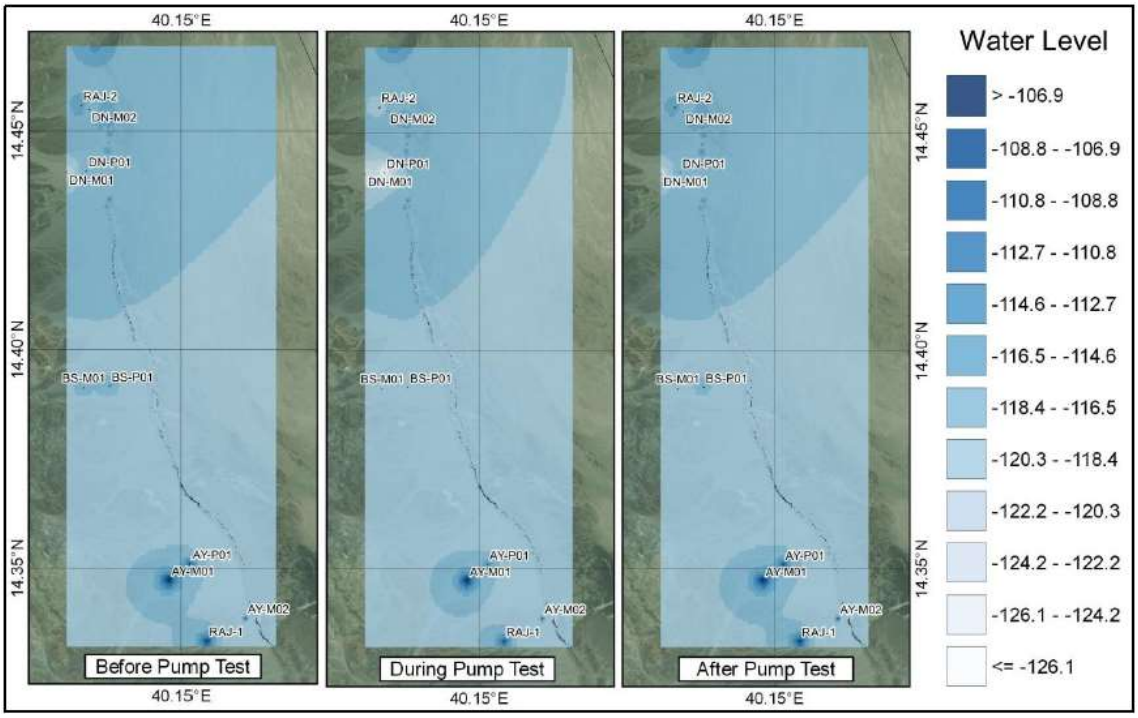

Figure 6-26 Water level contour map of the aquifer pre, during and post AST.

Water level measurements from AY-M01, AY-P01 and AY-M02 boreholes showed that the water table is sub-horizontal, with a gradient of 0.0085 m between the boreholes and the level of the seep from the fan toe. The water table gradient in the Bussaba and North Dogua Fans differed slightly at 0.007 and 0.12 m respectively but decreasing from the fan toe seep. This water table gradient was useful when determining the potential volume of the specific fans as the saturated portion of the fan is not perfectly horizontal.

6.6 AQUIFER SUSTAINABILITY

Discharge rates from all five production boreholes were recorded using flow meters or a V-notch throughout individual testing and the AST. **Figure 6-27** illustrates the discharge rate of each individual borehole and the period that it was flowing for during the AST. This varied between 25 l/s, 62.5 l/s, 45 l/s, 62.5 l/s and 66.7 l/s for RAJ-1, AY-P01, BS-P01, DN-P01 and RAJ-2 respectively. The combined flow rate of the five production boreholes throughout the AST is shown by the solid black line, peaking at 245.5 l/s but averaging at 216.7 l/s with only four boreholes flowing together because of BS-P01 being forced to shut down. The total volume discharged from the aquifer during the AST was 603 370.7 m^3, represented by the solid red line.

The dashed black line represents the achievable combined flow rate from all five production wells if they were equipped with the correct equipment and flowed simultaneously. Challenges in the AST hindered this, such as BS-P01 only pumping for 10 days before it was shut down and RAJ-1 only being able to yield 25 l/s with the pump used, when in Umvoto (2015) the data showed that 50 l/s was sustainable. At the achievable combined discharge rate of 286.7 l/s, a total volume of 842 209.9 m^3 could have been discharged during the AST.

Figure 6-28 predicts the total volume to be discharged over an entire year from the five production boreholes at the AST discharge rate and the potential discharge rate, yielding 6.5 million m^3 (6.5 hm^3) and 9.2 million m^3 (9.2 hm^3) respectively. If the five current boreholes were to function at their full potential that would already yield 31% of the full-scale mining requirement of 30 million m^3/annum.

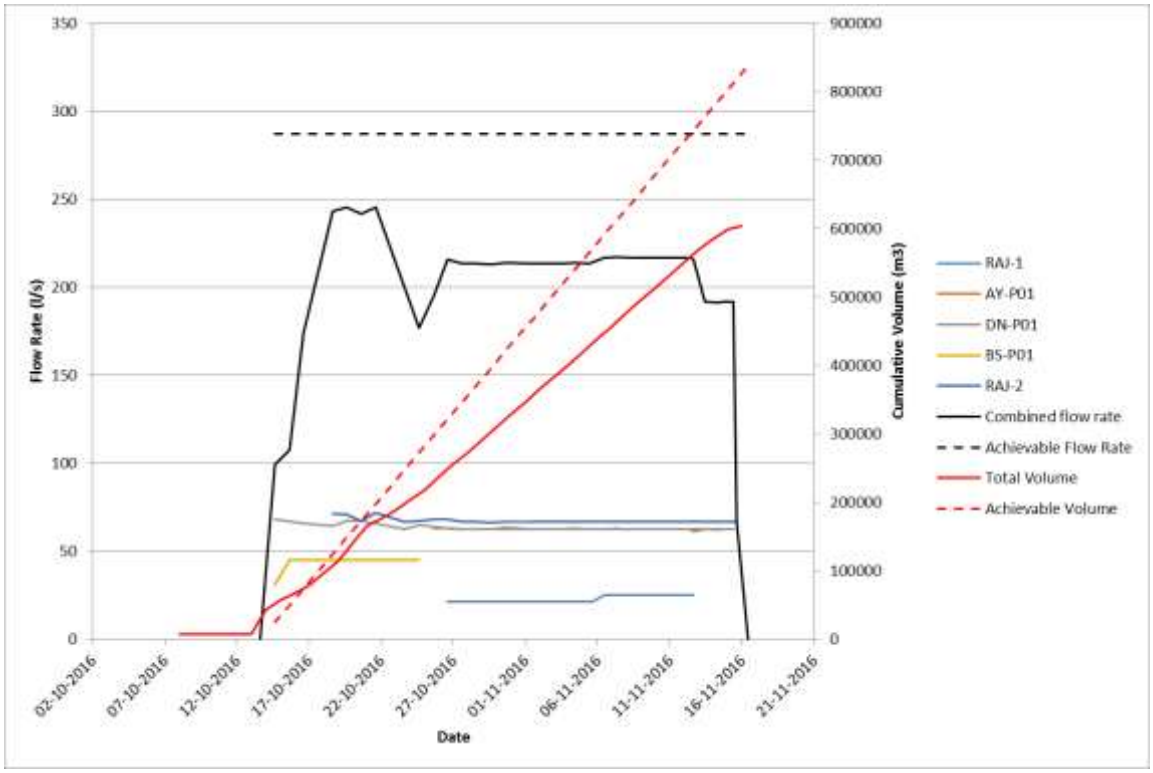

Figure 6-27 **Summary of individual borehole flow rates, combined total flow rate and total discharged volume during the AST. The dashed lines represent the potential combined flow rate and volume if all equipment functioned correctly.**

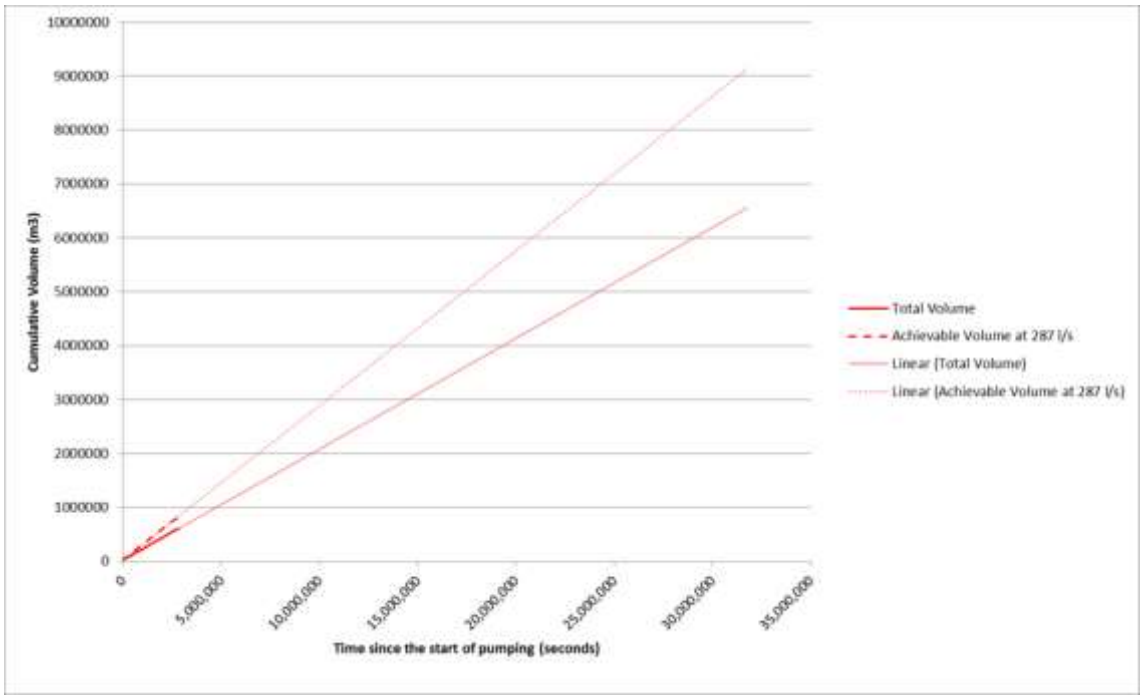

Figure 6-28 **Prediction of the total volume discharge for one year by extrapolating the actual discharge rates from the AST and the potentially achievable discharge rates, represented by dashed lines.**

CHAPTER 7
HYDROCHEMISTRY

7.1 INTRODUCTION

Natural groundwater often contains amounts of dissolved solids or gasses. The chemical constituents of a groundwater sample are a function of the various soil- or rock-water interactions that occur during its passage through the hydrological cycle. In areas with multiple aquifers of varying geological material, such interactions should generate a variety of bulk groundwater compositions, reflecting the variety of chemical sources in the given region. Analyses of groundwater chemistry are therefore useful for discerning between various groundwater sources and possible groundwater flow paths. Identifying recharge sources to the alluvial fans is crucial from a sustainability perspective as well as in terms of protecting potential fresh water sources form contamination by the hypersaline and brine waters known to be present. Hydrochemical analyses and trends offer valuable insight into determining where water recharging an aquifer may originate from. The presence of a hydrothermal system and the complex geological setting within the rift, however made such determinations challenging.

Hydrochemical data within the mining concession were sparse and were mostly concentrated to the south of the concession boundary, in the Gehertu, Musley and Bacarti fans.

7.2 METHODOLOGY

Water samples were collected for detailed hydrochemical analysis. These measurements were used, in addition with sample results by MWH (2015d), Umvoto (2015) and WWDSE (2013) to compare the chemistry of various borehole, seep and spring samples collected to identify possible recharge sources to the Asabuya, Bussaba and North Dogua fans. Most samples were collected between August and November 2016, during the Aquifer Stress Test (see **Chapter 6**). Samples were collected using best practice sampling protocol, and were packaged and transported to an ISO 17025 and SANAS accredited laboratory in Pietermaritzburg, South Africa for analysis.

Samples were analysed for macro and micro (trace metals) chemical constituents. In addition to these, stable and radiogenic isotope sampling was also carried out. Nitric acid was used as the preservative for the radiogenic isotope samples. An ion balance was

conducted on all results obtained from the laboratory to ensure accuracy. Here, the major anions and cations should ideally achieve a ratio balance of 1:1. Results were first converted to milliequivalents per litre (meq/l) by multiplying the concentration in milligrams per litre (mg/l) by the charge of the ion. Most samples showed a balance of 0.9-0.95, but some did range between 0.85-0.88. These results were considered to have a “good” to “excellent” balance and were deemed acceptable.

The possibility of the mine having a fresh water requirement of 5% of the total demand was considered when interpreting and discussing the hydrochemical results. While solution mining can be undertaken with poorer quality water, the analysed samples were compared to a combined drinking water quality standard to account for the possibility that groundwater may be used to fulfil the mine’s fresh water demand as well. The combined standard used was developed from a combination of standards set by the World Health Organisation in 2011 (WHO, 2011), Ethiopian Ministry of Water drinking water quality specifications (MoWE, 2002) and the South African National Standard (SANS) 241-1:2011 Standard Limit for Health (SABS, 2011). Constituents that exceeded these standards were highlighted in red (see **Appendix D**). Results of specific samples and constituents were plotted against each other to highlight specific trends and indicators of water quality, type and origin. Hydrochemical plots were used to illustrate the results graphically and to assist in classification and interpretation. **Figure 7-1** details the location of all the samples collected within the vicinity of the mining concession. The results have been discussed per fan from north to south and then discussed holistically. For the discussion, fresh, saline and brackish waters were based on the TDS concentrations as presented in **Table 6-1** below.

Table 7-1 TDS concentrations for water classification

Water Type	TDS range (mg/l)
Fresh	< 1 000
Brackish	1 000 - 10 000
Saline- Hyper saline	10 000 - 100 000
Brine	>100 000

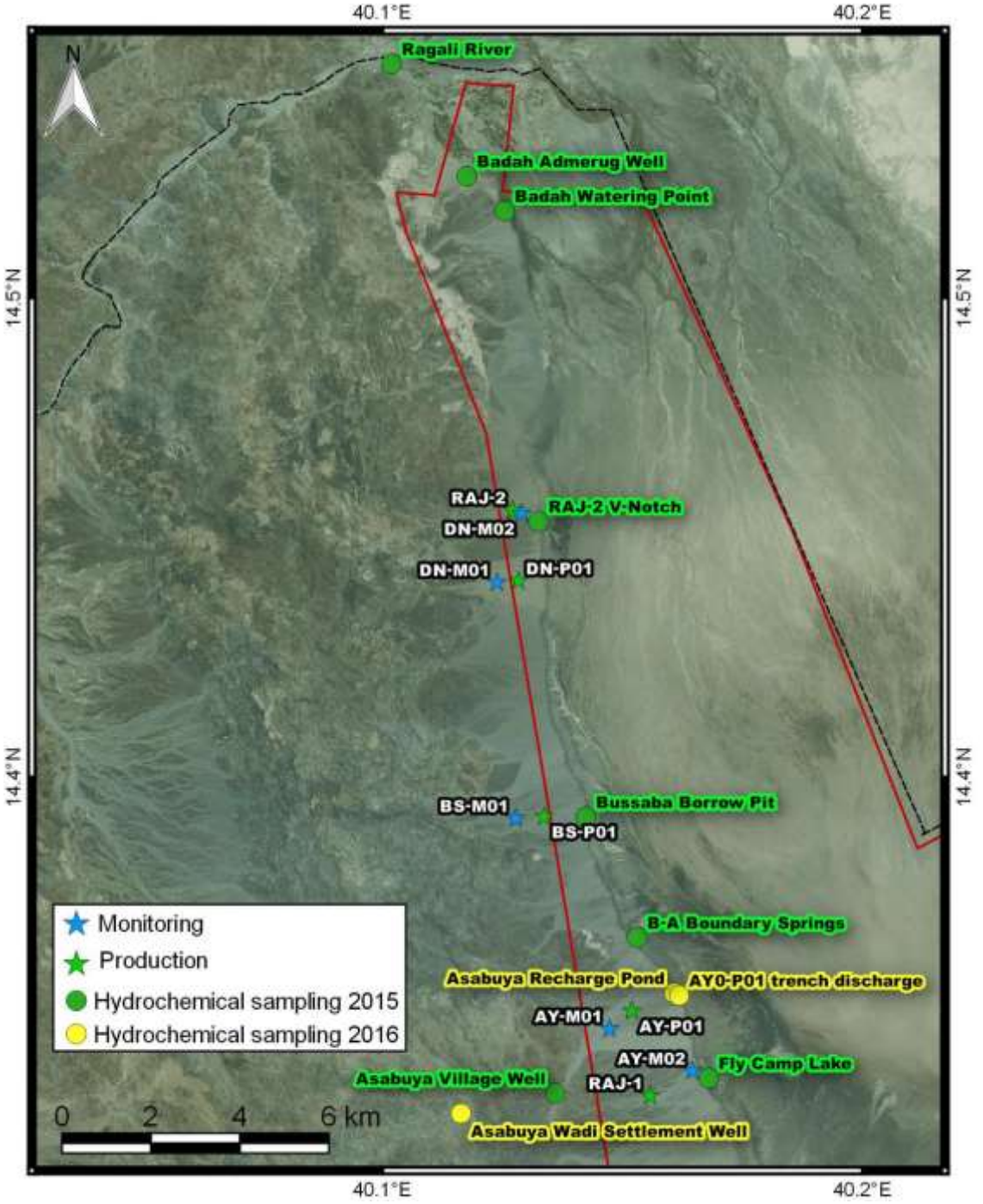

Figure 7-1 Map illustrating the location of samples collected for hydrochemical analyses (Umvoto, 2016c).

7.3 RESULTS

The hydrochemistry of samples collected were plotted in figures below and tabulated in **Appendix D**. **Figure 7-2** is a Piper Diagram of all samples collected within the vicinity of the mining concession. Piper diagrams illustrate bulk groundwater chemistry and are

useful for discriminating different groundwater groups. Most of the deep groundwater plotted in the Na-Cl type waters while samples from shallow wells appeared to plot in the Ca- HCO_3^- type waters. While a Piper diagram did not give any spatial context, it was useful in discerning potential recharge sources to the different fans.

Figure 7-3 is a bar graph showing the borehole Total Dissolved Solids (TDS) values compared from north to south. RAJ-1 and DN-P01 were in the North Dogua fan, BS-P01 in the Bussaba fan and AY-P01 and RAJ-1 in the Asabuya fan. A general decrease in TDS over the duration of pumping was observed in the North Dogua and Bussaba fans production boreholes, whereas the TDS increased in the Asabuya Fan production boreholes. Overall TDS was significantly lower in southern fans, indicating better water quality.

Figure 7-4 shows a lower TDS in the monitoring wells further up the fans and that TDS increased in production wells from south to north. It illustrates the change in TDS from the production boreholes to the seeps at the toe of the fans, which possibly indicates dilution by a less dense, fresher water layer that overlies the highly saline waters derived from deep fracture flow.

Figure 7-5 is a plot of Na versus Cl. Major ion patterns of sodium and chlorine showed that for the northern fan boreholes, water quality improved with continued pumping. The blue line indicates the overall trend. Northern fan areas (RAJ-2 and DN-P01) showed generally higher concentrations in Na and Cl compared to the southern fans (AY-P01 and RAJ-1).

Figure 7-6 is a Sodium/Potassium versus TDS plot. Fresh and recent rain waters with low flow path length are characterised by low Na/K ratios and depending on the formation, low TDS (Umvoto, 2016c). This is the opposite for groundwater that has a longer residence time as there is more time for water-rock interactions. Potassium is concentrated in certain layers of rift-valley evaporitic sequences hence the potash potential. Waters derived from these formations correspondingly have low Na/K ratios, but have very high TDS concentrations due to the saline nature of the water (Umvoto, 2015). Na/K ratios were significantly higher in northern fans (blue ring) than in southern fans (green ring). A slight trend of decreasing ratios in each borehole was visible. The moderate Na/K and TDS values observed in the Asabuya fan samples implied a potential mixing between fresher bedrock groundwater and saline rift waters. The wells located close to the rift-boundary fault had the highest ratios which possibly infer a deeper groundwater origin, such as up-flow of groundwater along faults.

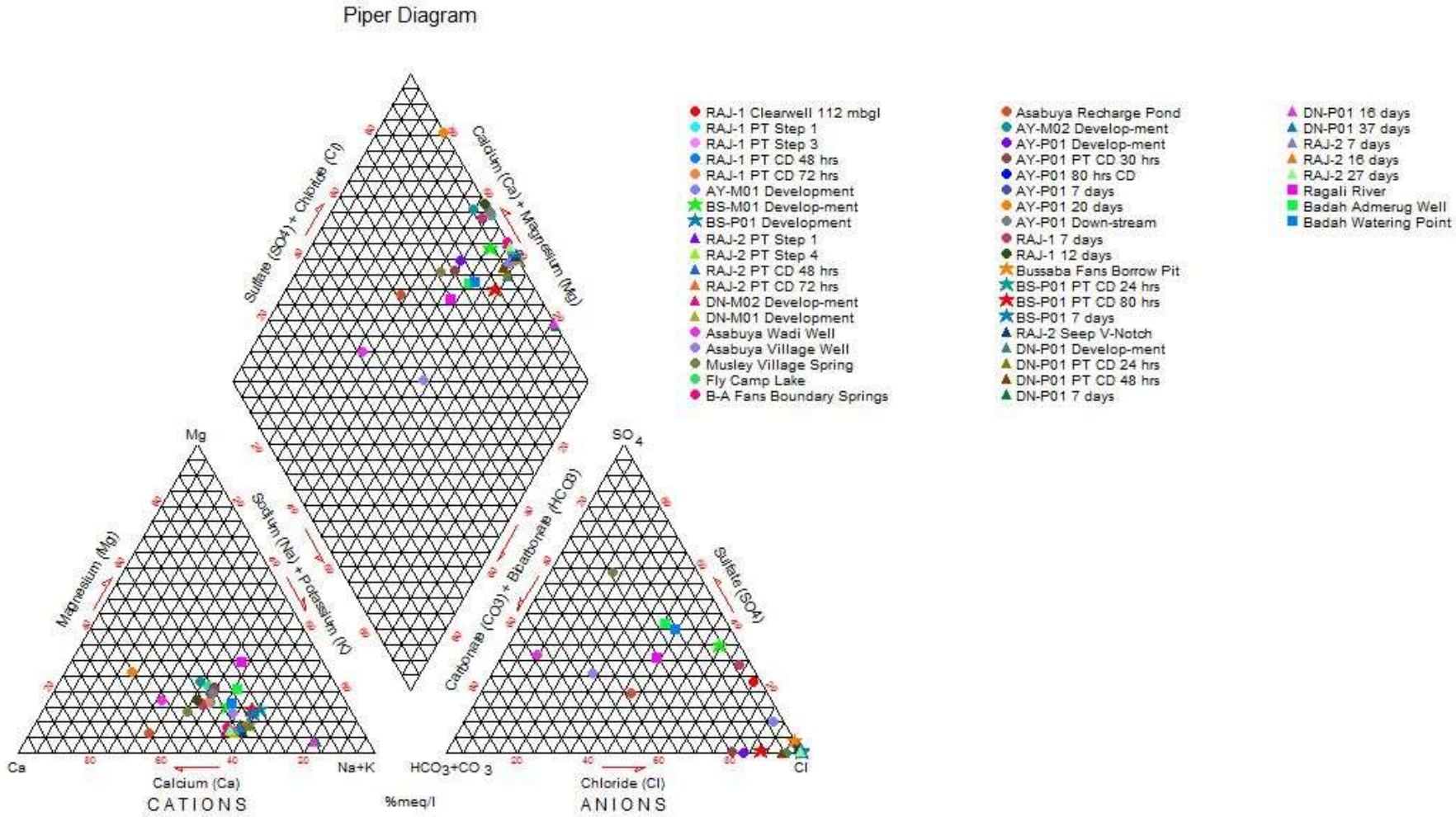

Figure 7-2 Piper Diagram indicating the major anion and cations in the samples collected from the Dogua Alluvial Fans and their respective wadis.

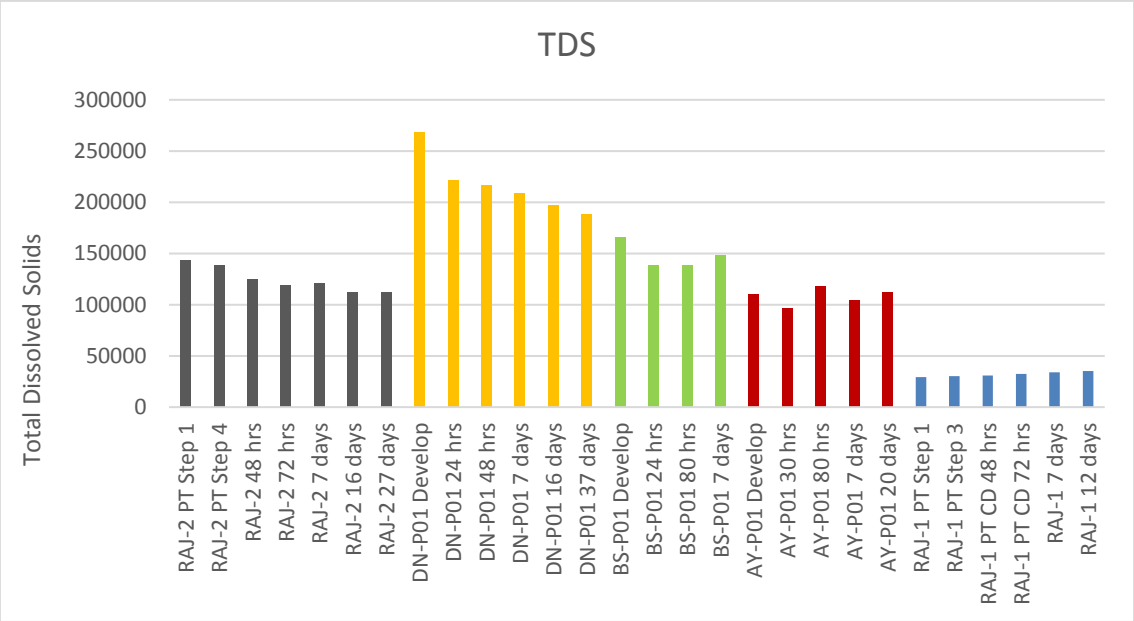

Figure 7-3 **Bar graph indicating the decreasing trend in salinity from north to south within the alluvial fans.**

Figure 7-7 is a Sulphate versus TDS plot. No distinct trends were visible. Per MWH (2015a), a straight-line trend typically indicates two or more sources. The lack of any significant trend affirmed the assumption of extensive mixing of different waters present in the fans. These were determined to be direct infiltration from run off and rainfall, hydrothermal influx, ancient red sea waters and formation waters. Samples from individual boreholes plotted together and concentrations can be seen in **Appendix D**.

Figure 7-8 is a plot of select dissolved metal concentrations in mg/l. If vertical thermal groundwater convection is present, it could also be a feasible pathway for the transportation of elevated metal concentrations commonly found in magmatic fluids (Umvoto, 2015). The high strontium concentrations were possibly derived from contact with basement rocks, especially in the northern fans. A trend of decreasing concentrations was noted as pumping continued. Manganese concentrations showed a similar trend, being higher in northern areas as opposed to the south. Boron is a strong indicator for hydrothermal and seawater influences (Umvoto, 2016c).

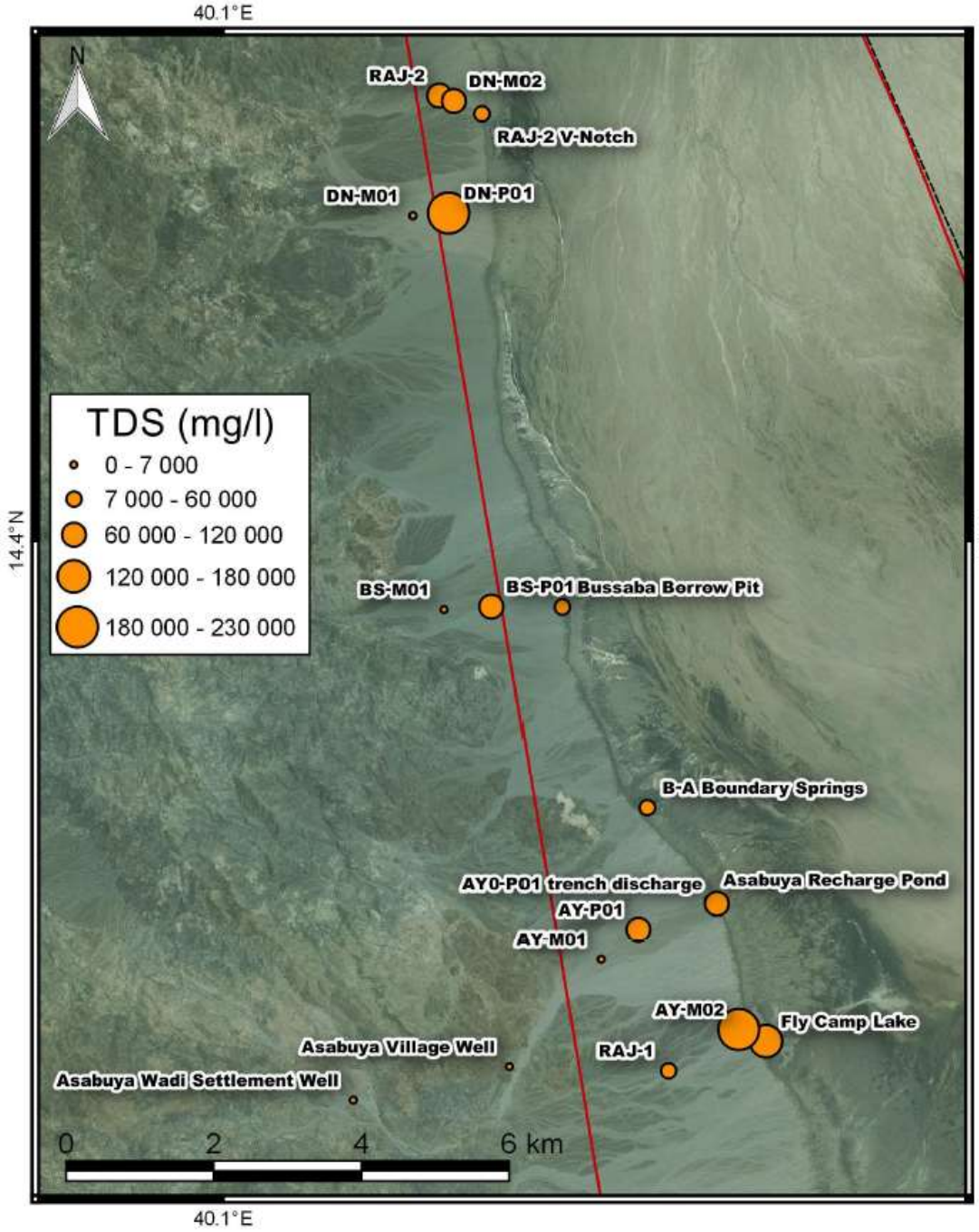

Figure 7-4 **Map illustrating where certain hydrochemical samples were collected and their TDS concentrations.**

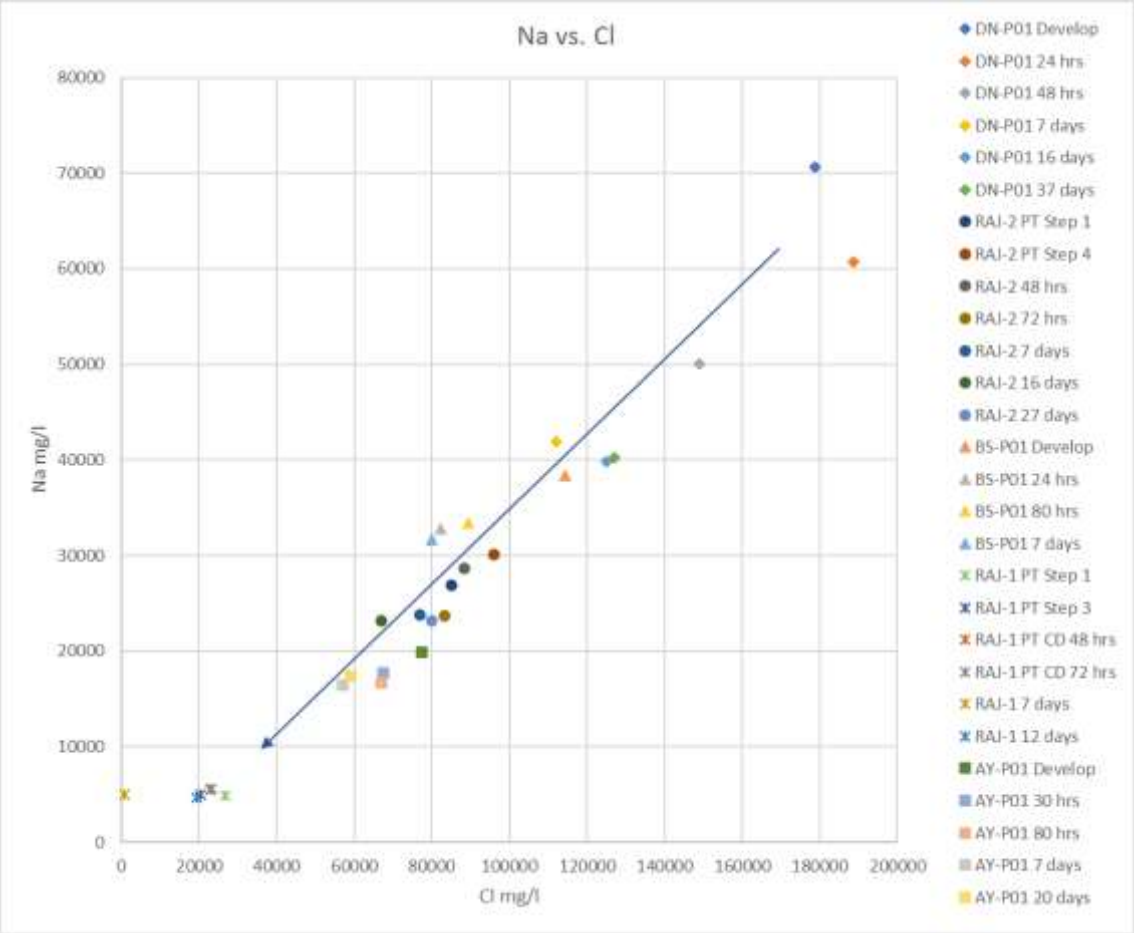

Figure 7-5 Sodium versus Chloride graph indicating a decreasing trend from north to south.

Figure 7-9 is a stable isotope plot of Deuterium and ^{18}O. Temporal trends represented by arrows also indicated that water quality could improve with prolonged pumping. A possible seawater signature was evident in the Dogua North fan which supports a possible ancient marine sourced recharge scenario for the northern fan. Local Meteoric Water Line (LMWL) and Red Sea composition field, shown by the ellipse are from the Alid area, Eritrea (Lowenstern *et al.*, 1999). Southern fans showed more depleted values, that trended towards the LMWL and Global Meteoric Water Line (GMWL).

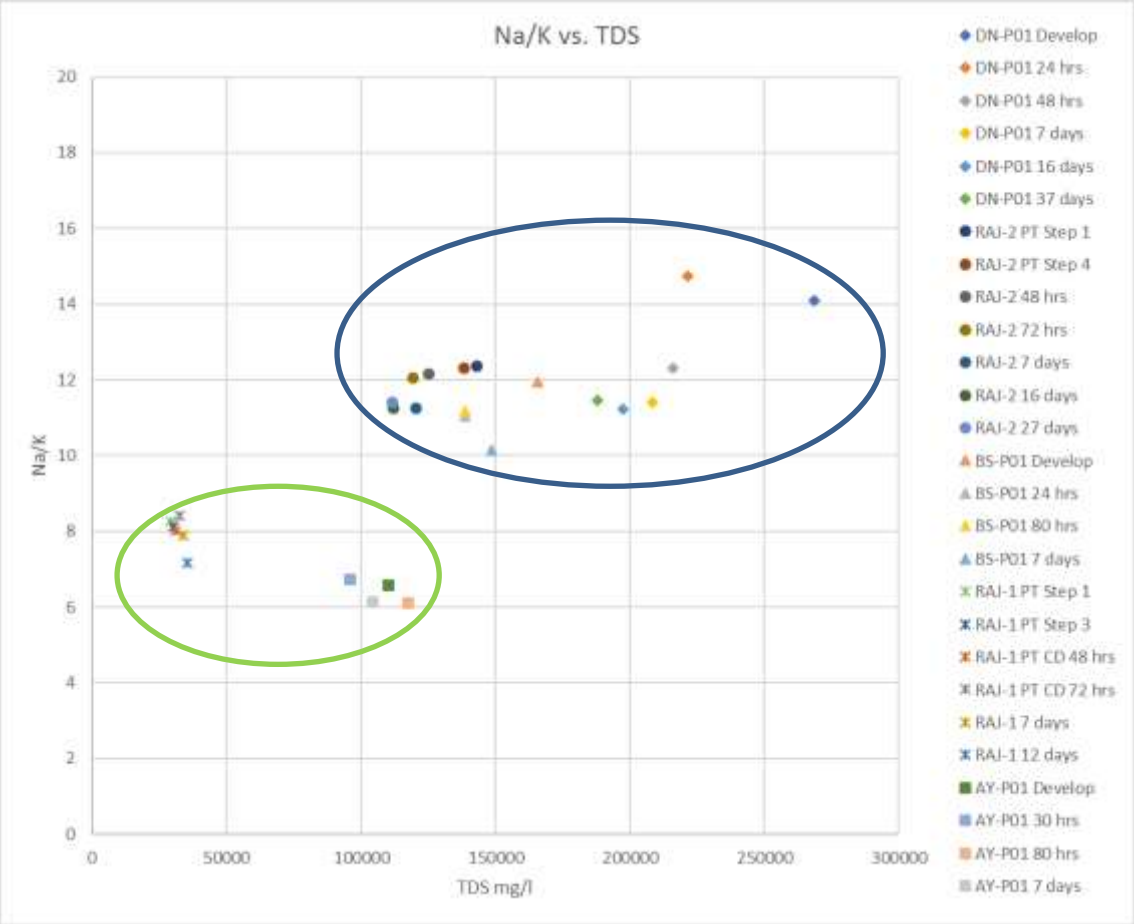

Figure 7-6 Na/K vs TDS diagram.

Figure 7-10 is a plot of ^{18}O versus TDS and indicated the brine character of most groundwater samples in the fans, except for RAJ-1 (Asabuya fan). The interpretive overlay (blue lines) are from Gat (1996). A general mixing trend between marine brine and brackish waters was observable, supporting ancient Red Sea waters flowing up via faults from the north into the fans as a possible recharge scenario.

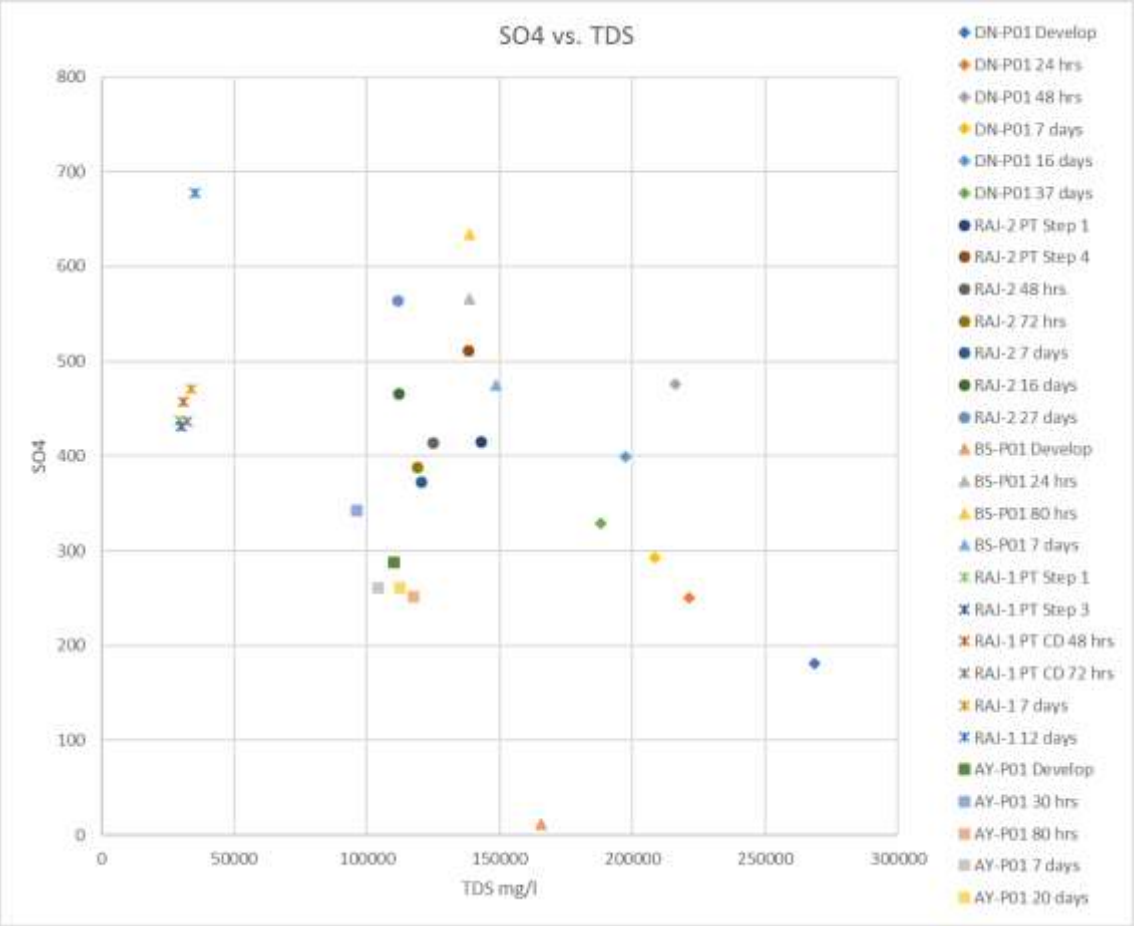

Figure 7-7 SO_4 vs TDS plot.

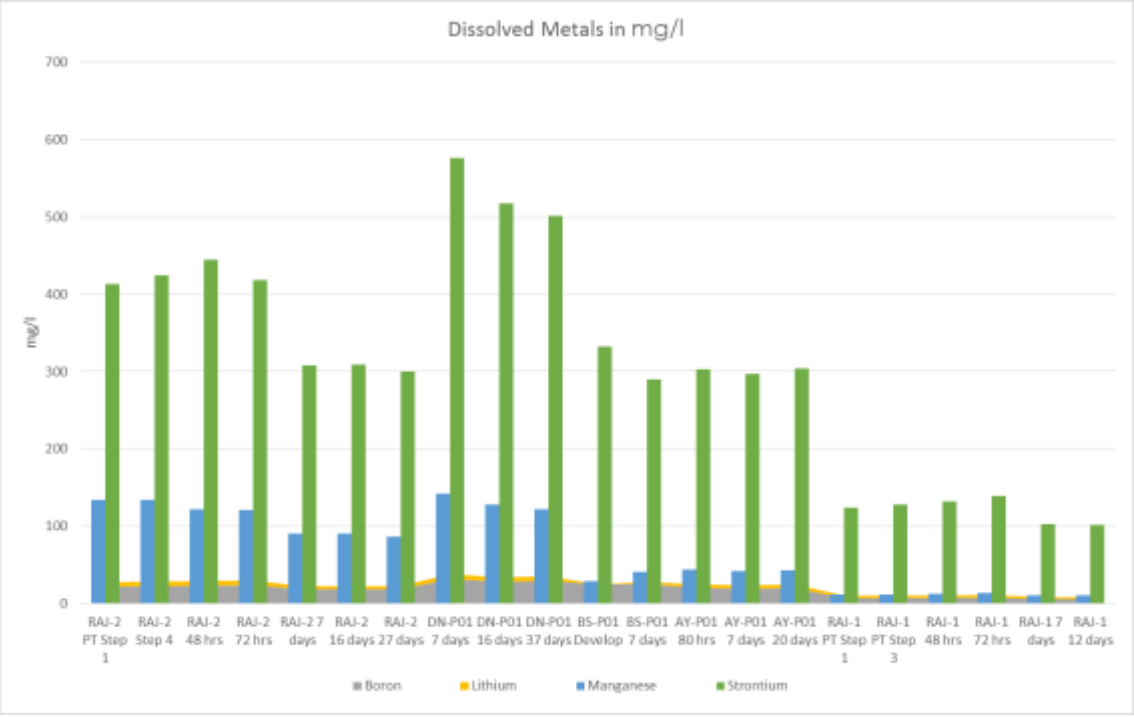

Figure 7-8 Diagram illustrating selected dissolved metals in mg/l.

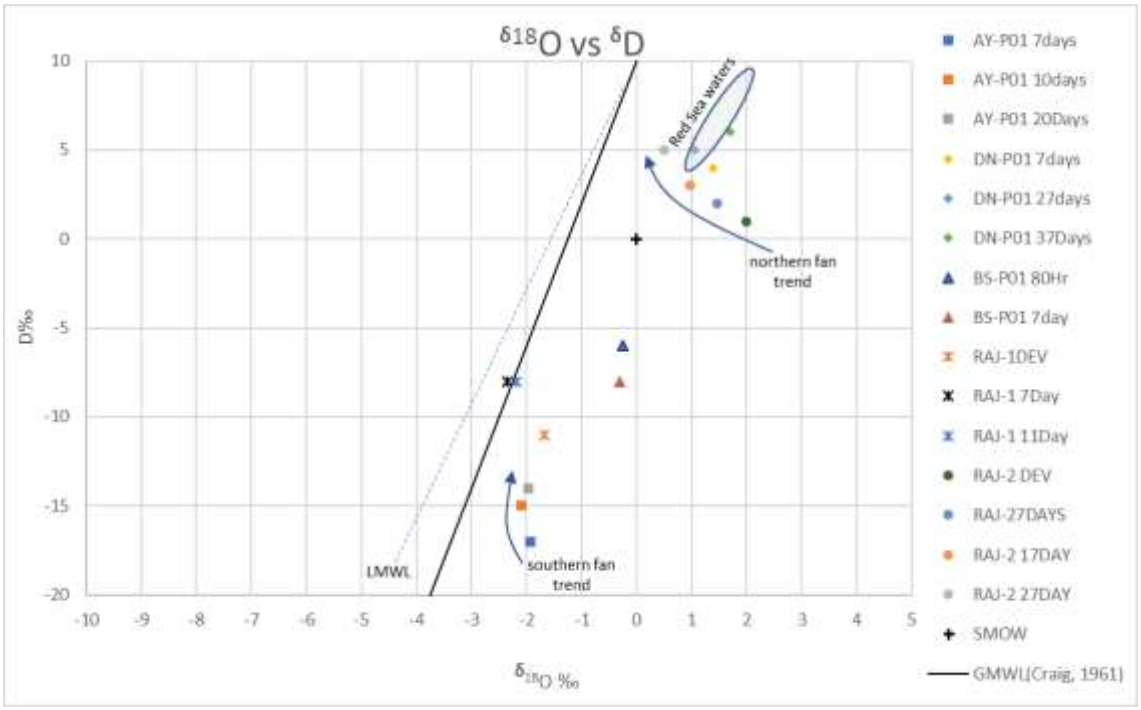

Figure 7-9 Stable isotope plot of Deuterium and ^{18}O.

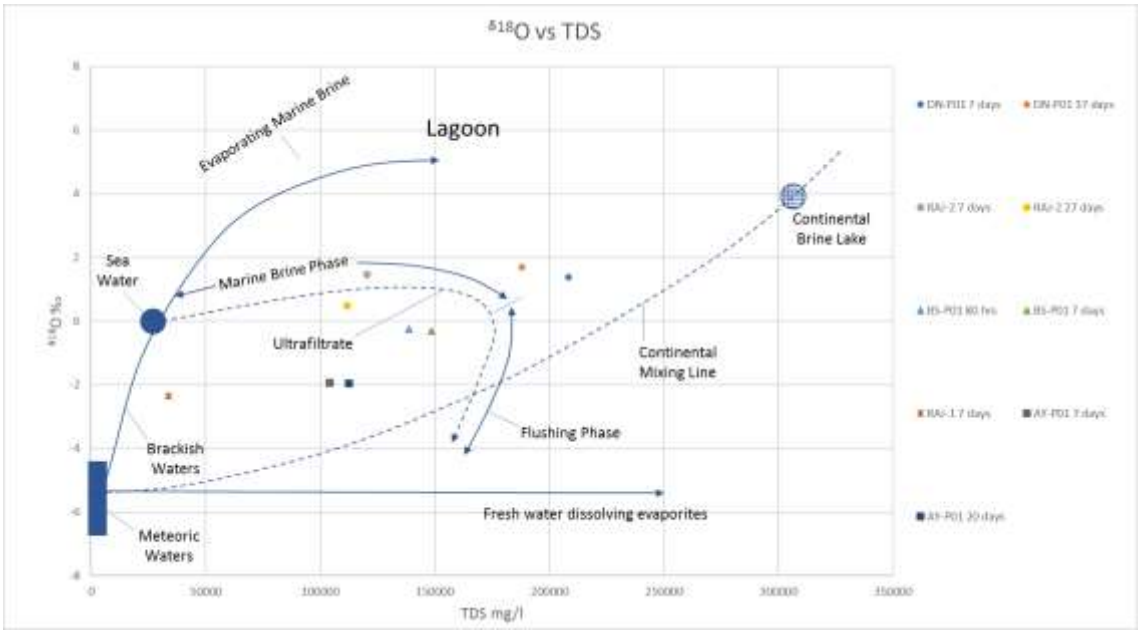

Figure 7-10 ^{18}O vs TDS plot after Gat (1996).

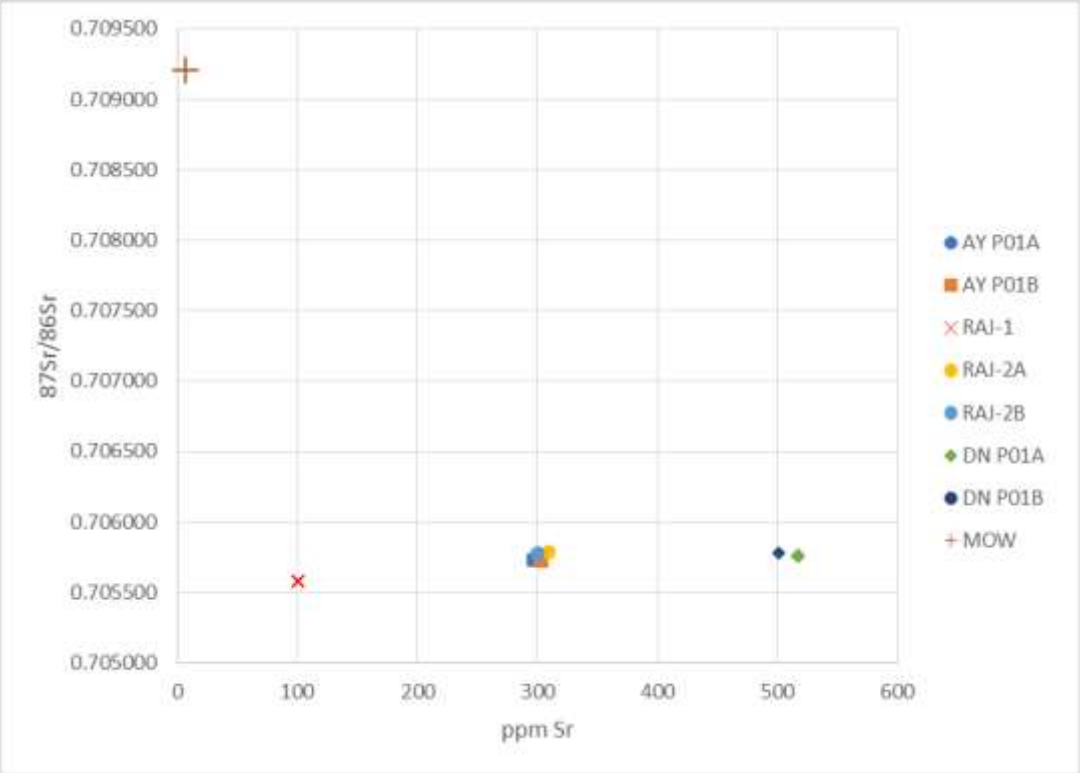

Figure 7-11 Radiogenic isotope plot of $^{87}Sr/^{86}Sr$ vs ppm.

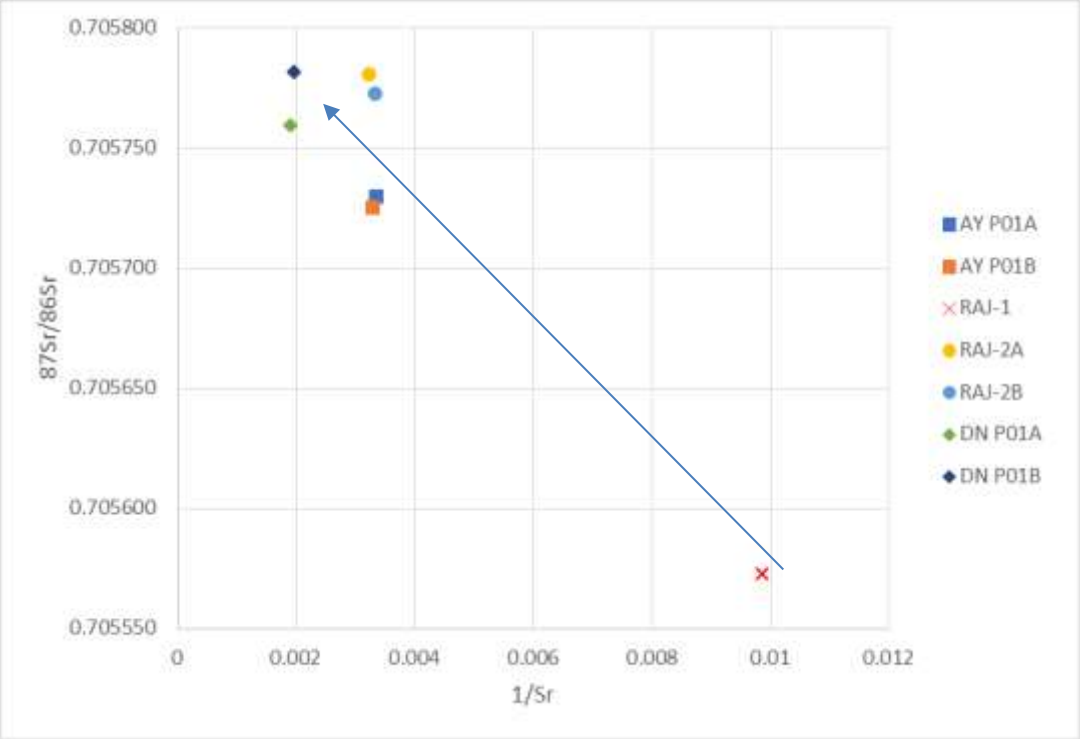

Figure 7-12 Radiogenic isotope plot of $^{87}Sr/^{86}Sr$ vs reciprocal Sr composition.

Figure 7-11 and **Figure 7-12** are radiogenic isotope plots of Strontium (Sr). MOW is the Mean Ocean Water composition (0.7092) which is similar to the Red Sea water composition (0.70916). The range of Sr ratios (0.705725 – 0.705781) indicated possible

fluid rock interaction in basaltic, possibly mantle derived rock types within the oceanic crust (Umvoto, 2016c). The low ratios could have derived from hydrothermal alteration thereof. There was a trend of Sr enrichment from south to north across the fan which could indicate that the source is water originating from the north for the northern fans, possibly the Afar or Red Sea Basalts in Eritrea (Umvoto, 2016c).

7.4 DISCUSSION

Water quality for potash mining is highly reliant on density. Sample results in **Appendix D** show that density across all the samples expectedly increased with increasing TDS, ranging from 0.99 g/cm^3 for BS-M01, AY-P01 and Asabuya Wadi Settlement Well samples to 1.15 g/cm^3 for AY-M01. Generally, the production boreholes showed water densities ranging from 1.00 g/cm^3 to 1.14 g/cm^3 in for RAJ-2 and DN-P01 respectively and 1.02 g/cm^3 to 1.07 g/cm^3 in the Asabuya fan, for RAJ-1 and AY-P01 respectively. BS-P01 ranged between 0.99 g/cm^3 and 1.11 g/cm^3 with an average of 1.09 g/cm^3. Personal communication with engineers involved in the potash mining operation indicated that water with a density of above 1.05 g/cm^3 was not ideal for solution mining, but this was not confirmed. If so, then considerable water treatment restraints may become a factor in the mine receiving the required volume of water.

The following results were noted from the hydrochemical tables (see **Appendix D**), summarised per fan from north to south.

7.4.1 Badah Fan

EC from the Ragali River and the Badah Watering Point in the northernmost, Badah fan, showed slightly elevated values of 293 and 404 mS/m respectively. The reduced EC in comparison to the other fans was likely due to flood recharge influence from the fresher Ragali River. The extensive Zariga Formation outcrop in the area possibly also had an effect by damming rainwater and therefore increasing freshwater infiltration into the fan.

Badah watering point and Badah Admerung Well had pH values of 7.6 and 7.8 respectively, with the Ragali River sample being the highest at 8.4.

The Ragali River, Badah Admerung Well and Badah Watering Point had TDS of 974 mg/l, 2 136 mg/l and 2 368 mg/l respectively. The latter two were classified as brackish water (1 000 – 10 000 mg/l) and the Ragali River sample as freshwater (<1 000 mg/l).

Badah Admerung and Badah Watering point showed elevated concentrations of sodium, magnesium, chloride and sulphate which were slightly above the drinking water limits. Nitrate concentrations were also slightly elevated which is often indicative of human and animal waste and sewage. The Ragali River only showed elevated chloride concentrations, all other macro constituents showed concentrations within the drinking water quality standards.

Dissolved trace elements were generally low in the Badah fan. Boron and strontium showed elevated values which could have indicated a hydrothermal influence, or residual sea waters (boron), or contact with the Jurassic carbonate and Precambrian basement rocks (strontium) in the Badah region.

7.4.2 North Dogua Fan

EC readings at DN-P01, DN-M02, DN-M01 and RAJ-2 showed elevated values of >20 000 mS/m, 11 380 mS/m, 16 080 mS/m and 17 570 mS/m respectively. There was a tendency for EC at RAJ-2 to decrease during continued pumping, for example in 2015 it decreased from 17 570 mS/m to 16 430 mS/m and in 2016 from 14 600 mS/m 14 210 mS/m. EC readings in the northern Dogua fans were generally higher than in the southern fans. This may be due to the influence of deep groundwater through-flow from the Tsaliet Group basement or additional upward injection of thermal brines along the MDRF.

Samples from DN-P01 development and DN-M01, within the North Dogua fan, had a pH of 5.9 and 6.9 respectively. The pH at DN-P01 became more neutral with continued pumping, it increased from 5.9 –6.3. The pH at RAJ-2 varied between 6.4 and 6.8. The more acidic pH values of DN-P01 were possibly the result of elevated sulphate concentrations in the basement rocks, as well as thermal upwelling.

TDS measurements at RAJ-2 and DN-P01 showed values of 142 910 – 111 720 mg/l and 268 562 – 188 052 mg/l respectively, which classified them as brines (>100 000 mg/l). A steady decrease in TDS was observed with continued pumping (see **Figure 7-3**). DN-M02 was also classified as brine with a TDS of 107 548 mg/l. The TDS of DN-M01 could not be analysed.

The elevated (above drinking water quality standards) concentrations of magnesium, sodium, potassium, chloride, fluoride and bromide in the DN-M02, DN-M01, DN-P01 and RAJ-2 samples indicated a possible strong basement rock or marine influence on the groundwater in the North Dogua fan. Concentrations of sodium, chloride and bromide

decreased with continued pumping (**Figure 7-5**, **Figure 7-7**). Fluoride and ammonia concentrations of >2 mg/l and 10.6 – 93 mg/l respectively, were both above the drinking water quality standard. Sulphate concentrations were within drinking water quality standards for most of the North Dogua fan samples**.**

DN-M01, DN-M02, DN-P01 and RAJ-2 had elevated concentrations of strontium, manganese, lithium and boron (**Figure 7-8**)**.** The high manganese content (up to 141 586 µg/l in DN-P01) was possibly the result of acid waters from hydrothermal upwelling in the northern fan. This was also likely the case for the elevated boron and lithium which are indicators of a hydrothermal influence. The elevated strontium concentration (up to 576 165 µg/l in DN-P01) was possibly from groundwater interactions with the metasedimentary basement rocks, carbonates and gypsum. DN-M01 also had elevated concentrations of arsenic, mercury and molybdenum. A decrease in trace metal concentrations was observed with continued pumping.

7.4.3 Bussaba Fan

BS-P01 had an elevated EC that decreased from 24 400 mS/m to 16 650 mS/m as pumping progressed. BS-M01 had a lower EC of 788 mS/m. BS-P01 likely had a higher EC because it was situated on the MDRF, possibly receiving hydrothermal brines, whereas BS-M01 was situated higher up on the fan, further away from the MDRF.

BS-P01 was slightly acidic with pH values of 6.4 –6.5. BS-M01 however, was slightly alkaline with a pH of 7.5, which was possibly the result of recharge from the gypsum (Zariga Formation) higher up on the fan.

BS-P01 had TDS values of 165 552 – 148 442 mg/l, classifying it as a brine. BS-M01 had significantly lower TDS values of 5 220 mg/l, classifying it as brackish water.

Elevated concentrations of sodium, potassium, chloride, magnesium and bromide were found in the BS-M01 and BS-P01 samples, possibly from interactions with the basement rock or a marine influence. **Figure 7-6** illustrates a decrease in sodium and chloride concentrations with continued pumping. Elevated sulphate concentrations were found in the Bussaba Fan Pit and BS-M01 of 1 540 mg/l and 1 280 mg/l, respectively (see **Figure** 7-7).

Elevated concentrations of barium, boron, manganese, nickel, strontium and thallium were found within the Bussaba fan boreholes. Because of the more neutral pH, less

dissolved manganese was found in the Bussaba fan. Strontium concentrations of 332 759 µg/l and 10 803 µg/l were found in BS-P01 and BS-M01 respectively. Similar to the trend observed with the EC, this showed a decrease in concentration away from the MDRF. In the North Dogua fan, the monitoring borehole BS-M01, located at a higher elevation, was enrichment in arsenic, mercury, molybdenum and selenium, possibly associated to its proximity with the basement rocks.

7.4.4 Asabuya Fan

The AY-M01, AY-M02, AY-P01 and RAJ-1 boreholes had elevated EC concentrations of 1 042 mS/m, >20 000 mS/m, 15 370 – 12 940 mS/m and 987 – 5 360 mS/m respectively. AY-M01, situated high up on the Asabuya fan, away from the MDRF, had the lowest EC, much the same as BS-M01. AY-M02 had the highest EC of >20 000 mS/m, presumably because it was drilled into the toe of the fan, interacting with the salt evaporites.

The pH in AY-P01 and RAJ1 was slightly acidic at 6.2 and 6.9 respectively. AY-M01 and the Asabuya Village Well were slightly alkaline with a pH of 7.7 and 7.6 respectively. These were likely influenced by the Antalo Group limestones and gypsums within the Zariga Formation. AY-M02 had an acidic pH of 5.9 which can be related to the influence of rift evaporites and thermal upwelling at the bottom of the fan.

Total dissolved solids in AY-P01 and RAJ-1 were 96 050 – 112 448 mg/l and 29 212 – 35 256 mg/l, respectively. The TDS increased with continued pumping which was opposite to the northern fans (**Figure 7-3**). This was possibly the result of AY-P01 intersecting the MDRF and therefore increasing geothermal recharge. The Musley Village spring, Asabuya recharge pond and AY-M01 had TDS of 830 mg/l, 1 432 mg/l and 6 762 mg/l, respectively. The Musley Village Spring was classified as freshwater, with AY-M01 and the Asabuya recharge pond been classified as brackish waters.

Concentrations of sodium, chloride, potassium and magnesium were elevated in RAJ-1, AY-M01, AY-M02 and AY-P01, but still generally lower than in the northern fan areas (**Figure 7-5 and Figure 7-6**). The water quality was still largely poor but improved the further south the boreholes were positioned. The Asabuya Village well, Musley Village spring and Asabuya recharge pond showed elevated nitrate concentrations which were possibly due to the influence of human and animal waste.

As with TDS, the southern Asabuya fan had less dissolved trace metals compared to the northern fans. Nevertheless, elevated strontium, manganese, boron and barium concentrations were found in RAJ-1, AY-M02 and AY-P01. As with the TDS a slight

increase in manganese and strontium concentrations were seen in AY-P01 and RAJ-2 as pumping continued, which was opposite to the northern fans.

7.5 SUMMARY AND CONCLUSIONS

From the hydrochemical plots in the sections above, as well as from results in **Appendix D**, the following conclusions are summarised:

- Individual fan samples distinctly plotted together;
- Salinity increased from south to north;
- Salinity decreased with the duration of pumping, apart from Asabuya fan where it increased. This was interpreted to be due to hydrothermal fluid upwelling along the MDRF, diluting the extremely saline northern fan water and increasing the salinity of the relatively good quality Asabuya Fan water. Extended pumping would likely bring all the fans water qualities to that of the hydrothermal upwelling, better than the northern fans, but worse than the southern fans, possibly in the region of 110 000 mg/l TDS;
- Salinity decreased from the production wells situated on the MDRF to the seeps at the toe of the fans and springs and wells within the wadi at the top of the fans. The dilution of the seeps could possibly represent interaction with a freshwater layer overlying the denser more saline water in the alluvial fans;
- Water quality was generally worse in the northern fans and along the MDRF;
- Dissolved trace metal concentrations decreased in the northern fans and increased in the southern fans with continued pumping, much the same as salinity;
- Stable isotope plot Deuterium and ^{18}O underlay the trend of increasing water quality with continued pumping. The plot showed that the North Dogua fan possibly had an ancient Red Sea signature and the Asabuya fan had a signature closer to the LMWL;
- Strontium isotope results showed that groundwater was relatively un-radiogenic, with $^{87/86}$ Sr ratios in the 0.705 range. This is indicative of fluids that have leached very young oceanic crust, exclusively near hot spots, such as the Afar and Red Sea basalts which have $^{87/86}$ Sr ratios in the range 0.704 (Drescher, 2014). The slightly higher $^{87/86}$ Sr ratios in boreholes could be due to mixing with enriched

sea water (0.70920) or meteoric water that has interacted with hydrothermally altered oceanic crust;

- The source of fluids was therefore not conclusive, but could be a combination of ancient Red Sea, meteoric water, hydrothermal fluid and evaporite waters. Samples from Dallol show that the surface acidic brines consist partly of meteoric water that has mixed with geothermal steam that originates from a magmatic source (Franzon *et al.*, 2015);
- If the mine had a fresh water requirement (TDS < 1 000 mg/L) of 5% of the total mine water demand of 30 hm^3/a then results indicate that shallower boreholes at the top of the alluvial fans near the wadis would be the best target as there is potential inflow from the wadis that act as drains and channel water from the larger catchment into the alluvial fans and there is a greater distance from the MDRF which possibly acts as a conduit for brine upwelling.
- The considerable difference in TDS values between samples collected in AY-M01 and AY-P01 and BS-M01 and BS-P01 respectively, indicate the possibility that a fresher water layer may be present above the denser, more saline water stored in the fans, although no E.C. profiling was conducted to further substantiate this.
- Water treatment options may have to be considered if there is a quality constraint on the water used for the potash solution mining operation. Possible options include desalination treatment through reverse osmosis, extensive blending and mixing of better quality groundwater or surface water with hypersaline waters and potential artificial recharge. Water samples collected at the base of the discharge trench during the AST indicate water quality improved marginally merely by allowing oxidation to occur, as was observed in the field by extensive red iron oxide staining on the plastic and boulders in the trench (see Figure 7-7).

Figure 7-13 Iron oxide precipitation in the discharge trench down the Asabuya fan after pump testing.

A comparison of the northern hydrochemical results with results from the southern fans display a clear trend of improving water quality towards the southern part of the Danakil Depression. This is possibly the result of fresher water recharge from the Antalo Group limestones and Adigrat Formation sandstones to the west and the boreholes being situated further away from the MDRF.

CHAPTER 8

REVIEW OF NUMERICAL MODELLING

8.1 INTRODUCTION

The conceptual model adopted by Umvoto (2016e) was an adaptation of two earlier conceptual models developed by MWH (2015d) and Umvoto (2015). The model developed and described by MWH (2015d) pertained predominantly to the southern fans. This chapter serves as a summary and review of the Umvoto (2016e) numerical model and its results. The author did not personally develop the model but played an integral part in refining the conceptual model and advising as to boundary conditions, hydraulic parameters, recharge scenarios, required predictive simulations, and co-authoring the modelling report. This chapter therefore aims to describe the Umvoto (2016e) model and comment on assumptions applied in the modelling of the natural system.

8.2 MODELLING METHODOLOGY

All numerical groundwater models are based on a conceptual model, that aims to provide an approximation of the groundwater conditions. This is because aquifers display increasing complexity as the scale is reduced, even in simple groundwater flow systems, and because natural systems have high spatial variability.

The purpose of the conceptual model was to identify all the relevant groundwater processes that have a significant effect on the groundwater flow system, so that these processes could effectively be captured in a regional numerical model. The numerical model was therefore constructed to incorporate the processes identified in the conceptual model, and confirmation of the effectiveness and accuracy of the model simulation was provided by the steady state and transient model calibration analysis. If this did not meet the required accuracy, the numerical model was adjusted iteratively until it met the calibration requirements as well as the conceptual model philosophy. The sensitivity analysis identified the hydraulic parameters that the model was particularly sensitive to, which allowed the reliability of the model to be determined from the accuracy of field measurements. Ultimately the sensitivity analysis and model calibration ensured the model was as true a representation of natural conditions as possible. Finally, once

all these steps had been achieved, the model was used to simulate planned developments. The model steps of Umvoto (2016e) are thus summarised as:

- conceptual model development;
- numerical model construction;
- steady state calibration and iterative adjustment;
- transient calibration and iterative adjustment;
- sensitivity analysis;
- development simulations; and
- numerical model reporting.

The prescribed standards as layout by the ASTM standard “D5718-13: Standard Guide for Documenting a Groundwater Flow Model Application” (ASTM International, 2013) were followed as part of the modelling methodology. Umvoto (2016e) offered a written and graphical presentation of model assumptions and objectives, the conceptual model, code description, model construction, model calibration, predictive simulations, and conclusions all of which are summarised and reviewed below.

8.3 MODELLING OBJECTIVES

The objectives of the modelling study can be summarised as:

- Evaluation for alternative regional groundwater flow-regime scenarios;
- Assessment of sensitivities of model outcomes to conceptual model assumptions, different mesh designs, hydraulic-parameter data sets and boundary conditions,
- Establishment of mesh refinement and boundary conditions for more detailed, local-scale simulation of the alluvial aquifers.

8.4 CONCEPTUAL MODEL

The conceptual model adopted by Umvoto (2015) followed approximately that which was developed and described in MWH (2015d) but was more extensive on the eastern side. The modelling study of MWH (2015d) focused on the wadi-drained catchments that discharge across the alluvial fans and subsequently outflow onto the playa salt mud flats,

in Asabuya, Gehertu, Musley and Bacarti Fan catchments. Umvoto (2016e) further refined the conceptual model to increase its applicability to the three alluvial fans under investigation. Revised lithological and structural mapping, data analysis and interpretation of the AST, hydrochemical and isotope analyses, static and dynamic water levels and field observations all contributed to the revision of the conceptual model. This revised model was more extensive on the eastern and northern sides of the previous model domain and included more detailed fault mapping (Umvoto, 2016e). It allowed for the following:

- Direct rainfall infiltration and runoff infiltration as per **Figure 8-1**.
- Limited lateral flow from the Antalo and Adigrat Formations in the west to recharge the Asabuya fan, but not the Bussaba and Dogua North fans. A clear distinction was thus made between the recharge scenarios of the southern and northern fans (see **Figure 8-1**).
- Recharge to the northern fans by deep seated, upward, vertical flow of hypersaline water from N-S and NW-SE trending faults associated with the MDRF.
- The conceptual model and numerical model focussed on three different recharge scenarios to the Dogua Alluvial Fan complex.

Figure 8-1 is a graphical representation of the regional conceptual model used in Umvoto (2016e). In summary, the aquifer system can be described by water flowing from the highlands, as bedrock throughflow down into the Lelegheddi valley (MWH, 2015c). Some bedrock throughflow then discharges into tributaries of the Ragali River and Saba River. Some is shown to pass under the river alluvium down to the Danakil Rift. A deeper, brackish flow is also shown to rise from depth along the margin of the rift, some of it transferred upwards along the MDRF and its associated faults. The fresh groundwater zone at the top of the Precambrian bedrock is of unknown proportional quantity and depth, but a significant percentage of fresh, shallow bedrock flow is captured by wadi sands and gravels, acting as drains that transport these flows into their respective alluvial fans. Within the alluvial fans, this fresh water is assumed to flow on top of the denser saline groundwater as a fresh water layer maintained by a density interface. In the playa salt flats evaporation is known to be very high, groundwater levels show loss by soil evaporation, the rate of which is controlled by the water table depth (Umvoto, 2015). The brines generated by groundwater evaporation and rift evaporites are denser than fresh and brackish water flows from the plateau bedrock and rainfall infiltration, and this density interface is an impenetrable barrier forcing the bedrock and alluvial throughflow to the surface around the toes of the alluvial fans (Umvoto, 2016e). Jurassic Adigrat Formation

and Antalo Group as well as the Danakil Group hydrostratigraphic units are also expected to transmit fresh and brackish groundwater from the Precambrian bedrock as throughflow via the alluvial fans to the density-interface zone (MWH, 2015c).

The spatial patterning of hydrochemistry and isotope results from individual boreholes, including available hydrochemistry data from earlier studies in the southern fans (MWH, 2015c; WWDSE, 2015), was combined with an analysis of probable flow paths using the revised hydrostratigraphy, structural geology, climatic data, and observed patterns and processes in the field to summarise components of the modelled recharge scenarios.

These data and information informed the differences and in some cases the similarities in the hydrogeological setting of the Dogua alluvial fans in the north compared to the Musley, Gehertu and Saba fans in the south. **Table 8-1** summarises the regional scale components of the modelled recharge processes that as per Umvoto (2016e) contribute to groundwater in storage in the Asabuya, Bussaba and North Dogua fans.

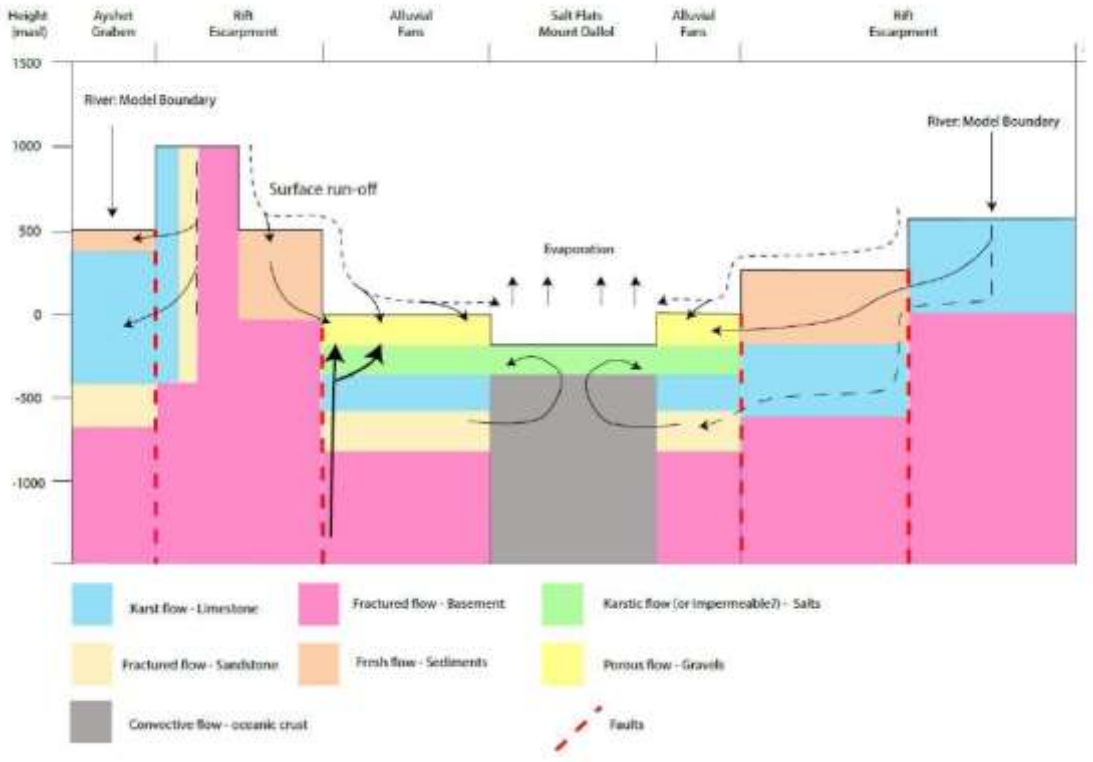

Figure 8-1 Regional conceptual model (Umvoto, 2016e).

Table 8-1 Summary of regional scale components of recharge scenarios to the Dogua Alluvial Fans after Umvoto (2016e).

	Recharge Component	Motivation

1	• Rainfall Related Recharge:
	  ○ Direct rainfall onto fans;
	  ○ Infiltration of surface runoff from the head of the fan;
	• Deep seated, upward vertical recharge from faults;
	• Lateral recharge from Antalo limestones in the west recharging only the Asabuya fan.
		• Measured rainfall from weather stations;
		• Runoff from catchments after rain events;
		• Isotope and hydrochemical signature, temperature variations during pumping and presence of regional and local structural features;
		• Groundwater gradient from west to east

2	• Rainfall related recharge identical to scenario 1 • Deep seated recharge from faults identical to scenario 1 • No lateral recharge from the Antalo limestones in the west;	• Isotope and hydrochemical signature, temperature and quality variations during pumping and geological structures (faulting); • Basement lithology adjacent to Bussaba and Dogua North fans acts as an aquitard
3	• Rainfall related recharge identical to scenario 1 • Lateral recharge from Antalo limestones identical to scenario 1 • Bussaba and Dogua North fans recharged by deep seated, upward vertical recharge with a northern source.	• Stable isotope and hydrochemical signature in northern fans vs Asabuya fan; • Faulting and volcanism north of the study area • Improved water quality of northern fans during pumping.

The above three components informed the conceptual model and lead to an upgrade and re-configuration of the numerical groundwater flow model. The groundwater flow model was calibrated under three different recharge scenarios (see **Table 8-2**) to improve confidence in the choice of a preferred interpretation of the natural system.

Table 8-2 Summary of the investigated recharge scenarios or pathways to the Dogua alluvial fans (Umvoto, 2016e).

Recharge Scenario	Summary
1	Recharge to Musley, Gehertu & Asabuya fans through fracture flow from the west. Vertical infiltration into the fans equivalent to surface flow. Vertical recharge to Bussaba, Dogua North & Badah fans from the south and lateral flow from the Ragali River.
2	No basement fracture flow from west. Lateral recharge to Musley, Gehertu and Asabuya fans (southern fans) from Antalo Bussaba, Dogua North & Badah fans recharged laterally by Ragali River. Vertical infiltration into the fans equivalent to surface flow.
3	Recharge to Musley, Gehertu & Asabuya fans through fracture flow from the west. Vertical infiltration into the fans equivalent to surface flow. Bussaba, Dogua North & Badah fans are recharged by fracture flow from the north and lateral flow from the Ragali River.

Density and thermally driven flows were not part of the numerical modelling outcomes which may be disadvantageous to potential insights for locating and distinguishing between groundwater of varying quality. Additionally, the numerical simulation of the eastern zone units was given a low priority due to its lesser relevance to the western alluvial fans and the complexity of deeper geothermal and brine circulation between Lake Assale and the Red Sea (Umvoto, 2016e). These factors are considered here as potential over simplifications of the conceptual and consequently the numerical model.

8.4.1 Hydraulic Properties

There was uncertainty in the hydraulic properties applied to the model due to there being a significant lack of stream or river data in the region and proxy catchment data had to be used which was sourced from MWH (2016c). This created potential for under or over estimating recharge, runoff and infiltration rates. This will be discussed further in **Section 8.4.3.**

The hydraulic conductivities and Transmissivities obtained during the analysis of the AST data were applied to the modelled alluvial fans. While this data was used with confidence, the possibility of vertical recharge to the alluvial aquifers by rift related faulting could

decrease confidence as numerous inherent assumptions applied may be rendered invalid. Storage values used were initially the same as were used in MWH, 2015 but were adjusted during calibration of the model. Due to the lack of any observation data obtained during test pumping and the AST, the sensitivity analyses of Specific Yield was of great importance in determining a representative Sy value. Calibration allowed for a Sy value of 0.2 being determined for each of the three fans. This correlates well with Sy values quoted in literature for the type of aquifer material and is thus considered representative of the natural system. The Sy value of 0.2 (or 20% effective porosity) will be applied when calculating a storage yield model.

8.4.2 Sources and Sinks

The main area sources were limited recharge from the higher catchments of the Dogua Mountains in the west and the Danakil Alps in the east and infiltration from wadi runoff. The main area sink was evaporation from the playa-salt mud flats. Evaporation in the model was applied as per the methodology described in **Section 8.4.3**. The methodology employed is open to error due to the large amount of uncertainty regarding spatial distribution of rainfall and actual versus potential evaporation rates. An additionally limiting factor is the short range of data sets collected and used from the different weather stations in the area (WS1, WS2, Solmin-1 and Badah weather stations), comprising only approximately 18 months of data. A data set of minimum 5 years would increase confidence.

8.4.3 Rainfall Related Recharge

There was one recharge process common to all the fans (see **Figure 8-2**), which was direct vertical recharge from rainfall and from lateral surface flows as the waters entering the heads of various fan components dissipated over, along and down the sides of the surface of the fan during flash flood events. These recharge elements were used to discretise the vertical recharge contribution from rainfall using the climate data. Direct rainfall infiltration, wadi runoff infiltration and fan runoff infiltration was calculated using three different approaches (see **Table 8-3**).

Table 8-3 Rainfall related recharge volumes entering the Dogua alluvial fans

Rainfall related recharge		Asabuya	Bussaba	North Dogua
Method 1 Total	(hm^3/year)	0.39	0.16	0.16
Method 2 Total	(hm^3/year)	0.84	0.37	0.36
Method 3 Total	(hm^3/year)	1.03	0.42	0.43

Method 1 referred to in **Table 8-3**, was formulated based on the methodology used by MWH (2015c) and MWH (2015d). This method made use of updated values of 90 mm/year rainfall and a 6 mm/year rainfall infiltration rate throughout the catchment of each fan. Due to a lack of streamflow data in the relative catchments, a runoff rate of 20% was obtained through stream flow data from a proxy catchment. Wadi and fan runoff volumes were reduced based on sequential infiltration and the remainder forming the subsequent runoff component. Infiltration coefficients used for the wadis and fans were based on results obtained for the Asabuya fan during soakage tests carried out in the region by MWH (2015b).

Method 2 referred to in **Table 8-3** may be considered a first order estimate based on field observations. It was devised on the premise that rainfall between 5-30 mm had a 30% infiltration rate, while rainfall >30 mm had a 60% infiltration rate.

Method 3 followed the exact same methodology as was used by MWH (2016c) and MWH (2016d), where the only changes made were the input values of rainfall and an assumed infiltration coefficient for the Bussaba and North Dogua fans. While Method 1 values were considered a conservative estimation, Method 2, although lacking key catchment data inputs, yielded results between the estimations obtained from the other two methods.

The groundwater model incorporated the results from the Method 1 approach, which were considered a conservative estimation (Umvoto, 2016e).

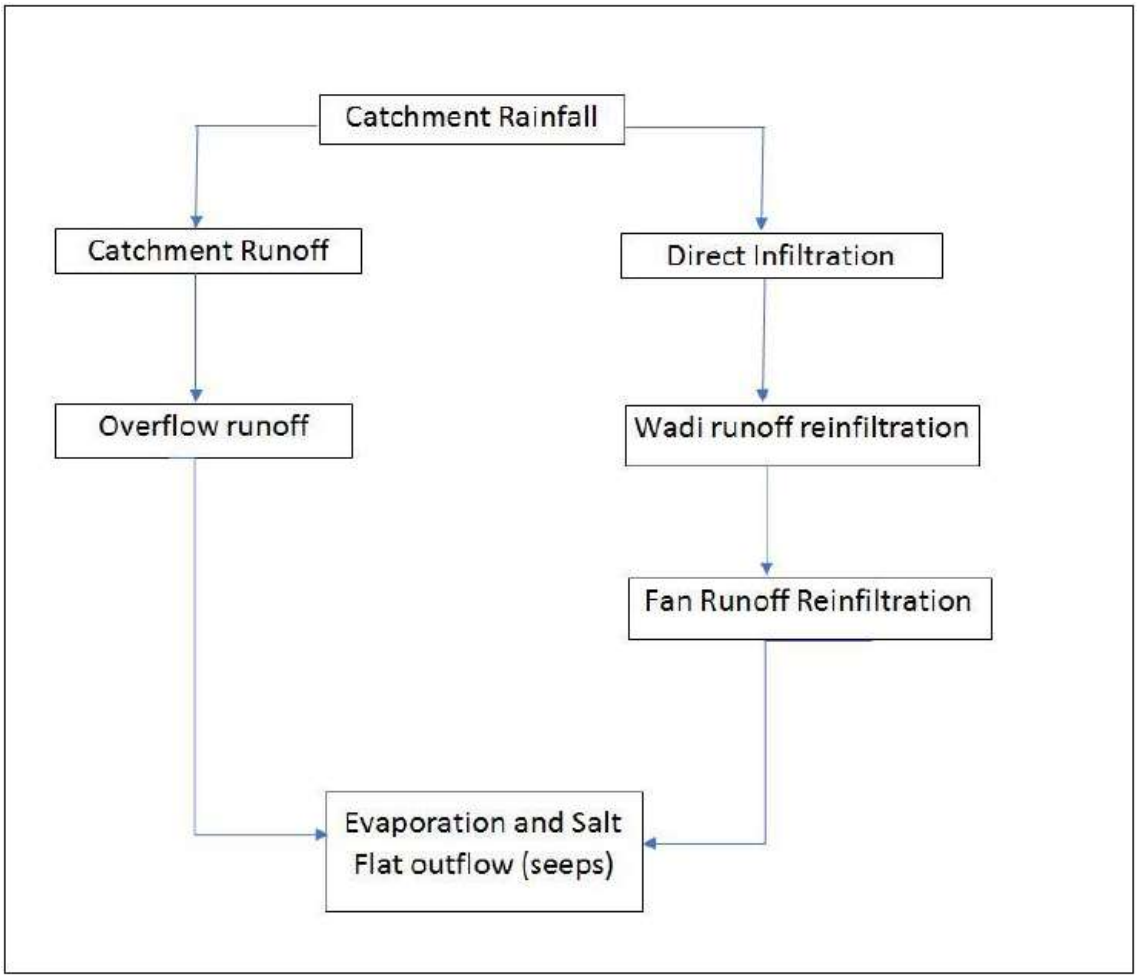

Figure 8-2 **Flow chart for various fresh water components involved in the recharge process to the northern Dogua alluvial fans (Umvoto, 2016e).**

To calculate rainfall infiltration recharge, the infiltration rate needed to be calculated. This was done based on the equation below initially from (MWH, 2015d):

$$I=P-Ro-Evap \qquad (2)$$

Where *I* is infiltration rate, *P* is precipitation, *Ro* is runoff and *Evap* is the evaporation rate.

Precipitation and evaporation were derived from the four weather stations situated in the study area, namely Dogua WS1, Dogua WS2, Solmin-1 and Badah Camp (see **Section 3.2.5**). Precipitation based on a year and a half of data was set at 90 mm/a for the recharge area. Evaporation was measured theoretically as ETos and by an evaporation pan as potential evaporation. Potential evaporation was on average 1.8 greater than ETos. An average of the two methods were used for actual evaporation which was calculated as 7.33 mm/d. This value was then multiplied by the amount of

rainfall events per year to give a total actual evaporation rate of 66 mm/a. This accounted for 76% of rainfall which is comparable with what MWH (2015d) obtained. Rainfall events were used because actual evaporation only took place when there was water to evaporate and this was only on the day of a rainfall event.

The runoff rate was taken at 20% of rainfall based on the proxy catchment data from MWH (2015d) which was equal to 18 mm/a. Therefore, the infiltration rate was calculated to be:

$$I=90mm-18mm-66mm$$

$$I=6\ mm/a$$

The measured rainfall data and calculated infiltration rate were then used to calculate direct rainfall recharge into the catchment, wadi runoff infiltration and fan re-infiltration based on the catchment and fan areas (see **Table 8-4**).

Table 8-4 Rainfall infiltration recharge calculations for the Asabuya, Bussaba and North Dogua fans based on catchment, wadi and fan infiltration (Umvoto, 2016e).

Direct catchment infiltration					
			Asabuya	Bussaba	North Dogua
Fan area		km^2	28.24	12.45	12.22
		m^2	28240000	12450000	12220000
Rainfall infiltration rate		mm/year	6	6	6
		m/year	0.006	0.006	0.006
Catchment infilitration		hm^3/year	0.17	0.07	0.07
Wadi runoff infiltration			**Asabuya**	**Bussaba**	**North Dogua**
Catchment area		km^2	80.67	36.77	37.52
		m^2	80670000	36770000	37520000
Wadi area		km^2	52.43	24.32	25.3
Area Wadi/Total		%	64.99	66.14	67.43
Rainfall rate		mm/year	90	90	90
Run-off coefficient		%	20	20	20
Run-off rate		mm/year	18	18	18
Wadi infiltration coefficient		%	16.5	15.5	15
Annual Wadi infiltration rate		mm/year	2.97	2.79	2.7
Wadi runoff infiltration		hm^3/year	0.15	0.06	0.06
Fan reinfiltration			**Asabuya**	**Bussaba**	**North Dogua**
Catchment area		km^2	80.67	36.77	37.52
		m^2	80670000	36770000	37520000
Fan area		km^2	28.24	12.45	12.22
Area Fan/Total		%	35.01	33.86	32.57
Rainfall rate		mm/year	90	90	90
Run-off coefficient		%	20	20	20
Run-off rate		mm/year	15.03	15.21	15.3
Fan infiltration coefficient		%	16.5	15.5	15
Annual Fan infiltration rate		mm/year	2.47	2.35	2.29
Fan infiltration		hm^3/year	0.07	0.03	0.03
Rainfall related recharge			**Asabuya**	**Bussaba**	**North Dogua**
Total		(hm^3/year)	0.39	0.16	0.16

The methodology is bulleted below, highlighting the variations applied to MWH (2015d):

- Direct rainfall infiltration was calculated using the figure of 6 mm/year rainfall infiltration rate, with the addition of new catchment area measurements.
- Wadi-runoff infiltration was calculated using the figure of 90 mm/year rainfall rate, a run-off coefficient of 20%, and run-off rate of 18 mm/year. The wadi-infiltration coefficient for the Asabuya, Bussaba and North Dogua Fans were taken from the same source. The wadi infiltration coefficient of the catchments was estimated

using the wadi catchment length in comparison with the southern catchments coefficients. The new catchment area measurements were used.

- Fan-runoff infiltration was calculated using a 90 mm/year rainfall rate, a run-off coefficient of 20%, and run-off rate of 18 mm/year. The fan infiltration coefficient for the Asabuya Fan was taken from MWH (2015d). The fan infiltration coefficient of the Bussaba and North Dogua catchments was estimated using the length of the fan in comparison with the southern catchment coefficients. The new catchment area measurements were used.
- Runoff over flow was calculated using the MWH (2015c) methodology, but with a 90 mm/year rainfall rate, 18 mm/year runoff rate and an overflow coefficient equal to the remainder of the fan infiltration coefficients. The new catchment area measurements were used.
- Total evaporation was calculated as described in **Section 8.4.3**;

8.5 COMPUTER CODE DESCRIPTION

Groundwater flow within the model domain was interpreted as normal gravity-driven flow and was represented by the fluid continuity equation (Umvoto, 2016e):

$$\frac{\partial}{\partial x}\left(K_x \frac{\partial h}{\partial x}\right)+\frac{\partial}{\partial y}\left(K_y \frac{\partial h}{\partial y}\right)+\frac{\partial}{\partial z}\left(K_z \frac{\partial h}{\partial z}\right)=S_s \frac{\partial h}{\partial t} \quad (3)$$

where x, y, z are the principal components of space (L); h = hydraulic head (L); S_s is specific storage (L-1); K is hydraulic conductivity (L/t), and t is time. The code used for numerical modelling was FEFLOW 6.2.

8.5.1 Assumptions

The major assumptions with the continuity equation and its application are that the fluid is incompressible, groundwater flow follows Darcy's Law, and the fluid throughout the model domain has a constant density (Umvoto, 2016e).

8.5.2 Limitations

In the Danakil area of application, the wide range of groundwater temperatures and salinities leads to variable density flows. The model assumption of constant fluid density is a therefore a limitation in this context. The hydrothermal system present also implies that heat transport modelling would be a useful tool to better represent the natural system and highlight different flow regimes present within the model domain.

FEFLOW 6.2 includes Solute Transport, Heat Transport and Density-dependent Flow packages for hydrochemical- and heat-transport studies. These modules were not incorporated in the groundwater modelling study nor were any automated solution or optimization techniques which may have increased the certainty with which the natural system was modelled. The complex hydrogeological setting of the area does however, promote the development of simplistic models that are slowly and iteratively made more complex as new data and insights are attained.

8.6 MODEL CONSTRUCTION

The regional model domain (see **Figure 8-3**) was defined based on aerial extent, geology and interpreted groundwater flow patterns. The model domain covered an area of 3,866 km² (Umvoto, 2016e). **Figure 8-3** shows the model domain mesh overlaid on the ALOS DEM, with blue tones representing parts of the northern Danakil basin that lie below sea level with the concession boundary outlined in red.

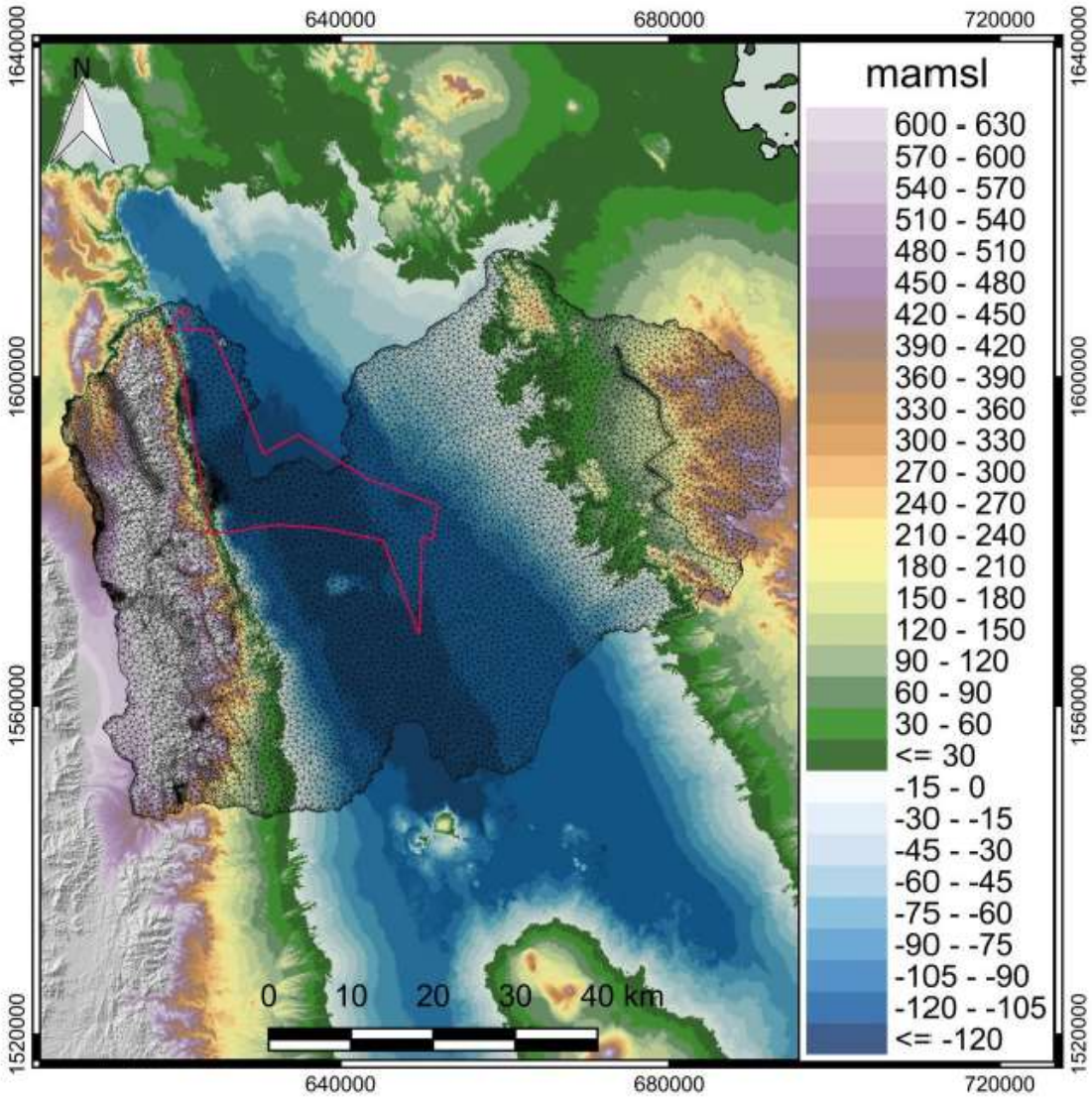

Figure 8-3 Model domain mesh overlaid on the ALOS DEM (Umvoto, 2016e).

8.6.1 Model Domain

The boundaries of the model domain were based on geographic features as described in **Table 8-5** adapted from Umvoto (2016e):

Table 8-5 Model domain boundaries

Boundary Segment	Geographic Feature	Comment
West (1)	Lelegheddi River	flows in a northerly direction to a confluence with the Ragali River
West (2)	Stream tributary segments	across a divide draining southwards to the Saba River and northwards to the Lelegheddi River
North West	Ragali River	flows east towards Badah, turning south at Badah into the Danakil Depression
North East	Zariga River	flows from the Danakil Alps in Eritrea southwest to the Danakil Depression
East	Danakil Alps drainage divide	separates the northern Danakil catchments from Red Sea catchments
South East	Unnamed wadi stream	drains Danakil Alps towards Lake Assale
South West	Saba River	flows eastward from the plateau into Lake Assale
South	Lake Assale	-

8.6.2 Finite-Element Mesh

Within the model domain, a two-dimensional finite-element pattern was discretized with a mesh of 15782 nodes per layer. The average node spacing was 4 - 2000 m and the element size between 0.000015 and 1.0 km^2 (Umvoto, 2016e). Node spacing was made finer near and along key geological features, such as faults or boundaries of known hydraulic difference. For local-area modelling around the Dogua Formation fans, the element size was refined to between 0.000159 km^2 and 0.027 km^2 (Umvoto, 2016e).

After the processing, the smoothed ALOS DEM was imported into FEFLOW 6.2 on a 30 m grid, and the elevation table integrated with model Layer 1 (Umvoto, 2016e).

The degree of discretization around the faults plays an important role in simulating deep vertical recharge via faults into the fans. Little explanation is supplied in Umvoto (2016e) as to the degree that node- and element-size and spacing was adjusted along these portions within the model and how such adjustments allowed for additional inflow into the aquifer.

8.6.3 Model Layering

Vertically, the model was discretized into 11 layers (see **Figure 8-4**), with the first layer was made 3 m thick and the rest of the layers 100 m thick each. The layering in the model followed the requirements of the conceptual model (see **Figure 8-1**). Generally, any one layer incorporated more than one hydrostratigraphic unit, each of which was differentiated by assigned parameter zones (see **Table 8-5**). The drawback of a regional model and such extensive model layering is that local modelling of the alluvial fans becomes increasingly complex.

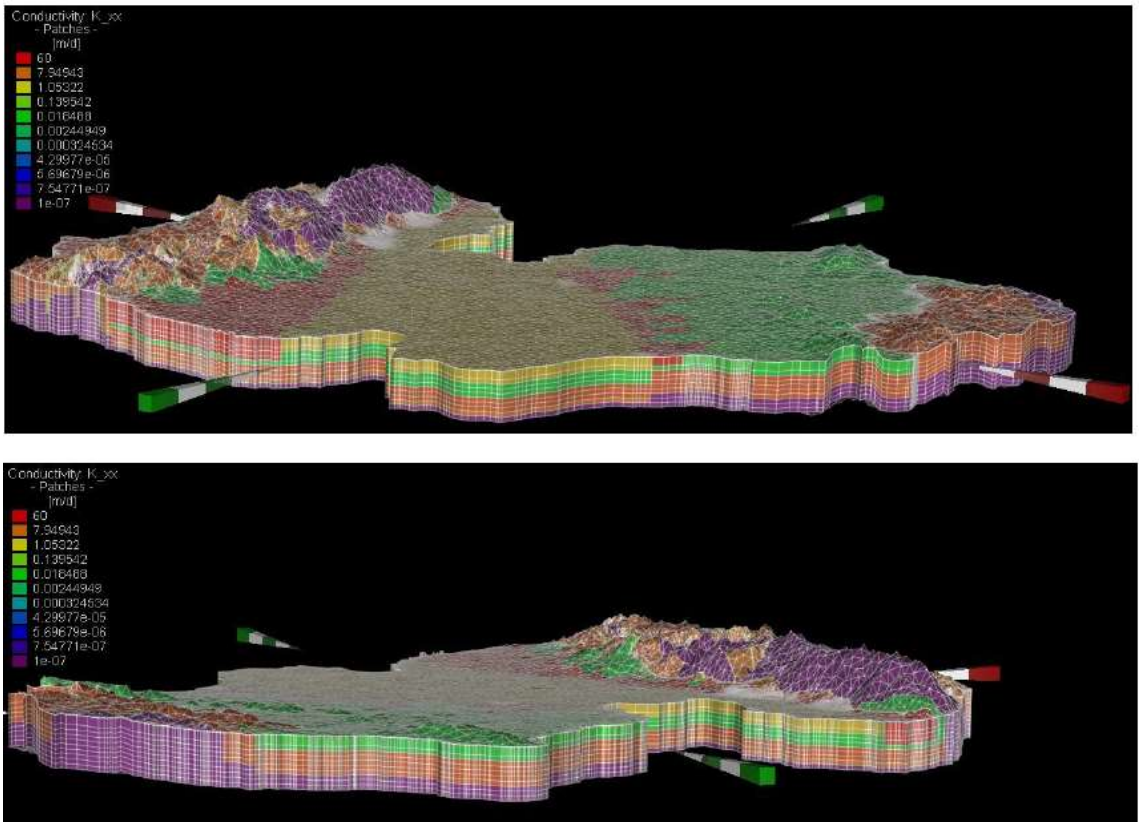

Figure 8-4 Perspective 3D views of vertical discretisation of the model to represent geological layering (Umvoto, 2016e).

8.6.4 Hydraulic Parameters

Hydraulic parameters, such as hydraulic conductivity (K), porosity (n), specific yield (S_y) or specific storage (S_s), were assigned to each model layer in hydrostratigraphic parameter zones (HPZs) as can be seen in **Figure 8-5** and **Table 8-6**.

Table 8-6 **Summary of relationships between HPZs, hydrostratigraphy, model layers and assigned hydraulic zones for Layer 1 (Umvoto, 2016e).**

Parameter Zone	Hydrostratigraphic unit	Layer	Hydraulic conductivity m/d	
			Kx &Ky	Kz
1	Recent Sediments	1	45	4,5
1	Alluvial fans	1-4	45	4,5
1	North Dogua Fan	1-4	16	1,6
1	Bussaba fan	1-4	20	2
1	Asabuya Fan	1-4	11	1,1
2	Salt	1-3	0,9	0,09
3	Gypsum	1	10	1
5	Danakil formation	1 - 4	0.01	0.001
6	Antalo Limestone	1-9	19	1.9
7	Adigrat Sandstone	1-10	9.5	0.95
8	Basement	1-11	0.000001	0.0000001

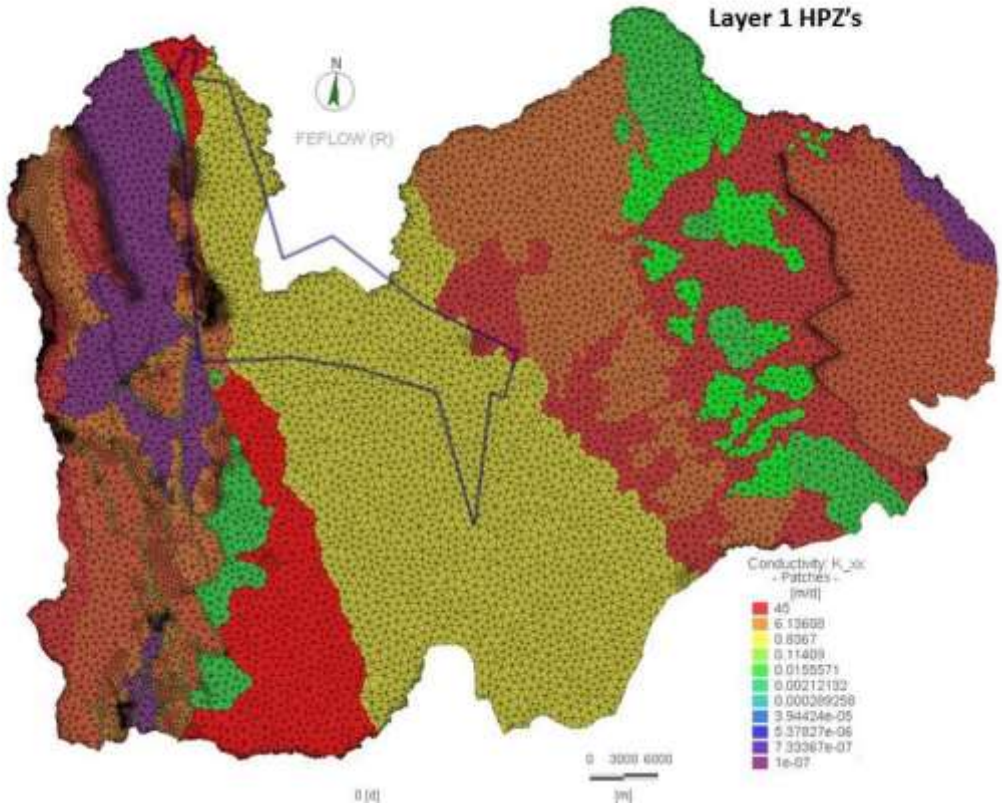

Figure 8-5 **Map view of spatial variation of HPZs throughout model Layer 1 (Umvoto, 2016e).**

Umvoto (2016e) reports K values as shown in **Table 8-6** and mention is made of hydraulic parameters being based on the calibrated MWH (2015c) model, however the K values obtained from pump test analysis are observed to be near double the values applied and in some cases exceed the MWH (2015c) values by nearly six times.

All the fans S_y values were adjusted until the model achieved acceptable calibration. Final S_y value for each fan was 0.2 were assigned an S_y value of 0.2 which correlates well with literature for the fan aquifer material and is considered feasible based on field observations.

8.6.5 Sources and Sinks

An important boundary line source within the numerical model was a portion of the western boundary across a catchment divide between the Saba and Ragali drainage basins. The main area source was documented by (Umvoto, 2016e) to be limited recharge from the higher catchments of the Dogua Mountains, which was then accorded a low priority as the model calibration was intended to only analyse the role of boundary conditions on the distantly originating component of lateral recharge via deep bedrock through-flow. There is no documented water balance calculation that details this through flow component.

The main area sink was evaporation from the playa-salt flats (Umvoto, 2016e). There was difficulty in achieving calibration when applying measured evaporation rates as well as with the application of extinction depths of evaporation applied to the playa-salt flats. These uncertainties were overcome by applying values for these parameters obtained from previously documented works by MWH (2015c). While this allowed for a calibrated model to be obtained, the uncertainty surrounding this crucial component may be an indication of problems involved in the initial mesh design, delineation of HPZs and discretisation applied to specific elements.

8.6.6 Boundary Conditions

Per Umvoto (2016e), boundary conditions were chosen to approximate regional groundwater flow patterns within the model domain. Edge boundary conditions were assigned to simulate features identified as per **Table 8-1** (see **Table 8-7** and **Figure 8-6**). The specified head value assigned to each boundary node at the ground surface was equal to the topographic elevation at the node (Umvoto, 2016e). The main purpose of these edge boundary conditions was to establish the larger-scale pattern of hydraulic-

head elevations and to constrain groundwater flow directions and flow gradients (Umvoto, 2016e).

In all scenarios, the perennial Ragali River, in the north and north-west, and the ephemeral Zariga River in the north-east, were represented by specified-head boundary nodes placed in the surface Layer 1 (see **Figure 8-6**). For constant head cells a water-level at the topographic surface was assigned. In **Figure 8-6**, DM represents the location of Dallol Mound and the concession boundary area is represented by the purple polygon. The alluvial fans in the model were recharged by wadi run off set as vertical infiltration at 11 mm/a and inflow from depth through the fault at 0.09 m/d. This inflow rate from the fault was determined from experimentation during the calibration of Scenario 1 and Scenario 2 (Umvoto, 2016e). However, no true measured data is available for the conductivities of the faults.

Table 8-7 Edge boundary conditions used to numerically simulate the three recharge scenarios as described in Table 7-2 (Umvoto, 2016e).

Region	Type of Boundary condition Recharge Scenario 1 (20170119_838RM_V27.1_LN)	Type of Boundary condition Recharge Scenario 2 (20170119_838RM_V24.1_LN)	Type of Boundary condition Recharge Scenario 3 (20170119_838RM_Sc3_V4_LN)	Motivation
West and Northwest	Specified head elevations along perennial stretch of the Lelegheddi and Ragali Rivers (W1,N1 &N2) Fluid-flux boundary (WF1)	Specified head elevations along perennial stretch of the Lelegheddi and Ragali Rivers (W1, N1 &N2)	Specified head elevations along perennial stretch of the Lelegheddi and Ragali Rivers (W1, N1 &N2) Fluid-flux boundary (WF1) Fluid flux at depth from layer 7-10	Lelegheddi River headwater tributary connected to Antalo Group limestone aquifer along W and supplies groundwater all year round Accommodation of bedrock through flow from the Ethiopian (Mekelle-Adigrat Highlands escarpment This is to simulate an alternative recharge source for the northern fans (Badah, Dogua North & Bussaba
North	Specified head elevations along ephemeral Zariga River (N3 & E1)	Specified head elevations along ephemeral Zariga River. (N3 & E1)	Specified head elevations along ephemeral Zariga River (N3 & E1)	Zariga River connected to the recent deposits and supplies water into system through those deposits.
South and Southwest	Specified head elevations along perennial Saba River and left-bank tributary in SW (S1 & S2) Constant head, Lake Assale (yellow segment)	Specified head elevations along perennial Saba River and left-bank tributary in SW (S1 & S2) Constant head, Lake Assale (yellow segment)	Specified head elevations along perennial Saba River and left-bank tributary in SW (S1 & S2) Constant head, Lake Assale (yellow segment)	Saba River headwaters and lower Saba River reach in Dogua Mountains gorge, connected to the Antalo Group (supplies groundwater all year round). Lake Assale water level in equilibrium with Saba River runoff and evaporation
East	No flow (E2)	No flow (E2)	No flow (E2)	Catchment boundary divide along crest of Danakil Alps

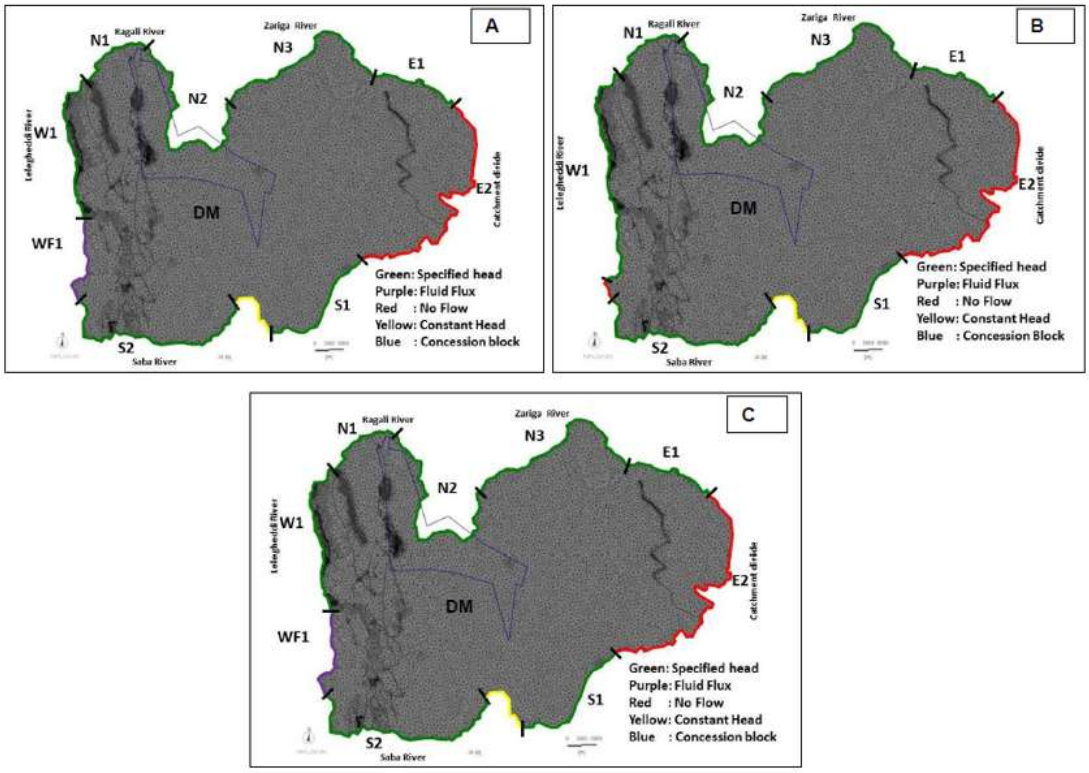

Figure 8-6 **Regional model domain illustrating edge-boundary conditions for Scenario 1 (A), Scenario 2 (B) and Scenario 3 (C) after Umvoto (2016e).**

Final steady state calibration of inflows and outflows on model edge boundaries and elsewhere in the model can be summarised as follows:

- Scenario 1: Different recharge processes were outlined, with a fluid flux boundary on the western edge of the model, fault recharge from depth and vertical infiltration were the main recharge sources to the fans. The main sink in the model was evaporation applied to the playa-salt flats. The model, after calibration, showed an imbalance of -4 .39 hm^3/a (Umvoto, 2016e).
- Scenario 2: Different recharge processes were outlined, with a specified head along the Lelegheddi River (Segment W1 in **Figure 8-6**) contributing lateral recharge to the Asabuya fan from the western edge of the model and the Ragali River (N1 & N2 in **Figure 8-6**) contributing lateral recharge to the Badah, North Dogua and Bussaba fans from the north. Other main recharge sources were fault recharge from depth and vertical infiltration from above. The main sink in the model was evaporation applied to the playa-salt flats. The model, after calibration showed an imbalance of -4.32 hm^3/a (Umvoto, 2016e).

- Scenario 3: Different recharge processes were outlined, with a specified head along the Lelegheddi River (Segment W1 in **Figure 8-6**) contributing lateral recharge to the Asabuya fan from the western edge of the model and the Ragali River (Segment N1 & N2 in **Figure 8-6**) contributing lateral recharge to the Badah, North Dogua and Bussaba fans from the north. Other main recharge sources were fault recharge from depth and vertical infiltration from above. A fluid flux boundary provided another recharge component through fracture flow from the west. The main sink in the model was evaporation applied to the playa-salt flats. The model after calibration showed an imbalance of -1.51 hm^3/a (Umvoto, 2016e)

A no-flow boundary was assigned along the eastern groundwater divide (segment E2 in **Figure 8-6**). In addition to the model-edge boundary conditions imposed by a fluid-flux along the western boundary and hydraulic-head elevation constraints elsewhere (see **Figure 8-6**), the elevations and discharge rates of seep-zones along the toe regions of the alluvial fans on both the western and eastern flanks of the playa-salt flats were also used to constrain the groundwater flow patterns. After experimental variation and adjustment, the constraints were inserted as outflows (sinks) of 0.05 l/s on internal nodes, based on the observed flow rate measured at a V-notch near borehole RAJ-2 (Umvoto, 2016e).

A further constraint was added around Mount Dallol. The Dallol Mound is "…not a volcanic cone, rather it is an anticlinal dome of uplifted and eroded bedded salt, capped and surrounded by hydrothermal crater features typified by karst pools and brine outflows but, as yet, there has been no breakout of volcanic rock material in the mound area…" (Warren, 2015). In the model, boiling springs from the Dallol Mound area were represented by a central fixed head at- 88 mamsl elevation, with surrounding nodes fixed at head values ranging from -119 to -79 mamsl (Umvoto, 2016e).

8.7 MODEL CALIBRATION: RESULTS AND DISCUSSION

8.7.1 Steady State

Several calibration experiments were performed with the aim of testing model sensitivity to different rates of groundwater flux from the western boundary, different assumptions about seepage rates and localised surface- and soil-water evaporation around the

alluvial fan seeps (Umvoto, 2016e). In later versions of these simulation experiments, an aerial region of soil evaporation was established over the playa salt flats east of the Dogua Formation alluvial fans, extending to a maximum depth of 3 m (Umvoto, 2016e). For this purpose, the original 100 m-thick top Layer 1 in the model was subdivided into an upper 3 m-thick Layer 1a and a lower 97 m-thick Layer 1b (Umvoto 2016e).

Graphical comparison of observed versus simulated model calibration results obtained from Umvoto (2016e), indicated the problematic nature of specific wells, for which the modelled water levels were below the observed water table. The explanation of the poor performance of the model in fitting the borehole data may possibly be related to these wells recording the potentiometric levels within confined or semi-confined aquifer units. This was observed throughout all three of the simulated scenarios.

A comparison focusing on the wells that intersect the Dogua Formation alluvial fan aquifers or monitoring piezometers on the salt-flats, revealed a scatter above and below the line of exact model fit. The results for the three different scenarios are summarised below as per Umvoto (2016e):

- Scenario 1: for steady state modelling the deviation was generally less than 10% for the fans. Only a single well was greater than 10% but the deviation was low at 10.2%.
- Scenario 2: for steady state modelling the deviation was generally less than 10% for the fans. Only a single well was greater than 10% but the deviation was low at 10.6%.
- Scenario 3: for steady state modelling the deviation was generally less than 10% for the fans. Only one well was greater than 10% but the deviation was low at 10.2%.

The representation of regional hydraulic head contours for the three scenarios (see **Figure 8-7**) indicated that there were some unresolved issues with boundary elevations along the upper Zariga River in the north-eastern part of the model domain and some problems with thicknesses and hydraulic conductivity parameters for the youngest alluvial deposits along the eastern boundary of the playa salt flats. These eastern domain issues did not, however, impact significantly on the western area of the model domain (Umvoto, 2016e).

Umvoto (2016e) reported that in all scenarios, the southwestern part of the model domain, influence of the Saba River on the groundwater flow of the larger alluvial-fan and outwash area between the Saba and the Bacarti fans was evident. North of the Saba

Fans and east of the fluid-influx boundary along the southwestern boundary of the model, the stepped pattern of the hydraulic head contours reflected the pattern of block faulting affecting the Adigrat, Antalo and Danakil aquifer units of contrasting K, relative to the low-K of the underlying Precambrian bedrock (see **Figure 8-7**). In the north-western part of the model domain, the pattern of head contours across the bedrock showed a very limited groundwater flow through the basement due to its low K, the groundwater instead flowed through the Antalo in a northerly direction towards the Ragali River. The head contours around the Ragali River boundary showed roughly stream-parallel groundwater flow until the outflow region near Badah, where the groundwater flow diverged from the main channel (Umvoto, 2016e).

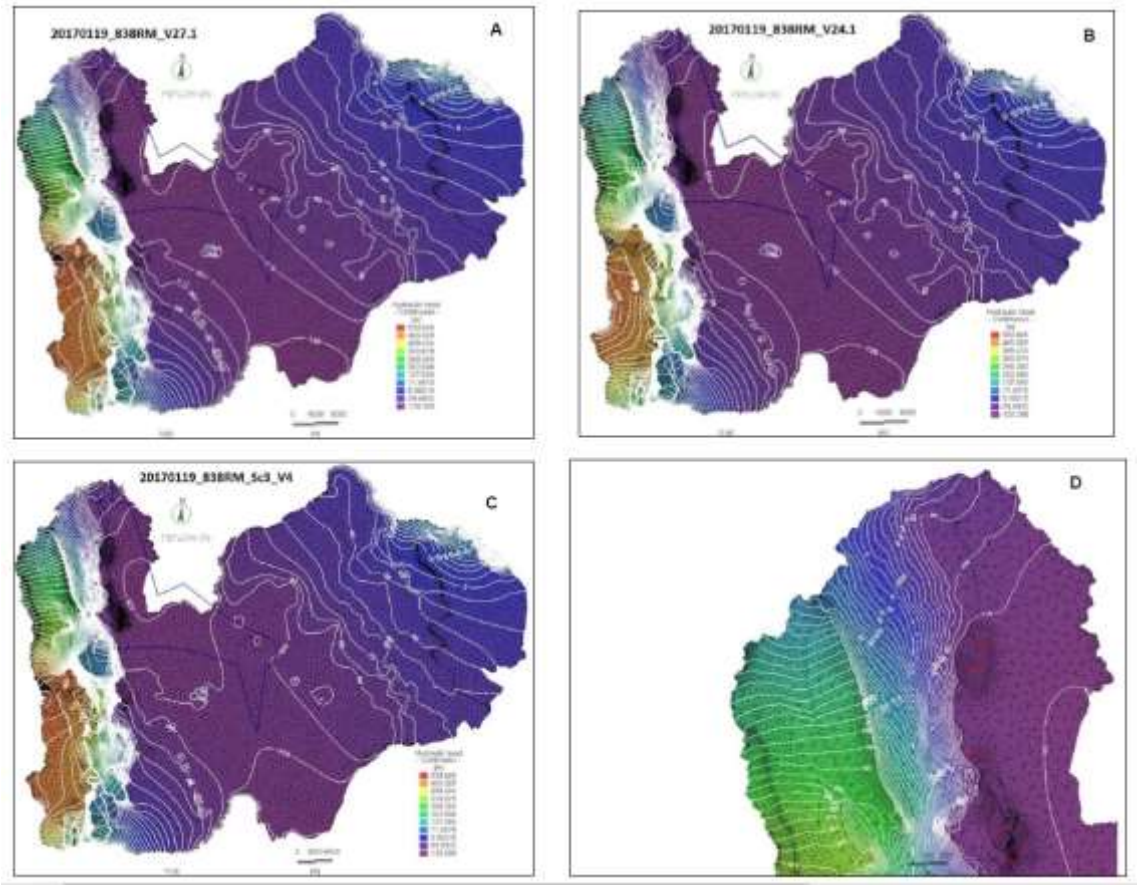

Figure 8-7 **Distribution of hydraulic head contours (A-C) for the final calibration run. Figure D details hydraulic head contours over the northern part of the Dogua Mountains (Umvoto, 2016e).**

8.8 QUALITATIVE AND QUANTITATIVE ANALYSIS

The purpose of the sensitivity analysis was to test uncertainties in the conceptual model.

8.8.1 Sensitivity Analysis

Per Umvoto (2016e), the following sensitivities were undertaken:

- Evaluation of K ranges in the fans;
- Evaluation of K values of the Antalo and Tsaliet groups;
- Variation of the influx from the west to evaluate influx ranges.

In summary, the outcomes from the steady state modelling did not aptly differentiate between different scenarios or offer insight to which may be a preferred or a more likely scenario. The next phase involved transient modelling and assessed which of the three, if any, scenarios achieved a history match to the AST data. The K values were however never made to be representative of the values determined during the test pump analysis and revealed to offer only marginal sensitivity the the calibration of the model.

8.8.2 Transient Modelling and Calibration

Drawdown measurements from the production boreholes (RAJ-2, DN-P01, BS-P01, AY-P01 and RAJ-1), obtained from the AST, were selected as calibration targets for the transient modelling. Due to a lack of drawdown data in any of the monitoring boreholes during the AST, no monitoring boreholes were used as calibration targets.

Initial conditions for the transient calibration were obtained from the calibrated steady state model. Due to the difference between the transient model initial water levels and the water levels at the start of the AST, the drawdown curves could not be matched. For calibration, the drawdown and the drawdown trends were used as calibration standards (Umvoto, 2016e).

Scenario 1 and 2 did not calibrate. Application of well skin effect and local mesh refinement was a possible cause. Scenario 3, however, achieved an acceptable degree of calibration to adequately represent the natural system. During the transient calibration, S_y and K of the North Dogua, Bussaba and Asabuya fans were adjusted to improve the match between measured and simulated water levels (Umvoto, 2016e). The adjusted K was applied to elements directly around the wells. The conductivity was decreased to simulate possible well skin effects present in the well (Umvoto, 2016e). It was determined that a S_y value of 0.22 for the Asabuya fan resulted in the best match, while S_y values of the other two fans remained 0.2.

8.9 PREDICTIVE SIMULATIONS

Predictive simulations were conducted on Scenario 3, since this was the only scenario which attained an acceptable transient calibration. The model simulated the abstraction of 30 hm^3/a over a 20-year period of water supply from North Dogua, Bussaba and Asabuya fans. This volume was allocated between 20 wells across the three fans, with the North Dogua and Asabuya fans having 7 wells each and Bussaba having the remaining 6 wells. Each of the wells abstracted at a rate of 60 l/s for 22 hours a day (Umvoto, 2016e).

The resulting spatial distribution of boreholes around the fans after running the simulation for 20 years is shown in **Figure 8-8**, with the water level drawdown (see **Figure 8-9**) showing an average drawdown of 5.5 m across all three fans (Umvoto, 216e). The North Dogua, Bussaba and Asabuya fans showed drawdowns of 5.3 m, 6.1 m and 5.1 m respectively (Umvoto, 2016e). These results suggested that water can be abstracted at the proposed rate and pumping regime over the life of mine without resulting in considerable drawdown of the water table within the fans. It must be noted that no drawdown was seen in the observation boreholes during the AST implying that pumping would need to continue for an extended period for measurable drawdown data to be obtained.

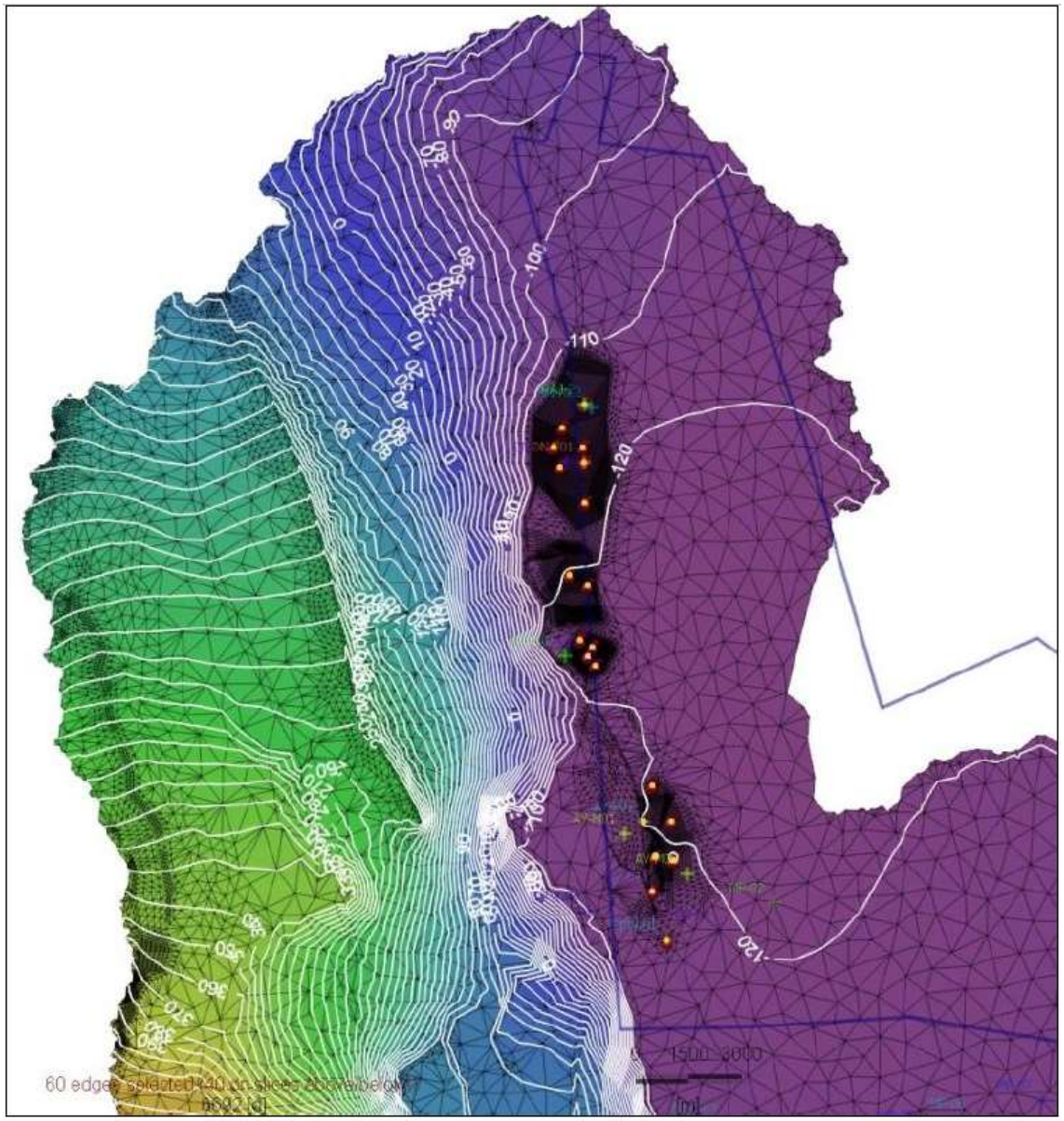

Figure 8-8 **Water level decline after 20 years of abstracting at 60 l/s from 20 wells, totalling 34.6 hm^3/a (Umvoto, 2016e).**

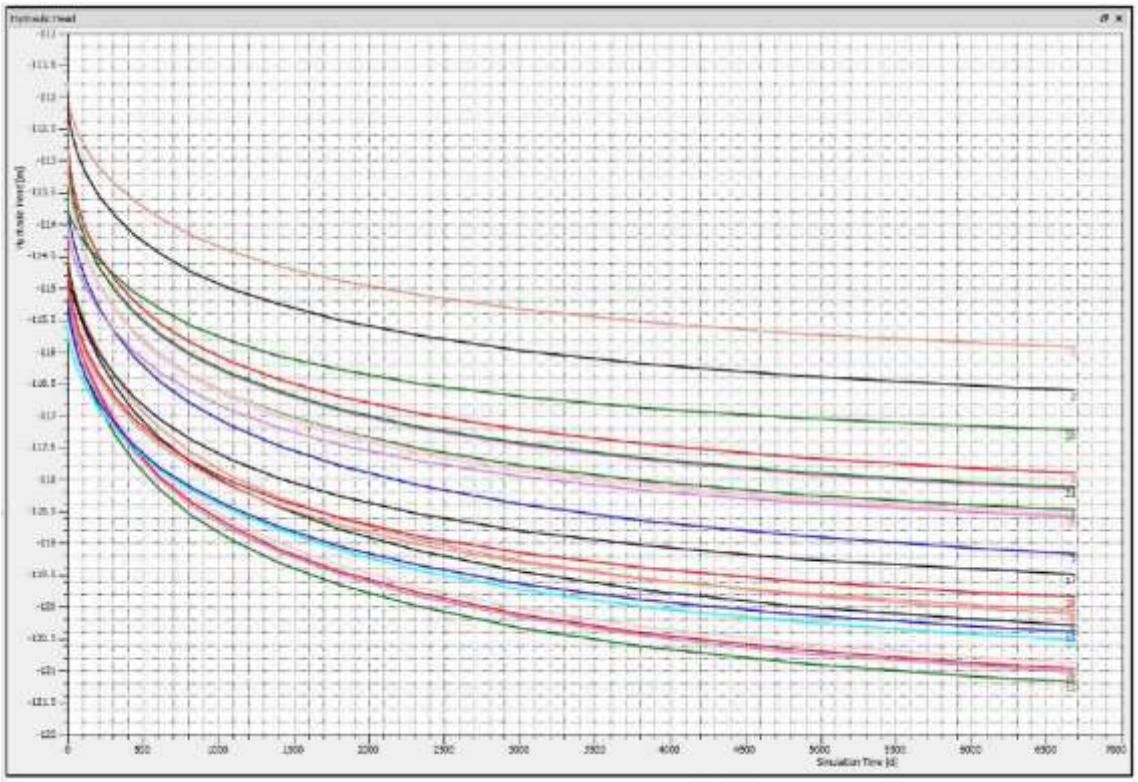

Figure 8-9 **Simulated water level drawdown in the monitoring boreholes after 20 years of pumping. Average drawdown of 5.5 m was observed (Umvoto, 2016e).**

With the configuration and distribution of the abstraction wells within the fans, the model simulated that water flowing into each of the fans may be able to sustain the proposed rates of abstraction (see **Table 8-8**). Extending the pumping period to 40 years also increased the flow rate into the fans to accommodate the abstraction (see **Table 8-9**).

Table 8-8 **Transient simulated volume through the Dogua Alluvial Fan Complex after 20 years of pumping after Umvoto (2016e).**

Fan	Inflow (hm^3/a)	Abstraction (hm^3/a)
North Dogua	18.3	12.2
Bussaba	13.8	10.4
Asabuya	21	12.2

Table 8-9 **Transient simulated volume through the Dogua Alluvial Fan Complex after 40 years of pumping after Umvoto (2016e).**

Fan	Inflow (hm^3/a)	Abstraction (hm^3/a)
North Dogua	18.4	12.2
Bussaba	14.0	10.4
Asabuya	20.9	12.2

The low drawdown in the fans after long periods of abstraction reflects the high transmissivity in the alluvial fans which implies a vast supply of water can be transmitted to the pumping wells. A short coming of the predictive simulations carried out is the lack of variation in the potential well field design and abstraction rates of a differing number of boreholes per fan.

8.10 SUMMARY AND CONCLUSIONS

The model was upgraded to include drilling, hydrochemistry and AST data, and calibrated to represent the three possible recharge scenarios as informed by these data. The developed models provided a basis for numerical experiments related to inherent assumptions of the conceptual model and the boundary conditions related to regional flow regimes.

The model tested the possible entry of deeper through-flow in the basement from the western boundary, with the model assuming it to be no more than 500 m deep, based on geological analysis related to the westward dip of the Adigrat-Antalo package (Umvoto, 2016e). In addition, the model included a fresh water recharge component into the Alluvial fan aquifers from run off infiltration.

In the evaluation of alternative regional groundwater flow-regimes, the model highlighted several issues worthy of closer attention, namely:

- Importance of quantitative constraints on bedrock through-flow and west to east water level gradients;
- Hydrogeological significance of the Dallol Mound;
- Role of the elevation of the active boiling Dallol springs which are flowing and boiling at an elevation of approximately -90 mamsl elevation or slightly higher, which is above the seepage face elevation in the fans which was measured as and set to -110 mamsl.

Deeper connections between the lower levels of the northern fans and the fault systems beneath them were also made apparent in the model which supports the hypothesis of influx of hydrothermal waters into the fans.

The results suggest boundary conditions primarily influence the regional flow gradient, but most importantly influence the water-table gradient in the fans. This is shown by the

non-unique steady state calibration attained using different boundary conditions, with all three of the model scenarios showing realistic gradients in the fans (Umvoto, 2016e).

Due to reported mesh design complications encountered in Scenario 1 and Scenario 2, only Scenario 3 attained a fair transient water level calibration (Umvoto, 2016e). The transient calibration also highlighted the possibility of positive skin effects of the well influencing the water levels. The results showed that the model slightly underestimated the water level drawdown in the abstracting boreholes. Calibration allowed a Sy value of 0.2 to be determined for the fans.

A predictive simulation of the mine's 30 hm^3/a requirement for the 20-year life of mine was run using Scenario 3. The results showed an average water level drop of 5.5 metres over the 20-year period. While this is supportive for a resource estimation, insufficient predictive scenarios were simulated to determine which scenarios would strain the aquifer system and so make known which ought to be avoided.

The model showed that sustainable abstraction rates required for adequate water supply can be attained without adversely impacting the aquifer. This was emphasised by the insignificant drawdown in the aquifer after long periods of abstraction.

The lack of modelling scenarios to investigate the influence of geothermally-driven convection beneath the fans and the possible influence of up-flow along the rift-border fault system was evident, however modelling of density-driven flows was not incorporated. Future development towards this objective, augmented by field measurements, would benefit a possible investigation of geothermal energy and fresh water sources, which may be relevant to mining or post-mining development needs.

A more local scale model of the fan may be useful in elucidating some of the uncertainties which remain in the Umvoto (2016e) model. A potential conceptual model is given by a detailed cross section of the Asabuya Fan, based on drilling results and stratigraphic understanding of the Dogua Alluvial Fans, which shows possible recharge sources to the Dogua Alluvial Fans (see **Figure 8-10**). Drilling chips revealed an alluvial fan thickness of 79 m at the toe of the fan (AY-M02) and a minimum thickness of 170 meters in the middle of the fan (RAJ-1). Literature implied a wedge shaped alluvial fan that is inter-fingered with the clay and salt deposits of the Danakil Depression. The older, lower section of the alluvial fan is also inter-fingered with the Zariga Formation gypsums. Water level measurements showed that the water table is sub-horizontal between the boreholes and the level of the seep at the fan toe. The dashed line and supplied temperatures include the possibility for density and thermally driven flows to be incorporated into a

local scale fan model. Constructing a local scale model would also offer greater accuracy in determining representative S_y values for each individual fan.

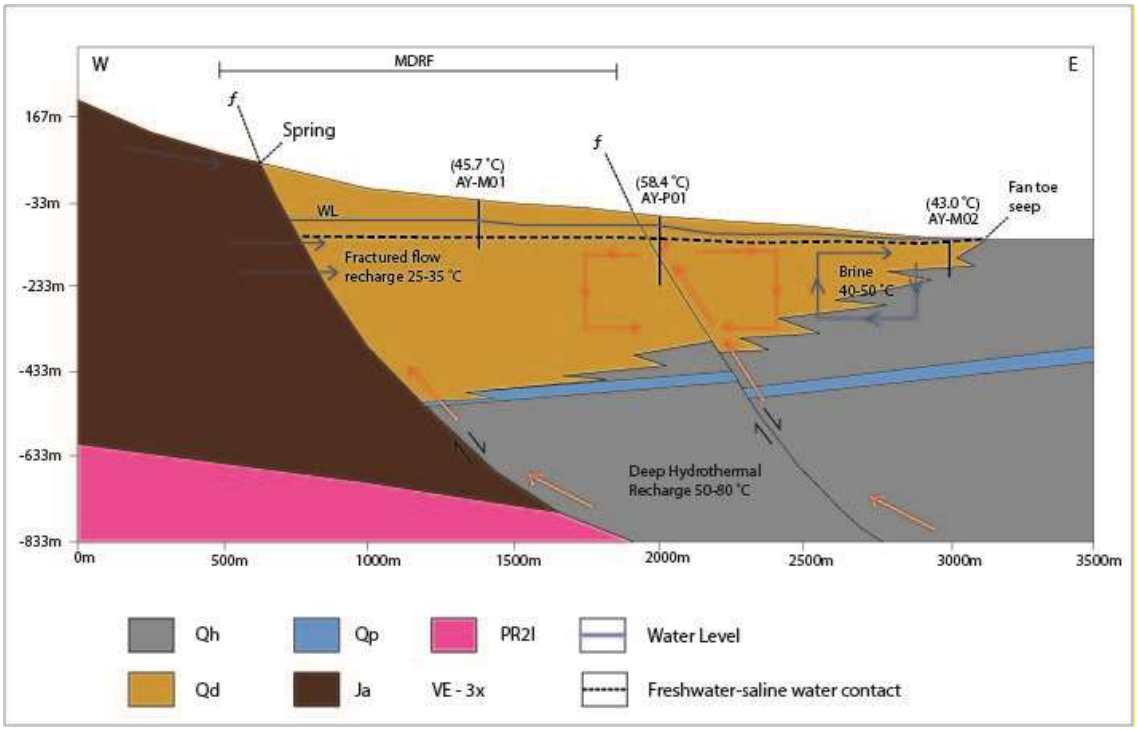

Figure 8-10 Detailed cross section of the Asabuya Fan illustrating the various paths of recharge, fractured flow through the MDRF and daylighting as springs along the basement contact and hydrothermal fluid from the magmatic rift.

CHAPTER 9

GROUNDWATER RESOURCE ESTIMATION

9.1 GROUNDWATER STORAGE ESTIMATION

Key considerations in evaluating resource availability are confidence in groundwater and resource estimation and sustainability of proposed abstraction over life time of the mine. These considerations are to better manage impacts from the abstraction of groundwater on groundwater flow, recharge and surface- groundwater interactions.

Furthermore, the quality constraints posed by the hypersaline-brine waters found in substantial quantities along the regional faults that transect the fans need to be considered as these waters may have to be treated prior to being used for solution mining practises.

The groundwater resource estimation is based on a culmination of the data interpretation and modelling presented thus far. The estimates are summarised below in the context of mine water demand.

The groundwater resource estimate is based on the volume of groundwater in storage in each of the alluvial fans regardless of quality. The geomorphological, geological associations and structural context of the large alluvial fan aquifers are believed to influence the quality and the quantity of recharge received, but storage calculations exclude any recharge as a matter of caution in quantifying the groundwater resource.

While there appears to be a significant supply of hypersaline water discharging vertically into the alluvial fan aquifers along the rift fault system, these volumes cannot be quantified nor relied on in determining the groundwater resource potential of the fans for the mine. High level estimates based on test pump data indicate boreholes that target the fault system would be capable to supply considerable amounts of water but would require extensive research to determine the exact source of these waters.

The total mine and plant demand of 30 hm^3/a or 30 gigalitres per annum (GL/a) is a significantly large water demand. Works carried out to this point indicate a potential quality constraint remains. If the mine were to have a fresh water demand (TDS < 1 000 mg/l) of 5% of the total water demand, then specific shallow boreholes in the Asabuya fan would likely be the most reasonable target to meet this demand without extensive water treatment being required. This is based on the lower TDS values encountered in

the AY-M01 samples collected during borehole development compared to those of AY-P01. Additionally, the increased likelihood of bedrock throughflow of better quality groundwater into the Asabuya fan from the Adigrat Limestones further supports this statement.

The water requirement scenarios discussed in this section were calculated by the author and form part of Umvoto (2016g). **Table 9-1** was constructed from data provided verbally by engineers associated with the solution mining operation (Fliss, 2017). The demand units are measured as cubic hectometres (hm^3) per annum and indicate the possible water requirement growth as the mining operation develops per year for the 20-year life of mine.

A strategic approach to groundwater development involving "…adaptive management…" (Umvoto, 2015) is recommended for a supply-development scenario during the growth stage (0-7 years) of the mine. In this context, a monitor-model-manage framework to groundwater exploration, exploitation and ecological monitoring, is considered vital.

Table 9-1 Mine water demand for the first seven years to full production in year 8 through to year 20.

Year	1	2	3	4	5	6	7	8	9-20
Total Mine Demand (hm^3/a)	0,1	0,4	2,9	7,58	8,91	16,12	24,09	30,05	30,05
Cumulative demand (hm^3/a)	0,1	0,5	3,4	10,98	19,89	36,01	60,1	90,15	450,75

9.1.1 Fan Volume

Total fan volume was calculated based on the thickness, width and length of the fan (see equation 4 and **Table 9-2**). The Specific Yield used in storage yield calculations was based on the S_y value obtained during model calibration. This value was determined to be 0.2 for each fan, although the Asabuya fan received a S_y of 0.22 during model calibration. The thickness is based on a minimum proven depth of 79 m during drilling, where only alluvial fan material was intersected. Two additional scenarios are included based on an additional 50 meters and an additional 100 meters' fan thickness (see **Table 9-2**). These calculations were done based on Equation 4 and **Figure 9-1**. The backstop of the fan was given a dip (δ in **Figure 9-1**) of 60°; a typical dip for normal faults in regions undergoing tectonic extension (Umvoto, 2016a). The saturated portion of the fan was taken to be the area below the measured water level within the boreholes and the fan toe seeps. The result of the various fan thickness scenarios on the total saturated volume is shown in **Table 9-2**.

$$V = \frac{hxb}{2} L \qquad (4)$$

where h is the maximum thickness of the fan based on the distance along a line passing through the heel of the fan that is perpendicular to its slope, b is the distance between the head and toe of the fan and L is the strike length of the fan, the extent in the lateral dimension, perpendicular to the profile view.

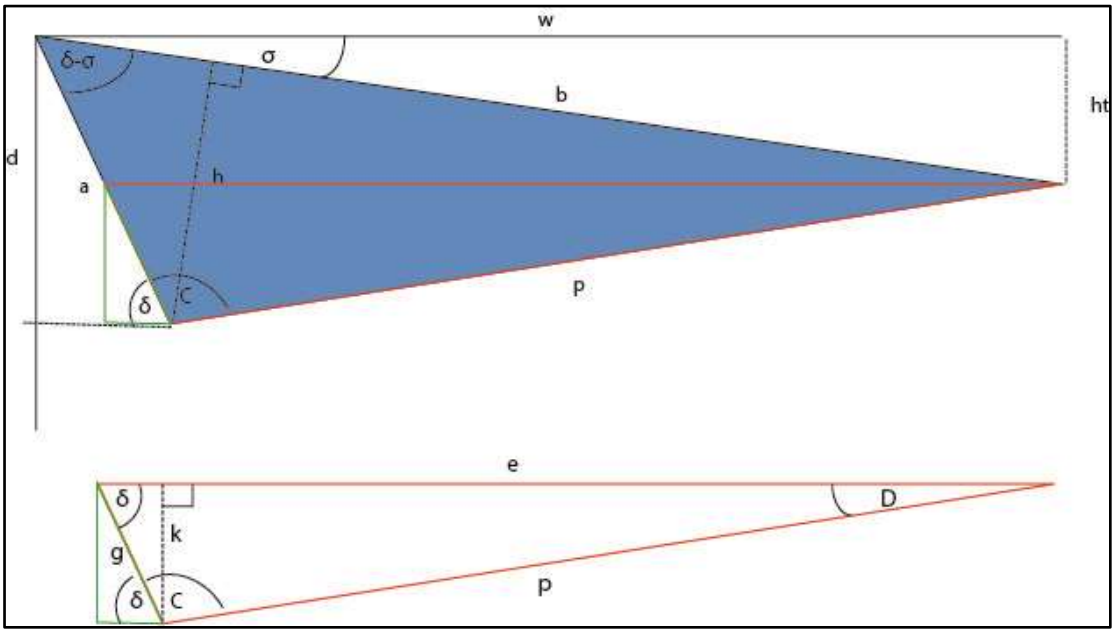

Figure 9-1 **Schematic cross-section through Dogua Formation alluvial fan sedimentary deposits (blue), with lengths and angles used to compute cross-sectional area and saturated fan-sediment volume.**

9.1.2 Storage Yield Model

Table 9-2 **Volume of water present in the fans based on a minimum proven thickness, minimum thickness with an additional 50 meters and an additional 100m thickness respectively.**

Fan	Total Volume	Saturated Volume	S_y
			0,20
	hm^3		
North Dogua	1765,34	448,47	89,69
Bussaba	4262,59	699,34	139,87
Asabuya	3639,17	894,46	178,89
Total	9667,09	2042,26	408,45
% of total mine demand	-	-	91
Additional 50 m			
North Dogua	2063,54	746,67	149,33
Bussaba	4792,76	1229,51	245,90
Asabuya	4030,48	1285,76	257,15
Total	10886,77	3261,94	652,39
% of total mine demand			145
Additional 100 m			
North Dogua	2361,74	1044,86	208,97
Bussaba	5322,93	1759,68	351,94
Asabuya	4421,79	1677,07	335,41
Total	12106,45	4481,62	896,32
% of total mine demand			199

Table 9-1 indicates a cumulative demand of 450.75 hm^3 over the life of mine, it can be seen that based on a storage calculations in **Table 9-2** a fan thickness of an additional 50 meters to the minimum thickness, there is sufficient water in storage to meet the overall demand if all recharge to the fans and quality constraints are neglected. Based on the life of mine demand and the minimum proven thickness, the water available in storage accounts for 91 % of the mines water demand.

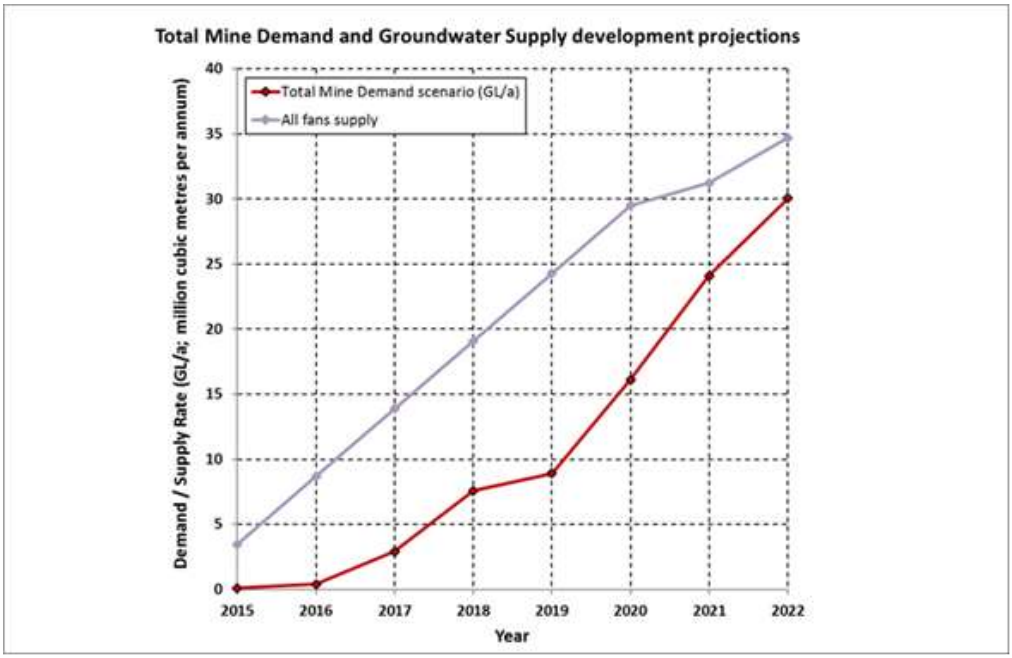

Figure 9-2 **Total mine demand versus groundwater supply development projections over the next 7 years.**

The projection in **Figure 9-2** and the results obtained in **Table 9-3** clearly implies that there is sufficient quantity of water to meet the demand throughout the development stages, but not for the entire LoM and that by year 18, 95.46 % of water will have been removed from storage. Further to this a minimum Sy value of 0.22 would be required to meet the mine water demand based on the minimum proven thickness. While this is very near to the S_y value used in the storage estimation, it is still larger than 0.2 used. A sufficiently small minimum S_y value (order of magnitude smaller i.e. 0.02) would offer undeniable confidence in the groundwater resource to meet the LoM in the absence of recharge.

Table 9-3 **Groundwater supply scenario, without special recharge augmentation, for the first seven years to full production in Year 8 through to year 20.**

Year	1	2	3	4	5	6	7	8	9-20
Total Mine Demand (hm^3/a)	0,1	0,4	2,9	7,58	8,91	16,12	24,09	30,05	30,05
Cumulative volume abstracted from storage (hm^3)	0,1	0,5	3,4	10,98	19,89	36,01	60,1	90,15	450,75
% of storage (S_y= 0,2: 408,46 hm^3)	0,02%	0,12%	0,83%	2,69%	4,87%	8,82%	14,71%	22,07%	110,35%

9.1.3 Recharge Estimation

Based on geophysical results, drilling, test pumping, hydrochemical analyses and interpretation as well as numerical groundwater modelling, it is evident that there is an

unquantified supply of poor quality water to the alluvial fan aquifers from upwelling of geothermally driven groundwater via the rift related faults that transect and underlie the aquifers. No quantification of the recharge potential of the faults is available, as too little information and understanding on the hydraulic character, spatial and geometric nature and extent of the faults is known. Rainfall related recharge was discussed and quantified via three different methods in **Section 8.4.3**.

9.2 WATER RESOURCE IMPLEMENTATION OPTION

The hydrochemical classification carried out suggests that conjunctive use of surface and groundwater would optimise the supply of water to the mine operation, minimise negative impact on aquifer integrity, promote sustainable water supply to local communities and in so doing present a solution to improving the quality of groundwater supplied. Key to this principle is Water Conservation and Water Demand Management. Water Conservation is to conserve water or use less and Water Demand Management (WDM) is to have water available when and if required (Umvoto, 2016g). A typical example in an area that experiences variability in rainfall is to harvest water during high flow events and slowly release it during low flows to meet the required water demand. The water demand can further be reduced by recycling or re-using water.

Based on field observations and hydrological model results reported on in Umvoto (2016g), it is evident that there is potential to harvest streamflow from the Ragali River, particularly during the months of July and August when streamflow is highest. These average monthly flows range from zero during the dry months of November to March peaking at approximately 9 m^3/s during August. This equates to approximately 23 million m^3 of water for August flowing down the Ragali River (Umvoto, 2016g). This is made evident in the field through regular flooding of the floodplains. Other additional considerations including international boundary and associated streamflow sharing as well as existing water users need to be considered prior to the potential harvesting of streamflow.

These surface waters may be useful for improving the water quality within the fans through harvesting the streamflow and artificially recharging the alluvial fans and in so doing suppressing the denser hypersaline waters. Considerations for such an undertaking would include the construction of off channel storage (OCS) facilities within or adjacent to the Ragali River or possibly even the Lelegheddi River. Umvoto (2016g) elaborates on this and supplies numerous potential Integrated Water Resource Management models. These would allow water to be stored and used as and when

needed. Additional physical challenges may arise such as overcoming significant elevation differences, sedimentation creating the need for large sediment traps and high evaporation rates requiring close management and control

Table 9-4 Implementation options for meeting mine water demand with advantages and challenges.

	Implementation Options	**Advantages**	**Disadvantages/challenges**
1	Target Faults within alluvial fans	• Substantial supply • Additional recharge source	• Poor quality • Decrease in quality over time • Significant mixing with fresh water to realise density targets • Unknown recharge potential and sustainability
2	Target fresh water layer or lens from artificial or managed recharge from surface water	• Supplementary source • OCS Facilities as supply • Control of water quality • Quality improvement through blending	• Evaporation losses • System maintenance • Implementation costs • Lowering of saline water interface requiring potential for large volumes of water to be pumped for sufficient storage

CHAPTER 10

KEY FINDINGS AND CONCLUSIONS

10.1 GEOLOGY AND CLIMATE

Lithological, structural and hydrostratigraphic investigations based on available literature, satellite imagery and field reconnaissance revealed that the Precambrian basement rocks of the Dogua Mountains outcrop in the west adjacent to the Bussaba and North Dogua fans, while further south, Cenozoic-Jurassic rocks of the Antalo Limestones and Adigrat sandstones are juxtaposed against the Asabuya fan. Structural mapping showed the presence of north-south trending rift related faults, including the Main Danakil Rift-boundary Fault, which transect and underlie the alluvial fans.

To augment climate data, two additional weather stations were established in the recharge zone of the alluvial fans. An average temperature of 34.4°C, an average rainfall rate of 90 mm/a and an evaporation rate of 60mm/a was determined for the study area. Measurements spanning a longer period would increase confidence in these calculations.

10.2 GEOPHYSICS, DRILLING AND TEST PUMPING

Results from the MLEM geophysical surveys showed minimum depths of up to 160 m for the alluvial fans. Low conductivity zones identified further supported the existence of rift related faults transecting the alluvial fans. Three production and five monitoring boreholes were sited in low conductivity zones and active depositional channels of the alluvial fans under investigation.

Lithologies encountered during drilling showed alluvial material of varying composition with no major confining clay layers. While drilling of production boreholes targeted faults, only AY-P01 intersected the fault at approximately 70 mbgl. Monitoring boreholes were drilled below and above production boreholes on low conductivity zones and active depositional portions of the fans. Drilling depths near the toe of the Asabuya fan proved a minimum thickness of 79 m while maximum depth was deduced from RAJ-1 drilling depth of 170 meters below ground level (mbgl). Greater understanding of the N-S boundary fault between the basement and the alluvial fan is needed, to determine if it is also transporting hydrothermal fluid and if fractured flow from the highlands is flowing

through it or not. The recharge from the west is a critical factor in resource estimation as would be upwelling of hydrothermal water in response to large scale abstraction.

The AST showed that pumping rates of up to 60 l/s were sustainable at each production well for up to 2 years. Production boreholes showed minor drawdown and rapid recovery. Steady state conditions are proposed to have been achieved, drawdown stabilised and laminar flow was never achieved during the AST, likely due to the partial penetration of the aquifer. High T values obtained from pump test data analysis implied vast amounts of groundwater could be transmitted to the boreholes during abstraction. These values were however, determined to be open to error due to the conclusion that the aquifer was recharged vertically with hypersaline hydrothermal waters and brine via rift related faults. This is proposed to act as a recharge source and not be evident as a recharge boundary in the test pump data. No drawdown was observed in the monitoring boreholes which prevented Storativity (specifically Specific Yield) values from being determined. The 603 370.7 m^3 discharged from the aquifer during the AST showed no negative effect on water levels. To give insight into any major boundary conditions and increase confidence in hydraulic parameters and aquifer response, the boreholes need to be pumped for a longer period and observation boreholes installed within 5, 10, 20 m of the abstraction borehole to offer distance related data for input into analytical model solutions. Water was ultimately not being removed from storage as there was a recharge source.

If the five production boreholes functioned at their full potential, 31% of the full-scale mining requirement of 30 million m^3/annum was achievable with no apparent strain to the aquifer.

Transmissivity and Hydraulic Conductivity values obtained were of a similar magnitude and were thus concluded to be high. Storage values from test pump analysis could not be attained due to no observation data. S_y values were thus determined from model calibration and applied to the storage yield model as they were in line with values quoted in literature for the aquifer material present. Hydrochemistry

Hydrochemical plots illustrated that the water quality was poorer (highly saline) in the North Dogua and Bussaba fans but improved from north to south and from the fan toe seeps to the wadis at the head of the fans. Individual borehole samples plotted distinctively together as a single fan, indicating the variation in recharge to the fans. Extended pumping was noted to improve the water quality within the fans except for the Asabuya fan, where the groundwater quality within AY-P01 and RAJ-1 decreased. This was concluded to be due to abstraction taking place directly from a fault in the Asabuya fan. Stable isotope sampling indicated that the northern fans had a similar signature to

the Red Sea and that the southern fans samples plotted closer to the Local Meteoric Water Line (LMWL). The strontium isotopes showed that all samples were relatively un-radiogenic with 87/86 Sr ratios, in the range of 0.705. This was suggested to be the result of leaching from young oceanic crust, possibly the Afar and Red Sea Basalts.

The change in TDS from the production boreholes to the seeps at the toe of the fans, possibly indicated dilution by a less dense, fresher water layer overlying the highly saline waters. There was extensive mixing of different waters present in each fan. These were determined to be direct infiltration from run off and rainfall, hydrothermal influx, ancient red sea waters and formation waters.

If the mine had a fresh water requirement (TDS < 1 000 mg/L) of 5% of the total mine water demand of 30 hm^3/a then results indicate that shallower boreholes at the top of the alluvial fans near the wadis would be the best target. This is due to potential fresh water inflow from the wadis from the larger surface water catchments and a greater distance from rift faults.

Water treatment options may have to be considered if there is a quality constraint on the water used for the potash solution mining operation. Possible options include desalination treatment through reverse osmosis, extensive blending and mixing of better quality ground- or surface- water with hypersaline waters or artificial recharge of the aquifers with surface flows from the Ragali River.

Stable isotope, radiogenic isotope and trace metal sampling and analysis is recommended to further increase confidence in the source of recharge. This is relevant for both resource estimation, development and groundwater quality management.

If the mine had a fresh water demand (TDS < 1 000 mg/l) of 5% of the total water demand, then specific shallow boreholes in the Asabuya fan would likely be the most reasonable target to meet this demand without extensive water treatment being required. This is based on the lower TDS values encountered in the AY-M01 samples collected during borehole development compared to those of AY-P01. Additionally, the increased likelihood of bedrock throughflow of better quality water into the Asabuya fan from the Adigrat Limestones further supports this statement.

10.3 MONITORING AND WATER LEVELS

Water levels monitoring showed a water table gradient between the southern (Asabuya Fan) and northern boreholes (Bussaba and North Dogua Fans), the water level dropped 12 meters over 14 kilometres, at a gradient of 1:0.00086 meters (0.86 mm every meter). Water levels within all the monitoring boreholes remained constant throughout the monitoring period and showed no negative effects from the AST.

Water level maps showed that there were two water mounds or high points, the Asabuya Fan to the south and the North Dogua Fan to the north, with the Bussaba Fan in the middle formed a low point. The water therefore possibly flows northward and southward to the Bussaba Fan.

Continuous water level monitoring will establish greater confidence in baseline conditions and seasonal variations or trends.

10.4 MODELLING

Numerical groundwater flow modelling showed limited lateral flow from the Antalo and Adigrat Formations in the west to recharge the Asabuya fan, but not the Bussaba and Dogua North fans. A clear distinction was thus made between the recharge scenarios of the southern and northern fans.

There was one recharge process common to all the fans which was direct vertical recharge from rainfall and from lateral surface flows during flash flood events. Rainfall related recharge was conservatively determined to be 0.39, 0.16 and 0.16 hm^3 for the Asabuya, Bussaba and North Dogua Fans respectively.

The conceptual model and numerical model focussed on three different recharge scenarios to the Dogua Alluvial Fan complex. The steady state and transient numerical model was calibrated under three different recharge scenarios.

The outcomes from the steady state modelling did not aptly differentiate between different scenarios or offer insight to which may be a preferred or a more likely scenario.

Density and thermally driven flows were not part of the numerical modelling outcomes which may be disadvantageous to potential insights for locating and distinguishing between groundwater of varying quality

The results showed that the model slightly underestimated the water level drawdown in the abstracting wells. Scenario 1 and 2 did not calibrate. Application of well skin effect and local mesh refinement is a possible cause. Scenario 3, however, achieved an acceptable degree of calibration to adequately represent the natural system. Calibration allowed for a Specific Yield value of 0.2, 0.2 and 0.22 to be determined for the North Dogua, Bussaba and Asabuya fans respectively.

The model showed that abstraction rates required for adequate water supply could be attained without adversely impacting the aquifer. This was emphasised by the insignificant drawdown in the aquifer after long periods of abstraction.

Deeper connections between the lower levels of the northern fans and the fault systems beneath them were also made apparent in the model supporting the hypothesis of influx of hydrothermal waters into the fans.

Further attention to the modelling of the shallow groundwater levels on a regional scale is required to improve confidence regarding inferred regional flow paths.

Limited modelling scenarios to investigate the influence of geothermally-driven convection beneath the fans and the possible influence of up-flow along the rift-border fault system was possible. Modelling of density-driven flows was not incorporated. Future development towards this objective, augmented by field measurements, would benefit a possible investigation of geothermal energy and fresh water sources, which may be relevant to mining or post-mining development needs.

Hydrological modelling is suggested as an important planning tool to initiate understanding of the surface water regime and unexplored volumes of fresh quality water available. It would make evident the significant flows and how they could be harnessed for improved, more sustainable mine water resource development and management in a conjunctive use scheme. These surface waters may be useful for improving the water quality within the fans through harvesting the streamflow and artificially recharging the alluvial fans and in so doing suppressing the denser hypersaline waters.

Considerations for such an undertaking would include the construction of off channel storage facilities within or adjacent to the Ragali River or possibly even the Lelegheddi River. Additional physical challenges may arise such as overcoming significant elevation differences as well as sedimentation and evaporation control and management.

10.5 RESOURCE ESTIMATION

The groundwater resource estimate was based on no recharge scenarios contributing to the water resource and volumes of groundwater in storage and available for abstraction in each of the alluvial fans.

It was concluded that there appeared to be an unquantified, but significant supply of hypersaline water recharging vertically into the alluvial fan aquifers along the rift fault system. It was suggested, based on test pump results that boreholes targeting this would have the potential to supply the water demand for life of mine, but water quality and the impact on the hypothesised naturally occurring fresh water layer overlying the saline waters in the fans remained a potential constraint. Further to this was the limitation posed by the amount of water in storage available for abstraction.

With a cumulative demand of 450.75 hm^3 over the life of mine, it was seen that based on fan volume calculations with fan thickness of an additional 50 meters to the minimum thickness and S_y value of 0.2, there was sufficient water in storage to meet 18 years' worth of mine water demand. With a minimum S_y value of 0.22 being needed to perfectly meet the LoM water demand (based on minimum proven thickness), the overall conclusion is that additional water resources will need to be explored to meet the full LoM demand without putting the alluvial fan aquifer system at risk from a sustainability point of view.

10.6 CONCLUSION

Literature, physiographic considerations, geological and hydrogeological investigations allowed for the development of a conceptual model on a regional and local scale of a potential groundwater resource for the mining operation. This conceptual model formed the basis of the numerical model which evaluated specific uncertainties regarding aquifer parameters and regional boundary conditions. Insights gained through model calibration and sensitivity analyses were, in combination with numerous drilling and hydraulic testing outcomes, used to determine the amount of recharge entering the alluvial fan aquifer and the volume of water available for abstraction from aquifer storage. This was related to the life of mine requirement.

Through groundwater exploration and aquifer characterisation, it is concluded that the alluvial fans are excellent aquifers, with sufficient storage and yield to meet the mine water demand of 30 hm^3/a for up to 18 years (including 7 years to full development).

Additionally, the Ragali River has potential to provide freshwater into the system. The minimum S_y value needed to supply the life of mine water demand however, was in the order of 0.22 which is higher than the S_y values used to determine water availability for supply from storage. This resulted that with no recharge to the system, 96% of the available water in storage will be depleted after 18 years and is thus a high-risk water source if not used conjunctively. The risk posed is not only to the aquifer integrity but also to the mining operation from an economic and social aspect.

Mine and processing water quality requirements however, need to be carefully mapped out to assess these requirements in terms of the available water resource. Two crucial factors need to be considered, the first being water quality constraints of the available groundwater and the second being erratic availability of fresh water from the Ragali River throughout the year.

The challenges in supplying groundwater to the mining operation will thus be in optimising development, sourcing water of an acceptable quality. As needed in terms of sustainable volume, and as possible in terms of water quality requirements, the rift fault system can be targeted.

Harnessing the Ragali River as a constant freshwater resource can be done by refurbishing and maintaining existing infrastructure in the Ragali River and creating more storage, thereby harvesting water during the high rainfall period, storing it through artificial recharge and using it during the low rainfall season.

REFERENCES

Abiye, T.A. (2010). An overview of the transboundary aquifers in East Africa. Journal of African Earth Sciences, 58: 684-691

Abbate, E., Woldehaimanot, B., Bruni, P., Falorni, P., Papini, M., Sagri, M., Girmay, S. and Medhin Tecle, T. (2004). Geology of the Homo-bearing Pleistocene Dandiero Basin (Buia Region, Eritrean Danakil Depression). Rivista Italiana di Paleontologia e Stratigrafia, 10: 5-34

Acton, D., and Stein, S. (1991). Block Rotation and Continental Extension in Afar: A Comparison to Oceanic Microplate Systems. Tectonics, 10 (3): 501-526.

Alemayehu, T. (2006). Groundwater occurrence in Ethiopia. Addis Ababa University, Ethiopia.

Allen, R.G., Perira, L.S., Raes, P. and Smith, M. (1998). Crop Evapotranspiration: Guidelines for computing crop water requirements. Irrigation and drainage paper No. 56, FAO, Rome Italy.

American Society for Testing and Materials (ASTM International) (2013). Standard guide for documenting a Groundwater Flow Model Application. ASTM International, USA, 5 pp.

Ayenew, T., Demlie, D. and Wohlich, S. (2008). Hydrogeological framework and occurrence of groundwater in the Ethiopian aquifers. Journal of African Earth Sciences, 52, 97-113.

Blainey, J. B., and J. D. Pelletier (2008). Infiltration on alluvial fans in arid environments: Influence of fan morphology, Geophys Res., 113.

Blair, T.C. and McPherson, J.G. (1994) Geomorphology of Desert Environments. Processes and Forms of Alluvial Fans. 2nd ed., 25: 413-467.

Brinckmann, J. and Kursten, M. (1970). Geological sketchmap of the Danakil Depression. Bundesanstalt fur Bodenforschung, Hannover.

Chorowicz, J. (2005). The East African rift system. Journal of African Earth Sciences, 43, 379-410.

Cooper, H.H. and C.E. Jacob (1946). A generalized graphical method for evaluating formation constants and summarizing well field history, Am. Geophys. Union Trans., vol. 27, pp. 526-534.

Jacob, C.E. (1944). Notes on determining permeability by pumping tests under water-table conditions, U.S. Geological Survey, 25p.

Craig, H. (1961). Isotopic Variations in Meteoric Waters. Science, 133 (3465). 1702-1703.

Darrah, T.H., Tedesco, D., Tassi, F., Vaselli, O., Cuoco, E., Pored, R.J. (2012). Gas chemistry of the Dallol region of the Danakil Depression in the Afar region of the northern most East African Rift. Chemical Geology. 14pp.

Drescher, H. (2014). Global geochemical variation of mid-ocean ridge basalts. Master's Thesis, Geoscience, University of Oslo. August 2014, 80 pp.

Driscoll, F.G. (1986) Groundwater and Wells. 2nd Edition, Johnson Division, St Paul, 1089.

Eagles, G., Gloaguen, R. and Ebinger, C. (2002). Kinematics of the Danakil microplate. Earth Planet. Sci. Lett., 203(2): 607-620

Environmental Resource Management (ERM) (2012). Dallol Potash Project – ERM Project 0143047. Draft Environmental, Social and Health Impact Assessment Report. December 2012

Environmental Resource Management (ERM) (2014). Scoping Report for the Yara Dallol Potash Environmental and Social Impact Assessment Study. May 2014

Ethiopian Institute of Geological Surveys (1988). Hydrogeological map of Ethiopia. 1:2 000 000 scale. Ethiopian Institute of Geological Surveys, Addis Ababa, Ethiopia.

ERCOSPLAN Ingenieurgessellschaft Geotechnik und Bergbau mbH (Ercosplan). (2015). Technical Report: In support of disclosure of Preliminary Economic Assessment of SOP Production, Allana Potash Corp., Danakil Project, Afar State, Ethiopia. Prepared for Allan Potash Corp. by Dr H. A. M. Rauache and Dr S. van der Klauw, pp. 268.

Fliss, T. (2017). Solution mining engineer, KU-TEC, Germany. Personal Communication March, 2017.

Food and Agriculture Organisation of the United Nations (FAO) (2005). Irrigation in Africa in Figures-AQUASTAT survey 2005.14 pp.

Franzson, H., Helgadóttir, H. M. and óskarsson, F. (2015). Surface Exploration and First Conceptual Model of the Dallol Geothermal Area, Northern Afar, Ethiopia. Proceedings World Geothermal Congress, 2015, Melbourne, Australia.

Frostick, L. E. (1997). The East African Rift Basins. In: Selley, R. C. (Ed). African Basins. Sedimentary Basins of the World, 3, 18-209.

Gat, J. R. (1996). Oxygen and Hydrogen Isotopes in the Hydrogeological cycle. Annu. Rev. Earth Planet. Sci. 1996. 24: 225–62

Gebresilassie, S., Tsegab, H., Kabeto, K., Gebreyohannes, T., Sewale, A., Amare, K., Mebrahtu, A., Zerabruk, S., Mebrahtu, G., Gebrehiwor, K. and Haile M. (2011). Preliminary Study on geology, mineral potential and characteristics of hot springs from Dallol area, Afar Rift, northeastern Ethiopia: Implications for natural resource exploration. Momona Ethiopian Journal of Science, 3(2): 12-30

Geological Survey of Ethiopia (GSE) (2009). Geology of Ethiopia. 1:2 000 000 scale, Ethiopian Ministry of Mines, Addis Ababa, Ethiopia.

Hantush, M.S., (1961a). Drawdown around a partially penetrating well, Jour. of the Hyd. Div., Proc. of the Am. Soc. of Civil Eng., vol. 87, no. HY4, pp. 83-98.

Hantush, M.S., (1961b). Aquifer tests on partially penetrating wells, Jour. of the Hyd. Div., Proc. of the Am. Soc. of Civil Eng., vol. 87, no. HY5, pp. 171-194.

Hayward, N.J. and Ebinger, C.J. (1996). Variations in the along-axis segmentation of the Afar Rift system. Tectonics, 15 (2): 244-257.

Holwerda, J. G and Hutchinson, R. W. (1968). Potash-bearing evaporites in the Danakil Area, Ethiopia. Economic Geology, 63: 124-150.

Horner, D. R., (1951). Pressure Build-up in wells. Proc. Third World Petroleum Cong., The Hague, Netherlands pp 503-520.

Kazmin, V. (1972). 1:2 000 000 Geological map of Ethiopia. The Geological Survey of Ethiopia, Ministry of Mines, Addis Ababa.

Kebede, S. (2013). Groundwater in Ethiopia. Springer Hydrogeology, Springer-Verlag Berlin Heidelberg.

Knight Piesold Ltd (2012). South Boulder Mines Ltd Colluli Potash Project – Hydrogeological site investigation report. Phase 1 investigation of mining Areas “A” and “B”. Prepared by Knight Piesold Ltd for South Boulder Mines Ltd, 14 pp.

Lowenstern, J.B., Janik, C.J., Fournier, R.O., Tesfai, T., Duffield, W.A., Clynne, M.A., Smith, J.G., Woldegiorgis, W., Weldemariam, K., and Kahsai, G. (1999). A geochemical reconnaissance of the Alid volcanic center and geothermal system, Danakil depression, Eritrea: Geothermics, 28: 161-187.

Mesfin, A. and Yohannes, E. (2014). The Geology of Northern Danakil Depression and its Geothermal Significance. Proceedings 5th African Rift Geothermal Conference, Tanzania.

Ministry of Water. (2002). Ethiopian guidelines: Specifications for drinking water quality. Federal Democratic Republic of Ethiopia, Addis Ababa, 15pp.

Munevar, A. and Marino, M.A. (1999). Modeling Analysis of Ground Water Recharge Potential on Alluvial Fans Using Limited Data. Groundwater, 37(5). 649-659.

MWH UK Ltd (MWH) (2015a). Yara Dallol Potash Project Mine Water Supply Feasibility Study: Conceptual model, water balance and surveys report. January 2015, 189 pp.

MWH UK Ltd (MWH) (2015b). Yara Dallol Potash Project Mine Water Supply Feasibility Study: Well construction and testing report. January 2015, 105 pp.

MWH UK Ltd (MWH) (2015c). Yara Dallol Potash Project Mine Water Supply Feasibility Study: Groundwater model report. January 2015, 180 pp.

MWH UK Ltd (MWH) (2015d). Yara Potash Project Water Supply Feasibility Study: Final report. January 2015, 97 pp.

Neuman, S.P. (1974). Effect of partial penetration on flow in unconfined aquifers considering delayed gravity response, Water Resources Research, vol. 10, no. 2, pp. 303-312.

Orris, G.J., Cocker, M.D., Dunlap, P., Wynn, J., Spanski, G.T., Briggs, D.A., and Gass, L., with contributions from Bliss, J.D., Bolm, K.S., Yang, C., Lipin, B.R., Ludington, S., Miller, R.J., and Slowakiewicz, M. (2014). Potash—A global overview of evaporite-related potash resources, including spatial databases of deposits, occurrences, and permissive tracts: U.S. Geological Survey Scientific Investigations Report 2010–5090–S, 76 pp.

Pedgley, D.E. (1967). Air Temperature at Dallol, Ethiopia. Meteorological Magazine. 96: 265-271.

Peel, M. C., Finlayson, B. L. and McMahon, T. A. (2007). Updated world map of the Köppen-Geiger climate classification. Hydrology and Earth System Science, 11: 1633-1644.

Remote Exploration Services (Pty) Ltd (RES) (2014a). Memo on G&B field verification findings. Pinelands, RSA, 19 pp.

Remote Exploration Services (Pty) Ltd (RES) (2014b). Report on the Time Domain Electromagnetic Survey, Bada-Danakil Licence, Ethiopia. Prepared for G&B Central African Resources Ltd, September 2014, 28 pp.

Remote Exploration Services (RES) (2016). Report on the Phase 2 Time Domain Electromagnetic Survey, Danakil Project, Ethiopia. Prepared by Remote Exploration Services (Pty) Ltd for Circum Minerals Ltd. Report No. RES16/003R, March 2016, 25 pp.

South African Bureau of Standards (SABS). (2011). South African National Standard (SANS) 241-1:2011. Drinking Water. Part 1: Microbiological, physical, aesthetic and chemical determinants.

Taylor, C.D., Schulz, K.J., Doebrich, J.L., Orris, G.J., Denning, P.D., and Kirschbaum, M.J. (2009). Geology and nonfuel mineral deposits of Africa and the Middle East: U.S. Geological Survey Open-File Report 2005–1294-E, 246 p.

Theis, C. V. (1935). The relation between the lowering of the piezometric surface and rate and duration of discharge of a well using groundwater storage. Transactions of the American Geophysical Union, 2, 519-524.

Thieman, S. (2007). Detection and Assessment of Erosion and Soil Erosion Risk in the Watershed of the Bilate River-Southern Ethiopian Rift Valley. PHD dissertation Ch.4, Freie University Berlin, 27pp.

Umvoto Africa (2014a). Phase 1 geology, hydrology and hydrogeology desktop study. Danakil Potash Project, Danakil Depression, Northern Ethiopia. Prepared by K. Burgers, C. J. H. Hartnady, A. Kuhudzai and V. Shoko of Umvoto Africa (Pty) Ltd for Remote Exploration Services (Pty) Ltd on behalf of G & B Central African Resources Ltd. Report No. 838/04/01/2014, January 2014, 59 pp.

Umvoto Africa (2014b). Phase 2 hydrogeology study. Danakil Potash Project, Danakil Depression, Northern Ethiopia. Prepared by C. J. H. Hartnady, D. Blake and E. R. Hay of Umvoto Africa (Pty) Ltd for Remote Exploration Services (Pty) Ltd on behalf of Circum Minerals Potash Ltd. Report No. 838/05/01/2014, December 2014, 27 pp.

Umvoto Africa (2015). Danakil Potash Project – Groundwater Modelling and Water Resource Analysis. Prepared by C. J. H. Hartnady, D. Blake, M. I. H. Hartnady, Dr F. S. Botha, E. R. Hay, L. Nolakana, D. C. McGibbon, Dr K. Riemann and A. Kuhudzai of Umvoto Africa (Pty) Ltd for Circum Minerals Ltd. Report No. 838/06-08/01/2015, July 2015, 117 pp.

Umvoto Africa (2016a). Water Resource Assessment for Potash Mining: Volume 1. Physiography and Geology. Danakil Potash Project, Danakil Depression, Northern Ethiopia. Prepared by C. J. H. Hartnady, M. I. H. Hartnady, E. R. Hay, D. C. McGibbon, L. C. Towers, D. Blake and C. A. E. Olianti of Umvoto Africa (Pty) Ltd for Circum Minerals Ltd. Report No. 838/14/01/2016, January 2017, 44 pp.

Umvoto Africa (2016c). Water Resource Assessment for Potash Mining: Volume 3. Aquifer Stress Test: Results and Interpretation. Danakil Potash Project, Danakil Depression, Northern Ethiopia. Prepared by D. McGibbon, L. Towers, D. Blake, Dr C. J. H. Hartnady and E. R. Hay of Umvoto Africa (Pty) Ltd for Circum Minerals Ltd. Report No. 838/14/03/2016, January 2017, 46 pp.

Umvoto Africa (2016d). Water Resource Assessment for Potash Mining: Volume 4. Climatology – Six Month Review. Prepared by P. Lee, D. C. McGibbon, L. Towers, Dr C. J. H. Hartnady and C. A. E. Olianti of Umvoto Africa (Pty) Ltd for Circum Minerals Ltd. Report No. 838/14/04/2016, January 2017, 34 pp.

Umvoto Africa (2016e). Water Resource Assessment for Potash Mining: Volume 5. Overview of Model Results. Danakil Potash Project, Danakil Depression, Northern Ethiopia. Prepared by L. Nolakana, L. Towers, J. Frewin, D. C. McGibbon, C. J. H. Hartnady, E. R. Hay, F. S. J. Botha, W. Gouws and C. A. E. Olianti of Umvoto Africa (Pty) Ltd for Circum Minerals Ltd. Report No. 838/14/05.01/2016, February 2017, 45 pp.

Umvoto Africa (2016f). Water Resource Assessment for Potash Mining: Volume 6. Potential Seismic and Volcanic Hazards and Risk Mitigation. Danakil Potash Project, Danakil Depression, Northern Ethiopia. Prepared by C. J. H. Hartnady, M. I. H. Hartnady, E. R. Hay, D. C. McGibbon and C. A. E. Olianti of Umvoto Africa (Pty) Ltd for Circum Minerals Ltd. Report No. 838/14/06/2016, January 2017, 71 pp.

United Nations Educational, Scientific and Cultural Organisation (UNESCO) (2004). World Water Assessment Program. National Water Development Report for Ethiopia. Addis Ababa, 284 pp.

United Nations Environmental Programme (UNEP) (2010). Africa Water Atlas. Division of Early Warning and Assessment (DEWA), UNEP, Nairobi, Kenya.

Vivier, J.J.P. (2013). Determination of Sustainable Groundwater Yield: A Systems Management Approach Based on the Minimum Groundwater Balance. AGES Consulting, Pretoria.

Waltham T., 2010. Afar Triangle: Rift Valleys and Volcanoes over Plate Divergence. In: Migoń P. (ed.), Geomorphological landscapes of the world. Springer Science + Business Media, Dordrecht: 183–190.

Warren, J. K. (2015). Evaporites: A compendium (ISBN 978-3-319-13511-3) Released August 2015: Berlin, Springer, 1600 pp.

Warren, J. K. (2015). Salty Matters. Online blog. Accessed January 2017. http://saltworkconsultants.businesscatalyst.com/blog/geology-of-danakhil-potash-in-the-danakil-depression. January 2017.

Water Works Design and Supervision Enterprise (WWDSE) (2015). Dallol Area Groundwater Potential Assessment Project: The Upper Catchments of the Dallol Areas (Ayshet Graben) Groundwater Potential Evaluation. Annex-2: Well Completion Report. Prepared by WWDSE on behalf of the Ministry of Water, Irrigation and Energy, Federal Democratic Republic of Ethiopia, December 2015, 121 pp.

Water Works Design and Supervision Enterprise (WWDSE) (2013). Groundwater potential assessment and evaluation of Dallol area, Phase 1: Evaluation of groundwater potential for Musley and adjacent fan areas. Prepared for Ministry of Water, Irrigation and Energy, Addis Ababa, Ethiopia, December 2013, 210 pp.

World Health Organisation (WHO) (2011). Guidelines for drinking-water quality. Fourth edition, Geneva, 541 pp.

APPENDIX A – CLIMATE DATA

A1. WS2 TEMPERATURE

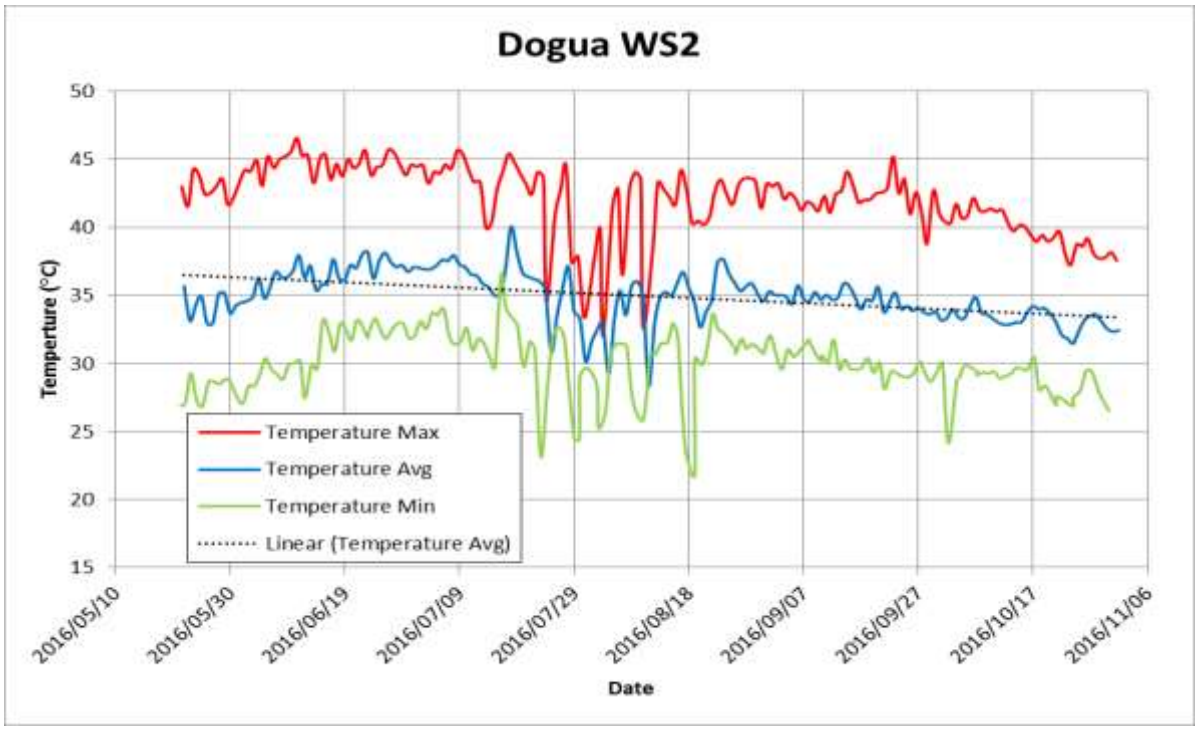

Figure A-1 **Dogua WS2 daily average, maximum and minimum temperature recordings between May and October 2016**

A2. WS2 RAINFALL

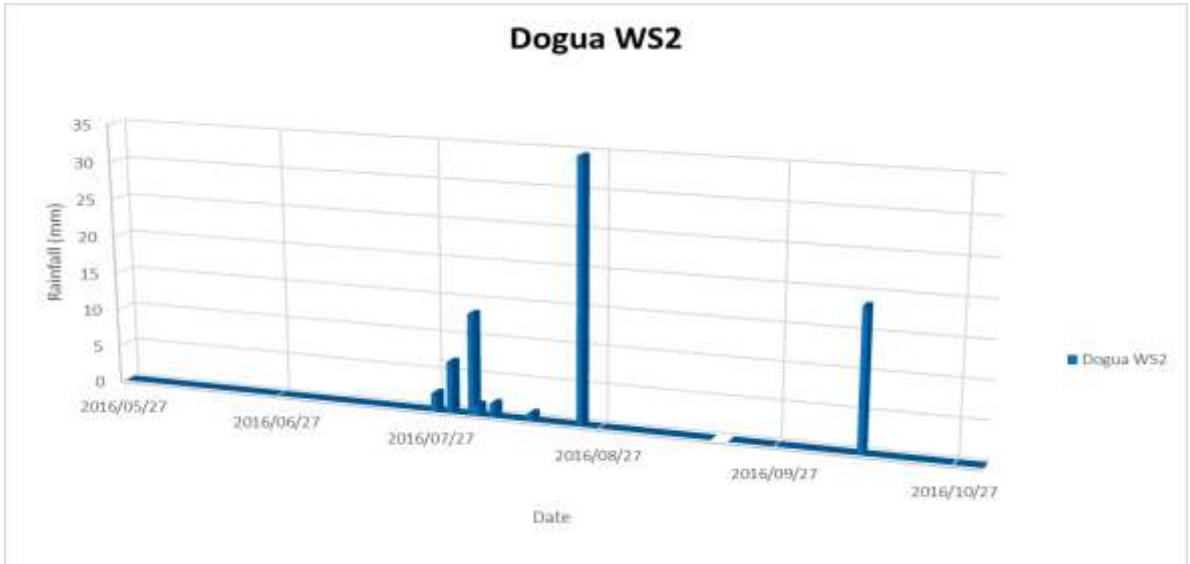

Figure A-2 **Dogua WS2 daily rainfall recordings between May and October 2016**

A3. WS2 EVAPORATION

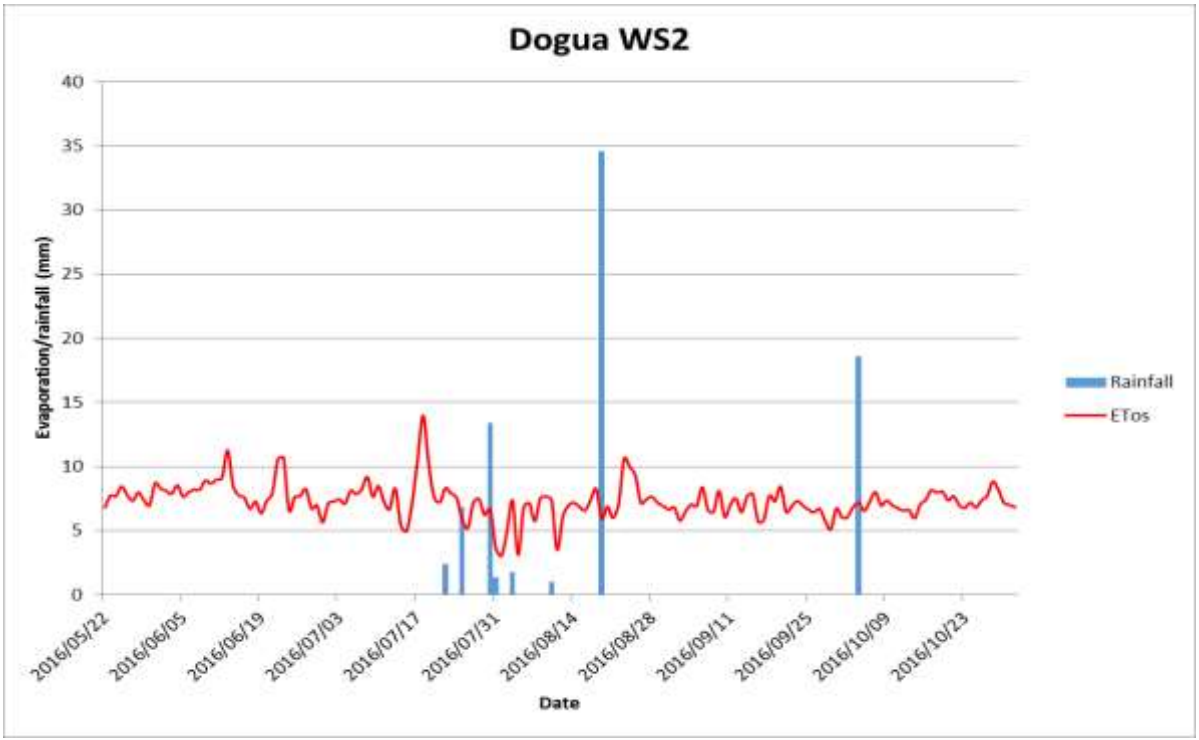

Figure A-3 **Dogua WS2 daily evaporation reordered as theoretical ETos along with daily rainfall between May and October 2016**

A4. WS2 WIND SPEED AND DIRECTION

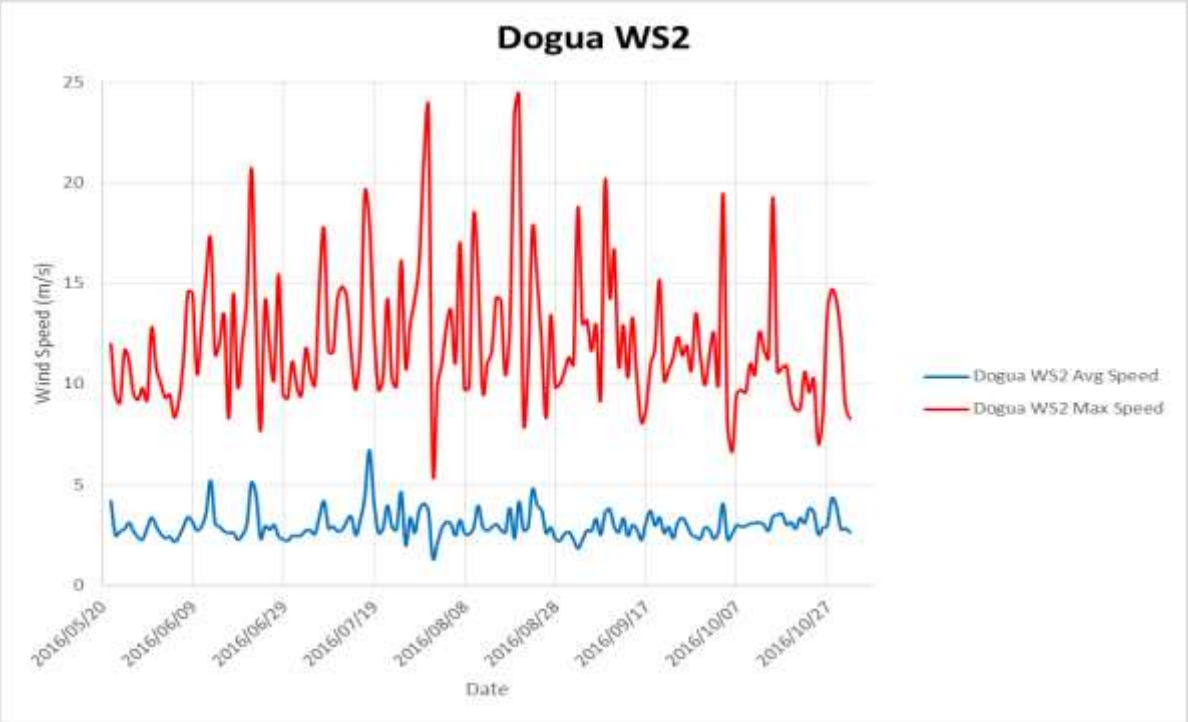

Figure A-4 **Dogua WS2 daily average and maximum wind speeds reordered between May and October 2016**

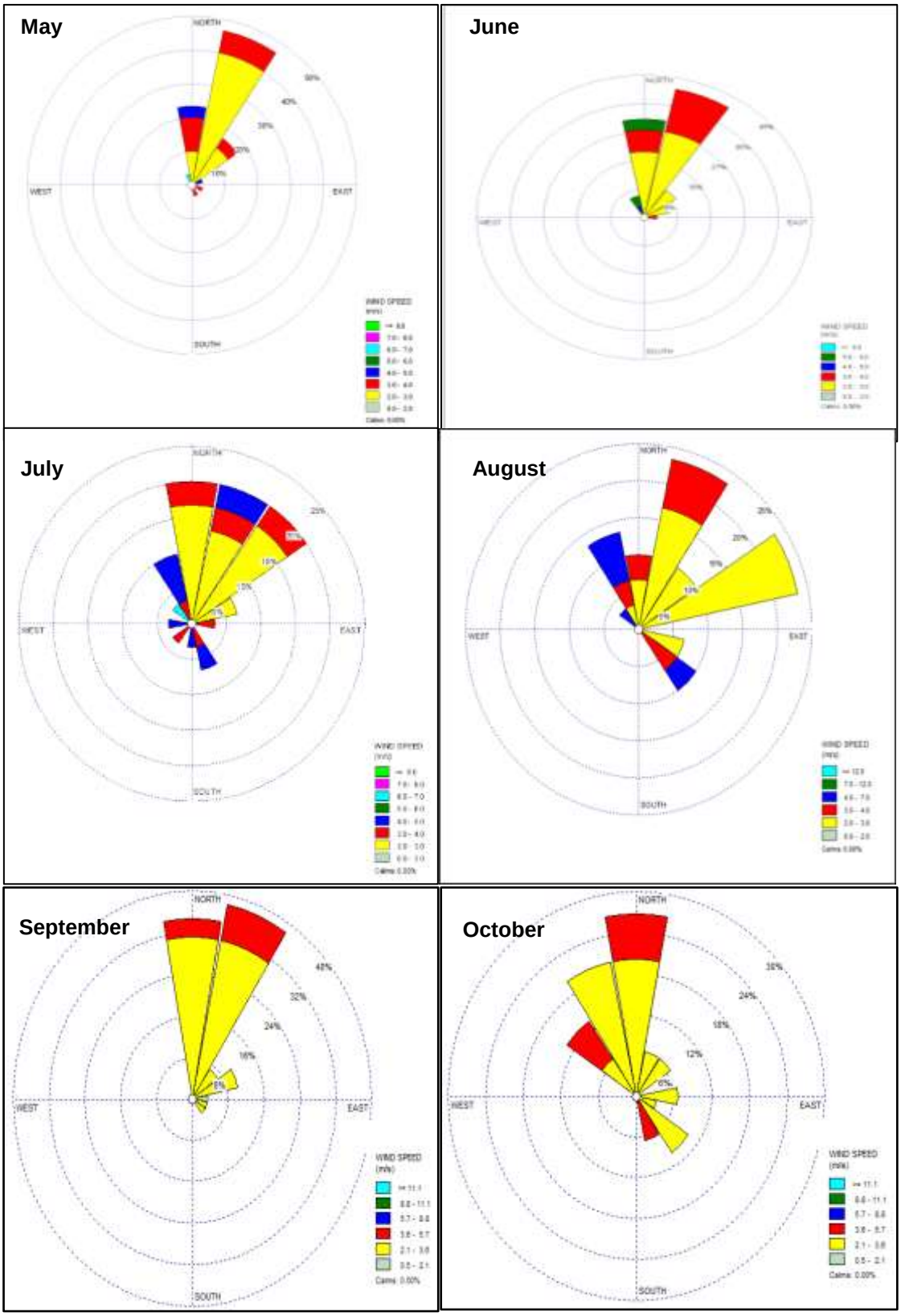

Figure A-5 Dogua WS2 monthly wind roses for May to October 2016

A5. WS2 RELATIVE HUMIDITY

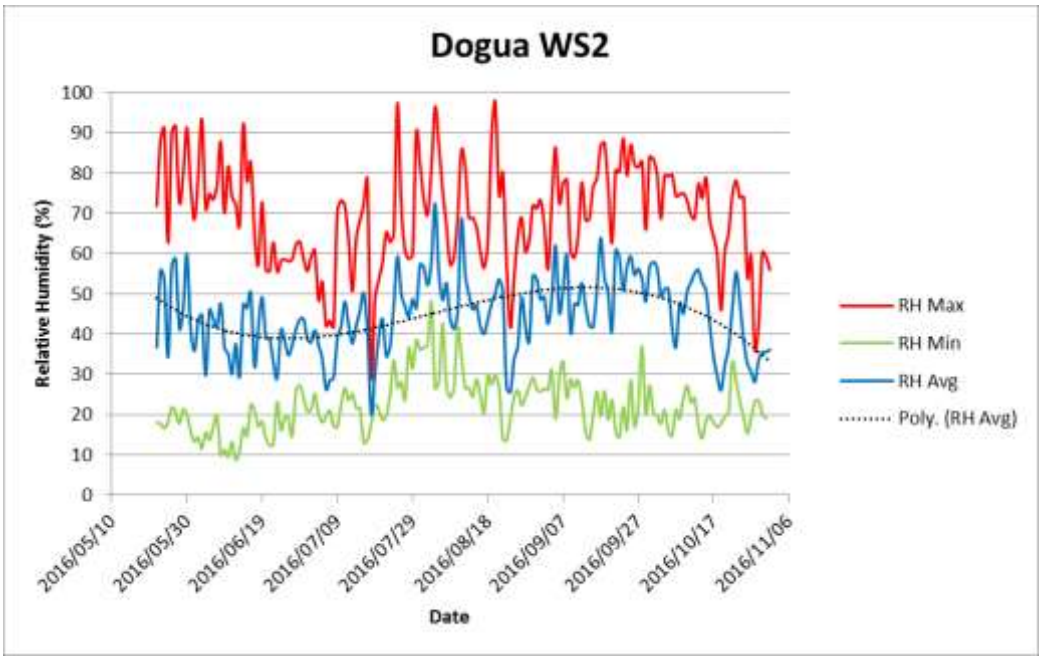

Figure A-6 **Dogua WS2 daily average, maximum and minimum relative humidity recorded between May and October 2016**

A6. WS2 SOLAR RADIATION

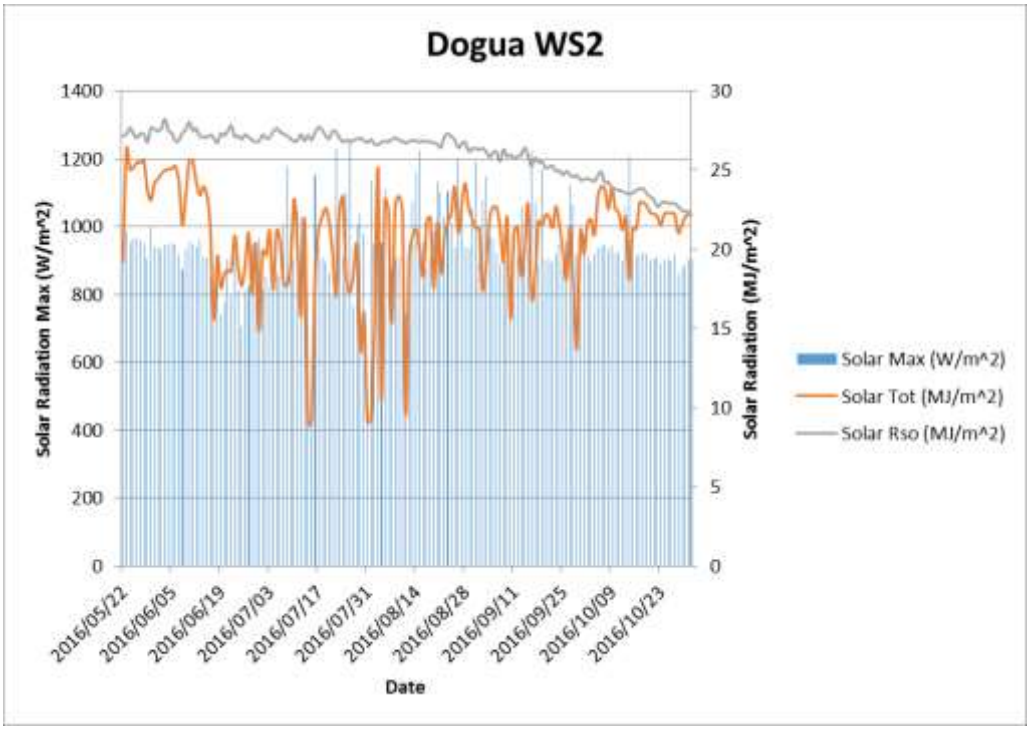

Figure A-7 **Dogua WS2 daily solar radiation recorded in terms of Rso, total and maximum between May and October 2016**

A7. WS2 PRESSURE

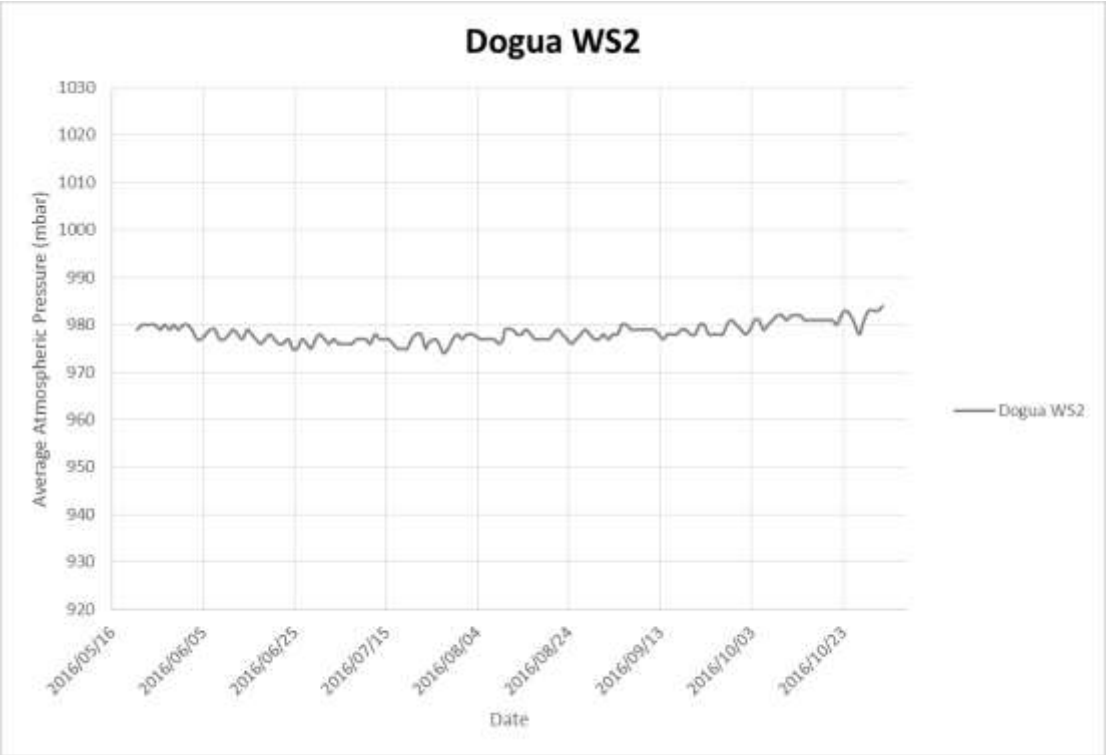

Figure A-8 **Dogua WS2 pressure recorded between May and October 2016**

A8. WS1 TEMPERATURE

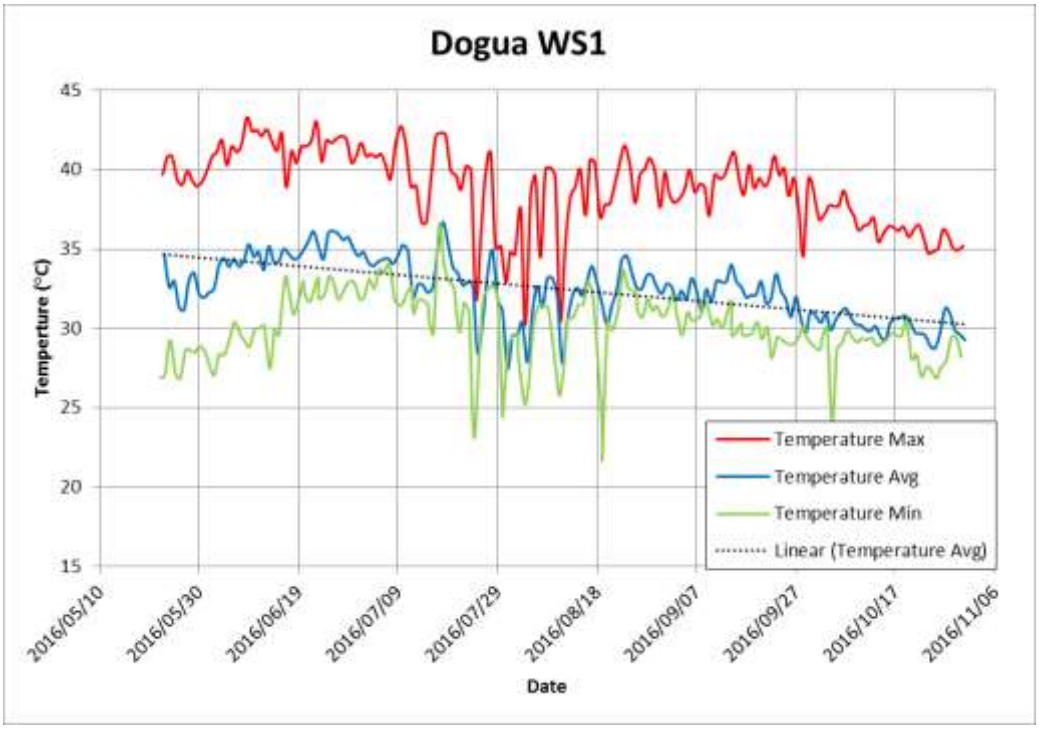

Figure A-9 **Dogua WS1 daily average, maximum and minimum temperatures recorded between May and October 2016**

A9. WS1 RAINFALL

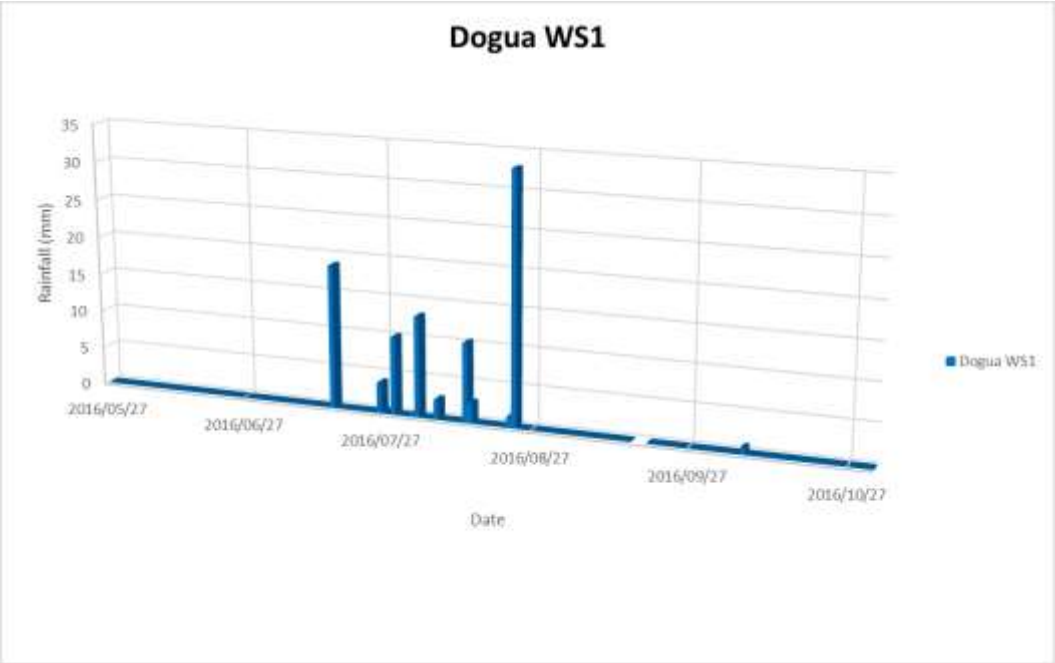

Figure A-10 **Dogua WS2 daily rainfall recorded between May and October 2016**

A10. WS1 EVAPORATION

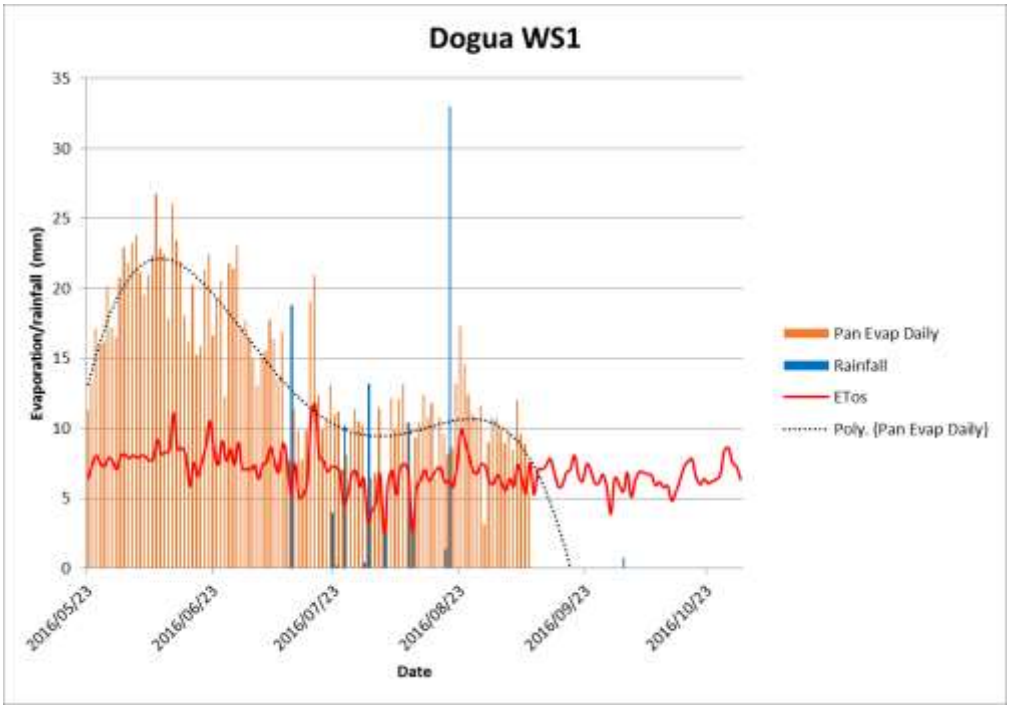

Figure A-11 **Dogua WS1 daily evaporation, measured as actual pan evaporation and theoretical ETos, along with daily rainfall recorded between May and October 2016**

A11. WS1 WIND SPEED AND DIRECTION

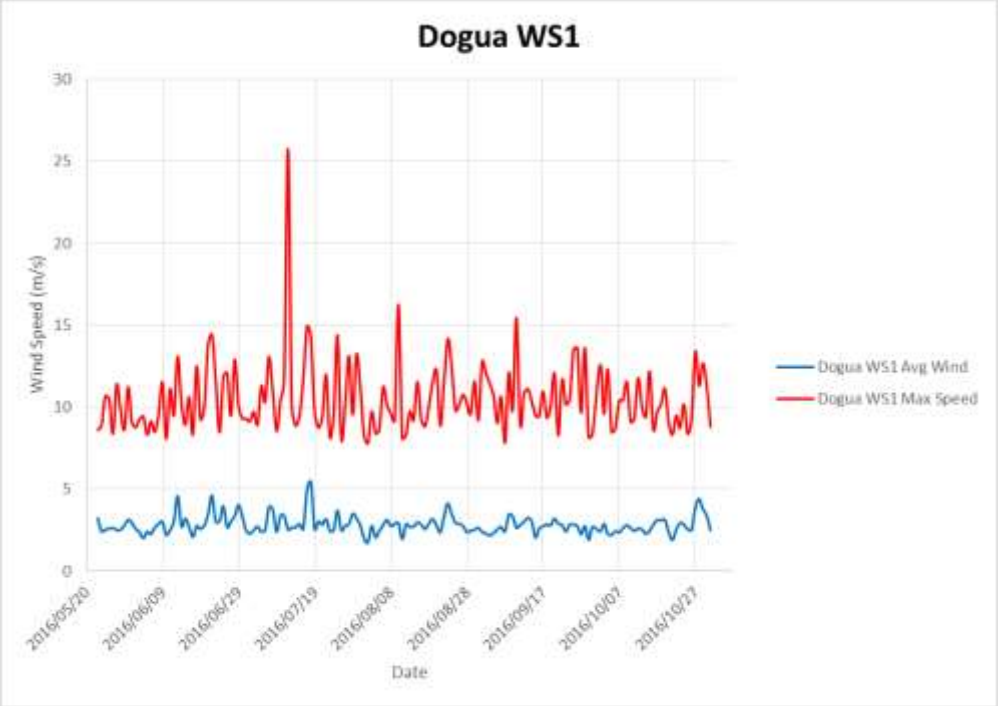

Figure A-12 Dogua WS1 daily average and maximum wind speed recorded between May and October 2016

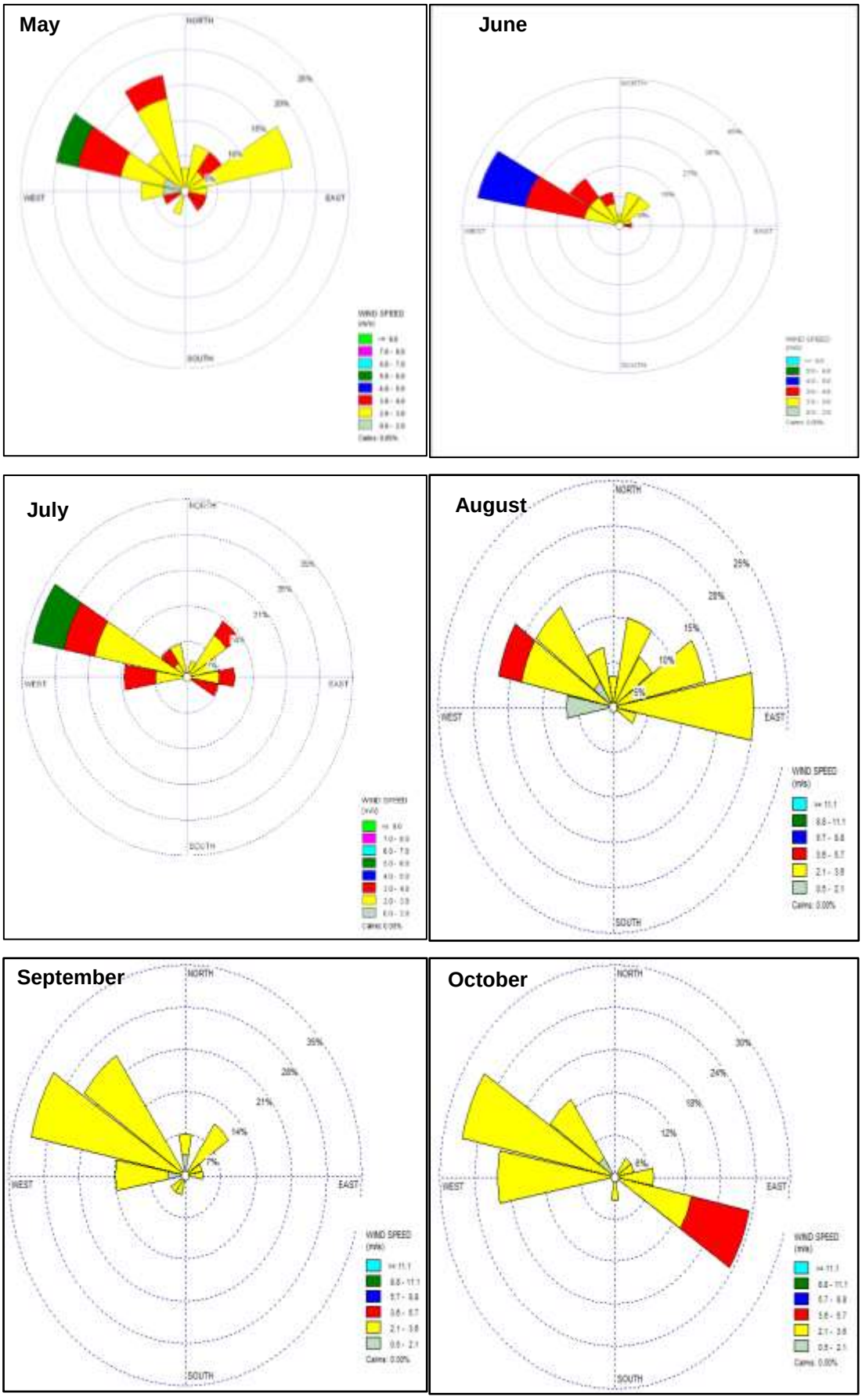

Figure A-13 Dogua WS1 monthly wind roses for May to October 2016

A12. WS1 RELATIVE HUMIDITY

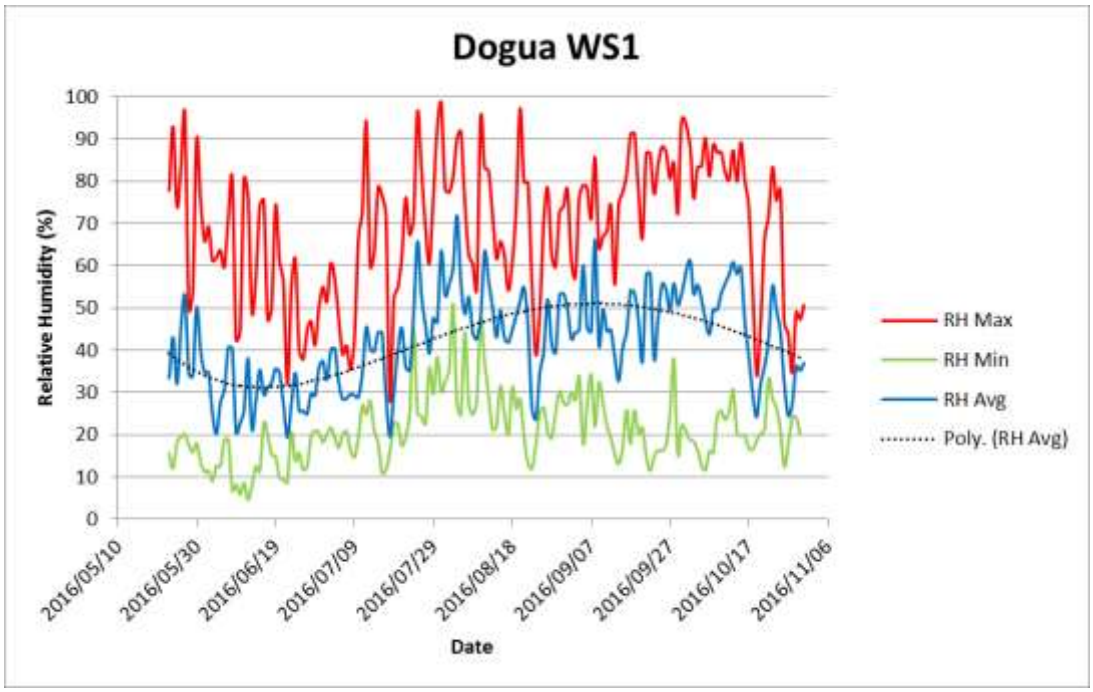

Figure A-14 **Dogua WS1 daily average, maximum and minimum relative humidity recordings between May to October 2016**

A13. WS1 SOLAR RADIATION

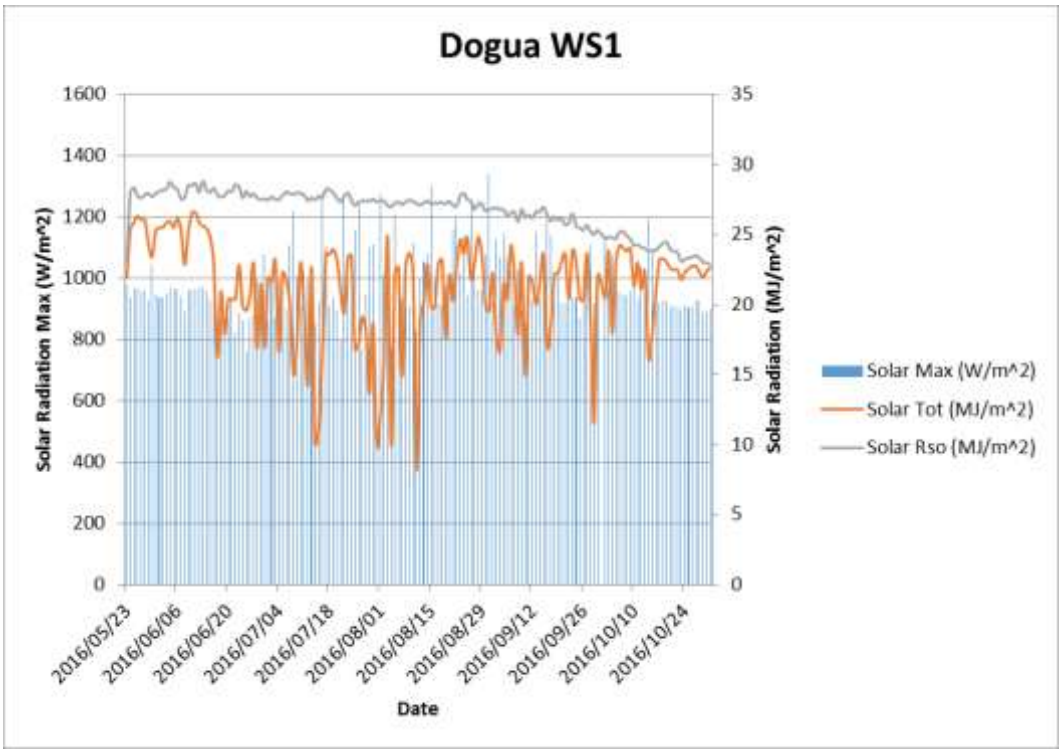

Figure A-15 **Dogua WS1 daily solar radiation recorded in terms of Rso, total and maximum between May and October 2016**

A14. WS1 PRESSURE

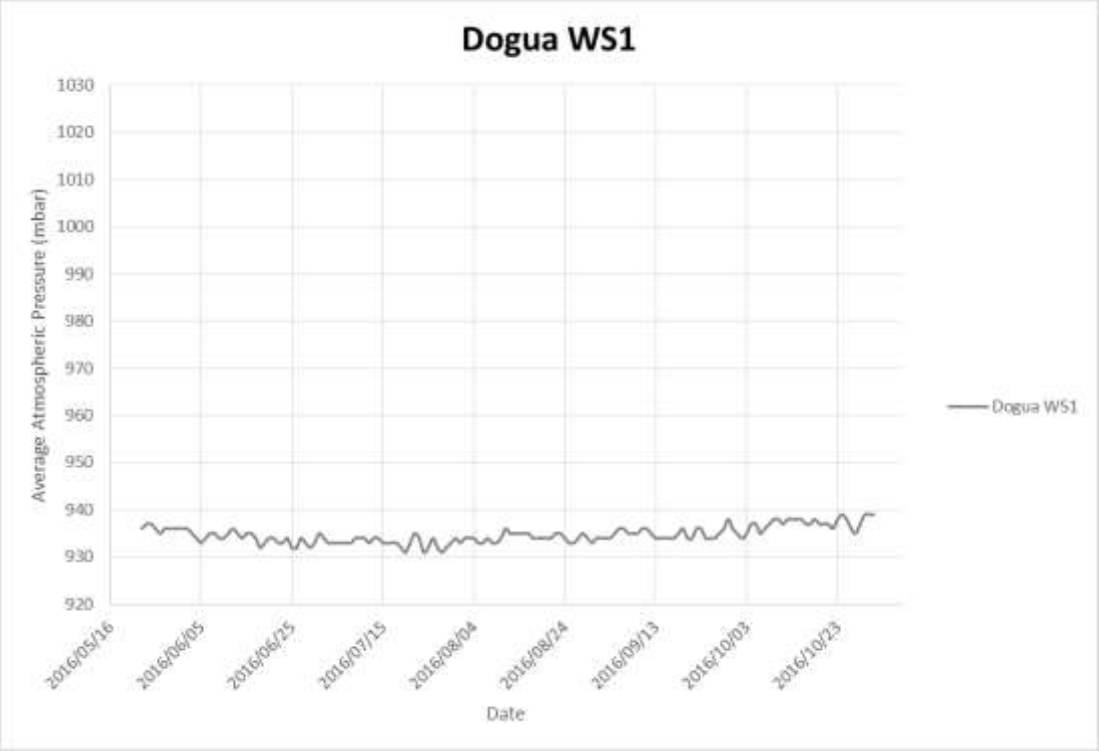

Figure A-16 Dogua WS1 pressure recorded between May and October 2016

A15. BADAH TEMPERATURE

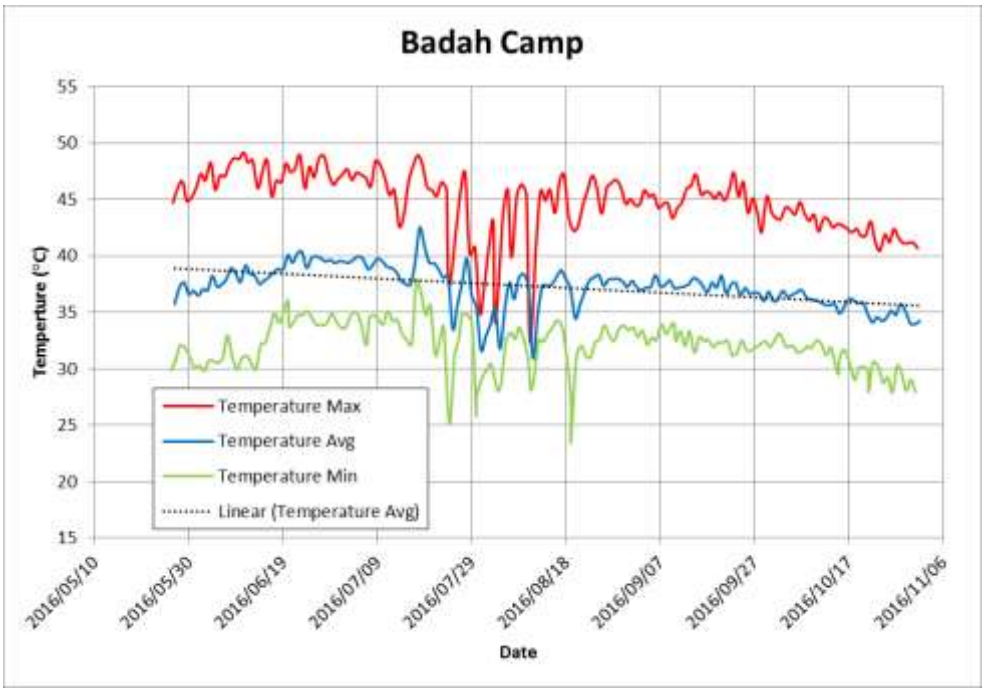

Figure A-17 Badah Camp daily average, maximum and minimum temperature recorded between May and October 2016

A16. BADAH RAINFALL

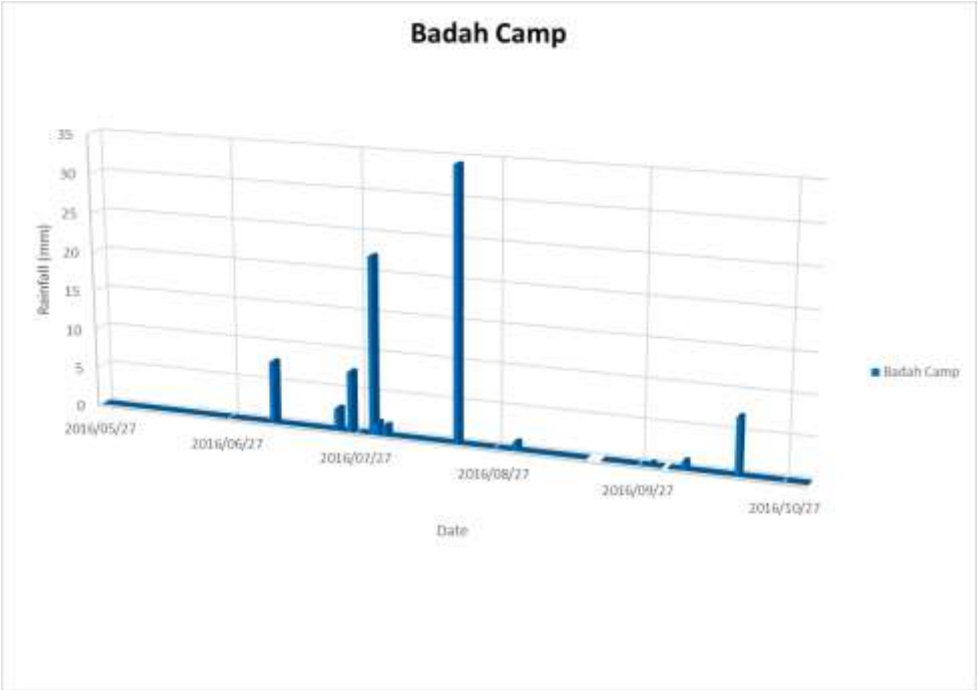

Figure A-18 Badah Camp daily rainfall recorded between May and October 2016

A17. BADAH EVAPORATION

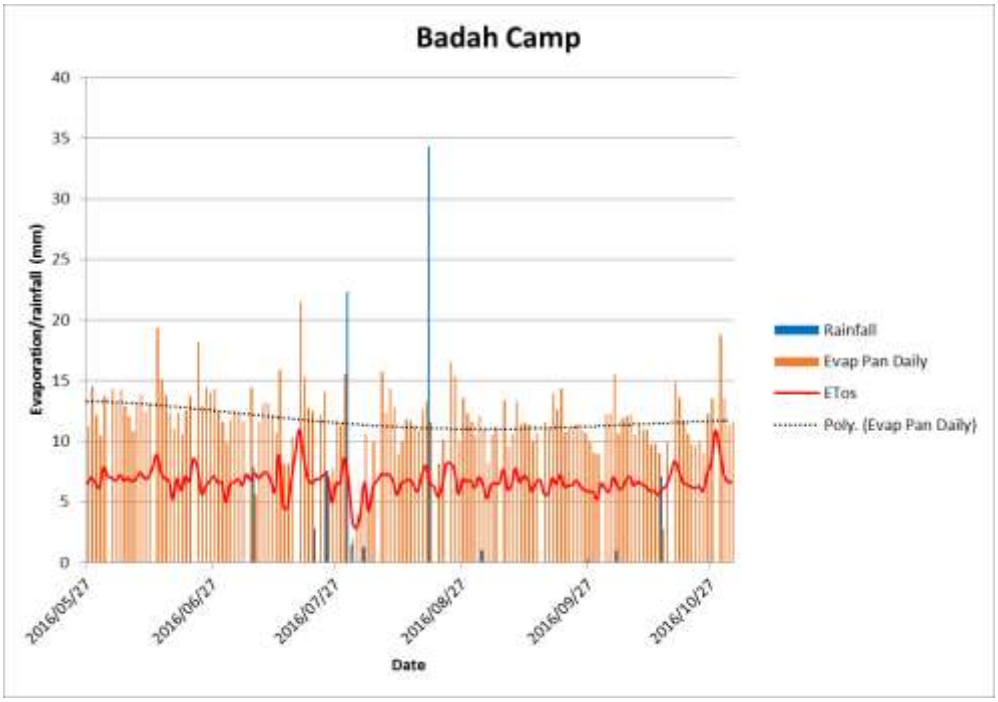

Figure A-19 Badah Camp daily evaporation, measured as actual pan evaporation and theoretical ETos, along with daily rainfall recorded between May and October 2016

A18. BADAH WIND SPEED AND DIRECTION

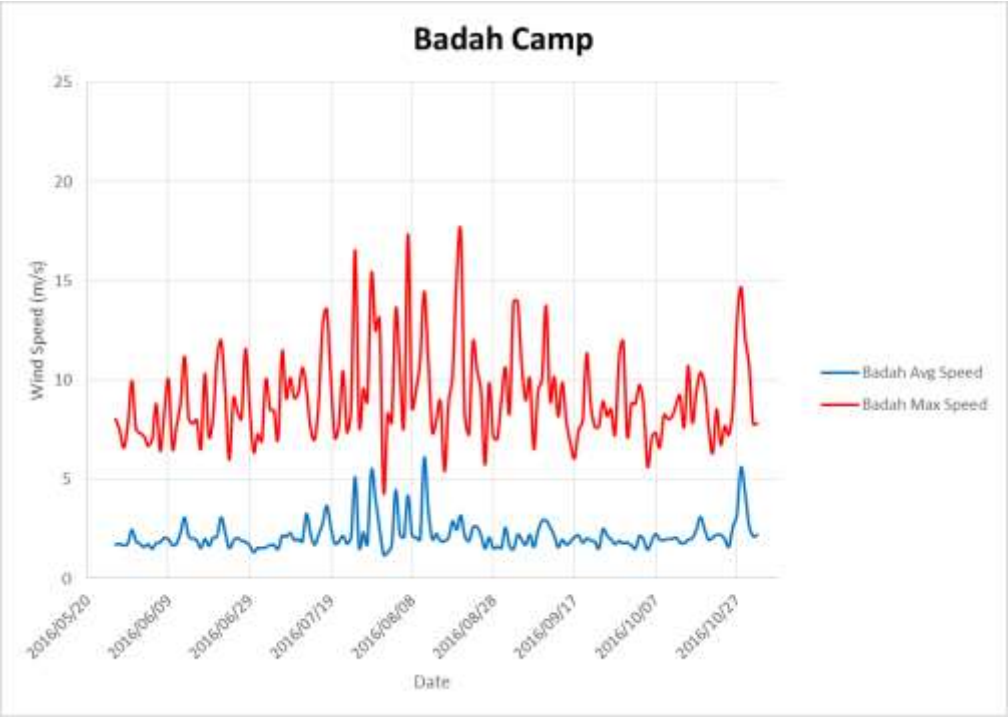

Figure A-20 **Badah Camp daily average and maximum wind speed recorded between May and October 2016**

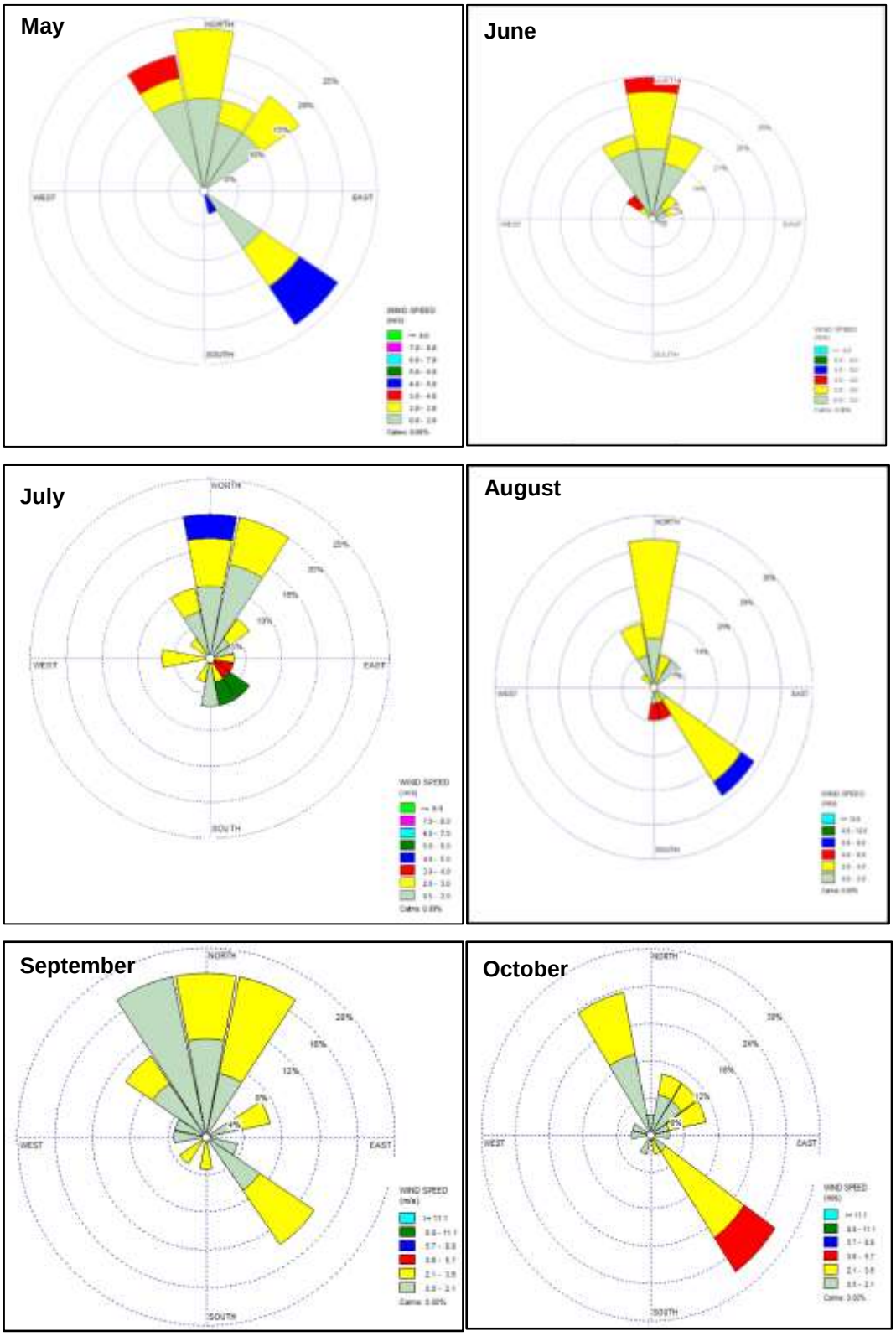

Figure A-21 Badah Camp monthly wind roses for May to October 2016

A19. BADAH RELATIVE HUMIDITY

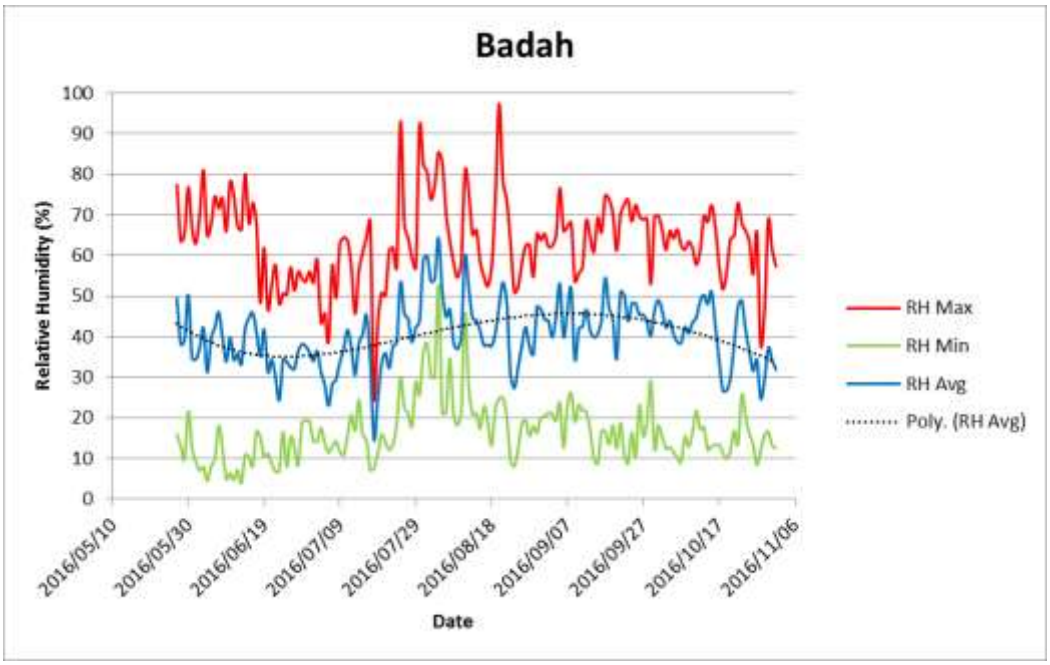

Figure A-22 **Badah Camp average, maximum and minimum relative humidity recorded between May and October 2016**

A20. BADAH SOLAR RADIATION

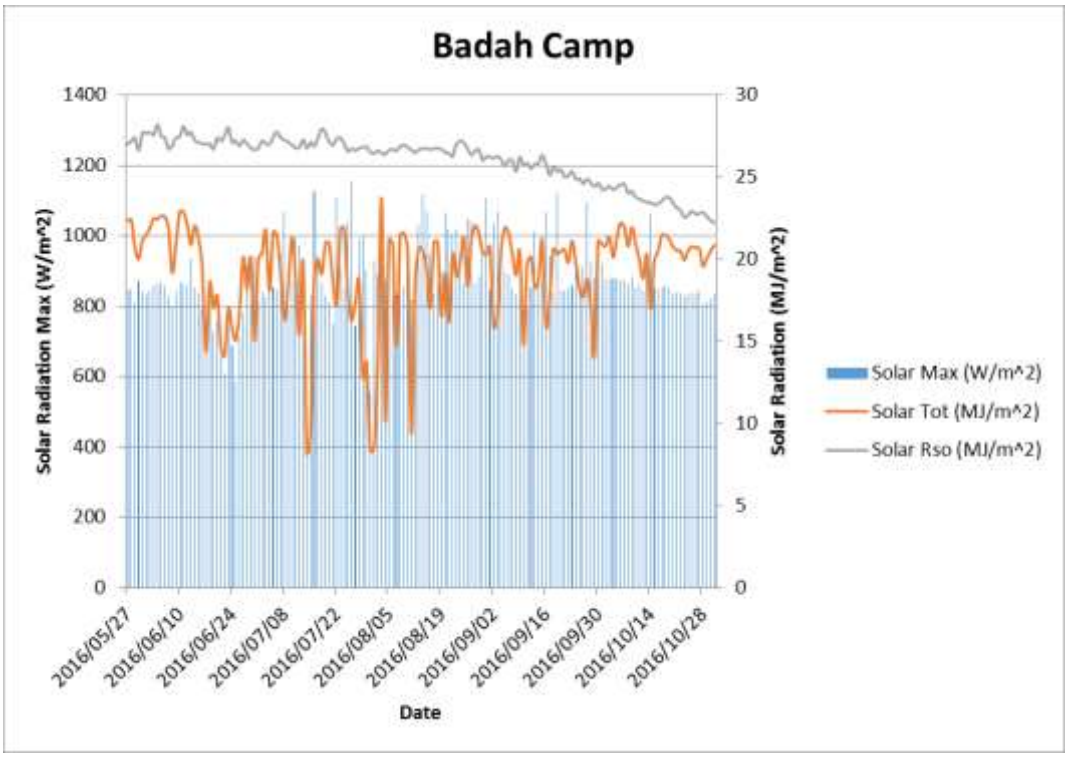

Figure A-23 Badah Camp daily solar radiation recorded in terms of Rso, total and maximum between May and October 2016

A21. BADAH PRESSURE

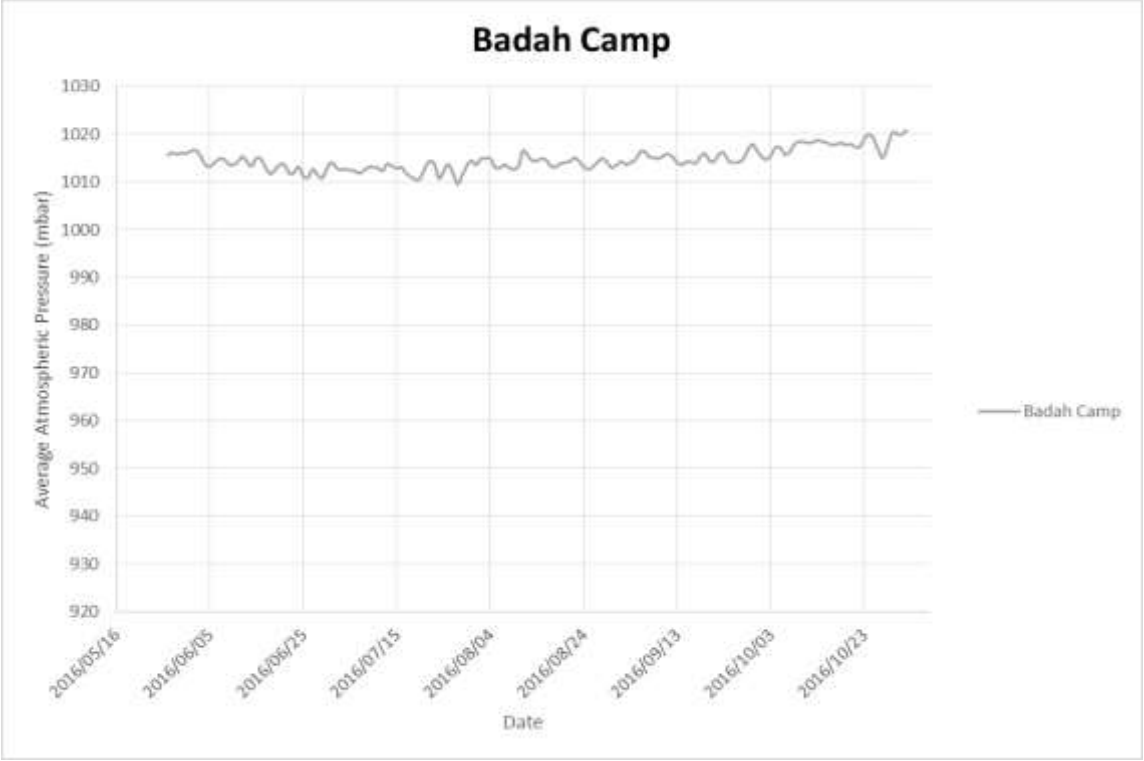

Figure A-24 Badah Camp daily pressure recorded between May and October 2016

A22. SOLMIN TEMPERATURE

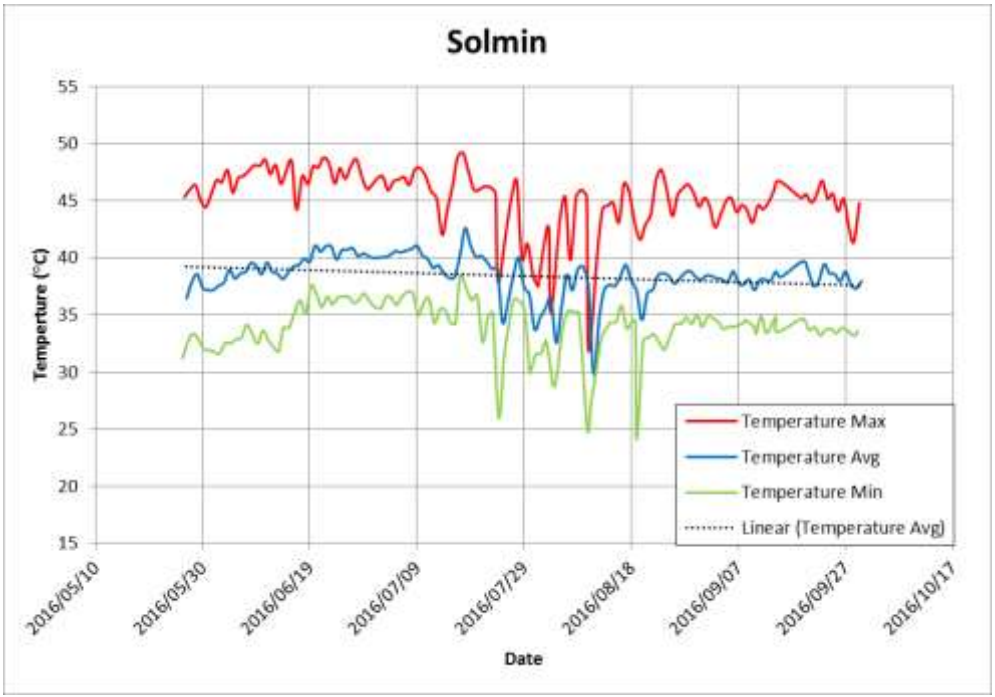

Figure A-25 Solmin daily average, maximum and minimum temperature recorded between May and September 2016

A23. SOLMIN RAINFALL

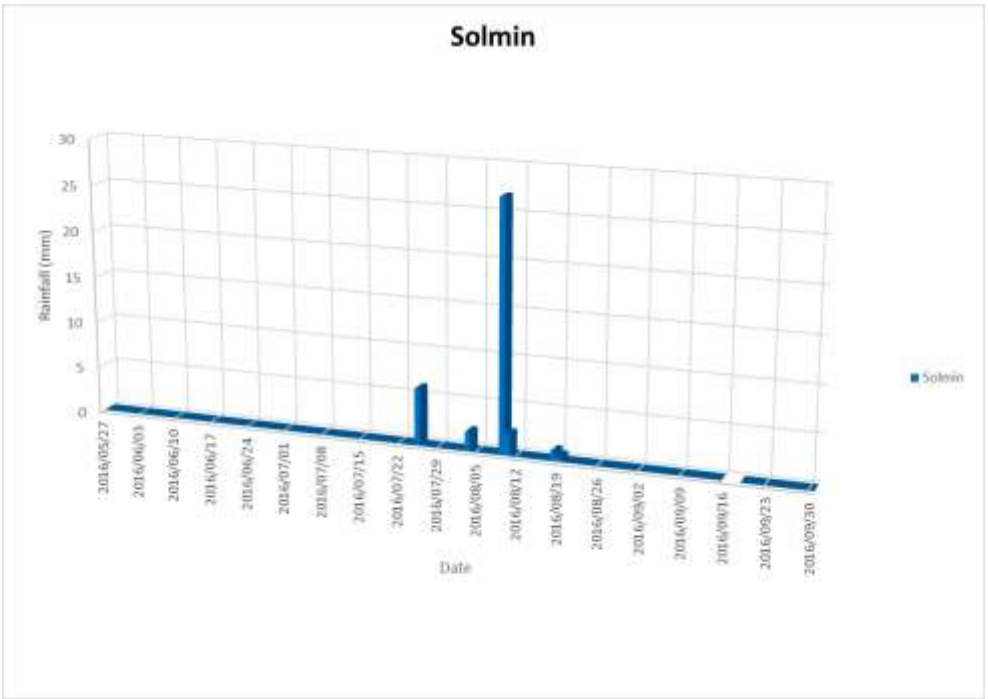

Figure A-26 Solmin daily rainfall recorded between May and September 2016

A24. SOLMIN EVAPORATION

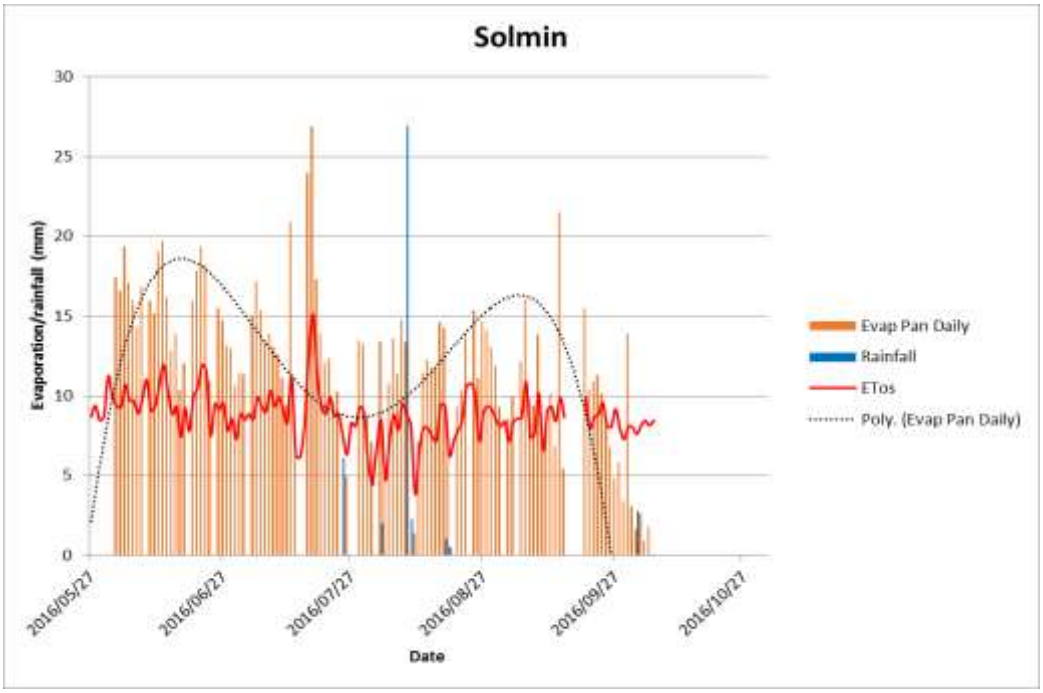

Figure A-27 **Solmin daily evaporation, measured as actual pan evaporation and theoretical ETos, along with daily rainfall recorded between May and September 2016**

A25. SOLMIN WIND SPEED AND DIRECTION

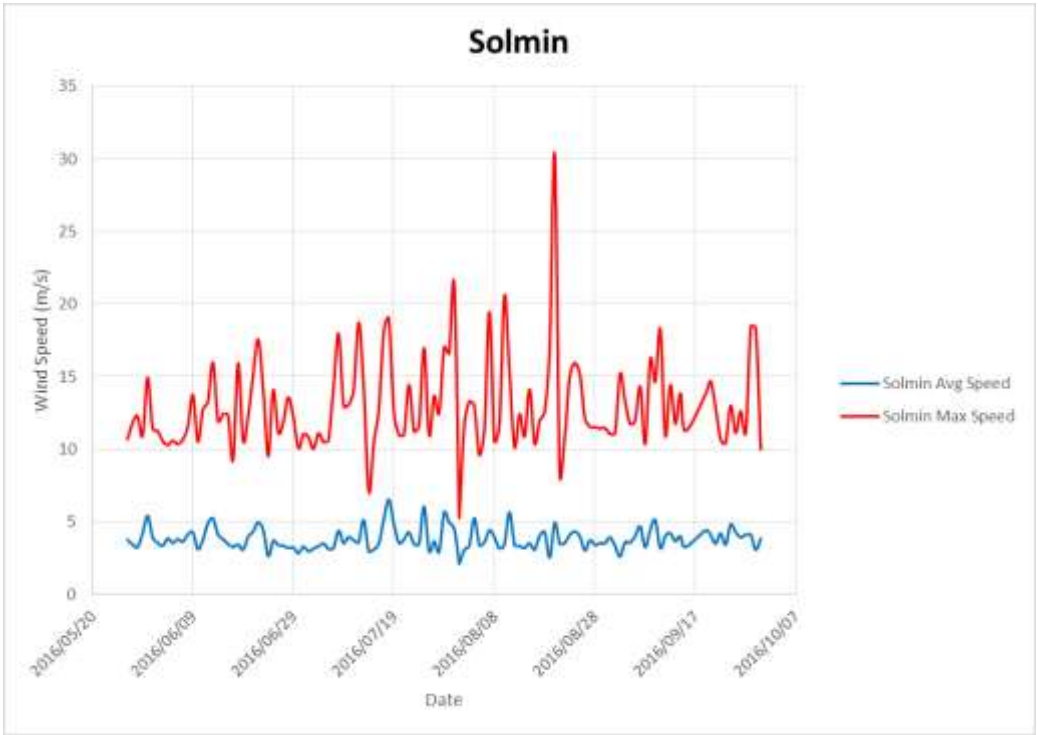

Figure A-28 **Solmin daily average and maximum wind speed recorded between May and September 2016**

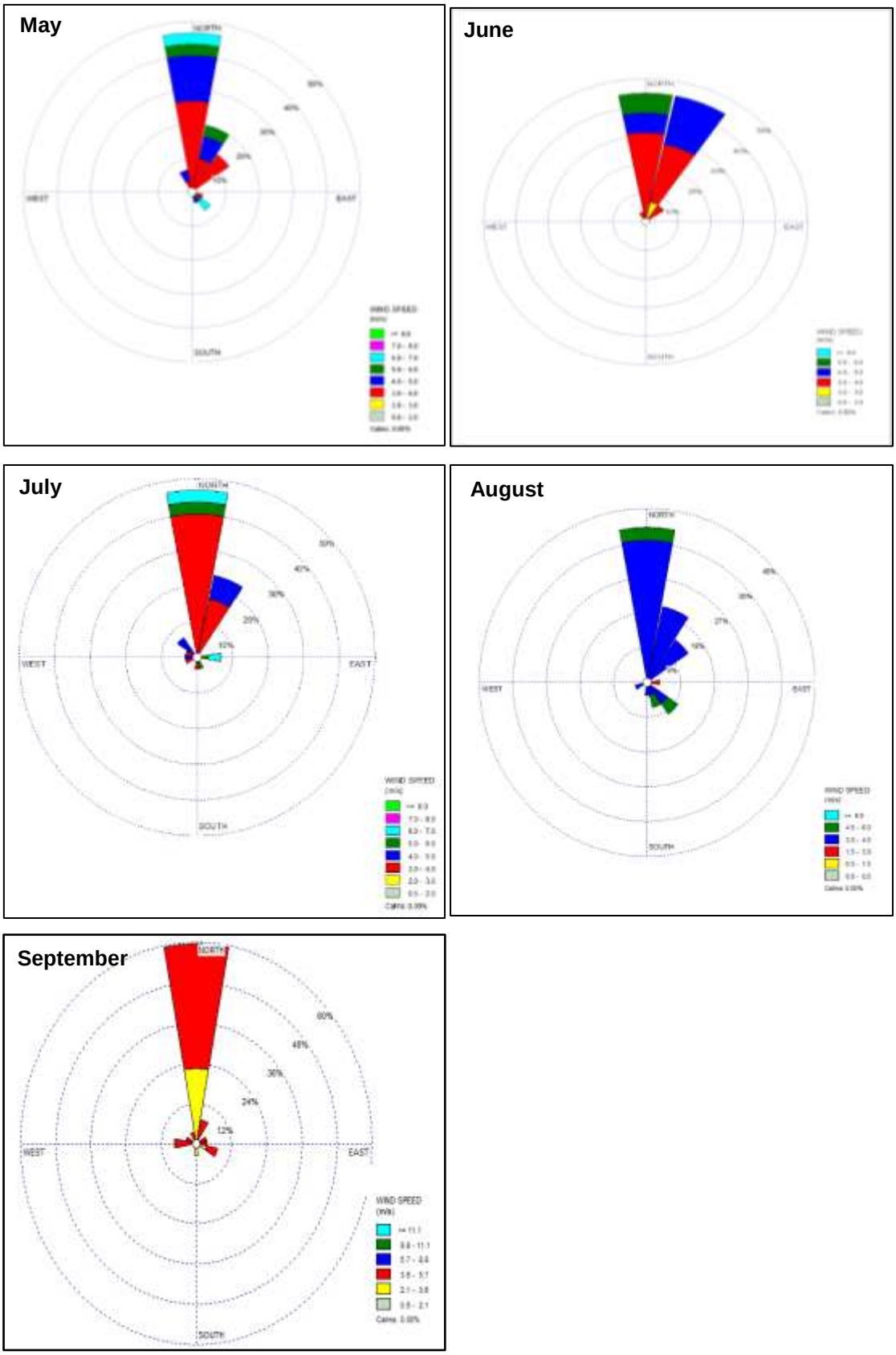

Figure A-29 Solmin monthly wind roses for May to September 2016

A26. SOLMIN RELATIVE HUMIDITY

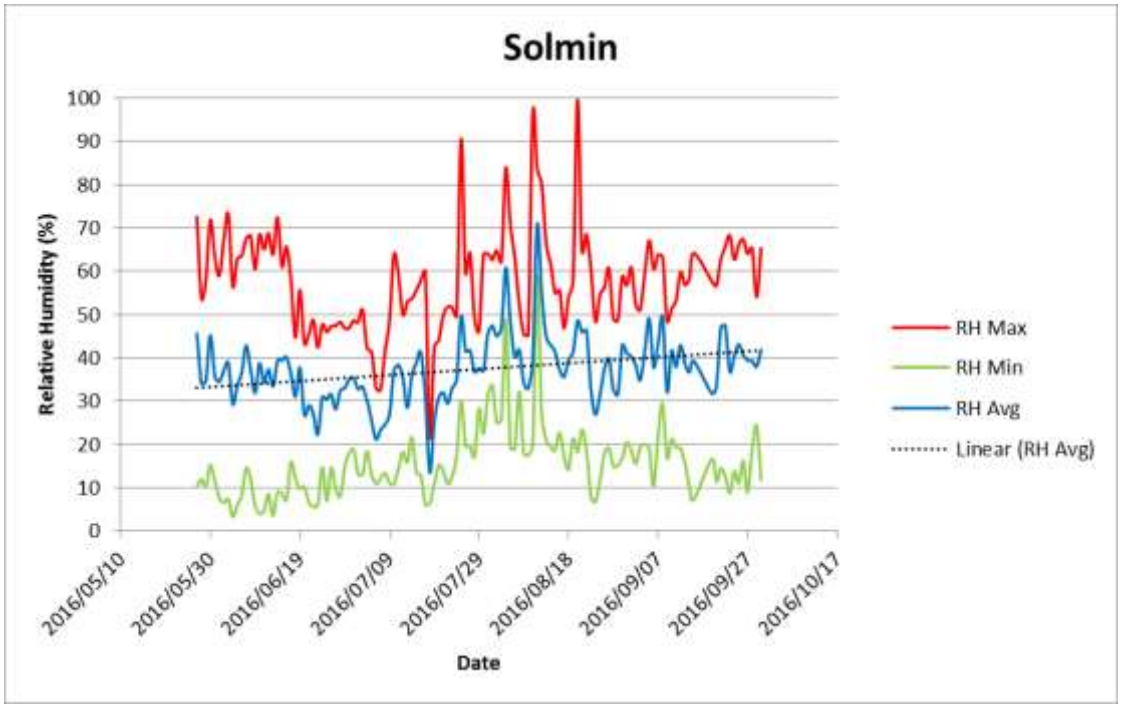

Figure A-30 **Solmin daily average, maximum and minimum relative humidity recorded between May and September 2016**

A27. SOLMIN SOLAR RADIATION

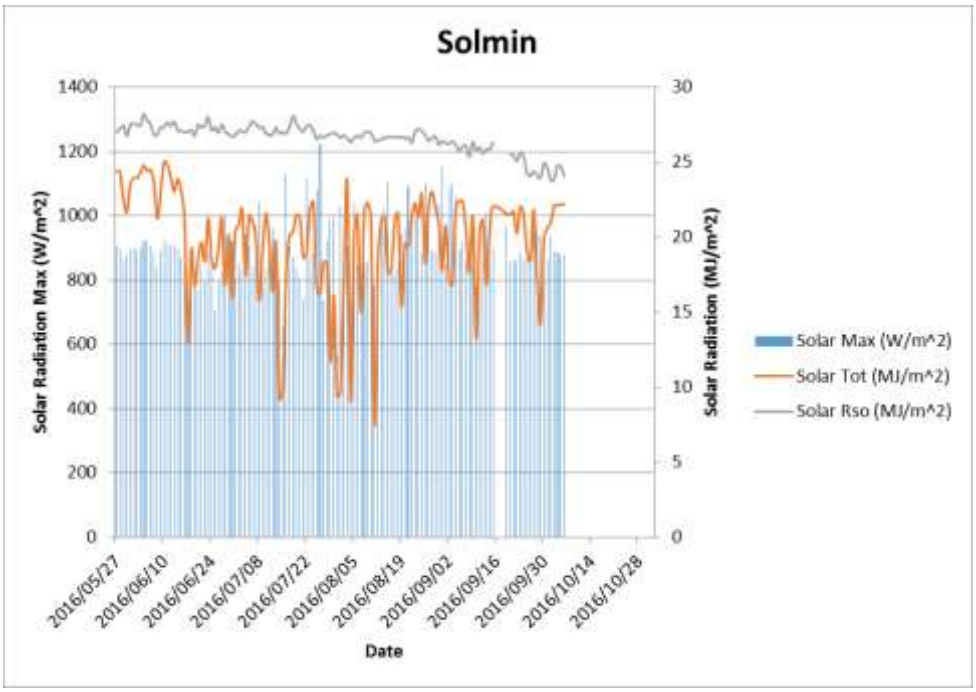

Figure A-31 **Solmin daily solar radiation recorded in terms of Rso, total and maximum between May and September 2016**

APPENDIX B – DRILLING DATA

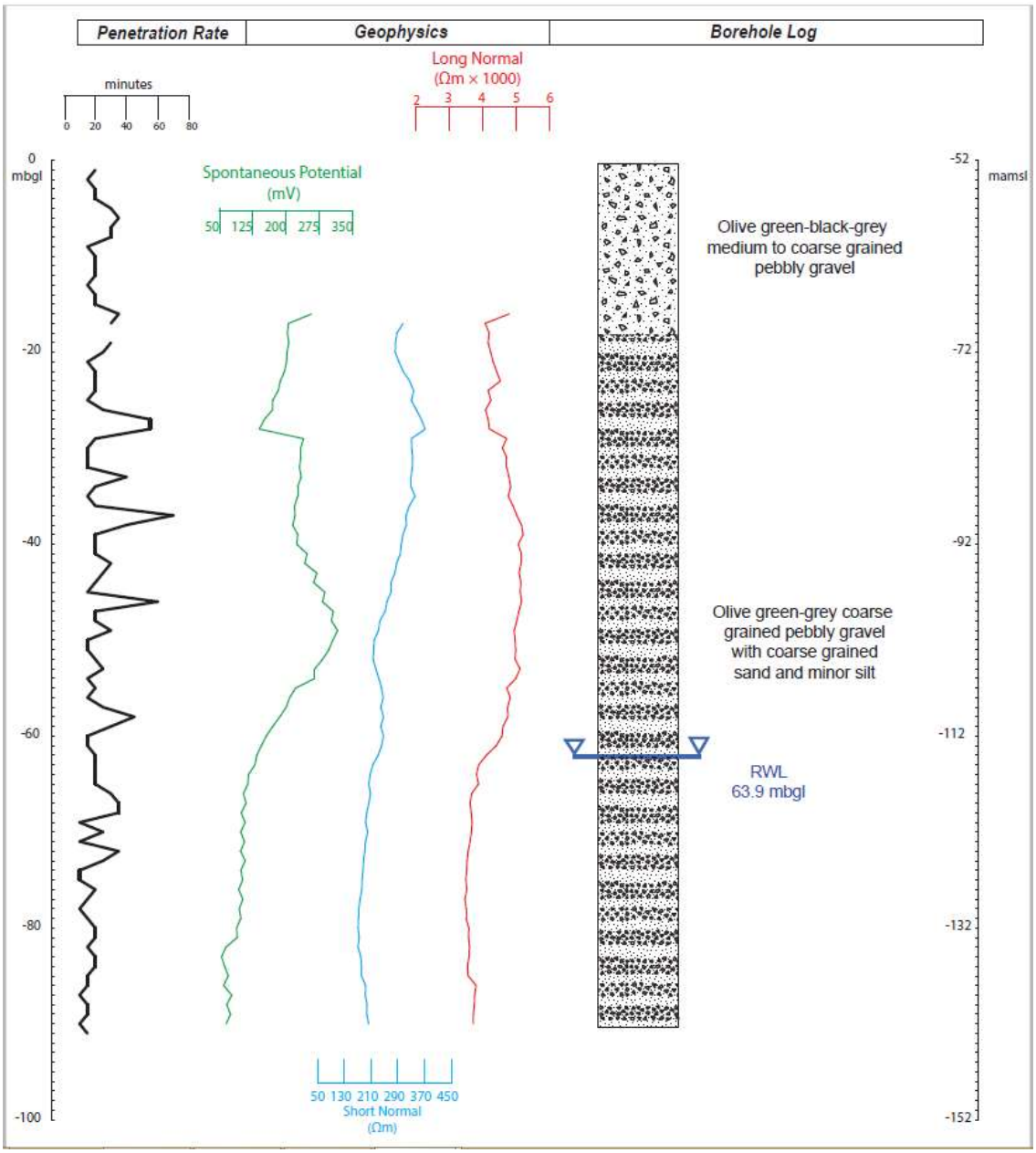

Figure B-0-1 Penetration rate, geophysical log compared to lithological log for DN-M01.

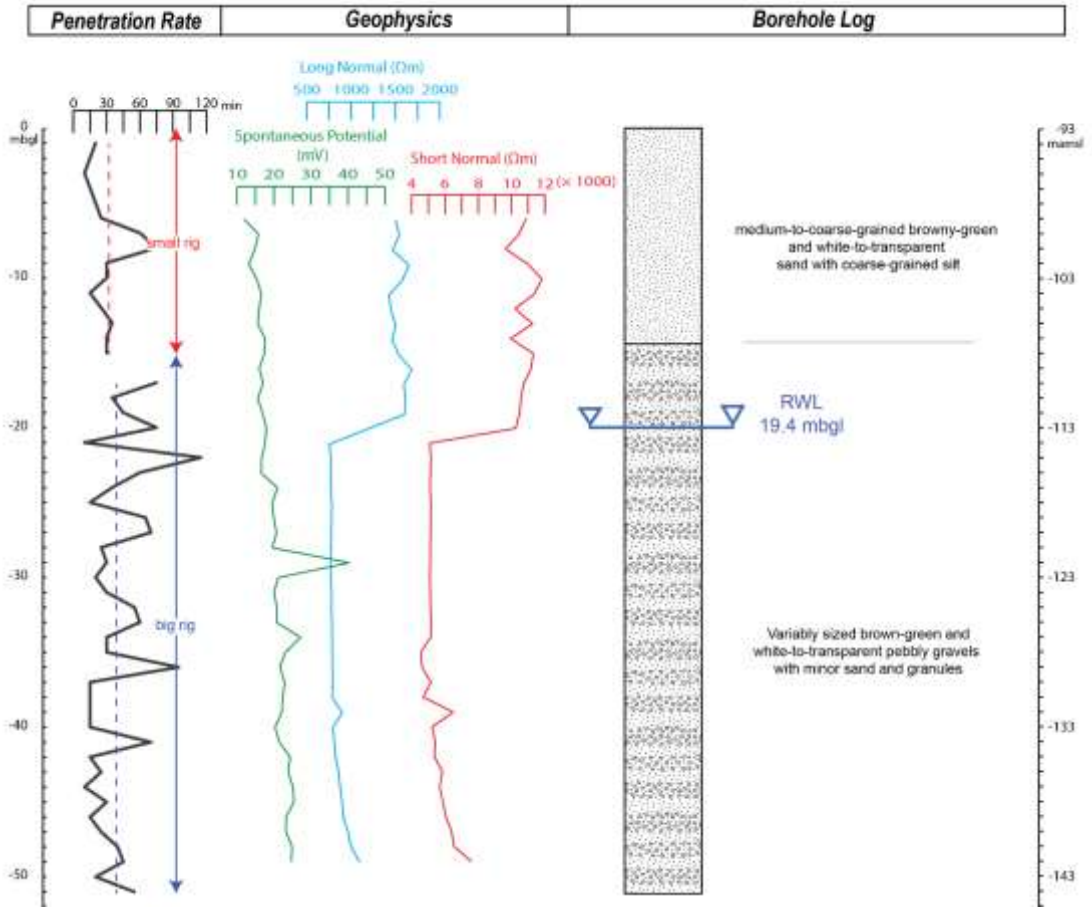

Figure B-0-2 Penetration rate and geophysical log compared to the lithological log for DN-M02.

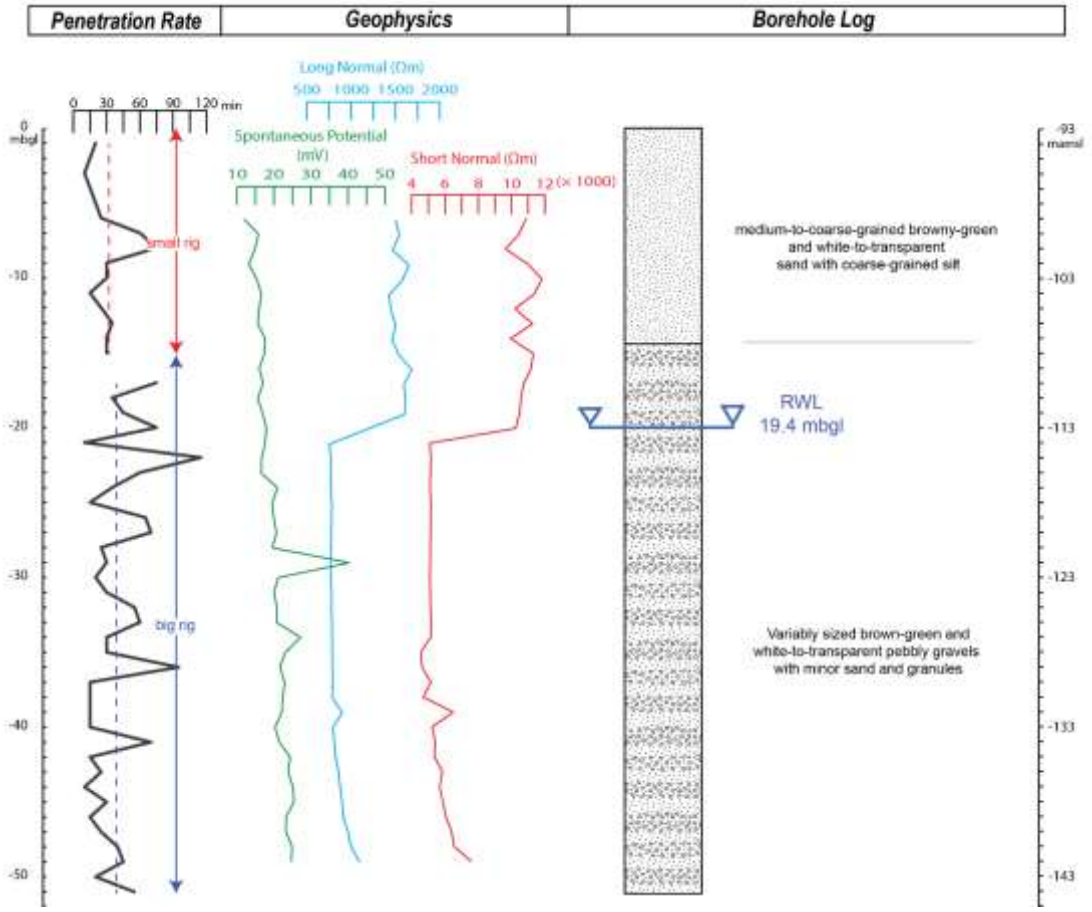

Figure B-0-3 Penetration rate and geophysical log compared to the lithological log for DN-M02.

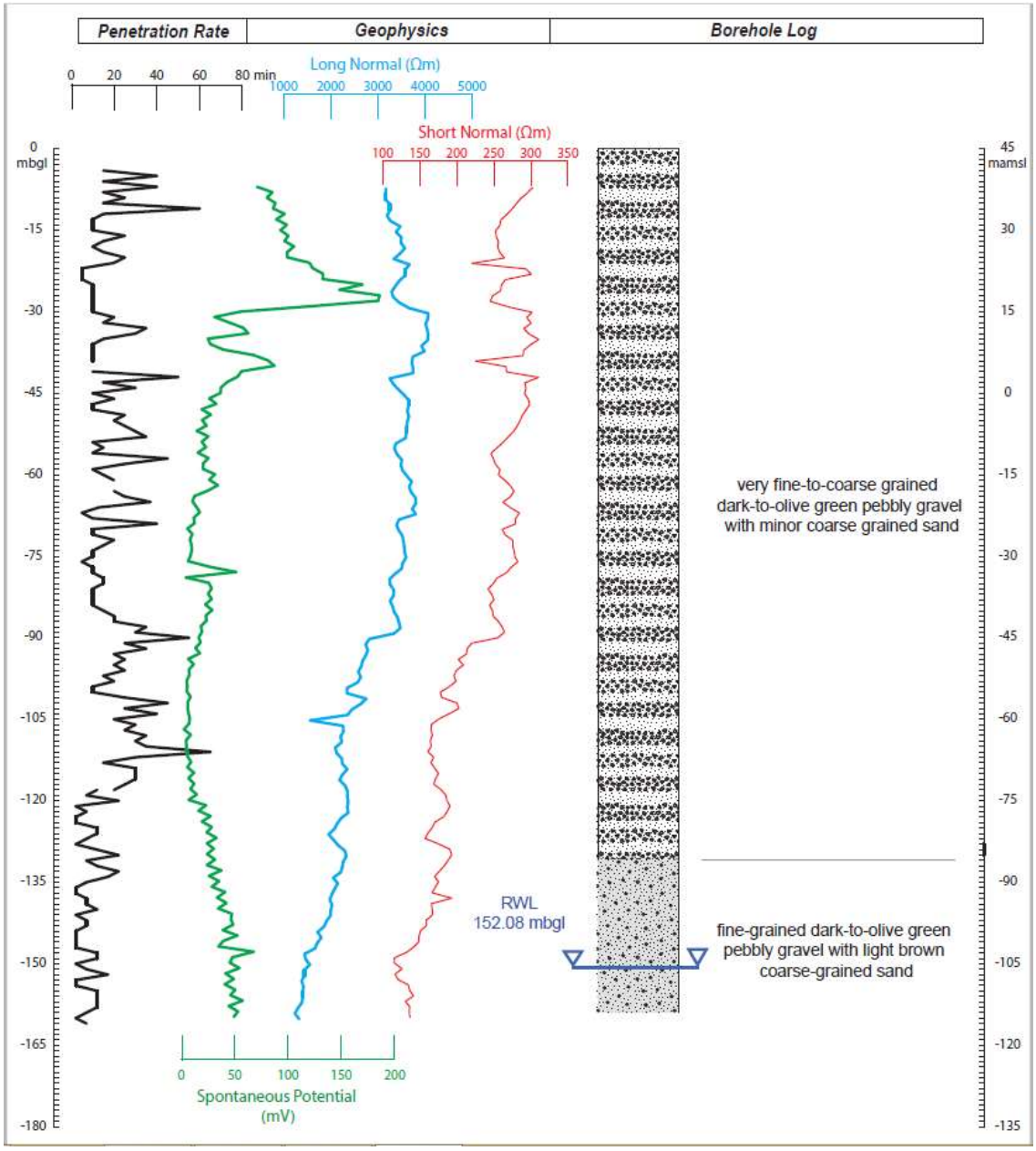

Figure B-0-4 Penetration rate and geophysical log compared to the lithological log for BS-M01.

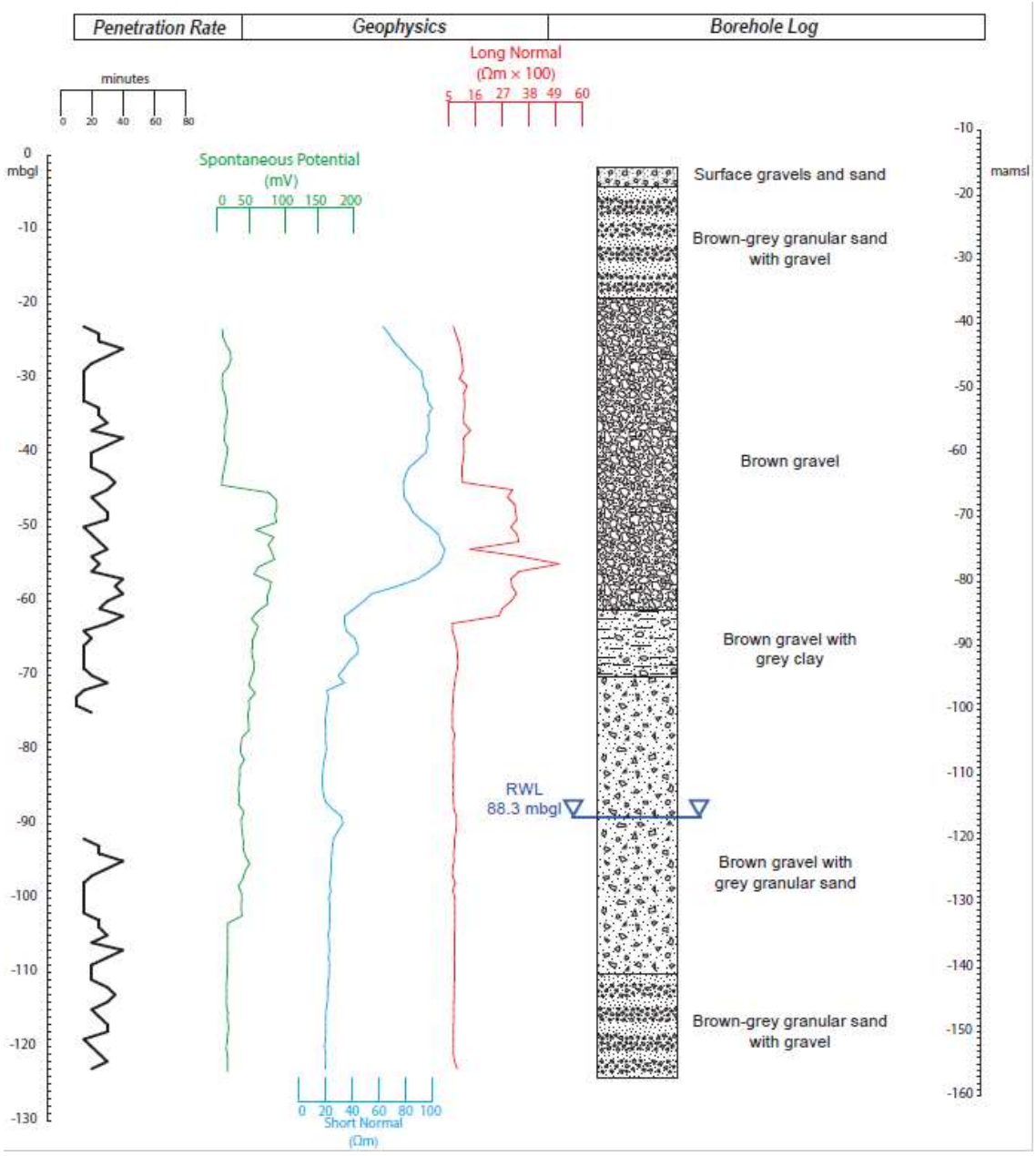

Figure B-0-5 Penetration rate and geophysical log compared to the lithological log for AY-M01.

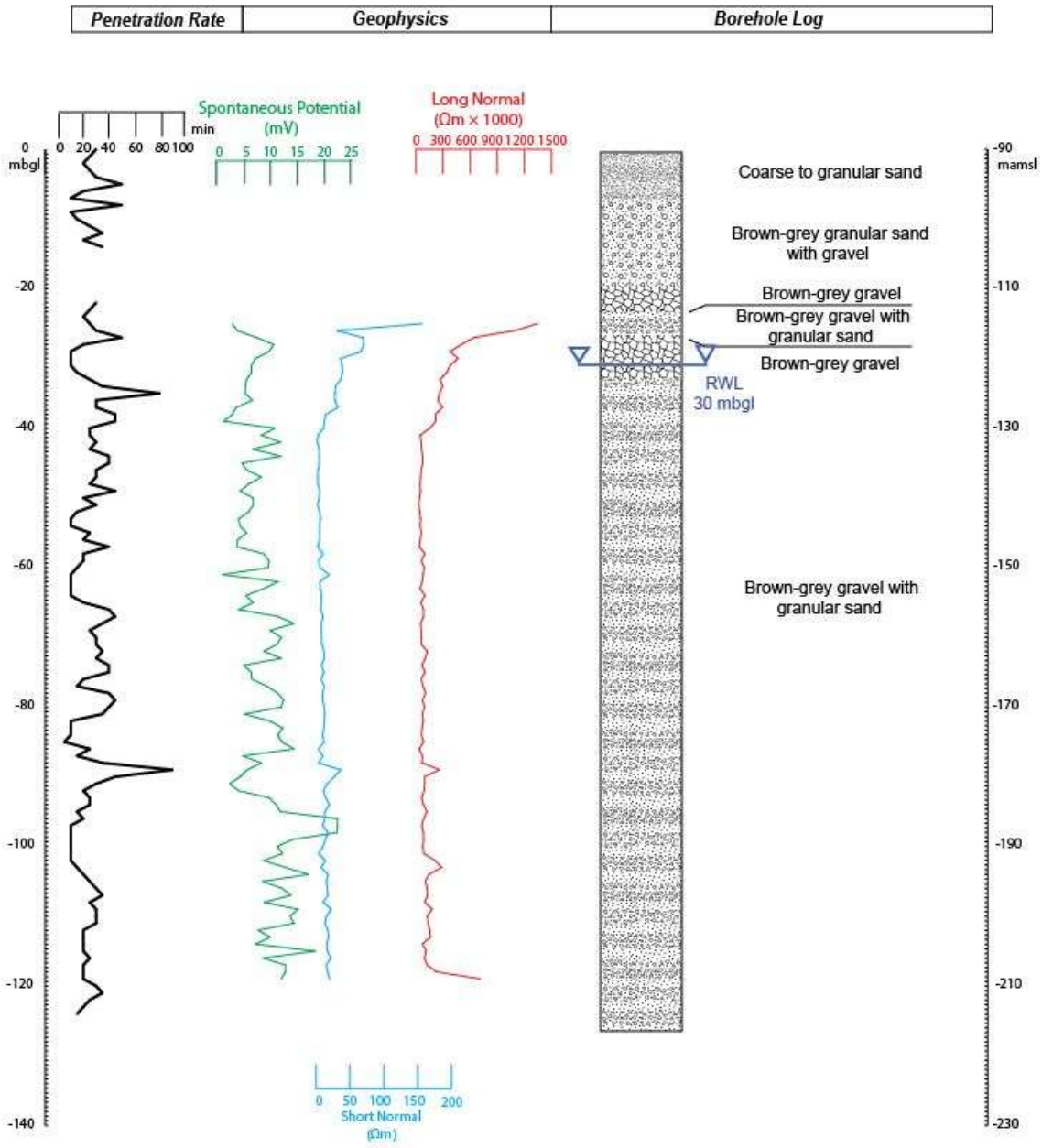

Figure B-0-6 Penetration rate and geophysical log compared to the lithological log for DN-P01.

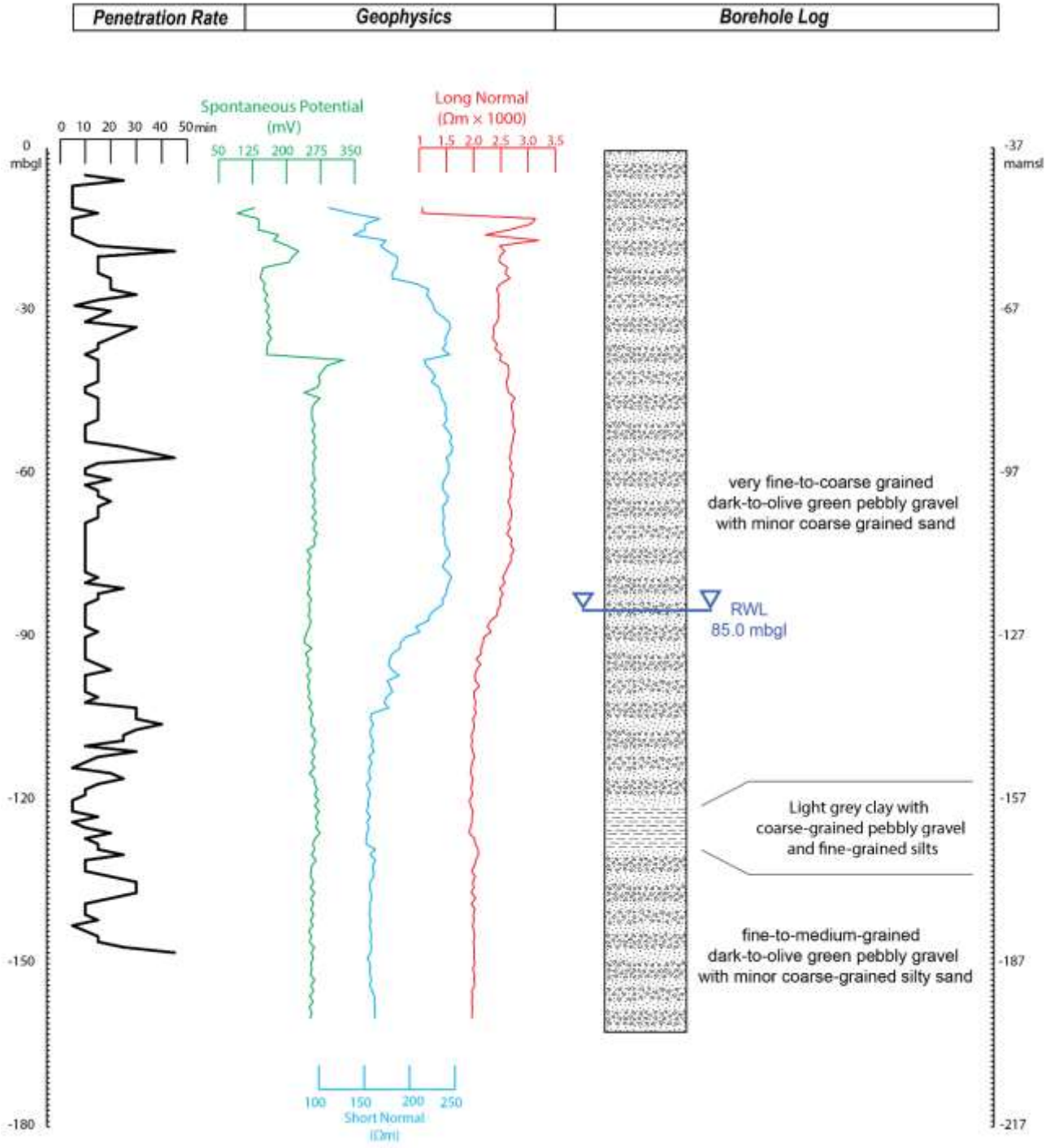

Figure B-0-7 Penetration rate and geophysical log compared to the lithological log for BS-P01.

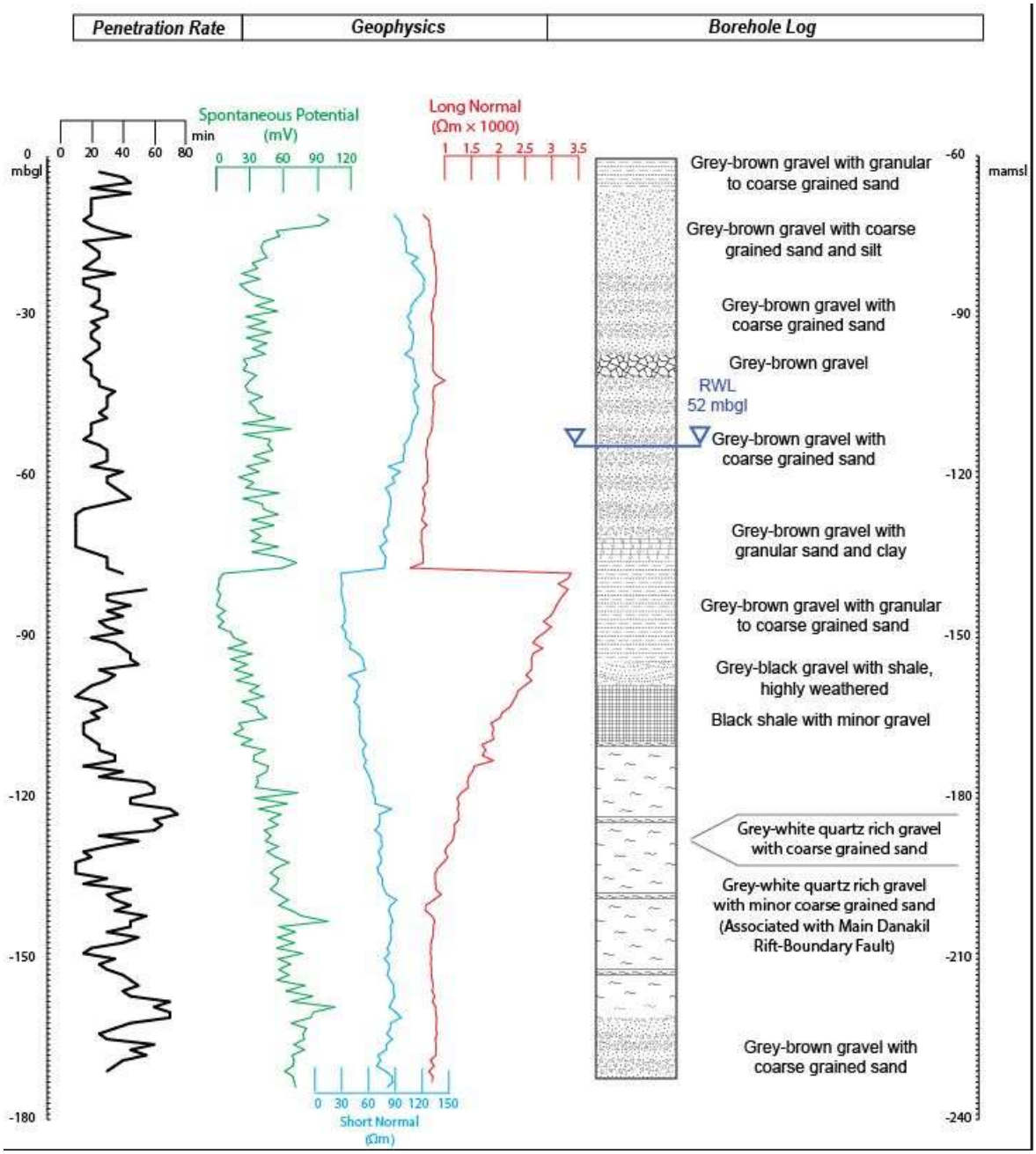

Figure B-0-8 Penetration rate and geophysical log compared to the lithological log for AY-P01.

APPENDIX C – AST DATA

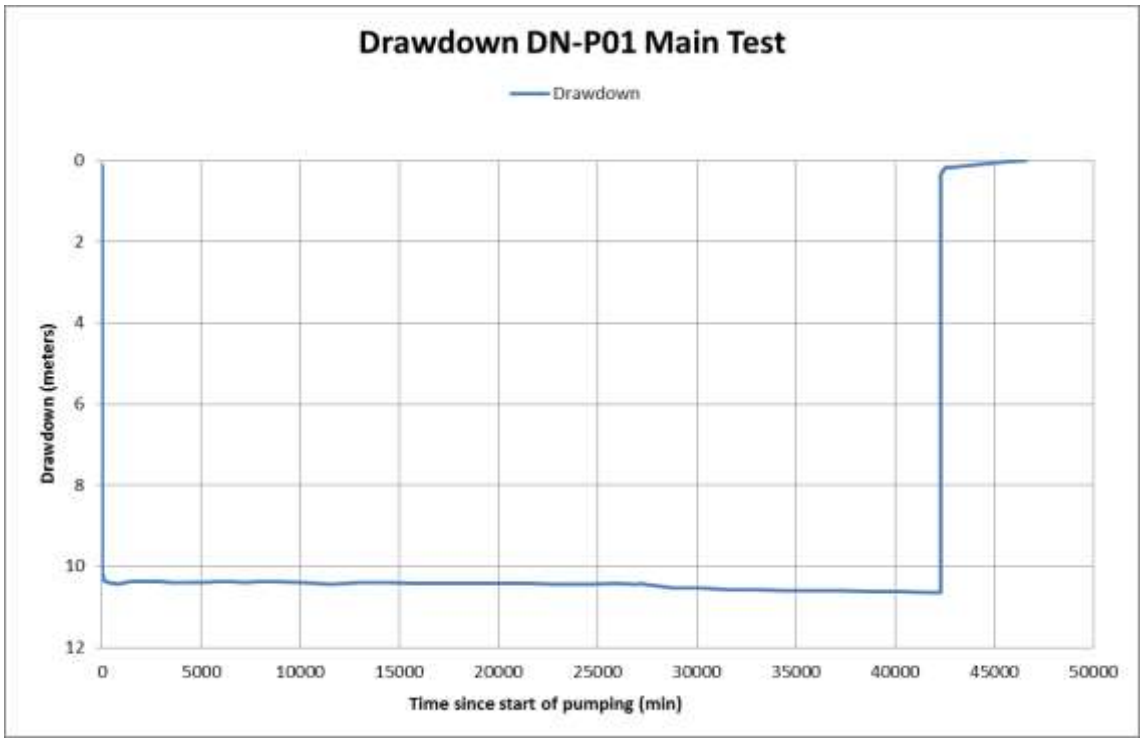

Figure C-0-1 Drawdown-time graph of the manually recorded data for AST of DN-P01.

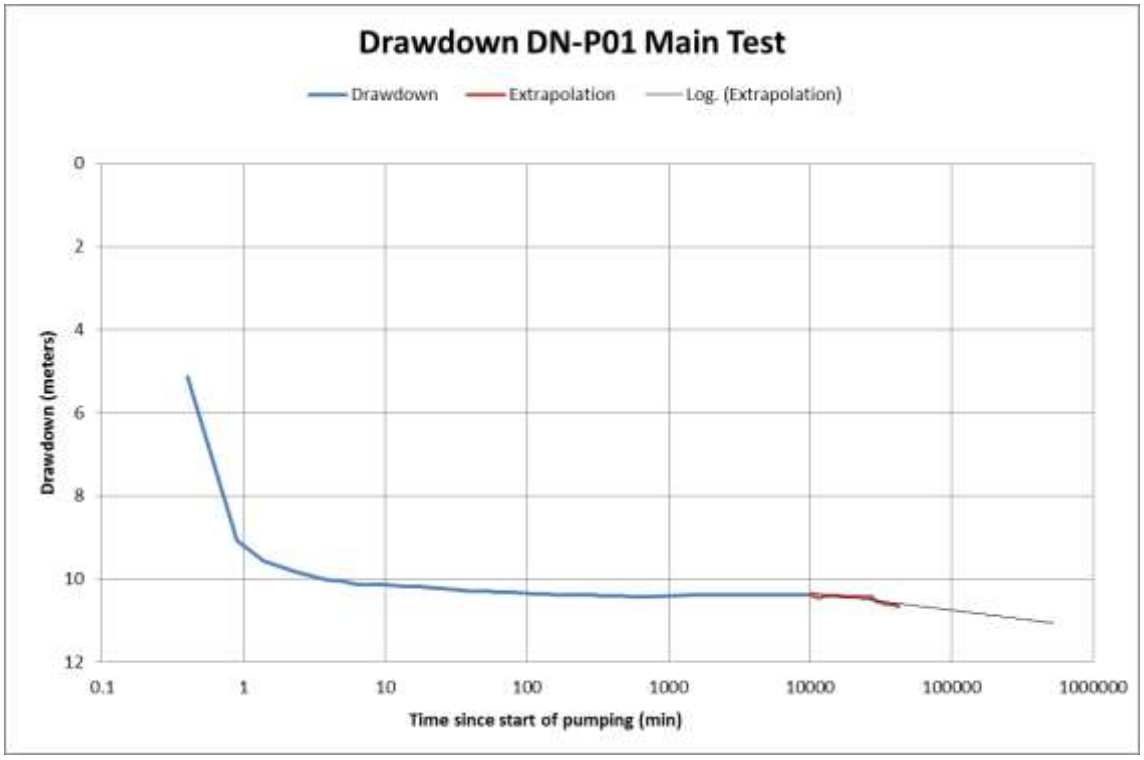

Figure C-0-2 Semi-log plot of drawdown-time data for AST at DN-P01.

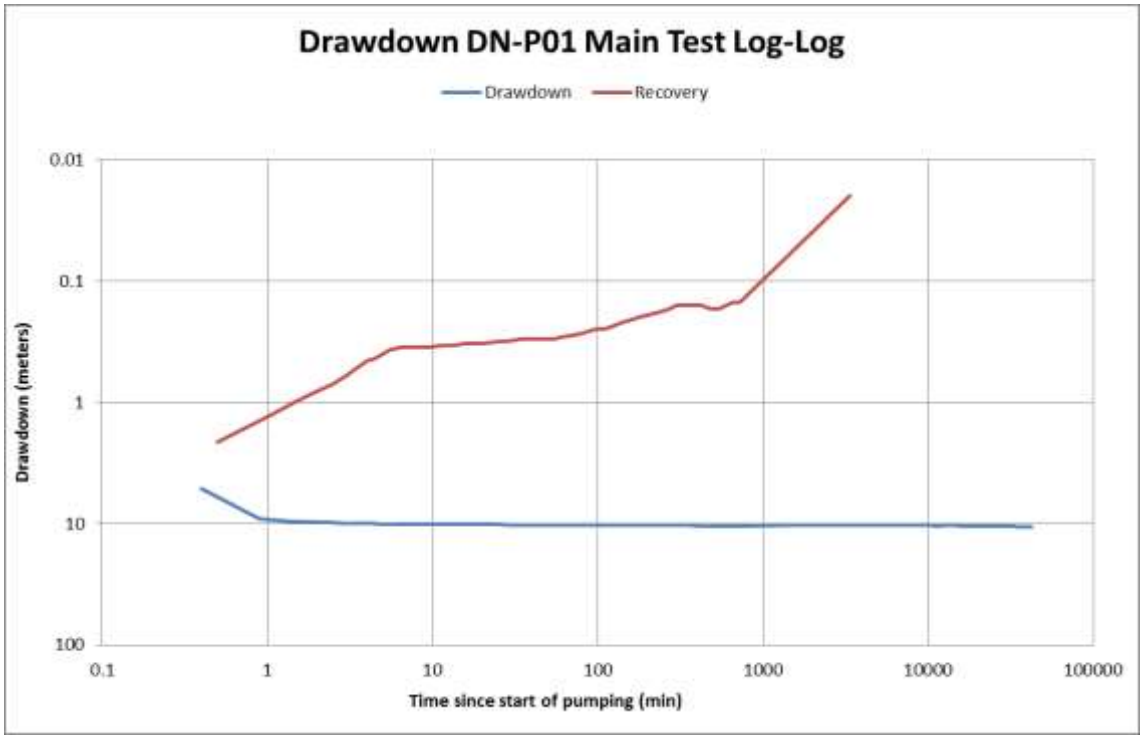

Figure C-0-3 Log-log plot of drawdown-time data for DN-P01 AST.

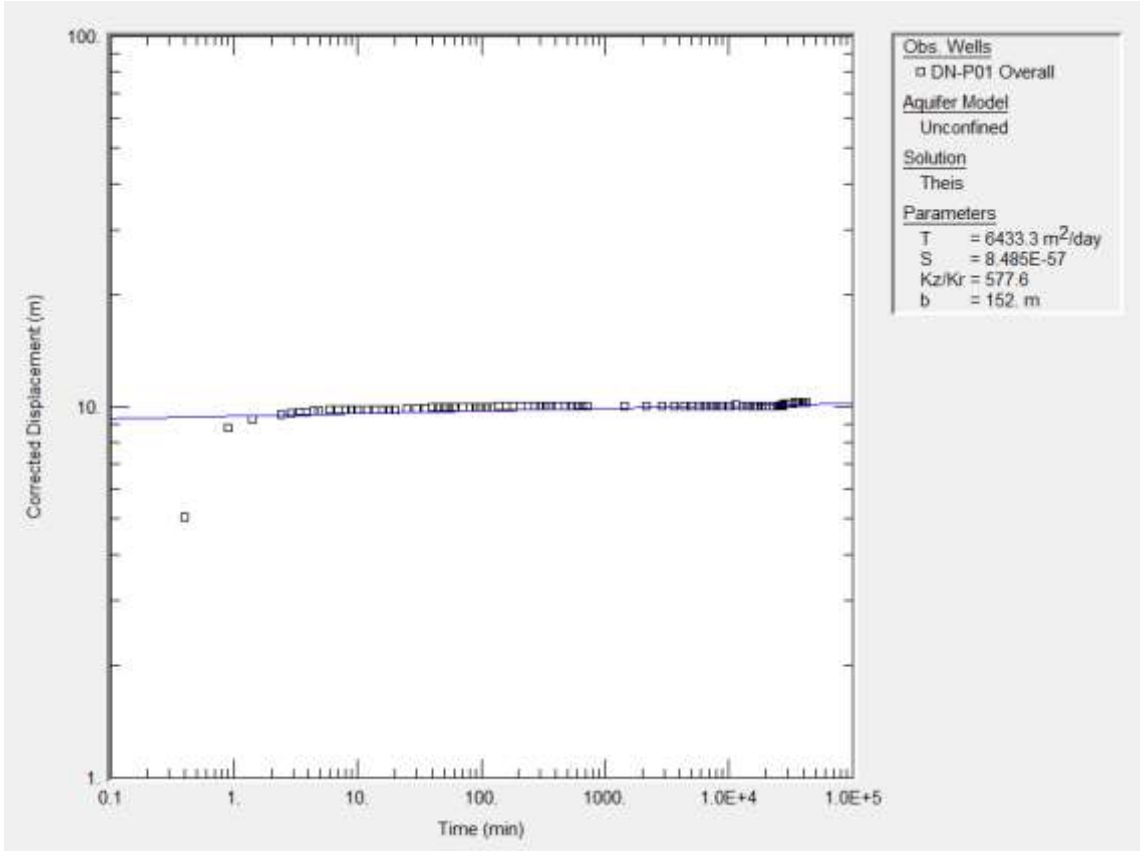

Figure C-0-4 Log-log curve in AQTESOLV software of DN-P01 time-drawdown data during AST

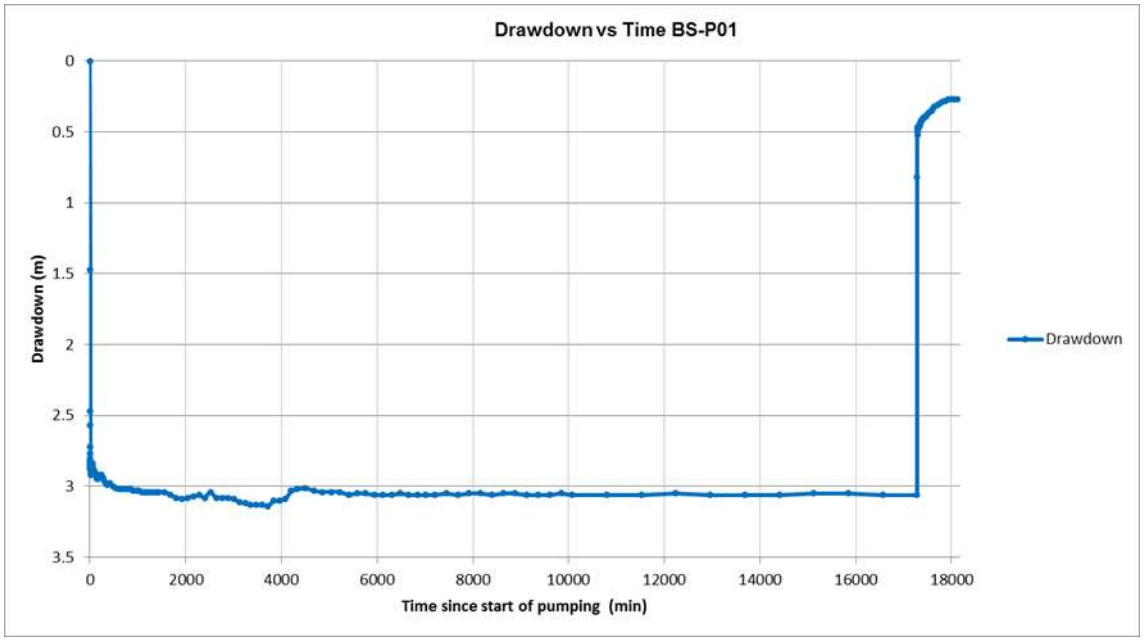

Figure C-0-5 Drawdown-time graph of the manually recorded data for the AST at BS-P01.

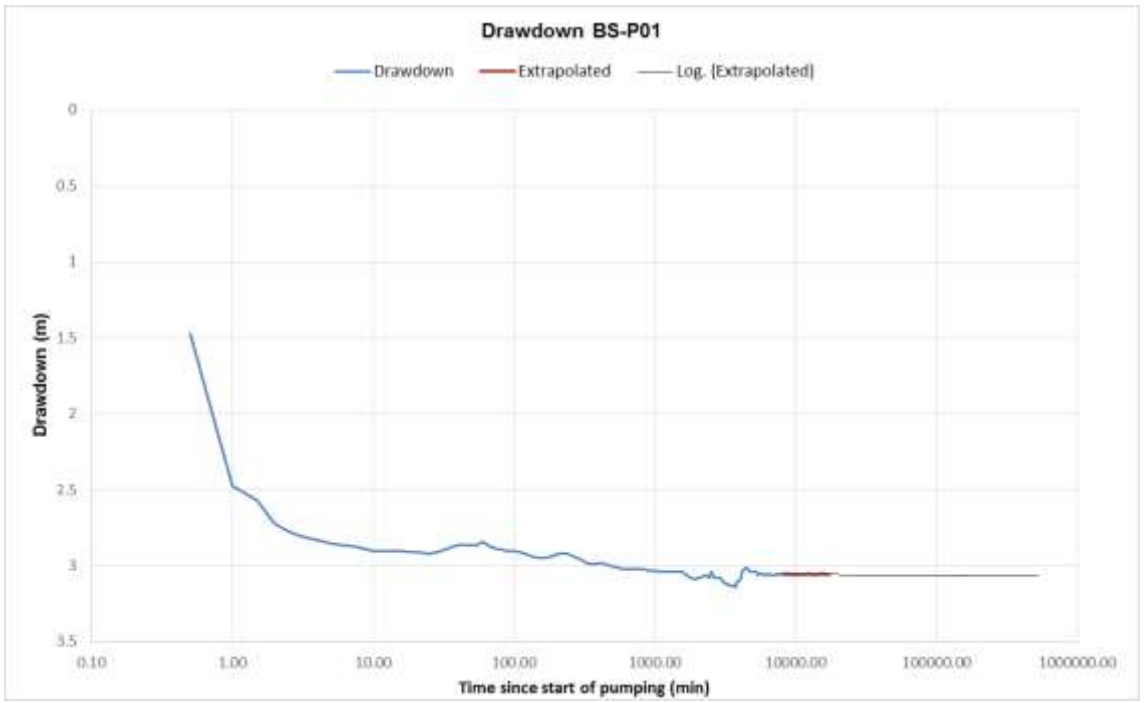

Figure C-0-6 Semi-log plot of drawdown-time data for BS-P01 AST

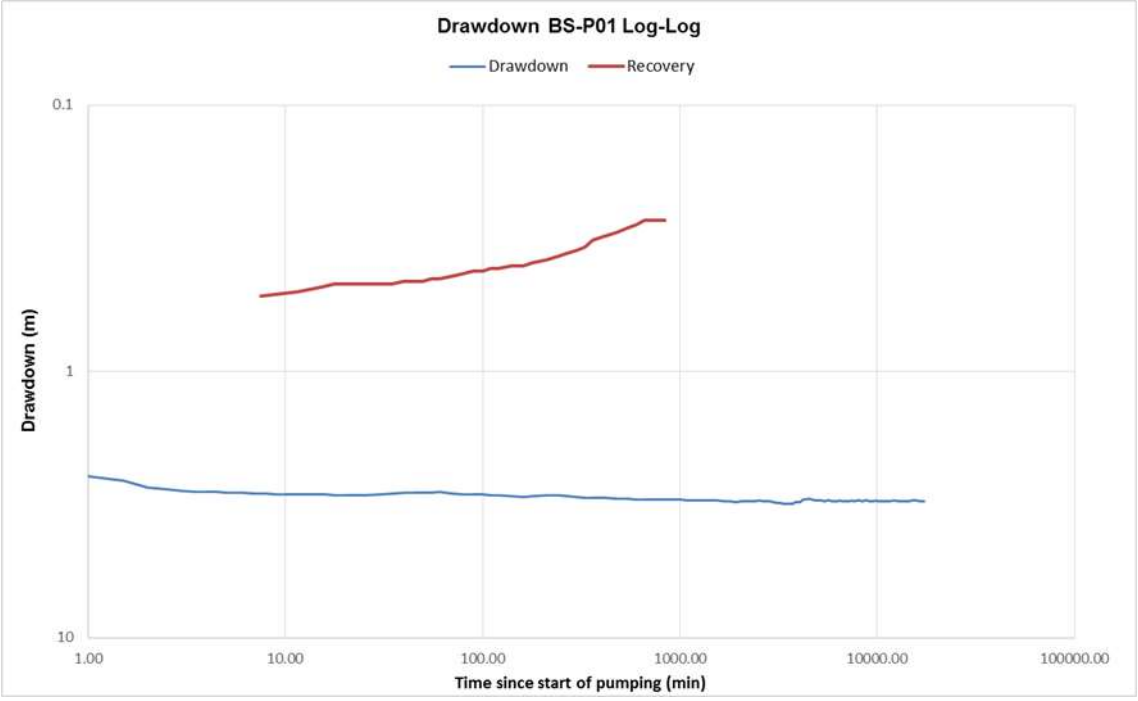

Figure C-0-7 Log-log plot of drawdown-time data for BS-P01 during the AST.

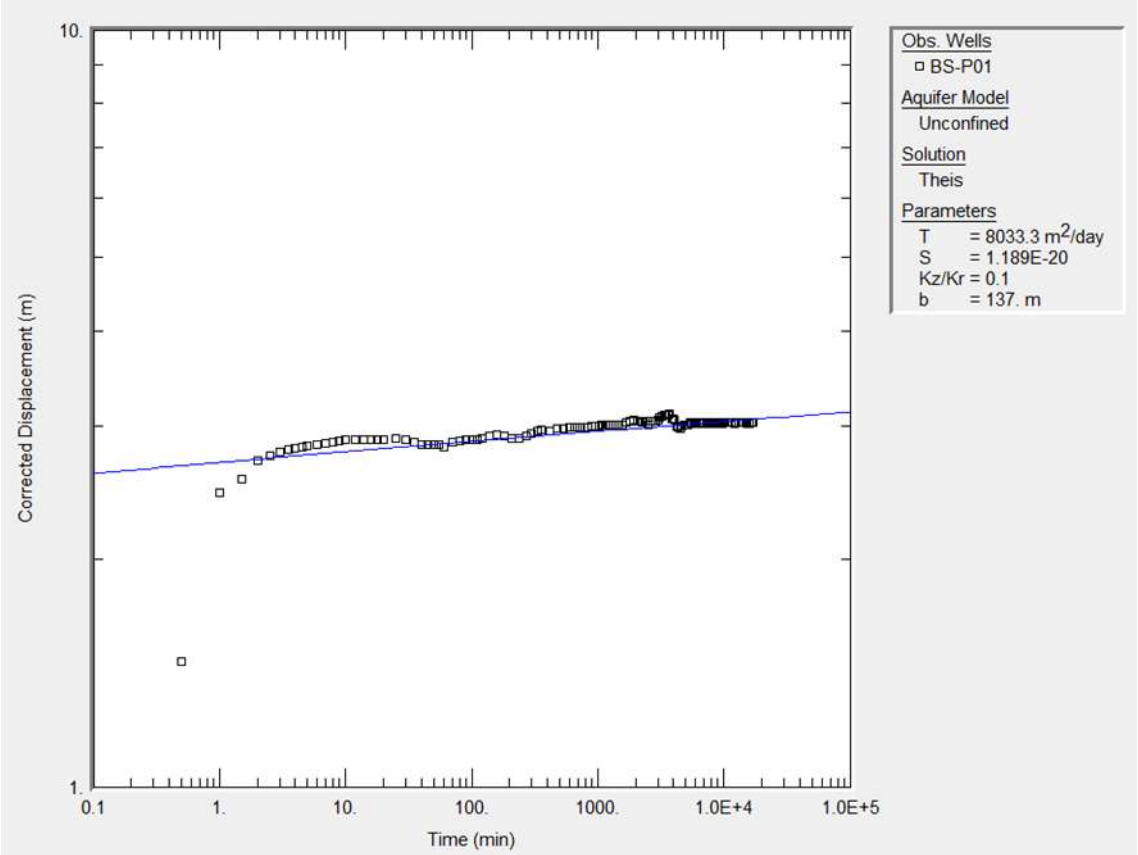

Figure C-0-8 Log-log curve in AQTESOLV software of BS-P01 AST

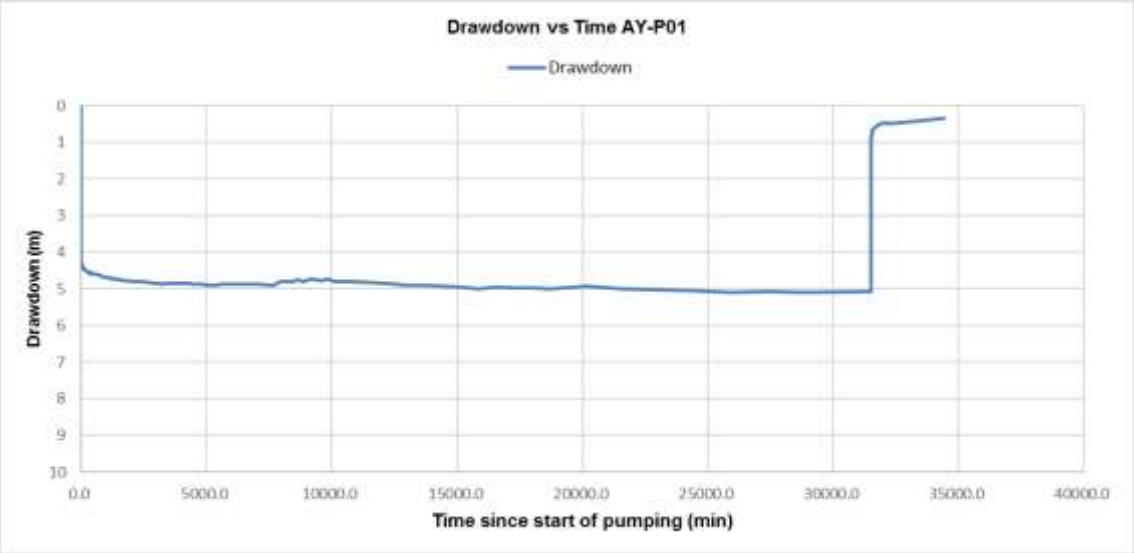

Figure C-0-9 Drawdown-time graph of the manually recorded data for AST at AY-P01.

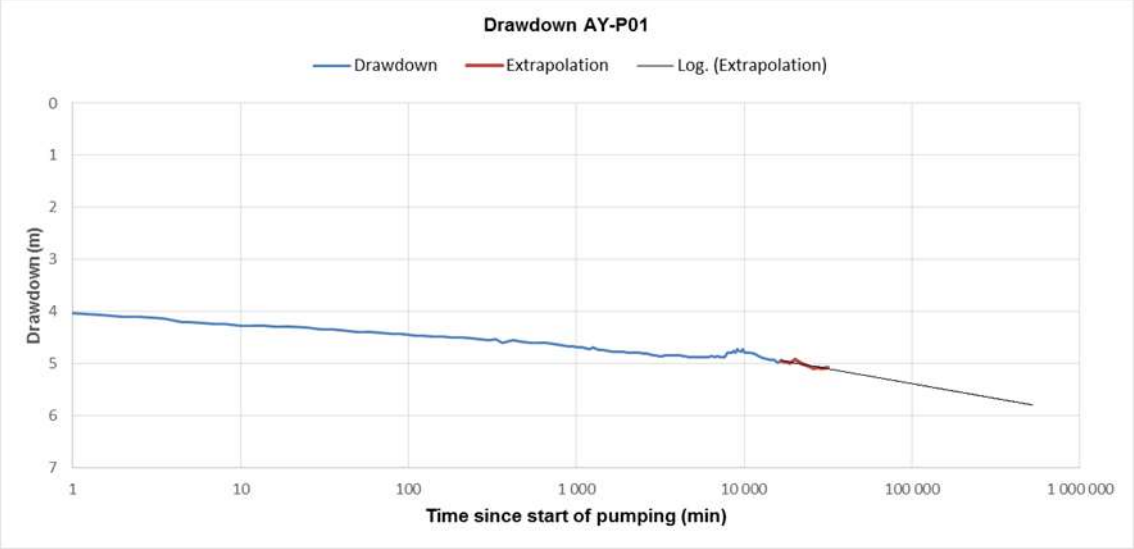

Figure C-0-10 Semi-log plot of drawdown-time data for AY-P01 AST

Figure C-0-11 Log-log plot of drawdown-time data for AY-P01 AST

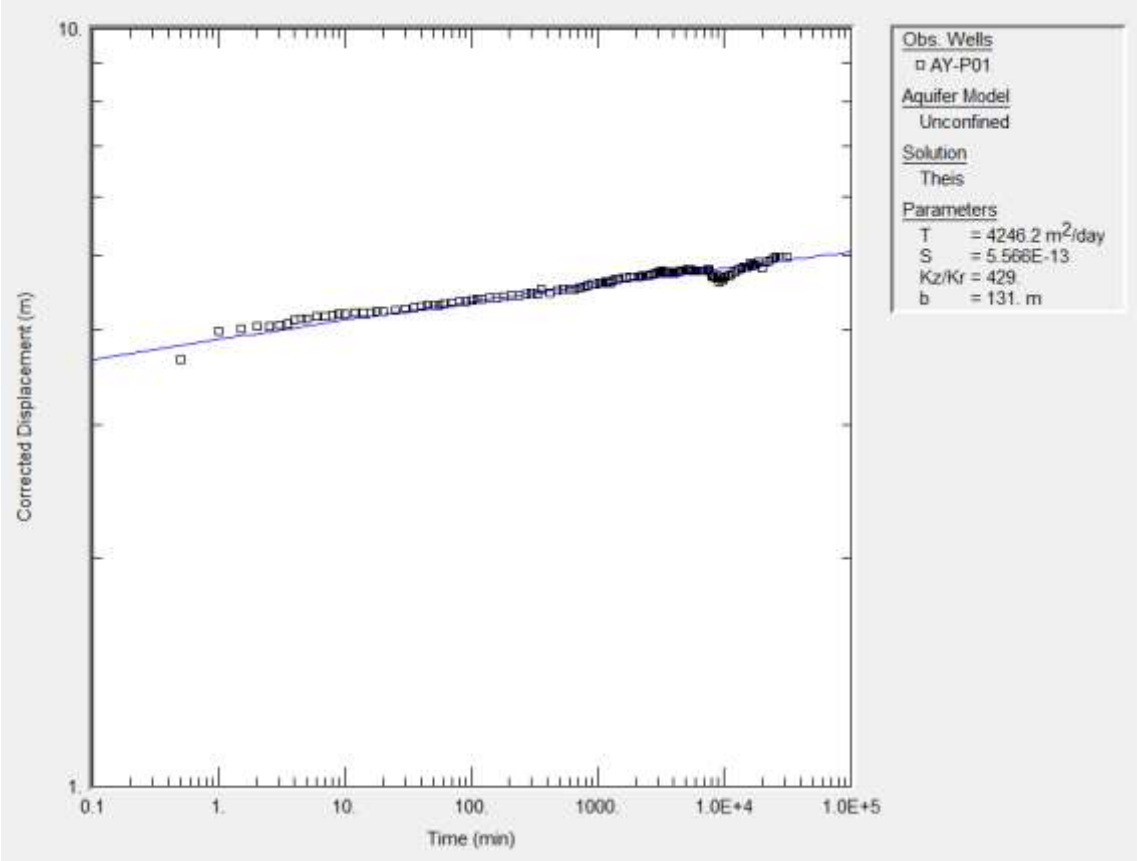

Figure C-0-12 Log-log curve in AQTESOLV software of AY-P01 time-drawdown data

APPENDIX D – HYDROCHEMICAL DATA

Table D 1 Hydrochemical results of all boreholes in the Badah area

Chemical Constituent	Drinking Water Quality Limits	Ragali River	Badah Admerug Well	Badah Watering Point
		17 May 2015	17 May 2015	21 May 2015
pH at 25°C	5-9.7	8.4	7.8	7.6
Conductivitiy at 25°C (mS/m)	≤170	293	361	404
Density (g/cm^3)	-	0.99	0.99	0.99
In mg/l				
Total Dissolved Solids at 180°C	≤1200	974	2136	2368
Total Alkalinity	-	98	134	140
Total Hardness	-	426	839	140
Bicarbonate	-	98	134	140
Calcium	-	75	194	239
Magnesium	≤70	58	86	74
Sodium	≤200	168	378	420
Potassium	≤50	18	32	39
Chloride	≤300	301	548	695
Bromide	≤5	<0.1	<0.1	<0.1
Fluoride	≤1.5	1.13	1.16	1.39
Sulphate	≤500	289	770	856
Orthophosphate	≤5	0.006	0.044	0.037
Ammonia	≤1.5	<0.08	0.7	<0.08
Nitrate	≤11	1.67	3.53	2.73
Nitrite	≤0.9	0.09	0.09	0.21
Chemical Oxygen Demand	-	20	29	51
Dissolved Metals (in µg/l)				
Aluminium	≤200	4.34	17.9	1.5
Antimony	≤20	<1	<1	<1
Arsenic	≤10	2.42	1.46	3.81
Barium	≤700	89	41	58
Beryllium	≤10	<1	<1	<1
Boron	≤300	260	616	632
Cadmium	≤3	<1	<1	<1
Chromium	≤50	<1	<1	<1
Cobalt	≤500	<1	<1	<1
Copper	≤2000	<1	<1	<1
Iron	≤2000	4.16	4.35	1.72
Lead	≤10	<1	<1	<1
Lithium	-	40	65	70
Manganese	≤400	<1	38	<1
Mercury	≤6	<1	<1	<1
Molybdenum	≤70	2.19	9.61	10.4
Nickel	≤70	<1	<1	<1
Selenium	≤10	1.46	6.56	1.64
Silver	≤100	<1	<1	<1
Strontium	≤4000	2151	4042	4532
Thallium	≤2	<1	<1	<1
Tin	-	<1	<1	<1
Titanium	-	<1	<1	<1
Uranium	≤15	1.12	2.2	2.13
Vanadium	≤200	4.22	14.4	54
Zinc	≤5000	<1	18.1	<1

Table D 2 Hydrochemical results of all boreholes in the north Dogua fan.

Chemical Constituent	Drinking Water Quality Limits	RAJ-2 PT Step 1	RAJ-2 PT Step 4	RAJ-2 PT CD 48 hrs	RAJ-2 PT CD 72 hrs	RAJ-2 Seep V-Notch	RAJ-2 7 days	RAJ-2 16 days	RAJ-2 27 days	DN-M01 Develop-ment	DN-M02 Develop-ment	DN-P01 Develop-ment	DN-P01 PT CD 24 hrs	DN-P01 PT CD 48 hrs	DN-P01 7 days	DN-P01 16 days	DN-P01 37 days
		03 June 2015	03 June 2015	06 June 2015	07 June 2015	26 May 2015	25 Oct 2016	3 Nov 2016	14 Nov 2016	28 June 2016	08 June 2016		23 Aug 2016	29 Aug 2016	15 Oct 2016	24 Oct 2016	14 Nov 2016
pH at 25°C	5-9.7	6.4	6.4	6.6	6.7	6.8	6.6	6.7	6.7	6.9	6.4	5.9	6.0	6.1	6.2	6.2	6.3
Conductivitiy at 25°C (mS/m)	≤170	17310	17570	17220	16430	6770	14600	14340	14210	11380	16080	>20000	>20000	>20000	>20 000	>20 000	19700
Density (g/cm^3)	-	1	1	1	1	1	1	1	1	1.05	1	1	1	1	1.14	1.14	1.13
In mg/l																	
Total Dissolved Solids at 180°C	≤1200	142910	138362	124998	119118	44810	120420	111960	111720	-	107548	268562	221372	216122	208366	197242	188052
Total Alkalinity	-	43	39	33	28	26	20	27	31	-	90	6153	5640	5128	35	27	33
Total Hardness	-	43318	51480	49295	39769	13800	41316	41773	41897	28075	45454	84780	106228	93947	70253	66905	66888
Bicarbonate	-	43	39	33	28	26	20	27	31	71	90	6153	5640	5128	35	27	33
Calcium	-	14505	17401	16585	13283	4567	13726	14028	14048	8811	15446	32456	29360	26614	22376	21398	21355
Magnesium	≤70	1724	1950	1914	1603	582	1710	1638	1656	1475	1672	6116	5011	4450	3492	3272	3294
Sodium	≤200	26859	30104	28688	23724	8858	23845	23206	23172	17577	24007	70684	60700	50075	41875	39878	40198
Potassium	≤50	2171	2444	2358	1969	636	2121	2061	2032	1347	1900	5012	4121	4065	3675	3551	3512
Chloride	≤300	85123	95936	88341	83378	37180	76976	66979	79975	47934	65554	178668	188594	148890	111965	124961	126961
Bromide	≤5	9	9	9	10	3	7592	7681	7593	5203	6541	-	-	-	14204	12350	12711
Fluoride	≤1.5	2	2	2	2	2	400	400	400	2	2	2	2	2	300	300	300
Sulphate	≤500	415	511	414	388	739	372	466	564	732	379	181	250	476	293	399	329
Orthophosphate	≤5	<0.002	<0.002	<0.002	<0.002	<0.002	<0.03	<0.03	0	<0,002	<0.002	<0,03	<0,03	<0,03	<0.03	<0.03	<0.03
Ammonia	≤1.5	23	24	23	23	1	21	20	21	10.6	22	93	72	60	40.4	46.9	37.3
Nitrate	≤11	0	0	0	0	0	<0.1	<0.1	0	<0,1	<0.1	<0.1	<0.1	<0.1	<0.1	0.14	<0.1
Nitrite	≤0.9	0	0	0	<0.01	0	0	0	<0.1	<0,1	<0.1	<0.1	<0.1	<0.1	<0.1	<0.1	<0.1
Chemical Oxygen Demand	-	5737	6182	4020	4183	1841	4513	3610	4021	1299	4531	6880	5200	5120	6892	7549	7385
Dissolved Metals (in µg/l)																	
Aluminium	≤200	52	26	243	237	97	<1	<1	8	3	147	58	<1	435	2.88	7.87	1.18
Antimony	≤20	<1	<1	<1	<1	<1	<1	<1	<1	2	<1	3	5	8	<1	<1	<1
Arsenic	≤10	1	1	<1	<1	2	<1	1	<1	28	<1	<1	<1	2	2.36	1.45	1.39
Barium	≤700	2899	2952	2623	2737	513	1671	1684	1665	437	3600	-	-	-	2984	2587	2622
Beryllium	≤10	<1	<1	<1	<1	<1	<1	<1	<1	1	<1	<1	<1	17	<1	<1	<1
Boron	≤300	21670	22198	22937	23486	7153	18297	18398	18366	11906	27390	-	-	-	31659	28034	29128
Cadmium	≤3	<1	<1	<1	<1	<1	<1	<1	<1	<1	4	<1	<1	7	<1	<1	<1
Chromium	≤50	<1	<1	<1	1	<1	<1	<1	1	<1	<1	2	<1	24	<1	1.28	46
Cobalt	≤500	2	2	2	2	<1	<1	<1	<1	3	<1	13	10	60	6.9	5.64	6.34
Copper	≤2000	6	<1	1	3	76	3	<1	31	4	94	12	19	29	33	38	27
Iron	≤2000	464	174	152	144	35	54	60	60	2	<1	312	170	721	102	87	92
Lead	≤10	45	45	64	76	11	16	41	33	9	6	197	135	126	70	61	59
Lithium	-	5924	6032	6113	6153	1676	4235	4207	4195	<1	6748	-	-	-	6537	5697	5971
Manganese	≤400	133603	134087	121434	120611	4	90597	90883	86186	26190	114265	-	-	-	141586	127739	122021
Mercury	≤6	<1	<1	<1	<1	<1	<1	<1	<1	72	<1	<1	-	1	<1	1.56	6.15
Molybdenum	≤70	11	9	15	14	13	7	7	8	127	94	9	7	22	8.5	8.18	7.85
Nickel	≤70	10	4	13	11	11	3	4	5	13	12	37	17	126	6.92	6.03	9.44
Selenium	≤10	<1	<1	<1	2	<1	2	<1	<1	<1	<1	5	38	<1	6.95	6.98	8.32
Silver	≤100	<1	<1	<1	<1	<1	<1	<1	<1	73	6	9	7	10	<1	<1	<1
Strontium	≤4000	413517	424317	444313	418268	119061	308104	309401	300157	177849	350107	-	-	-	576165	517733	500941
Thallium	≤2	16	17	36	39	2	7	10	11	153	6	40	34	29	24	19.6	19.9
Tin	-	<1	<1	<1	<1	<1	<1	<1	<1	6	<1	<1	<1	<1	<1	17.5	<1
Titanium	-	<1	<1	<1	2	<1	<1	<1	2	<1	<1	<1	<1	6	1.76	<1	<1
Uranium	≤15	<1	<1	<1	<1	<1	<1	<1	<1	2	<1	<1	<1	<1	<1	<1	<1
Vanadium	≤200	<1	<1	<1	<1	<1	<1	<1	<1	<1	<1	<1	<1	<1	<1	<1	<1
Zinc	≤5000	795	625	809	757	32	481	556	580	1	735	3064	2971	2575	1204	980	958

Table D 3 Hydrochemical results of all boreholes in the Bussaba fan.

Chemical Constituent	Drinking Water Quality Limits	Bussaba Fans Borrow Pit	BS-M01 Develop-ment	BS-P01 Develop-ment	BS-P01 PT CD 24 hrs	BS-P01 PT CD 80 hrs	BS-P01 7 days
		17 May 2015	08 June 2016	30 June 2016	14 Aug 2016	18 Aug 2016	19 Oct 2016
pH at 25°C	5-9.7	7.2	7.5	6.5	6.4	6.4	6.5
Conductivitiy at 25°C (mS/m)	≤170	7170	788	24400	17780	17750	16650
Density (g/cm^3)	-	1.03	0.99	1.11	1.09	1.09	1.09
In mg/l							
Total Dissolved Solids at 180°C	≤1200	49018	5220	165552	138694	138628	148442
Total Alkalinity	-	47	90	41	6153	6666	29
Total Hardness	-	15261	1723	56651	52515	54138	50145
Bicarbonate	-	47	90	41	6153	6666	29
Calcium	-	4784	479	14745	13971	14522	13845
Magnesium	≤70	805	128	4816	4281	4341	3782
Sodium	≤200	10162	778	38360	32758	33469	31651
Potassium	≤50	839	78	3214	2967	2997	3120
Chloride	≤300	29353	1614	114475	82386	89334	79975
Bromide	≤5	2.9	133	10.53	-	-	8863
Fluoride	≤1.5	3.2	1.25	2.8	2.72	2.72	400
Sulphate	≤500	1540	1280	11.7	566	634	475
Orthophosphate	≤5	<0.002	0.015	0.149	<0,03	<0,03	0.354
Ammonia	≤1.5	<0.08	0.77	0.6	19.9	19.8	20.3
Nitrate	≤11	0.41	<0.1	2.81	<0,1	<0,1	<0.1
Nitrite	≤0.9	0.12	<0.1	0.2	<0,1	<0,1	<0.1
Chemical Oxygen Demand	-	1868	147	5036	4080	4480	6236
Dissolved Metals (in µg/l)							
Aluminium	≤200	124	269	5.1	2527	5245	11
Antimony	≤20	<1	<1	5.9	9.68	5.43	<1
Arsenic	≤10	<1	1.18	11.8	<1	2.23	<1
Barium	≤700	212	258	414	1303	1595	1161
Beryllium	≤10	<1	<1	3.1	<1	<1	<1
Boron	≤300	7754	2118	24596	-	-	24918
Cadmium	≤3	<1	<1	<1	<1	1.58	<1
Chromium	≤50	<1	<1	1.6	141	-	4.58
Cobalt	≤500	<1	<1	3	4.05	10	2.9
Copper	≤2000	<1	22	41	108	170	188
Iron	≤2000	57	49	20	511	877	69
Lead	≤10	4.41	1.07	8.2	<1	<1	1.39
Lithium	-	1146	241	49	-	-	2810
Manganese	≤400	4.09	605	28264	-	-	41060
Mercury	≤6	<1	1.72	11.9	-	-	4.93
Molybdenum	≤70	16.1	5.9	215	5.52	9.58	3.71
Nickel	≤70	6.31	5.53	7.4	109	183	5.67
Selenium	≤10	4.56	2.79	53	6.07	36	3.75
Silver	≤100	<1	<1	137	8.91	8	<1
Strontium	≤4000	136480	10803	332759	-	-	289548
Thallium	≤2	2.89	<1	41	7.7	7.91	8.43
Tin	-	<1	<1	8.4	<1	<1	<1
Titanium	-	4.91	1.86	1.9	<1	6.97	<1
Uranium	≤15	<1	<1	2.8	<1	3.25	<1
Vanadium	≤200	<1	<1	<1	<1	<1	<1
Zinc	≤5000	22	47	4.2	-	-	38

Table D 4 Hydrochemical results of all boreholes in the Asabuya fan.

Chemical Constituent	Drinking Water Quality Limits	RAJ-1 CW 112 mbgl	RAJ-1 PT Step 1	RAJ-1 PT Step 3	RAJ-1 PT CD 48 hrs	RAJ-1 PT CD 72 hrs	RAJ-1 7 days	RAJ-1 12 days	Asabuya Village Well	Musley Village Spring	Fly Camp Lake	B-A Fans Boundary Springs	Asabuya Recharge Pond	AY-M01 Develop-ment	AY-M02 Develop-ment	AY-P01 Develop-ment	AY-P01 PT CD 30 hrs	AY-P01 80 hrs CD	AY-P01 7 days	AY-P01 20 days	AY-P01 Down-stream
		20 April 2015	11 June 2015	11 June 2015	15 June 2015	16 June 2015	31 Oct. 2016	5 Nov. 2016	17 May 2015	21 May 2015	15 June 2015	02 June 2015		20 July 2016		28 Sep 2016	30 Sep 2016	2 Oct. 2016	1 Nov. 2016	14 Nov. 2016	28 Oct. 2016
pH at 25°C	5-9.7	7.2	6.8	6.8	6.8	6.7	6.9	6.9	7.6	7.7	6.6	6.7	7.7	7.7	5.9	6.4	6.2	6.2	6.2	6.2	6.8
Conductivitiy at 25°C (mS/m)	≤170	987	4770	4940	5240	5360	4650	4690	145	164	>20000	7880	198	1042	>20000	15370	13910	13120	12940	13170	13420
Density (g/cm^3)	-	1	1.02	1.02	1.02	1.02	1.02	1.02	0.99	1	1.13	1.03	0.98	1	1.15	1.07	1.06	1.07	1.07	1.07	1.07
In mg/l																					
Total Dissolved Solids at 180°C	≤1200	7832	29212	30134	30914	32388	33914	35256	943	830	173630	53522	1432	6762	227174	110298	96050	117546	104154	112448	118102
Total Alkalinity	-	39	28	26	33	28	24	27	167	120	41	26	205	61	4614	8717	9320	35	31	29	33
Total Hardness	-	15634	13596	13983	15319	15903	15321	15248	311	120	92040	19531	590	2025	135127	59424	52656	49091	49298	66	50306
Bicarbonate	-	39	28	26	33	28	24	27	167	120	41	26	205	61	4614	8717	9320	35	31	29	33
Calcium	-	5265	3847	3954	4278	4454	4414	4314	90	112	22938	6410	213	666	33402	14698	13142	12788	12927	12459	13070
Magnesium	≤70	604	969	998	1126	1161	1044	1087	21	20	8442	856	14	88	12560	5518	4818	4167	4133	4159	4291
Sodium	≤200	9872	4908	4985	5457	5591	4988	4641	154	109	28430	10271	125	1257	36802	19896	17706	16637	16441	17411	17140
Potassium	≤50	646	594	613	680	665	632	647	19	7.3	4727	743	18	92	6465	3025	2630	2730	2683	12	2757
Chloride	≤300	2691	26800	20348	22830	23326	827	19494	180	155	130031	33022	397	3082	168742	77423	67497	66979	56982	58982	65980
Bromide	≤5	0.3	2.5	2.7	2.7	2.9	2394	2325	<0.1	<0.1	19	3.8	-	0.371	-	-	-	8185	7772	8004	8531
Fluoride	≤1.5	3.84	2.98	3	2.98	3.12	1 500	1 500	1.87	1.08	8.5	4.4	0.83	1.99	7.55	5.8	5.5	1000	1000	1000	1000
Sulphate	≤500	1130	438	431	457	437	471	678	225	702	786	552	244	500	467	288	342	251	261	261	269
Orthophosphate	≤5	0.02	<0.002	<0.002	<0.002	<0.002	0.083	0.08	0.016	0.006	<0.002	<0.002	<0.03	<0,03	<0.03	<0.03	<0.03	0.453	0.381	0.319	0.352
Ammonia	≤1.5	<0.08	2.32	2.47	2.71	2.83	2.68	2.73	<0.08	0.65	18.7	1.27	<0.22	<0.22	31.4	14.1	20.5	11.5	11.3	11.6	11.8
Nitrate	≤11	0.9	0.54	0.57	0.59	0.54	0.58	0.6	4.03	1.77	0.2	0.57	12.1	1.7	0.17	<0.1	<0.1	<0.1	<0.1	<0.1	<0.1
Nitrite	≤0.9	0.13	0.09	0.07	0.08	0.08	<0.1	<0.1	0.08	0.09	<0.01	0.1	0.12	<0,1	<0.1	<0.1	<0.1	<0.1	<0.1	<0.1	<0.1
Chemical Oxygen Demand	-	139	1076	853	1096	1584	827	720	<20	<20	3636	1212	94	106	5440	3280	2560	3446	3446	3774	4185
Dissolved Metals (in µg/l)																					
Aluminium	≤200	198	127	133	66	304	<1	2.33	1.35	1.25	422	53	-	<1	4132	540	381	43	6.13	<1	<1
Antimony	≤20	<1	1.05	<1	<1	<1	<1	<1	<1	<1	<1	<1	10.1	<1	16.7	10.4	13.4	<1	<1	<1	<1
Arsenic	≤10	<1	1.09	<1	<1	1.35	<1	<1	<1	<1	1.05	<1	<1	3	104	<1	<1	1.2	1.01	<1	<1
Barium	≤700	224	782	833	856	929	638	627	17.8	37	3151	352	205	55	4077	-	-	2070	2022	2406	2580
Beryllium	≤10	<1	<1	<1	<1	<1	<1	<1	<1	<1	<1	<1	<1	<1	<1	<1	1.56	<1	<1	<1	<1
Boron	≤300	2001	6712	6837	7081	7538	5694	5413	576	310	44980	7616	-	1350	-	-	-	20079	18929	19643	20697
Cadmium	≤3	<1	<1	<1	<1	<1	<1	<1	<1	<1	<1	<1	1.29	<1	1.01	<1	2.21	<1	<1	<1	<1
Chromium	≤50	<1	<1	<1	<1	<1	<1	<1	<1	<1	<1	<1	19.7	<1	554	<1	51	1.23	1.66	<1	1.77
Cobalt	≤500	<1	<1	<1	<1	<1	<1	<1	<1	<1	3.53	<1	4.08	1.4	104	4.04	6.04	1.83	1.45	1.64	2.04
Copper	≤2000	<1	10.1	<1	<1	4.76	32	7.17	<1	<1	4.23	<1	<1	17.2	311	4.43	29	3.81	3.96	11.4	9.6
Iron	≤2000	104	301	384	23	29	24	22	1.27	1.13	156	37	1050	<1	-	235	1269	83	427	839	59
Lead	≤10	7.16	6.24	1.72	2.05	14.2	<1	<1	<1	<1	35	2.51	<1	2.7	17.2	<1	<1	<1	<1	<1	<1
Lithium	-	1131	3409	3431	3335	3445	2607	2425	113	6.74	11114	4240	2413	62	-	7746	7595	4749	4396	4987	5287
Manganese	≤400	640	11008	11487	12268	13338	10704	10507	<1	<1	82180	2.47	278	370	-	-	-	43422	41623	42893	45392
Mercury	≤6	<1	<1	<1	<1	<1	1.97	<1	<1	<1	<1	<1	-	42	-	-	-	<1	<1	<1	<1
Molybdenum	≤70	25	7.02	6.26	6.72	5.08	5.15	5.65	8.79	7.11	15	5.32	2.97	38	136	14.3	11.3	9.77	10.3	5.78	6.3
Nickel	≤70	1.07	11	4.09	9.16	7.18	1.59	1.17	<1	<1	13.4	<1	11.4	23	1139	10	20	5.55	4.8	2.77	3.49
Selenium	≤10	1.56	<1	2.64	1.67	1.13	<1	8.43	4.17	2.35	5.81	<1	41	<1	15.6	29	27	1.57	1.29	5.42	6.43
Silver	≤100	<1	<1	<1	<1	<1	<1	<1	<1	<1	<1	<1	11.9	2.6	8.49	10.7	11.4	<1	<1	<1	<1
Strontium	≤4000	26726	123809	127815	132021	139100	102081	101056	2558	2077	791527	188973	3270	18853	-	-	-	303033	296971	303894	316602
Thallium	≤2	<1	<1	<1	3.07	2.88	<1	<1	<1	<1	3.66	5.26	<1	<1	<1	3.91	6.16	4.4	4.2	3.38	3.83
Tin	-	<1	<1	<1	<1	<1	<1	<1	<1	<1	<1	<1	<1	5.3	2.93	13.1	3.64	<1	<1	<1	<1
Titanium	-	1.28	<1	<1	<1	<1	1.45	<1	<1	<1	<1	2.37	<1	<1	<1	<1	<1	1.5	3.68	<1	3.03
Uranium	≤15	<1	<1	<1	<1	<1	<1	<1	1.48	<1	<1	<1	2.69	25	2.02	<1	<1	<1	<1	<1	<1
Vanadium	≤200	<1	<1	<1	<1	<1	<1	<1	3.56	3.76	<1	<1	<1	<1	<1	<1	<1	1.53	1.59	<1	<1
Zinc	≤5000	<1	165	2.96	217	170	8.84	<1	<1	1.65	49	<1	-	<1	-	83	174	43	36	33	34

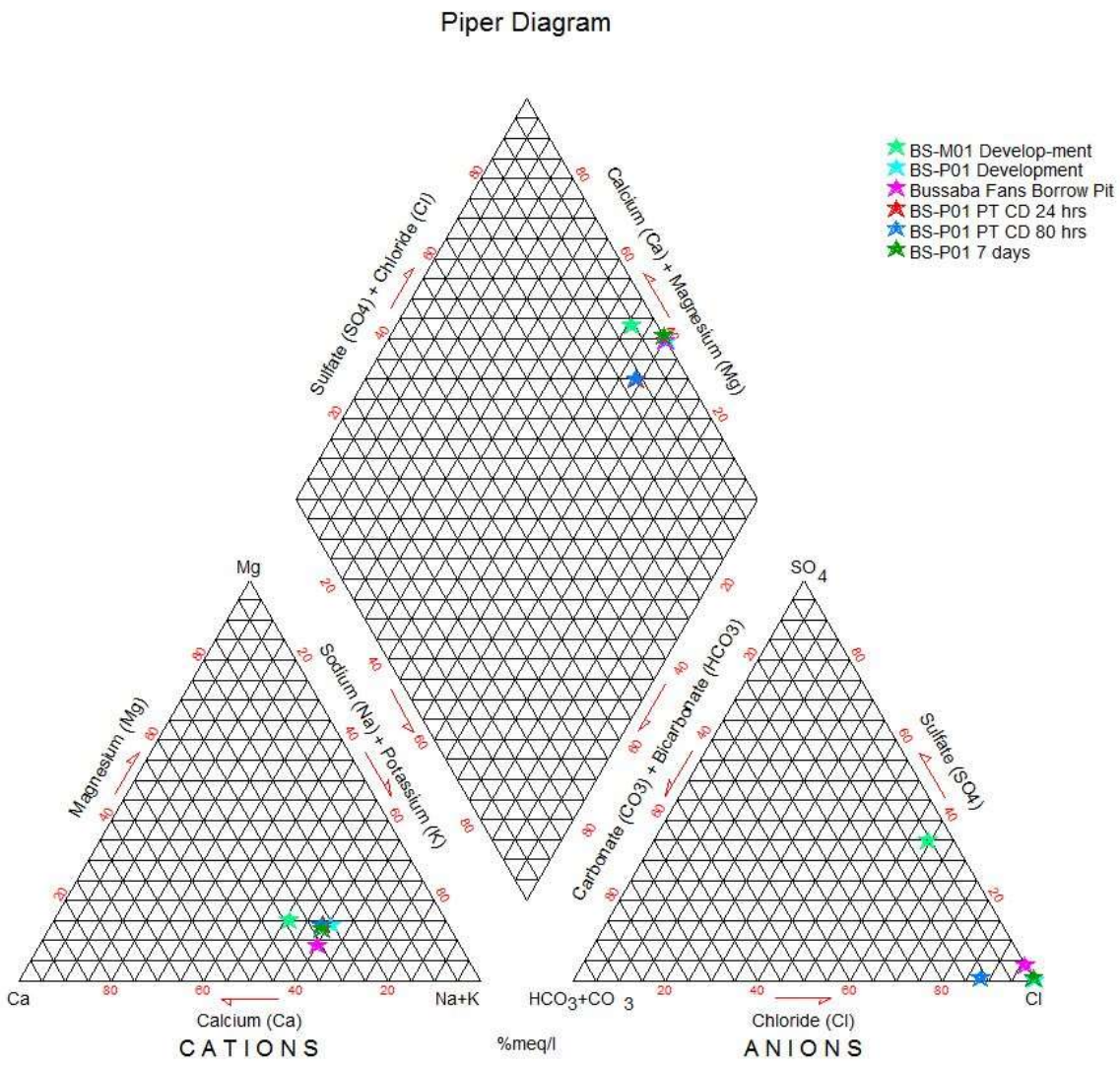

Figure D 5 Piper Diagram illustrating samples of the Bussaba fan.

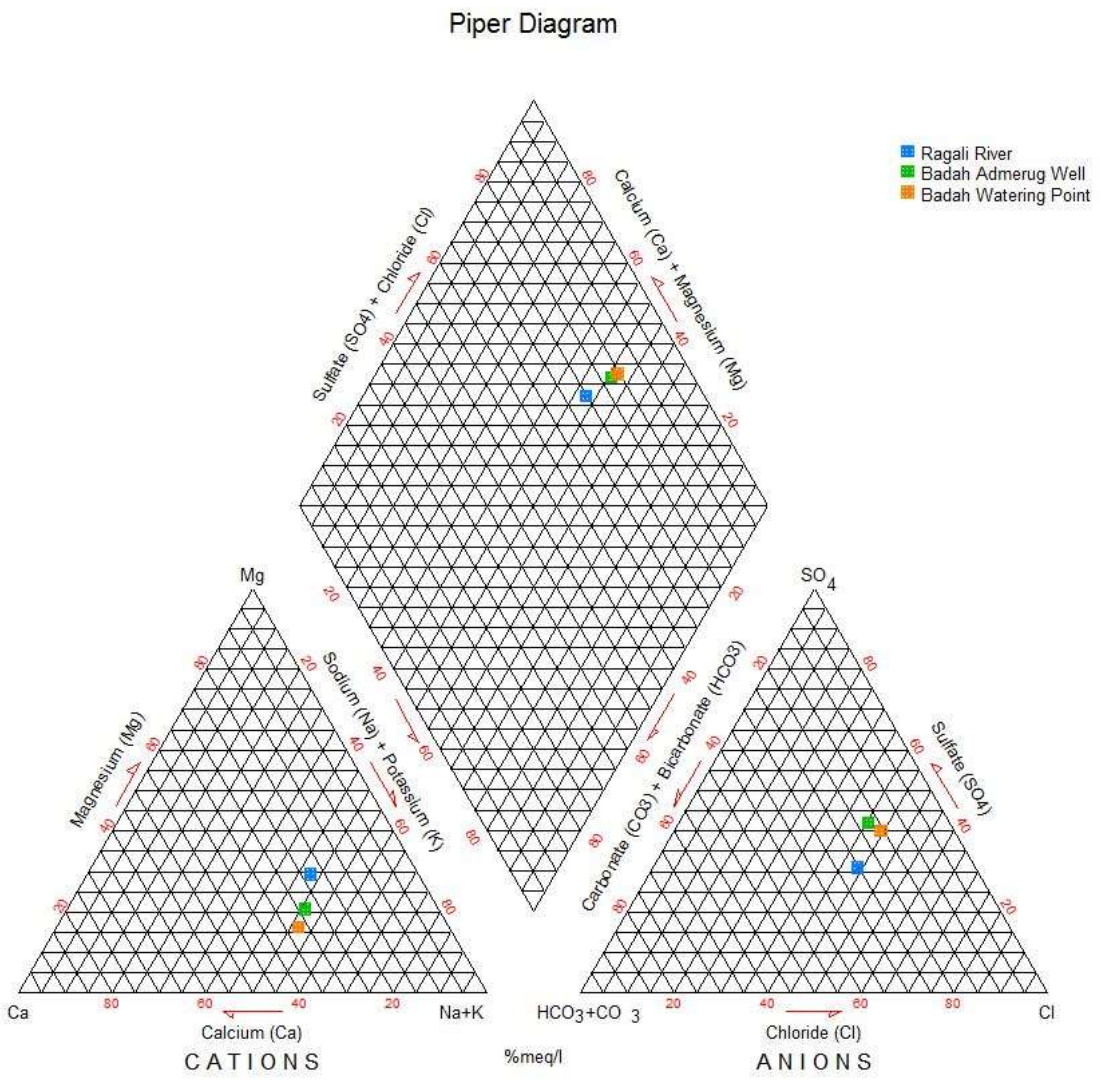

Figure D 6 Piper Diagram illustrating samples of the Badah area

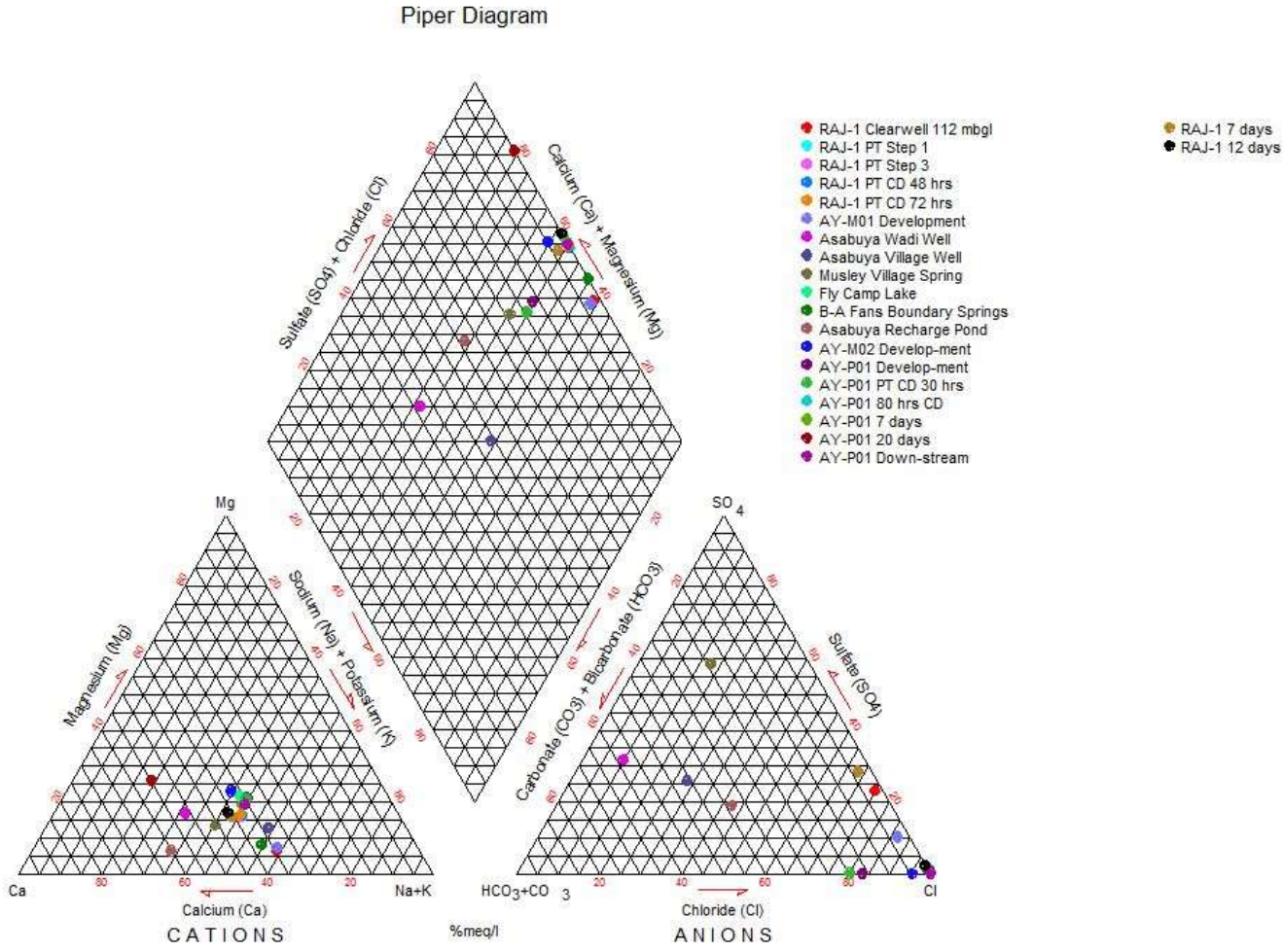

Figure D 7 Piper Diagram illustrating samples of the Asabuya fan

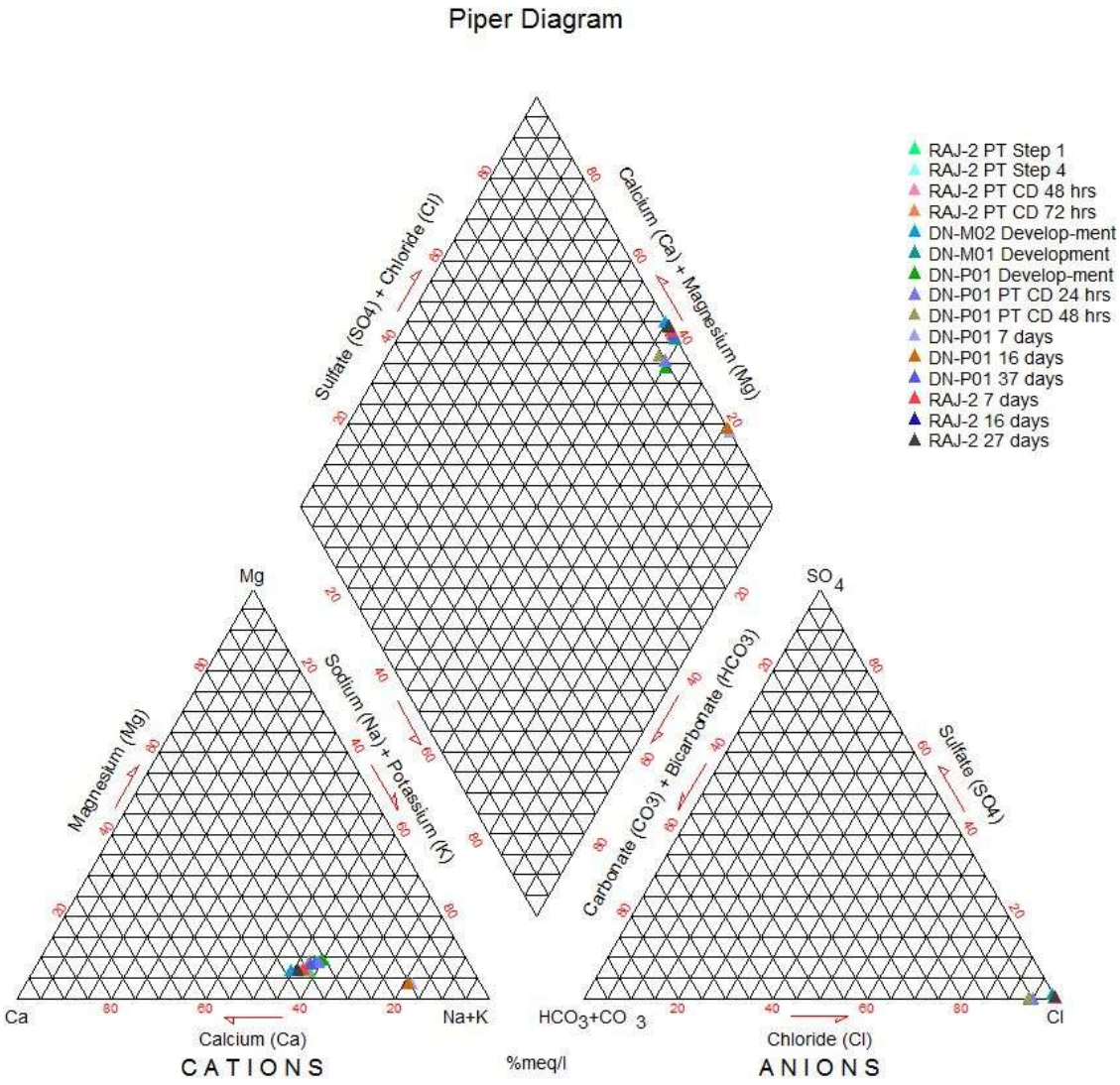

Figure D 8 Piper Diagram illustrating samples of the North Dogua fan

ABSTRACT

This dissertation investigates three alluvial fans in the Northern Danakil Depression, Ethiopia for potential groundwater supply to a solution mining operation. The presence of groundwater seeps at the toe of the alluvial fans further indicated the potential of the alluvial fans for groundwater exploration and possible abstraction to meet the mine water demand of 30 cubic hectometres (30 hm^3) or 30-million cubic meters per annum. Cumulative life of mine demand was determined to be 450.73 hm^3.

Lithological, structural and hydrostratigraphic investigations revealed that the Precambrian basement rocks of the Dogua Mountains outcrop in the west adjacent to the Bussaba and North Dogua fans, while further south, Cenozoic-Jurassic rocks of the Antalo Limestones and Adigrat sandstones are juxtaposed against the Asabuya fan. Structural mapping showed the presence of north-south trending rift related faults, including the Main Danakil Rift-boundary Fault, which transect and underlie the alluvial fans. These faults were determined to be likely pathways for deep hydrothermal fluids to vertically recharge the fans with hot, hypersaline groundwater and brines. Additionally, east-west trending fault and fracture zones identified in the Cenozoic-Jurassic rocks implied that fresh-brackish water is likely transmitted from the west into the Asabuya fan, but no such through flow is expected into the Bussaba and North Dogua fans due to the Precambrian basement rock acting as an aquitard. This was determined to cause a considerable difference in recharge sources and hydrochemical signatures between Asabuya fan in the south and Bussaba and North Dogua fans in the north.

Two automatic weather stations, were established in recharge zones of the Dogua Mountains. The annual average rainfall was determined to be 90 mm/a with an average evaporation rate of 66 mm/a.

Moving Loop Electromagnetic geophysical surveys showed low conductivity zones extending through each fan from south to north, confirming the presence of mapped faults transecting the alluvial fans. A maximum fan thickness of 160 m was determined to occur toward the centre of each fan. The low conductivity fault zones and active depositional channels informed the final positions for production and monitoring boreholes.

Drilling results of three production boreholes and five monitoring boreholes confirmed the unconfined nature of the aquifer. Drilling depths proved a minimum thickness of 170 m.

Analysis of time-drawdown data yielded high Transmissivity values in the order of 11 000-20 000 m^2/d. Due to a lack of observable drawdown in the monitoring holes, storage estimations were inconclusive. Water level response during pumping increased confidence in the assumption of recharge by hydrothermal water upwelling via rift related faults.

An Aquifer Stress Test (AST) showed minimal drawdown and rapid recovery proving that pump rates of up to 60 l/s were sustainable for up to two years. A total of 603 370.7 m^3 was abstracted during the AST. No cross-fan interaction was observed.

Hydrochemical analyses indicated boreholes nearer the wadis at the head of the fans had improved water quality compared to boreholes targeting the MDRF. Water quality in the Asabuya fan deteriorated as pumping continued, while the quality of the Bussaba and North Dogua fans both improved, implying different recharge sources to specific fans.

Insights gained from works carried out were used to inform a regional conceptual and numerical model. The numerical model assessed the influence of regional boundary conditions on the groundwater flow system as well as the feasibility of three different recharge scenarios to the alluvial fan aquifers. Calibration results indicated that only scenario 3 was feasible to use for predictive simulations. 20 wells spread across the fans were simulated to pump 22 hours/day at 60 l/s for 20 years and further for 40 years. Results showed an average drawdown of 5.5 m in the alluvial fans and that the mine water demand could be met in terms of quantity. Quality considerations however, were not incorporated into the model results and outcomes.

Resource estimation determined that with a S_y value of 0.2, the life of mine demand could be met for only 18 years at which time 96% of water in storage, without recharge contributions, would be depleted from the aquifer.

OPSOMMING

Hierdie verhandeling ondersoek drie alluviale waaiers in die Noordelike Danakil Depressie, Ethiopië vir moontlike grondwatertoevoer na 'n oplossing-mynbouoperasie. Die teenwoordigheid van grondwater syfering aan die toon van die alluviale waaiers dui verder op die potensiaal van die alluviale waaiers vir grondwater eksplorasie en moontlike abstraksie om die mynwater aanvraag van 30 hm^3/jaar te verskaf.

Lithologiese, strukturele en hidrostratigrafiese ondersoeke het getoon dat die Prekambriese keldergesteentes van die Dogua-berge teenaan die westelike grens van die Bussaba- en Noord-Dogua waaiers staan, terwyl die suidelike Cenozoic-Jurassic-gesteentes van die Antalo-kalkstene en Adigrat-sandstene teenaan die Asabuya-waaier staan.

Strukturele kartering het die teenwoordigheid van noord-suid-neiging verskywings, insluitend die Hoof Danakil-kloofgrensverskywing, getoon, wat die alluviale waaiers onderliggend maak.

Hierdie verskywings was bepaalend om waarskynlik vloei paaie vir diep hidrotermiese vloeistowwe te wees om die waaiers vertikaal te laai met warm, hipersaliene grondwater en pekelwater. Daarbenewens het oos-westelike verskywings- en breukgebiede wat in die Cenozoic-Jurassic-gesteentes geïdentifiseer is, geïmpliseer dat vars brakwater waarskynlik van die weste na die Asabuya waaier oorgedra word, maar daar word nie verwag dat hierdie vars brakwater in die Bussaba en Noord Dogua waaiers in sal vloei nie omdat die keldersteen nie as ‘n akwifer dien nie.

Dit was bepaalend om 'n aansienlike verskil in herlaaibronne en hidrochemiese handtekeninge tussen Asabuya waaier in die suide en Bussaba en Noord Dogua-waaiers in die noorde te veroorsaak.

Twee outomatiese weerstasies, is in herlaaissones van die Dogua-berge gevestig. Die jaarlikse gemiddelde reënval is vasgestel op 90 mm/jaar met 'n gemiddelde verdampingstempo van 66 mm/jaar.

Beweginde Lus Elektromagnetiese geofisiese opnames het lae geleidingsvermoë sones wat deur elke waaier van suid na noord voorkom geidentifiseer en die teenwoordigheid van onderliggende gekarteerde verskywings bevestig.

Maksimum waaierdikte van 160 m is bepaal. Die lae geleidingsvermoë sones en aktiewe deposisionelekanale het die finale posisies vir produksie en moniterings boorgate ingelig.

Boorresultate van drie produksie boorgate en vyf moniterings boorgate het die onbeperkte aard van die akwifer bevestig. Boordieptes het 'n minimum dikte van 170 m bepaal.

'n Akwifer Spanning Toets (AST) het getoon dat daar ‘n minimale mate van vermindering en ‘n vinnige herstel van watervlakke was. Dit toon aan dat pompkoers van 60 l/s in die produksie boorgate volhoubaar is.

'n Totaal van 603 370,7 m^3 is gedurende die AST uit gepomp. Ontleding van mate van vermindering en tyd data het hoë Transmissiwiteitswaardes in die orde van 11000-20000 m^2/d opgelewer.

Weens 'n gebrek aan waarneembare mate van vermindering in die moniteringsgate was opbergingsberamings onbevredigend. Watervlak reaksie tydens pomp afskakeling gee verhoogde vertroue in die aanname van groundwater herlaaing deur hidrotermiese water wat deur middel van verskywings vloei.

Hidrochemiese ontledings dui op dat boorgate nader aan die wadis aan die hoof van die waaiers beter waterkwaliteit het in vergelyking met boorgate nader aan die Hoof Danakil-kloofgrensverskywing.

Waterkwaliteit in die Asabuya-waaier het agteruitgegaan, terwyl die pompe gehardloop het terwyl daai van die Bussaba en Noord Dogua-waaiers albei verbeter het, wat verskillende herlaaibronne aan spesifieke waaiers impliseer.

Insigte verkry uit werke uitgevoer is gebruik om 'n konseptuele en numeriese model in te lig. Die numeriese model het die invloed van streeksgrenstoestande op die grondwatervloeistelsel beoordeel, sowel as die uitvoerbaarheid van drie verskillende herlaai-scenarios aan die alluviale waaier akwifers.

Kalibrasie resultate het aangedui dat slegs scenario 3 moontlik was vir voorspellende simulasies. 20 boorgate versprei oor die waaiers is gesimuleer om 22 uur per dag by 60 l/s vir 20 jaar en verder vir 40 jaar te pomp.

Resultate het 'n gemiddelde mate van vermindering van 5.5 m in die alluviale waaiers getoon en dat daar in terme van hoeveelheid genoeg water aan die myn verskaf kan

word. Kwaliteit oorwegings is egter nie opgeneem in die modelresultate en uitkomste nie.

Waterbron bepalings toon aan dat met 'n konserwatiewe effektiewe porositeit van 0.2 kan 96% van die myn se water benodiging verskaf word. Binne 18 jaar sal daar niks meer water beskikbaar wees nie in die akwifer. Saam oppervlak waters is dit voldoende om die hoeveelheid water aan die myn te bevredig, maar moontlike gehaltebeperkings bly nog ‘n probleem.